Heinrich Heine Universität Düsseldorf

Ultrasonic monitoring of the tablet compression process using different pharmaceutical excipients

Inaugural-Dissertation

zur Erlangung des Doktorgrades

der Mathematisch-Naturwissenschaftlichen Fakultät

der Heinrich-Heine-Universität Düsseldorf

vorgelegt von

Melinda Kern

aus Lörrach

Darmstadt, Juli 2022

aus dem Institut für Pharmazeutische Technologie und Biopharmazie
der Heinrich-Heine-Universität Düsseldorf

Gedruckt mit der Genehmigung der
Mathematisch-Naturwissenschaftlichen Fakultät der
Heinrich-Heine-Universität Düsseldorf

Berichterstatter:

1. Prof. Dr. Jörg Breitkreutz

2. Prof. Dr. Anne Seidlitz

Tag der mündlichen Prüfung: 26.10.2022

Table of Contents

Publications

Parts of this thesis have already been published in the peer reviewed journal International Journal of Pharmaceutics or presented at conferences.

Original Publication

- Kern, M., Riedel, T., Breitkreutz, J., 2022. *Investigating key properties of model excipients and binary powder blends using ultrasonic in-die measurements on a compaction simulator.* International Journal of Pharmaceutics 613
  DOI: 10.1016/j.ijpharm.2021.121381

The idea was defined by Melinda Kern and Thomas Riedel. The study design was developed by all three authors. Experimental work was performed by Melinda Kern. The data evaluation was primarily performed by Melinda Kern with input by Thomas Riedel and Jörg Breitkreutz. The manuscript was written by Melinda Kern and optimised by Jörg Breitkreutz, and revised by Thomas Riedel and Jörg Breitkreutz.

Evaluation of Authorship: "Investigating key properties of model excipients and binary powder blends using ultrasonic in-die measurements on a compaction simulator". Contributions in %.

Author	Idea	Study Design	Experimental	Evaluation	Manuscript
Melinda Kern	50	34	100	50	50
Thomas Riedel	50	33	0	30	20
Jörg Breitkreutz	0	33	0	20	30

Poster Presentations

Kern, M., Riedel, T., Breitkreutz, J., *Using Ultrasound to Characterise the Elastic Behaviour of Binary Mixtures.* 3rd European Conference on Pharmaceutics, Bologna, Italy (2019)

Kern, M., Riedel, T., Breitkreutz, J., *Investigating the Sensitivity of Ultrasonic In-Die Measurements to the Compaction Behavior of Different Mannitol Grades*. PharmSci 360, Virtual Event (2020)

Abbreviations

%ER	Elastic Recovery
%iER	Immediate Elastic Recovery
%V	Volume fraction
%w	Weight fraction
ACP	Anhydrous calcium hydrogen phosphate
API	Active Pharmaceutical Ingredient
AUC	Area under the Curve, in particular under the ultrasonic decompression curve
DEM	Discrete Element Method
DIA	Dynamic Image Analysis
ERW	Elastic Recovery Work
FEM	Finite Element Method
ICH	International Conference on Harmonisation
KIM	Kilian Inline Measurement System
L	Large
LM	Lactose monohydrate
LoD	Loss on Drying
LP	Lower Punch
M	Medium
MCC	Microcrystalline cellulose
MgSt	Magnesium stearate
MN	Mannitol
MS	Maize starch
µCT	X-ray microtomography
NetW	Net Work
Ph. Eur.	European Pharmacopoeia
PR	Poisson's Ratio
PSD	Particle Size Distribution
R^2	Coefficient of Determination
Ratio	Ratio between velocity decrease and solid fraction decrease
rpm	Rotations per Minute
S	Small
SEM	Scanning Electron Microscopy
sd	Standard Deviation

SDC	Solids Development Consult
SF	Solid Fraction
SF_{max}	Maximum Solid Fraction
SF_{end}	Solid fraction at which the contact between upper punch and compact is lost
Slope	Slope of the ultrasonic decompression signal
SM	Shear Modulus
SOS	Speed of Sound
TA	TabAnalyzer
Tab	Tablet
TH	Tablet Height
TOF	Time of Flight
TS	Tensile Strength
TWC	Total Work of Compaction
UP	Upper Punch
US	Ultrasound
YM	Young's Modulus

1 Introduction

1.1 The Need for Better Characterisation

Tablets are the preferred dosage forms for systemically acting small molecules (Zhong et al., 2018). Simple dosing, handling and administration, all of which increase patient adherence, as well as comparatively low manufacturing cost and high throughput, number amongst their benefits. Even so, there are many challenges involved in their development. One of the sub-processes which are not entirely understood in tablet manufacturing is the tablet compression step. As the active pharmaceutical ingredient (API) often does not exhibit favourable compaction properties, a combination of excipients needs to be identified to improve tableting performance of the API and form tablets which are strong enough to cope with further handling. However, towards the early stages of development, there are only small amounts of the API available and additionally at high cost. Furthermore, the development timelines are tight, and results of formulation experiments are expected and needed as fast as possible to ensure timely commencement of clinical trials. Even so, the development process is in many cases still trial-and-error driven and a large number of excipient combinations and process parameters need to be tested. In addition, once a suitable powder mixture is found, new challenges might arise such as changes in the API properties caused by changes in the chemical synthesis (Rasenack and Müller, 2002), batch-to-batch variability of the excipients (Thoorens et al., 2014), and challenges in the process scale-up, e.g. from eccentric single station to rotary tablet presses (Palmieri et al., 2005) which might make performing new sets of experiments necessary.

The implementation of compaction simulators capable of mimicking the punch movements and the speed of rotary tablet presses has improved the predictability of small-scale experiments (Wünsch et al., 2020). In addition, as they are fully instrumented, they generate force and displacement data over the whole compaction process which can help in the identification of variances within the materials, all the while only needing small amounts of material (Çelik and Marshall, 1989). However, the usage of compaction simulators is still time consuming as many different combinations might need to be assessed and should not override the desire to understand the process itself. Owing to the implementation of the concepts of quality by design (QbD) and process analytical technology (PAT), the thorough understanding of the different processes has become more of a focal point in drug product development in recent years (Leuenberger and Lanz, 2005). The emergence of new characterisation methods and analytical tools could be observed with the common goal to better characterise the materials, some of which

found their way into the European Pharmacopoeia (Ph. Eur.), e.g., the characterisation of flow properties via shear cell (Ph. Eur. 2.9.36).

To summarise, devising new methods to monitor the compaction process is crucial, as a thorough understanding of the mechanisms involved in powder compaction is an important step in the identification of parameters indicative of the tablet performance. This would be especially helpful when attempting direct compression. As there are fewer interim steps involved than in other routes, e.g., roller compaction or twin-screw granulation, it is comparatively cost effective (Leane et al., 2018). But, at the same time it is most prone to being sensitive to small changes in API or excipient properties (Leane et al., 2015) which need to be identified as early as possible.

1.2 Tablet Compression

1.2.1 Mechanisms of Powder Compaction

During tablet compaction, the powder is radially constricted by the die and subjected to axial forces which results in a reduction of the powder bed height and consequently the volume. At the same time the sample transforms from individual particles to a cohesive compact through the formation of bonds between individual particles (Nyström et al., 1993; Rumpf, 1958). The tabletting process is commonly divided into three stages: die filling, compaction and ejection (Wu et al., 2005b). The compaction step can be further separated into loading (= compression) and unloading (= decompression). During compression several sub-processes occur simultaneously: Rearrangement, fragmentation, plastic deformation and elastic deformation of the particles (Denny, 2002; Hiestand et al., 1977; Nordström et al., 2012). Rearrangement of the particles occurs primarily at lower compaction pressures when the powder particles or granules are still loose (Klevan et al., 2010). Once densification through movement is not possible anymore, i.e., the voids in the powder bed become smaller than the particles, deformation will start. This can occur through elastic deformation of the particles, fragmentation into smaller pieces, or irreversible plastic deformation on the contact areas between particles (Cooper and Eaton, 1962). Normally most, if not all, of the aforementioned deformation mechanisms will occur in a pharmaceutical powder (Sonnergaard, 2001), however, depending on the predominant mechanism, the materials will differ in their susceptibility when it comes to lubrication (Wang et al., 2010) or tabletting speed (Armstrong, 1989). In addition, plastic deformation is thought to be the main factor contributing to tablet strength owing to the pronounced increase in contact areas between different particles which furthers bond formation (Hiestand, 1997).

To determine whether a pharmaceutical powder deforms through fragmentation, the measurement of the surface area of a compact is often applied (De Boer et al., 1986; Westermarck et al., 1998). The assumption is that a brittle material will show an increase in surface area as a result of particle breakage. The comparison of scanning electron microscope images before and after compression to assess the degree of fragmentation is also a possibility (Hardman and Lilley, 1970; Nyström et al., 1982). Another approach was introduced by Skelbæk-Pedersen et al. (2019) who prepared compacts of different excipients blended with magnesium stearate, and then determined the particle size distribution after grinding of the tablets, and observed a correlation between decreased particle size and fragmentation propensity. All of the aforementioned techniques are performed out of die after tablet compaction and ejection. A more material-sparing method used in the characterisation of the deformation behaviour of

pharmaceutical powders is the in-die analysis through compression models, which will be further explored in Chapter 1.2.2.

It has to be noted that deformation behaviour is not solely dependent on the material investigated, but also the size and shape of the particles. It has been found that increasing particle size and surface irregularities generally lead to an increase in fragmentation (De Boer et al., 1986; Skelbæk-Pedersen et al., 2020; Wong and Pilpel, 1990). However, while a primarily plastically deforming material might show more fragmentation if the particle size is increased, the primary deformation mechanism will not change (Nordström et al., 2012).

Since the mass during compaction is constant, the volume reduction results in an increase in tablet density. This process is often depicted through the increase of relative density, also known as solid fraction (SF), or reversely, the decrease of porosity, i.e., the pore fraction, of the compact. The SF can be calculated using equation (1-1) and is related to the porosity according to equation (1-2).

$$\boldsymbol{SF = \rho_{rel} = \frac{\rho_c}{\rho_{true}}} \tag{1-1}$$

$$\boldsymbol{\phi = 1 - \rho_{rel}} \tag{1-2}$$

SF: *Solid fraction [-]*

ρ_{rel}*:* *Relative density [-]*

ρ_c*:* *Compact density [g/mL]*

ρ_{true}*:* *True density [g/mL]*

ϕ*:* *Porosity [-]*

Both, SF and porosity, can be used to compare different powder materials to each other in-die as well as out-die. However, as the true density of a material cannot easily be determined, the pycnometric density or apparent particle density is often used as an approximation (Gustafsson et al., 1999; Katz et al., 2013; Kuentz and Leuenberger, 1999).

Pronounced volume reduction and resulting low porosity does not necessarily mean the material will form a strong compact (Gustafsson et al., 1999). However, as it is associated with additional contact surfaces between particles, volume reduction does promote bond formation. While loading is generally associated with increased bonding, during unloading and elastic recovery bonds are expected to break (Hiestand et al., 1977). However, it has been shown that bond formation can continue during decompression, if to a lesser extent (DeCrosta et al., 2001).

1.2.2 Compression Models

Much work has been invested into the understanding of the processes taking place during powder densification within the die of the tablet press. Since fully instrumented tablet presses and compaction simulators have become common in pharmaceutical development, the use of force and displacement data has become increasingly popular in the characterisation of materials. The main advantage over the originally used out of die methods is the material- and time-sparing character as one compaction cycle is often sufficient to investigate different material properties. While many equations have been proposed to describe the deformation of powders under pressure (Cooper and Eaton, 1962; Kawakita and Lüdde, 1971; Kawakita and Tsutsumi, 1966; Leuenberger and Rohera, 1986; Masteau and Thomas, 1999; Sonnergaard, 2001), the parameter most commonly referred to is the yield pressure according to Heckel (1961). Heckel proposed the decrease in porosity with increasing compression pressure following a first order kinetic and thus linearised the compression using the empirical Equation (1-3).

$$ln\frac{1}{\phi} = kP * A \tag{1-3}$$

ϕ: *Porosity [-]*

P: *Compression Pressure [MPa]*

K: *Slope of the linear portion of the Heckel plot [1/MPa]*

A: *y-intercept of the extrapolated linear portion of the Heckel plot [-]*

k and *A* are constants with *1/k* being defined as the yield pressure (Hersey and Rees, 1971). While the Heckel equation was originally devised for plastically deforming metal powders, it has since found applications in the pharmaceutical field (Adams and McKeown, 1996; Dai et al., 2019; Denny, 2002; Kuentz and Leuenberger, 1999; Mahmoodi et al., 2013; Nordström et al., 2012). The general assumption is that the higher the yield pressure, the harder a material, which leads to lower plasticity and higher fragmentation propensity. However, the yield pressure is highly dependent on the experimental conditions (Chowhan and Chow, 1980). The density changes with applied pressure might change depending on the speed of the compression (Fell and Newton, 1971; Kim et al., 1998) or the tooling (Sinka, 2007), and the determined yield pressure is known to change with varying maximum pressure (Sonnergaard, 1999). Additionally, the accuracy of density and displacement determination has a significant impact on the slope of the Heckel plot (Krumme et al., 2000) which is especially challenging for materials with a relatively high moisture content where the accurate true density determination is difficult (Sun, 2005). In addition, while Heckel determined the porosity out-die by compacting the powder materials to different solid

fractions, the in-die method is usually preferred nowadays. In this case, the results are not directly comparable as the curve progression in-die will also be influenced by the reversible elastic deformation of the material (Sun and Grant, 2001). This problem was addressed by Katz et al. (2013) who proposed correcting the in-die porosity for the elastic recovery and thus being in better agreement with the out-die method. Another difficulty is the determination of the slope *k* due to the non-linear increase of the compression part of the plot of materials which are not plastically deforming (Klevan et al., 2009), the curvature at the beginning of the compression process associated with particle rearrangement (Rowe and Roberts, 1996), and the deviation from linearity in the high pressure range of elastic materials (Sonnergaard, 1999; Sun and Grant, 2001). An additional hurdle in the comparison of the yield pressure presented by different authors is the determination of the slope. In many cases no information is disclosed about the boundary conditions set for the definition of the linear part of the compression curve (Aburub et al., 2007; Van Der Voort Maarschalk et al., 1996; Zhang et al., 2003). In case some information is given, the definitions range from a specified pressure range (Dai et al., 2019; Gustafsson et al., 1999; Nicklasson and Alderborn, 2000; Salbu et al., 2010), determination of the first derivative minimum and a specified deviation thereof (Mahmoodi et al., 2013; Nordström et al., 2012), a specified porosity range (Van Der Voort Maarschalk et al., 1997) to a target coefficient of determination (R^2) (Paul and Sun, 2017). Consequently, the results of the Heckel analysis should only be used in the comparison of different materials if the same experimental conditions and method for yield pressure determination were used (Krycer et al., 1982).

1.2.3 Work of Compaction

Another approach to use the force and displacement data is the calculation of compression energies or the work of compaction. All in all, there are total work of compaction (TWC), network (NetW) and elastic recovery work (ERW). The energies are calculated according to the following equations as used by Schlack (2001):

$$\boldsymbol{TWC} = \int_{\boldsymbol{TH_0}}^{\boldsymbol{TH_{F(max)}}} \boldsymbol{F_{avg}} * \boldsymbol{dTH} \tag{1-4}$$

$$\boldsymbol{ERW} = \int_{\boldsymbol{TH_{min}}}^{\boldsymbol{TH_{end}}} \boldsymbol{F_{avg}} * \boldsymbol{dTH} \tag{1-5}$$

$$\boldsymbol{NetW} = \int_{\boldsymbol{TH_0}}^{\boldsymbol{TH_{min}}} \boldsymbol{F_{avg}} * \boldsymbol{dTH} - \boldsymbol{ERW} \tag{1-6}$$

TH_o: *Tablet height at the beginning of compression [mm]*

$TH_{F(max)}$: *Tablet height at force maximum [mm]*

F_{avg}: *Average force of upper and lower punch [kN]*

dTH: *Change of tablet height with applied force [mm]*

TH_{min}: *Tablet height at contact loss [mm]*

The TWC is a measure for the total energy put into the material before unloading. The ERW is the energy released during elastic recovery and the NetW is the energy put into the material through irreversible deformation. High values of ERW and NetW are associated with high elasticity and large amounts of irreversible deformation, respectively (Ragnarsson, 1996).

1.2.4 Elastic Recovery

If the dimensions of a tablet are determined in- and out-die, a discrepancy will be noted. Once out of the die, the volume of the compacts increases due to the elastic relaxation of the material. The volume change between the minimum tablet height in-die and the out-die volume after compression can then be used to quantify the elastic recovery according to equation (1-7):

$$\%\boldsymbol{ER} = \frac{\boldsymbol{V_{out-die}} - \boldsymbol{V_{in-die}}}{\boldsymbol{V_{in-die}}} * \mathbf{100}\% \tag{1-7}$$

%ER: *Elastic recovery [%]*

$V_{out-die}$: *Tablet volume out-die after ejection [mm^3]*

V_{in-die}: *Tablet volume at minimum distance between punches [mm^3]*

The expansion caused by elastic recovery can lead to the breaking of bonds and the loss of interparticular adhesion established during compression. The more elastic a substance, the more bonds will break as has been shown using compression calorimetry (DeCrosta et al., 2001). This has often been associated with the occurrence of capping or lamination of tablets (Paul and Sun, 2017), a defect that results in the rejection of the finished drug product.

1.3 Characterisation of Tablets

1.3.1 Tensile Strength

After compression, a number of additional process steps may follow such as coating, storage and packaging, which will put the tablets under mechanical strain. It is, therefore, of vital importance that the tablets are strong enough to cope with any further handling without exhibiting failures such as breakage. The most commonly applied method for the determination of mechanical strength is the diametral-compression test, where the tablets are being crushed between a static wall and a moving plate. The breaking force is then used for comparison. However, while the crushing force is often used synonymously with compact hardness and can be used to compare tablets of the same size and shape, it does not incorporate the influence of the tablet dimensions on the mechanical strength of a tablet. For the comparison of biplane tablets with different sizes Fell and Newton (1970) proposed to use the tensile strength (TS):

$$\boldsymbol{\sigma = \frac{2P}{\pi D h}} \tag{1-8}$$

σ: *Tensile Strength [MPa]*

P: *Applied load [N]*

D: *Tablet diameter [mm]*

h: *Tablet height [mm]*

To compare the performance of different blend compositions, the relationships between SF, TS and the applied pressure can be used. For a single material, the TS typically increases with increasing SF. It has been postulated that in order to cope with further handling, a tablet should exhibit a TS of over 1.7 MPa and a SF around 0.85 (Leane et al., 2015). However, different shapes and geometries are still difficult to compare.

1.3.2 Elasticity Parameters

Aside from the tablet strength, the elasticity parameters of a material might be of interest for the characterisation of the compacts. Two parameters that are often determined are Young's Modulus (YM) and Poisson's Ratio (PR). The YM describes the change in specimen length through elastic deformation when a force is applied. The higher the value, the higher the resistance against elastic deformation. The PR is defined as the ratio of length change to width change. It can therefore be used to describe the volume change of a material when pressure is applied. Solid materials typically exhibit values between 0 and 0.5, where the volume change decreases with increasing values until at 0.5 no volume change occurs (Rosato and Rosato, 2003).

Approaches to determine the YM of pharmaceutical compacts include three-point bending test (Busignies et al., 2004; Porion et al., 2010), application of axial load and simultaneous deformation measurement (Kachrimanis and Malamataris, 2004), micro and nano indentation (Lum and Duncan-Hewitt, 1996; Radovic et al., 2004; Wu et al., 2019), Terahertz time-delay measurements (Peiponen et al., 2015) or an instrumented die where the force exerted in radial direction is monitored during the compaction process (Akseli et al., 2008a; Mazel et al., 2012, 2013; Paul and Sun, 2017). Even though the PR can be experimentally determined using an instrumented die, for pharmaceutical materials in many cases a value of 0.3 is assumed over the whole compaction process and resulting porosity range (Roberts et al., 1994). However, for YM and PR it has been shown that there is a dependency on the porosity (Aliabouzar et al., 2018; Asmani et al., 2001; Cunningham et al., 2004; Mazel et al., 2012, 2013; Wang, 1984a). The YM increase with decreasing porosity was found to adhere to the following relationship (Spriggs, 1961):

$$\boldsymbol{E = E_0 e^{-b\phi}} \tag{1-9}$$

E: *Young's Modulus [GPa]*

E_0: *Young's Modulus at zero porosity [GPa]*

b: *Material dependent constant [-]*

ϕ: *Porosity [-]*

One application of the elasticity parameters is in the modelling and simulation of the powder compaction process. Simulation approaches have become increasingly popular over the last years as they help in better understanding of the compaction process, e.g., viscoelastic behaviour of materials (Desbois et al., 2020; Diarra et al., 2013), and the resulting tablet properties such as density distribution (Michrafy et al., 2002; Sinka, 2007; Wu et al., 2005b), break force (Shang et al., 2013) and structural anisotropy (Yohannes et al., 2016). As the correct determination of the elasticity parameters has a pronounced influence on the accuracy of the simulations in discrete (DEM) and finite element modelling (FEM) (Diarra et al., 2018; Paulick et al., 2015), finding methods to accurately measure those parameters is of high interest.

1.3.3 Porosity

In addition to the pore volume of the tablets, the pore structure is also used in the characterisation of pharmaceutical compacts. Porosity and also pore structure are known to have an impact on tablet disintegration and strength, both of which are essential parameters to keep in mind when formulating a new drug product (Sun, 2017). Some of the methods used in the determination of pore size are nitrogen adsorption (Westermarck et al., 1998, 1999), mercury

intrusion porosimetry (Van Veen et al., 2002; Wu et al., 2008), image analysis through scanning electron microscopy (SEM) (Chen et al., 2015; Wu et al., 2007; Yu et al., 2005), pulsed-gradient stimulated-echo NMR (Porion et al., 2010), X-ray microtomography (µCT) (Yang et al., 2014), and Terahertz domain spectroscopy (Markl et al., 2018a; Markl et al., 2017). However, all of these methods have their limitations (Markl et al., 2018b). Nitrogen adsorption and mercury intrusion porosimetry can help in the measurement of pore size distribution, however, as the measurement medium needs to fill the pores, only pores accessible from the outside are considered using these methods. Additionally, they do not yield any information about the pore orientation. In SEM images only the surface of the tablet is assessed. To get images of the compact interior, the sample needs to be cut, which might result in an alteration of the pore structure. A drawback of the µCT approach is the limited resolution of about 10 µm, which is not sufficient for microstructure analysis in pharmaceutical compacts (Wu et al., 2005c).

An additional tool in the assessment of porosity which is already used for a variety of materials is ultrasound which will be focused on in the following section.

1.4 Ultrasonic Testing

1.4.1 Fundamentals of Sound Transmission

A sound wave through a medium can be described by wavelength, velocity and frequency which are related according to the following equation:

$$\boldsymbol{c = \lambda f} \tag{1-10}$$

c: *Speed of sound [m/s]*

λ: *Wavelength [m]*

f: *Frequency [s^{-1}]*

Since the speed of sound (SOS) within a material is constant, an increase in wavelength will always result in a decrease of frequency. The sound frequencies perceptible by humans are between 20 and 20,000 Hz. Higher frequencies, starting at 20 kHz are called ultrasound (US). The SOS through a medium is related to the material properties. Furthermore, the velocity through a solid is generally decreased by the inclusion of small amounts of a foreign material or pores into the matrix (Krautkrämer and Krautkrämer, 1990).

The intensity and pressure of the sound wave transmitted through the medium are dependent on the acoustic impedance which is related to the velocity through the following equation:

$$\boldsymbol{Z = c\rho} \tag{1-11}$$

Z: *Acoustic impedance [Ns/m³] / [kg/sm²]*

c: *Speed of sound [m/s]*

ρ: *Material /True density [kg/m³]*

A material with a high impedance value is referred to as sonically hard (Krautkrämer and Krautkrämer, 1990). When a sound wave encounters a boundary surface between two materials exhibiting a high impedance mismatch, parts of the sound wave will be reflected which results in the decrease of the sound intensity. The sound intensity can be calculated according to equation (1-12).

$$\boldsymbol{I = \frac{p^2}{2Z}} \tag{1-12}$$

I: *Sound intensity [W/m²]*

p: *Sound pressure [Pa]*

Z: *Acoustic impedance [Ns/m³] / [kg/sm²]*

The sound pressure is related to the amplitude of the sound wave. The intensity of the sound wave in a medium decreases with distance to the sound source due to scattering and absorption. The combination of those two effects is called attenuation.

Two different wave forms are commonly used in the ultrasonic testing of materials: longitudinal compression waves and transverse shear waves. Both are mechanical waves and, therefore, propagate through oscillation of the medium. While in longitudinal waves the oscillation occurs in the same direction as the wave propagation, in the case of the transverse wave, the oscillation is perpendicular to the overall direction as is depicted in Figure 1-1. This results in several differences. The first is how the wavelength is determined. Longitudinal waves result in areas of varying densification caused by the delayed movement of neighbouring particles. One wavelength is then the space between two areas of identical density. Transverse waves on the other hand resemble the classic sine wave form. Here, a wavelength is defined as the space between two particles on the same vertical level moving in the same direction.

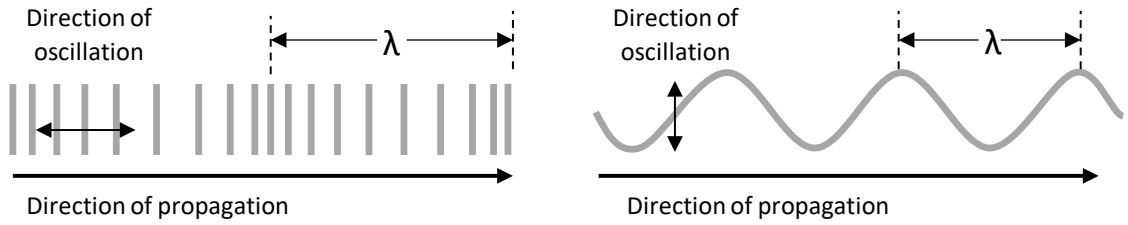

Figure 1-1: The two different kinds of sound waves; left: longitudinal, right: transverse.

The second difference is the speed of the sound waves. Longitudinal waves are in most cases about twice as fast as transverse waves (Schmerr, 2016). The third and last difference to be mentioned here is the medium through which the respective waves can propagate. While longitudinal waves traverse solids, liquids and gases, a solid medium is required for transverse waves (Krautkrämer and Krautkrämer, 1990).

The sound velocity though a material is dependent on its elastic properties and density. Through gases and liquids, it can be calculated using the Newton-Laplace equation:

$$\boldsymbol{c} = \sqrt{\frac{\boldsymbol{K}}{\boldsymbol{\rho}}} \tag{1-13}$$

c: *Speed of sound [m/s]*

K: *Bulk modulus [Pa]*

ρ: *Material / True density [kg/m³]*

Through equation (1-13), it becomes obvious that the SOS is reversely correlated to the square root of the material density. Furthermore, the SOS increases with increasing bulk modulus which in turn means it decreases with decreasing resistance against deformation i.e., increased compressibility. Additionally, there is a temperature dependence of SOS in gases and liquids. In solids the temperature effect is negligible (Krautkrämer and Krautkrämer, 1990). Here, the speed of sound can be calculated as follows:

$$\boldsymbol{c_L} = \sqrt{\frac{\boldsymbol{E}}{\boldsymbol{\rho}} \frac{(\mathbf{1}-\boldsymbol{v})}{(\mathbf{1}+\boldsymbol{v})(\mathbf{1}-\mathbf{2}\boldsymbol{v})}} \tag{1-14}$$

$$\boldsymbol{c_T} = \sqrt{\frac{\boldsymbol{G}}{\boldsymbol{\rho}}} \tag{1-15}$$

c_L: *Longitudinal wave velocity [m/s]*

c_T: *Transverse wave velocity [m/s]*

E: *Young's Modulus [N/m²]*

v: *Poisson's Ratio [-]*

G: *Shear Modulus [N/m²]*

ρ: *Material /True density [kg/m³]*

The longitudinal wave velocity is then related to Youngs's Modulus and Poisson's Ratio, while the transverse velocity is linked to the shear modulus of the solid. It needs to be kept in mind, however, that *E, v* and *G* are not independent of each other (Krautkrämer and Krautkrämer, 1990):

$$\boldsymbol{E} = \mathbf{2}\boldsymbol{G}(\mathbf{1}+\boldsymbol{v}) \tag{1-16}$$

E: *Young's Modulus [N/m²]*

G: *Shear Modulus [N/m²]*

v: *Poisson's Ratio [-]*

1.4.2 Applications of Ultrasonic Testing

Ultrasound has been used in the testing of materials for decades. The first patent for an ultrasonic testing apparatus was filed in 1940 by Firestone (1942). It was intended for the detection of density and elasticity inhomogeneities, as well as flaws within a material, otherwise inaccessible through non-destructive means. The author showed the sensitivity of the "reflectoscope" to holes in welds, which can negatively affect their strength, through the use of reflection signals (Firestone, 1946). He also found that lacking strength of the welds could not be determined using ultrasound, unless it was caused by a defect or discontinuity within the material.

Since then, ultrasonic testing has become a popular method in the characterisation and testing of materials.

Two measurement modes can be applied in general: pulse-echo, where only one transducer is needed which holds both functions, transmitting the sound wave into the specimen and then receiving the echo signal, and pitch-catch, where two transducers are placed on opposite sides of the specimen, one being the transmitter and the other one the receiver (Figure 1-2). The selection of the measurement mode depends on the intended purpose. The echo approach is useful in the determination of the thickness of different layers through the arrival times of the echoes reflected off the boundary surfaces, or the detection of cracks within the material. The transmission method on the other hand is faster since the sound wave only passes the specimen once which is an advantage in dynamic processes where short measurement windows are needed.

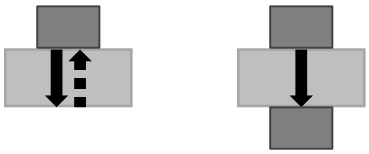

Figure 1-2: Schematic depiction of the pulse-echo (left) and pitch-catch (right) measurement set-ups. Solid arrow: transmitted signal, dashed arrow: reflected echo signal.

The utility of ultrasonic testing is not limited to the determination of welding integrity, but was also shown to be sensitive to defects in porcelain tiles. Artificially created cracks in the structure were found to decrease the amplitude of the ultrasonic echo signal reflected off the backwall of the sample (Eren et al., 2012).

In addition to the detection of defects, ultrasound has also been used in the characterisation of porous materials. As mentioned in Chapter 1.4.1, introducing pores into a medium reduces the phase velocity of the transmitted sound wave. Takatsubo and Yamamoto (1991) found that the time delay of an ultrasonic signal through perforated aluminium plates of the same dimensions but with different porosities and pore sizes was caused by the sound waves “creeping” around the pore surface. They could consequently correlate porosity and pore size with the delay time of the sound waves. In a later study (Takatsubo and Yamamoto, 1996) they found the delay time to be proportional to the porosity and independent of pore size if the pore shape was the same. Their findings confirm those of other authors who found the calculated velocity to be dependent on pore shape in sintered materials (Boccaccini and Boccaccini, 1997) and pore size (Sayers, 1981), and that the velocity is reversely proportional to porosity in ceramic samples (Asmani et al., 2001; Chang et al., 2000; Kohout et al., 2013), pressed aluminium (Nagarajan, 1971) and porcelain tiles (Eren et al., 2012).

Ultrasonic testing has also been applied in the determination of elastic parameters such as Young's Modulus and Poisson's Ratio in compressed alumina samples (Nagarajan, 1971), sintered materials (Boccaccini and Boccaccini, 1997), marble (Sarpün et al., 2009), alumina ceramics (Asmani et al., 2001; Chang et al., 2000) and other porous samples (Aliabouzar et al., 2018; Wang, 1984b). In addition, many of the authors found a correlation between Young's Modulus and porosity, as well as Poisson's Ratio and porosity which agrees with the findings when other methods were applied. It has been shown that in brittle materials the sonically determined elastic constants are in good agreement with those determined via indentation methods if the sample is isotropic (Wu et al., 2019). The SOS has even been found to be sensitive to the structural changes inside avocados during ripening (Fariñas et al., 2021).

In ultrasonic testing, the intensities of the sound waves are rather low while the frequencies are typically in the higher range (above 100 kHz) to prevent induced changes within the specimens (Krautkrämer and Krautkrämer, 1990). When high intensities are used, the oscillation has been shown to result in increased strength of the specimen when applied during compaction (Levina et al., 2000; Millán-Jiménez et al., 2017).

1.4.3 Ultrasonic Testing in Pharmaceutical Technology

In the past 20 years ultrasonic testing has found its way into the pharmaceutical area as a possible new tool in the characterisation of tablets. It has been proposed as an alternative method of tablet strength evaluation without the need to destroy the finished product as a correlation between tablet strength and measured velocity through the material has been observed (Akseli et al., 2011; Razavi et al., 2016; Simonaho et al., 2011; Xu et al., 2018a). However, there are two drawbacks. First, it is known that tensile strength of a powder compact decreases with increasing porosity as already mentioned in Chapter 1.3.1. Keeping in mind that ultrasonic velocity also decreases with increasing pore fraction, the correlation of tensile strength and ultrasonic velocity is obvious. Xu et al. (2020), however, found the ultrasonic results to be more sensitive to small changes in the pore structure of tablets, but how this could be translated into actual differences in tablet performance has not been shown yet. Second, while this trend could be observed for all materials, it was not possible to compare the measured speed/tensile strength relationship of different excipients (Simonaho et al., 2011). This means a calibration is needed for each new material or blend.

Another proposed application is the determination of the core centricity of dry coated tablets (Liu and Cetinkaya, 2010) which is crucial for their performance. The idea is that there are two boundary surfaces inside a dry coated tablet in addition to the actual outer surfaces of the

compact: one between the upper outer layer and the top of the included tablet, the second one between the lower outer layer and the bottom of the inner tablet as shown in Figure 1-3. At each surface, part of the ultrasonic wave is reflected due to the impedance mismatch of the materials. In pulse-echo mode it is then possible to compare the arrival times of the different reflected signals and determine whether upper and lower outer layer are of the same thickness.

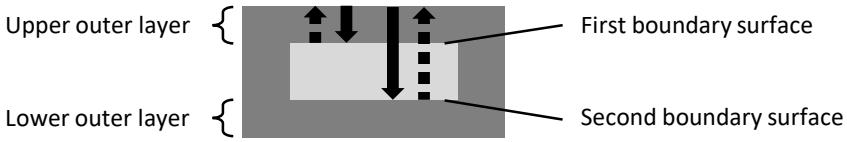

Figure 1-3: Depiction of the layer thickness measurement of a dry coated tablet using US. Dark grey: outer layer, light grey: inner layer, solid arrows: sound wave sent by transmitter, dashed arrows: sound waves reflected at boundary surface.

As ultrasound is related to the elasticity parameters of a material, it has also been used to calculate the Young's Modulus of tablets out-die (Akseli and Cetinkaya, 2008a; Akseli et al., 2010; Akseli et al., 2008a; Razavi et al., 2016; Stephens et al., 2013b; Xu et al., 2018a). The calculations were performed using the relationship between longitudinal velocity through the specimen, Young's Modulus, and compact density, as shown in Equation (1-17):

$$c_L = \sqrt{\frac{E}{\rho_c}} \tag{1-17}$$

c_L: *Longitudinal velocity [m/s]*

E: *Young's Modulus [GPa]*

ρ_c: *Compact density [kg/m^3]*

In addition to analysing a single component compact, the Young's Modulus of coat and core of tablets has been determined using the pulse-echo set-up described before (Akseli et al., 2009a; Akseli and Cetinkaya, 2008b; Liu and Cetinkaya, 2010).

In all the aforementioned publications, the speed of sound measurements were performed in axial direction, i.e. the same direction the force had been applied by the punches during compression. Akseli et al. (2009b) additionally measured the velocity in radial direction. Their specimens were uniaxially compressed cubical compacts. They found an increased longitudinal velocity perpendicular to the direction of applied stress for microcrystalline cellulose (MCC), while there was almost no change for lactose monohydrate (LM). They attributed their findings to a Young's Modulus anisotropy in MCC. However, it needs to be kept in mind that they used Equation (1-17) for the determination of the YM where an increased velocity always results in an increase

in YM if the density is constant as it was the case here. It should be mentioned that this equation is strictly speaking only valid in rods where the diameter of the specimen is smaller than the wavelength of the sound wave (Kinsler et al., 2000), which is not necessarily the case for tablets. Additionally, in an anisotropic material not only the longitudinal compression waves, where the vibration occurs in the direction of the sound wave, but also the transverse shear waves where oscillation is perpendicular to the direction of propagation should be used (Lum and Duncan-Hewitt, 1996). Equations (1-18) and (1-19) which use both wave velocities to calculate the elastic properties (Schmerr, 2016) might therefore give a better approximation of the parameters.

$$\boldsymbol{\nu} = \frac{\mathbf{1}(\boldsymbol{\kappa}^{\mathbf{2}} - \mathbf{2})}{\mathbf{2}(\boldsymbol{\kappa}^{\mathbf{2}} - \mathbf{1})} \tag{1-18}$$

$$\boldsymbol{E} = \frac{\boldsymbol{c}_{\boldsymbol{L}}^{\mathbf{2}}\boldsymbol{\rho}(\mathbf{1} + \boldsymbol{\upsilon})(\mathbf{1} - \mathbf{2}\boldsymbol{\upsilon})}{(\mathbf{1} - \boldsymbol{\upsilon})} \tag{1-19}$$

ν: *Poisson's Ratio [-]*

κ: c_L/c_T *[-]*

c_L: *Longitudinal velocity [m/s]*

c_T: *Transverse velocity [m/s]*

E: *Young's Modulus [N/m²]*

ρ: *Material / True density [kg/m³]*

In case of porous solids such as tablets, the compact density is sometimes used as an approximation similar to the approach presented in Equation (1-17) (Hagelstein et al., 2019). This is done to approximate the changes in elastic moduli with decreasing porosity.

Since no transverse measurements have been performed, the velocity anisotropy cannot unequivocally be attributed to the elasticity parameters but could also stem from anisotropic pore shapes (Piekarczyk and Kata, 2016). This is supported by the findings of Porion et al. (2010) who found an anisotropy in pore structure for MCC, but isotropy for YM determined via three-point single-beam test. As mentioned before (Chapter 1.4.2) the delay time of the ultrasonic signal and, therefore, the resulting calculated SOS are dependent on the pore shape. As the sound waves need to circumvent the pores in order to arrive on the other side of the specimen, their orientation will dictate the actual distance the sound wave has to cover as schematically depicted in Figure 1-4.

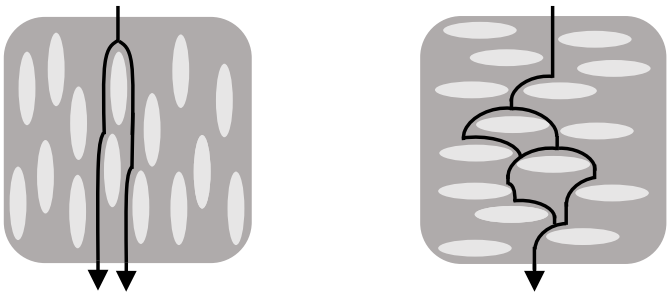

Figure 1-4: Schematic depiction of the sound wave propagation through a solid with flat pores assuming the pores are circumvented by creeping of the sound waves around the pore surfaces as proposed by Takatsubo and Yamamoto (1991).

Other proposed applications for ultrasound in pharmaceutics include the determination of swelling and erosion of matrix tablets (Leskinen et al., 2011), the determination of porosity changes caused by different initial particle sizes (Hakulinen et al., 2008), defect detection (Akseli et al., 2008b; Leskinen et al., 2010) or determination of capping risks (Akseli et al., 2013; Xu et al., 2018b).

One difficulty in ultrasonic testing is the transmission of the sound wave into the specimen. Due to the non-favourable acoustic properties of air, it is often necessary to apply a viscous liquid between transducer and tablet to transfer the signal into the compacts. This could potentially damage the tablet surface which would counteract the advantage of ultrasonic testing being non-destructive. However, Leskinen et al. (2010) showed it was possible to transfer the signal under applied pressure without the need of a coupling agent. In addition, they found the speed of sound to be independent of the frequency used. This, combined with the findings of Liu et al. (2011) which addressed the obstacle of impedance mismatch between compaction equipment and powder material, made ultrasonic in-die monitoring an achievable approach.

Since then, Leskinen et al. (2013) found the ultrasonic velocity measured during the compaction process to be sensitive to the blending time of magnesium stearate. Longer blending times resulted in higher wave velocities through the samples which they explained with better coupling between particles through the increased amounts of magnesium stearate filling smaller pores. In addition, they measured the velocity through binary mixtures of MCC and paracetamol as well as pure MCC and found a decrease in SOS with increasing paracetamol content. What has to be kept in mind when interpreting those results is that they were compared as a function of time and not the porosity. The pure MCC samples did not only show the highest velocities but also the lowest porosities which could be an explanation for the difference in SOS. They also interpreted changes in velocity they observed during the dwell time being indicative of ultrasonic measurements being sensitive to changes in the mechanical properties of the tablets.

Stephens et al. (2013a) calculated the apparent in-die YM of a mixture of MCC and α-lactose monohydrate using the changes in ultrasonic velocity on a hydraulic press. The authors further claimed that the ultrasonic wave forms could be used as indicator of geometric irregularities such as micro-cracks which could lead to capping or lamination of the tablets. They also observed good agreement between wired and wireless wave form acquisition which could make the implementation of ultrasonic measurement systems on rotary tablet presses feasible (Stephens et al., 2013b). Recently Hagelstein et al. (2019) introduced the Kilian Inline Measurement (KIM) system as an add on to the Styl'One Evolution compaction simulator. The KIM system has been shown to be capable of performing ultrasonic measurements at production relevant speeds. In addition, they could calculate apparent YM and PR throughout the entire compression process. They found their elasticity parameters to be in the same order of magnitude as those determined by other authors (Cunningham et al., 2004; Mazel et al., 2012) using different approaches. They further assumed the changes in PR with increasing SF to be indicative of the compaction behaviour (Hagelstein et al., 2018). Their studies suggested that ultrasonic in-line measurements were not only feasible, but also had the potential to assess the deformation properties of pharmaceutical materials and justify further investigation.

2 Aims and Outline

The processes occurring during the powder compaction process are, to this day, not wholly understood. Therefore, the development of new tools capable of monitoring the tablet formation process is indicated to help in the better understanding and prediction of the compaction behaviour of pharmaceutical materials. Hagelstein et al. (2019) recently introduced an ultrasonic in-line measurement system capable of performing ultrasonic measurements throughout the tablet compression process. However, while they proposed several possible applications, they did not systematically assess the derived results.

The aims of this thesis are fourfold:

- Assessing the robustness of the method and its applicability to pharmaceutical powders, exemplarily demonstrated on excipients acting as fillers. Here, the signal detection and recognition, as well as the repeatability of the measurements when conducted on separate days are of interest.
- Combining experimental data and knowledge about ultrasound propagation in porous solids such as the link between the velocity of sound through the material, and elasticity and porosity, to answer the question which parameters are responsible for differences in the velocity profiles.
- Mathematically describing both compression and decompression velocity profiles of the exemplary fillers, to derive parameters which could then be used in the evaluation and characterisation of the materials concerning their compression behaviour as well as changes in pore structure.
- Investigating the influence of a second component added to the material in question on the velocity profiles, the derived parameters and consequently the compression behaviour of the powder blends.

The results of this work can then be the next step in the possible establishment of ultrasonic in-die measurements in the characterisation of the compaction behaviour as well as pore structure evolution during of pharmaceutical powders and blends thereof.

3 Results and Discussion

Parts of this section have already been published in the International Journal of Pharmaceutics (Kern et al., 2022). The content was linguistically adapted, and data sets were partly extended. Additionally, several figures were already published in the article and will be referenced throughout the section.

For the experiments, five different excipients were used: microcrystalline cellulose (MCC), mannitol (MN), α-lactose monohydrate (LM), anhydrous calcium phosphate (ACP) and maize starch (MS). Since in most cases several grades of the materials were used depending on the experimental requirements, the grade names are referenced in the respective chapters. The trademarked names and abbreviations are indicated in Chapter 5.1. The excipients chosen for this work are commonly used fillers. Since they generally amount to the highest portion of the final blend, fillers have the highest impact on the overall behaviour of the mixture which makes studying them essential to the understanding of the tabletting process. In addition, the materials chosen are fairly well described in literature which in turn makes the impact of different deformation behaviours on the velocity profiles easy to identify. The substances chosen in this work can be described as brittle (ACP and LM) (Zhang et al., 2003), ductile (MCC) (Zhang et al., 2003) and primarily elastic (MS). In addition, both MCC and MS show viscoelastic, i.e., time-dependent, behaviour (Desbois et al., 2020; Ruegger and Çelick, 2000). The deformation behaviour of mannitol has mostly been described as brittle (Tarlier et al., 2015), however, structured mannitol grades have been shown to be more plastically deforming (Ohrem et al., 2014; Roopwani and Buckner, 2011).

3.1 General Considerations

Before going into the specifics and interpreting the results generated with the KIM system, some general considerations need to be discussed. The following pages are dedicated to identifying factors that may have an influence on the ultrasonic velocity through the compact during compaction, from here on shortened to velocity.

3.1.1 Data Pre-Processing

Prior to getting into the experimental results, it is worth looking at the data acquisition and pre-processing. As further explained in Chapter 5.2.3.2, the KIM software identifies the maximum or minimum amplitude of the ultrasonic raw signal to determine the time of flight (TOF) of longitudinal and transverse sound waves, respectively, which is needed to calculate the velocity. However, at low signal amplitudes towards the start of the compression process, the signal maximum is not necessarily unambiguous, i.e., the peak might be flat or there may be a plateau

with several small peaks caused by the fluctuations of the amplitude. A low amplitude signal at two consecutive time points is exemplarily shown for Tablettose 100 in Figure 3-1. While there was a clearly visible maximum in both cases (peak between dashed lines), it was slightly tilted in opposite directions. First to the left, then to the right, caused by the comparatively high noise of 0.01 V compared to the signal amplitude of 0.04 V. This resulted in small differences of the measured TOF which in turn was visible in fluctuations of the calculated velocity, from 1.810 mm/µs to 1.795 mm/µs.

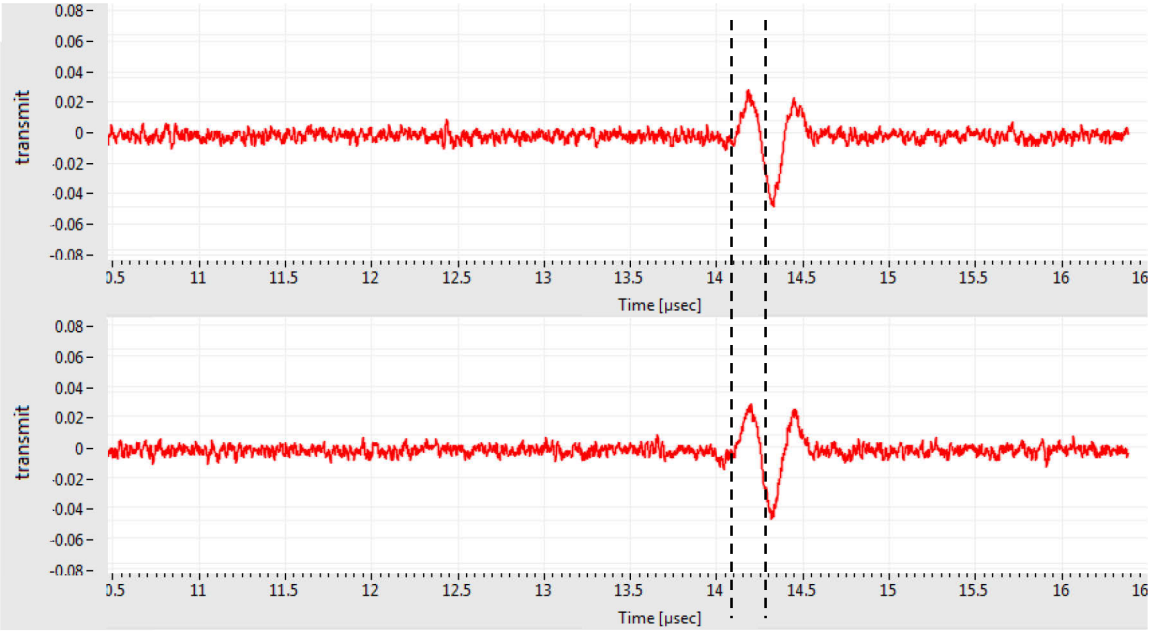

Figure 3-1: Transmitted longitudinal ultrasonic signal of two successive time points of the KIM measurement of Tablettose 100 as illustrated by the KIM++ software. Amplitude [V] over time since pulse generation [µs]. The maximum in question is depicted between the dashed lines.

To account for small fluctuations, the TabAnalyzer software applies a smoothing step by calculating the moving average over five subsequent velocity values. Figure 3-2 depicts the compaction of Vivapur 101 as proposed by Hagelstein et al. (2019) through the velocity of the ultrasonic wave as a function of SF. Both plots contain the velocity as calculated at a specific SF, as well as the smoothed values. The fluctuations were highest at low solid fractions where the amplitude of the signal was low as discussed before. However, the smoothing step did not influence the overall shape of the compaction signal and the smoothed results will from here on out be used in the discussion of the results.

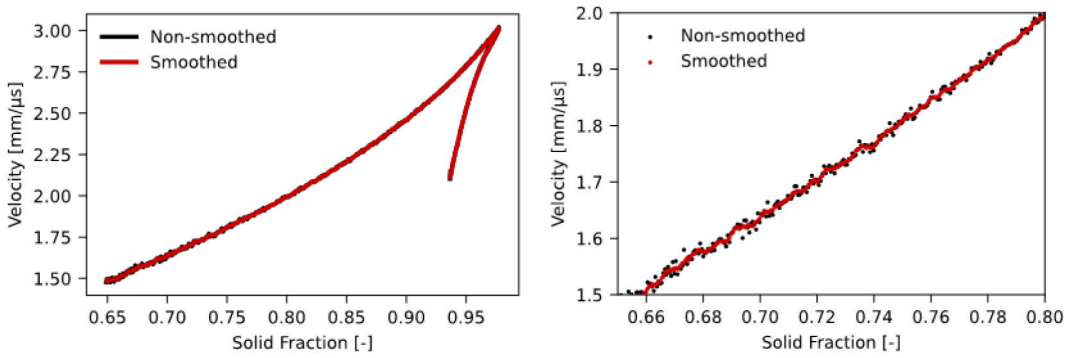

Figure 3-2: Ultrasonic velocity results of one longitudinal measurement, raw and smoothed. Left: entire compaction; Right: zoom into the start of compression.

Another possible difficulty with the peak detection at low amplitudes concerns the identification of the correct peak. In transverse mode, a minimum is used for the determination of the TOF. As shown in Figure 3-3 on the example of Tablettose 100, there was more than one minimum. The highest amplitude was first exhibited by the peak arriving later, then the amplitude of the first peak increased gradually with increasing solid fraction. As the KIM++ algorithm has been programmed to determine the arrival time of the peak with the highest amplitude (maximum for longitudinal and minimum for transverse sound waves, respectively), there was a jump to earlier arrivals once the amplitude of the first peak became higher than the second one around a SF of 0.7. The velocities calculated using the second peak did not represent the actual velocity of the sound wave and were thus filtered as described in Chapter 5.2.4.1.

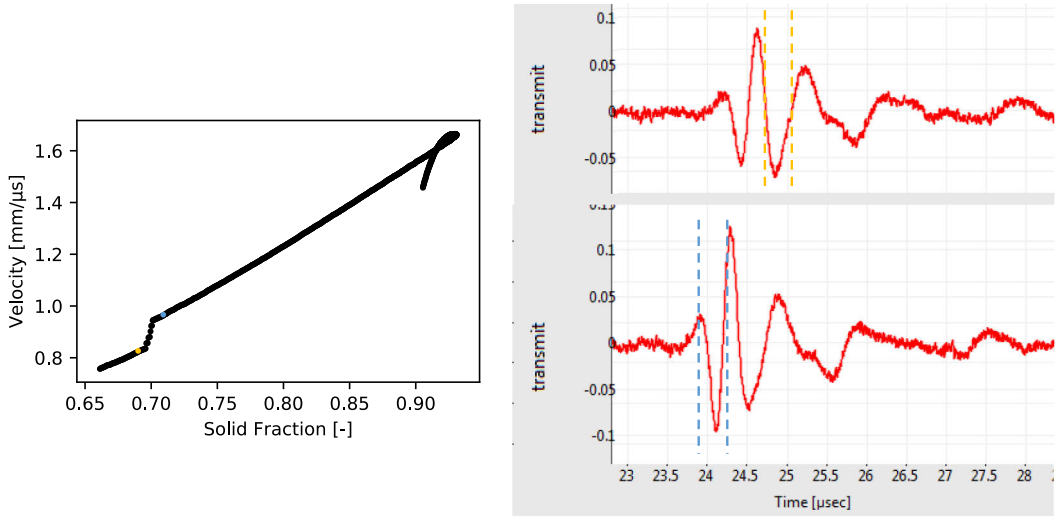

Figure 3-3: Transverse ultrasonic wave measurement of Tablettose 100 (left). On the right two raw signals of amplitude over time are depicted at a SF of 0.69 (top) and 0.71 (bottom). The peak used for the TOF determinations by the KIM++ software is shown between the dashed lines. Plots on the right share x-axis.

The maximum SF reached when a target pressure is applied differs between materials. Time and pressure, however, are pre-set and, therefore, independent of the sample under investigation. Hence, the SF adds another dimension to the plots. Since the SF changes during

compression as well as decompression it is possible to discern the different phases of the compaction process as shown in Figure 3-4. Here, compression and decompression were separated. The black data points at the beginning, most prominent for ACP and Tablettose 100, represent the data points where difficulties with the maximum detection occurred as described before. In addition, the single data point significantly lower than the rest is an artefact of the TabAnalyzer export. It is the mean value of four time points where a velocity was calculated, and the time point before the first signal was detected with the velocity set at zero. These values will not be shown in the subsequent figures. The results will be further discussed in Chapter 3.1.5.

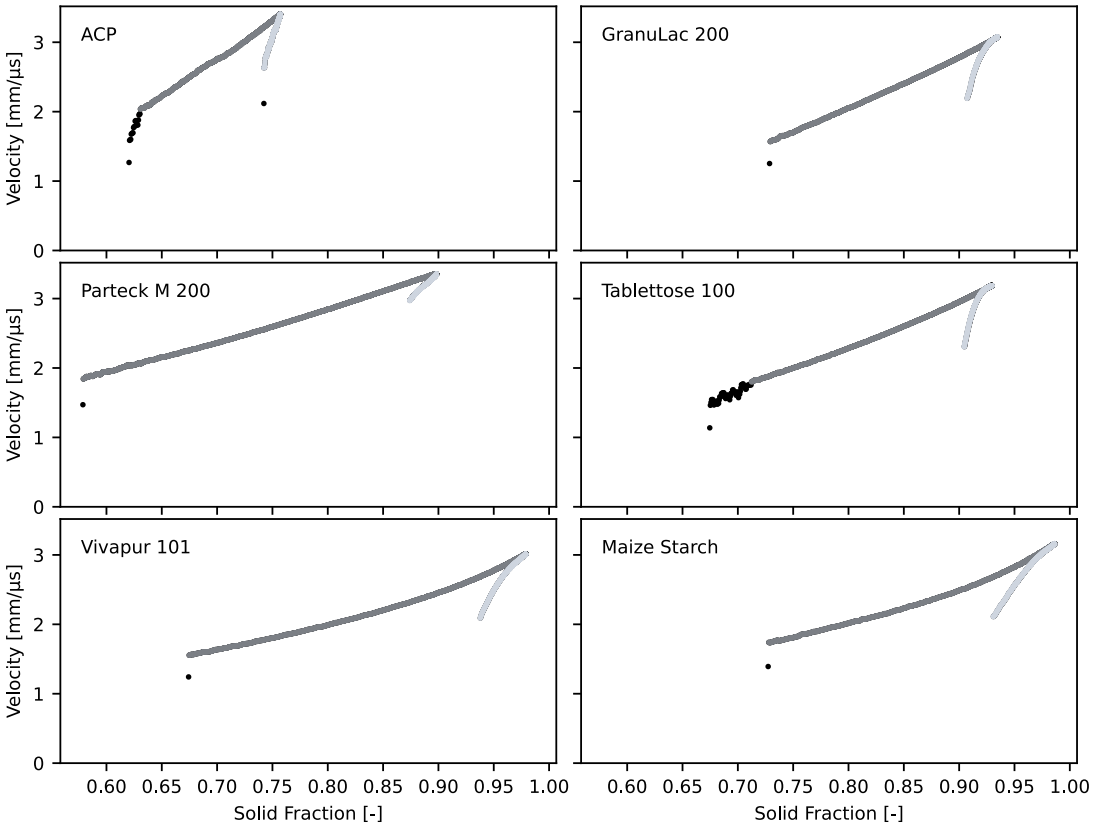

Figure 3-4: Compaction processes depicted as the longitudinal velocity as a function of SF. Black: Non--filtered data exported by the TabAnalyzer software; Dark grey: Compression phase; Light grey: Decompression phase. Plots in one row share y-axis; plots in one column share x-axis.

3.1.2 Amplitude

Depending on the acoustic properties of the powder materials, the signal needed to be amplified or dampened to reach amplitudes in the range where the peak was clearly discernible as described in Chapter 5.2.3.2. Low amplitudes, typically below 0.1 V, can be disturbed by the relatively high noise as previously shown in Figure 3-1. As the noise increases with increasing amplification of the receiver signal, the detectable amplitude minimum might vary. If the amplitude is too high, this may result in a small plateau of the raw signal which makes the TOF determination problematic. After the measurements the actual amplitude of the signal arriving at

the transducer in the lower punch could be calculated using the following relation to the detected amplitude:

$$\Delta I = 10 \log \frac{I_2}{I_1} = 10 \log \frac{{p_2}^2}{{p_1}^2} = 20 \log \frac{p_2}{p_1} = 20 \log \frac{AV_2}{AV_1} \quad (3\text{-}1)$$

ΔI: *Amplification / damping ratio [dB]*

I: *Intensity [W/m²]*

p: *Sound pressure [Pa]*

AV: *Amplitude [V]*

1: *Input values, e.g., measured amplitude*

2: *Output values, e.g., displayed amplitude after amplification or damping*

ΔI was manually set before the measurements. Since the intensity is proportional to the square of sound pressure and the pressure is proportional to the amplitude, the detected voltage can be used to compare different materials to each other concerning their ability to transmit sound waves.

Figure 3-5 shows the amplitude over the course of three consecutive maize starch measurements in transverse mode. Figure 3-5a) depicts the signal amplitude as recorded by the receiver unit. The first signal was transmitted from upper punch to lower punch 350 ms after the measurement had started at an amplitude of 0.15 V. From there it increased to 0.67 V at 440 ms and then decreased until the signal stopped after roughly 500 ms. As seen in Figure 3-5b) the actual voltage of the signal through the material was rather low which is why the signal had to be amplified (+15 dB) to make the TOF determination possible.

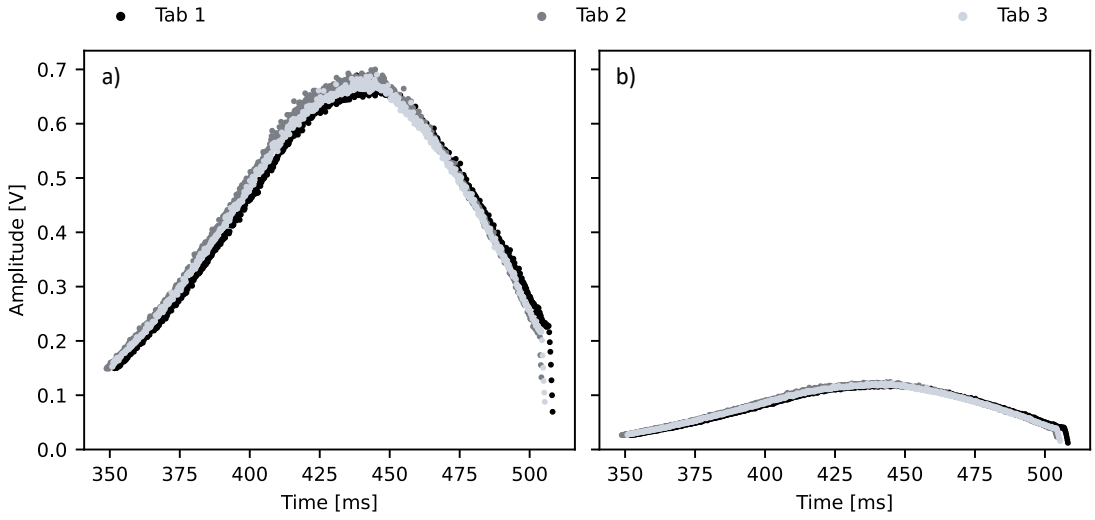

Figure 3-5: Amplitude as a function of time throughout three consecutive maize starch measurements in transverse mode, a) raw signal, b) data corrected for the applied amplification. Plots share y-axis.

When comparing the amplitude of starch to ACP, shown in Figure 3-6, several differences stand out. For one, while the maximum amplitude was not identical for the three starch measurements, the variability between the ACP tablets (Tab) was noticeably higher. The lowest detected maximum amplitude was slightly below 0.7 V as seen in Figure 3-6a), while the highest was over 0.8 V. In addition, the amplitude increase of the Tab 2 measurement started later and the decrease earlier compared to the other two measurements. Finally, while the signal through maize starch had to be amplified to be detectable, the ACP signal had to be dampened to be in the range required for the KIM software to determine the TOF (-9 dB for all measurements).

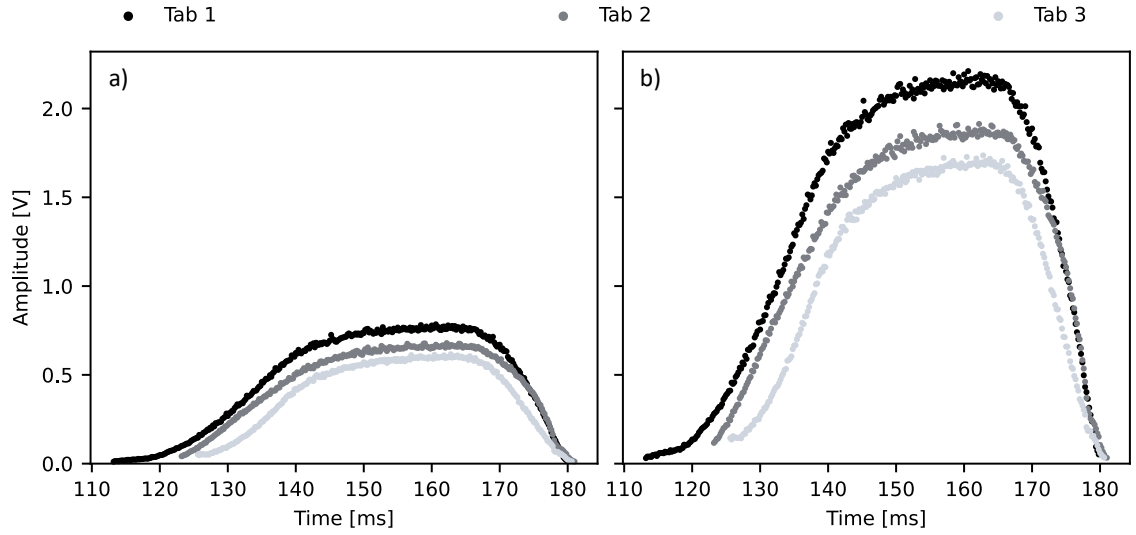

Figure 3-6: Amplitude as a function of time throughout three consecutive ACP measurements (Tab 1 - 3) in transverse mode, a) raw signal, b) corrected for the applied amplification. Plots share y-axis.

For all materials, the amplitude of the ultrasonic signal increased with increasing SF, as is evident in Figure 3-7, which matches the findings of Takatsubo and Yamamoto (1991) who found a decreasing amplitude of the transmitted sound signal with increasing porosity. This was to be expected as increased porosity leads to an increase in boundary surfaces which results in scattering and subsequent attenuation of the sound wave. The maximum amplitude reached by the various substances was more similar in longitudinal mode compared to transverse, where it ranged between 2.3 and 0.12 V. Which wave form (longitudinal or transverse) was transmitted more efficiently through a medium, could not be generalised. While the transverse amplitude was higher than longitudinal for ACP and LM, the opposite was found for MCC and MS. MN showed almost no difference between the maximum amplitudes of the two wave forms. This resulted in a change of the order of the maximum intensity: while in longitudinal mode the intensity was reversely correlated to the maximum in-die SF reached, MN and LM were swapped in transverse mode.

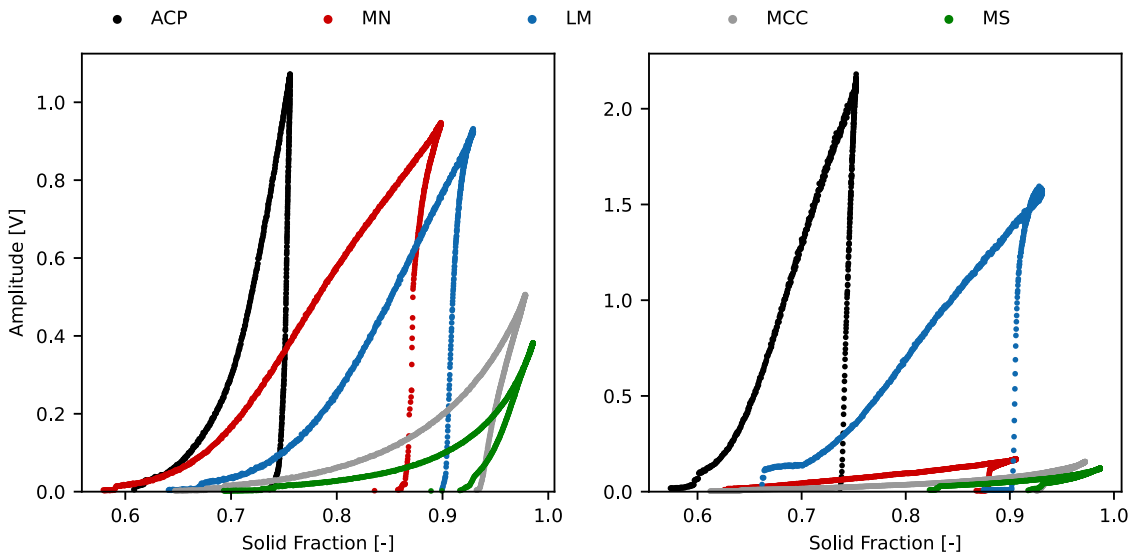

Figure 3-7: Amplitudes of the ultrasonic signal as a function of SF measured in longitudinal (left) and transverse (right) mode (n = 3). ACP = anhydrous calcium phosphate, MN = Parteck M 200, LM = Tablettose 100, MCC = Vivapur 101, MS = maize starch.

As shown Figure 3-7, the material under investigation had an influence on the measured signal amplitude of the ultrasonic waves. This was to be expected as the detected intensity of a sound wave is a result of the initial intensity of the signal and the acoustic properties of the permeated medium (Krautkrämer and Krautkrämer, 1990). However, using the maximum value or the changes in amplitude to compare the materials was difficult in this set-up since a) especially for ACP and several mannitol grades the intensity was not constant, even when measurements were done in succession, and b) the amount of couplant used to connect transducer and punch tips had an effect on the amplitude of the transverse signals which made comparing amplitude results obtained on different days virtually impossible.

3.1.3 Robustness

When introducing a new analytical tool, it is imperative to determine the robustness of the set-up to determine the error margin of the method and being able to identify actual differences between materials. Three exemplary materials were tested to ascertain the repeatability of the measurements. The results can be found in Figure 3-8.

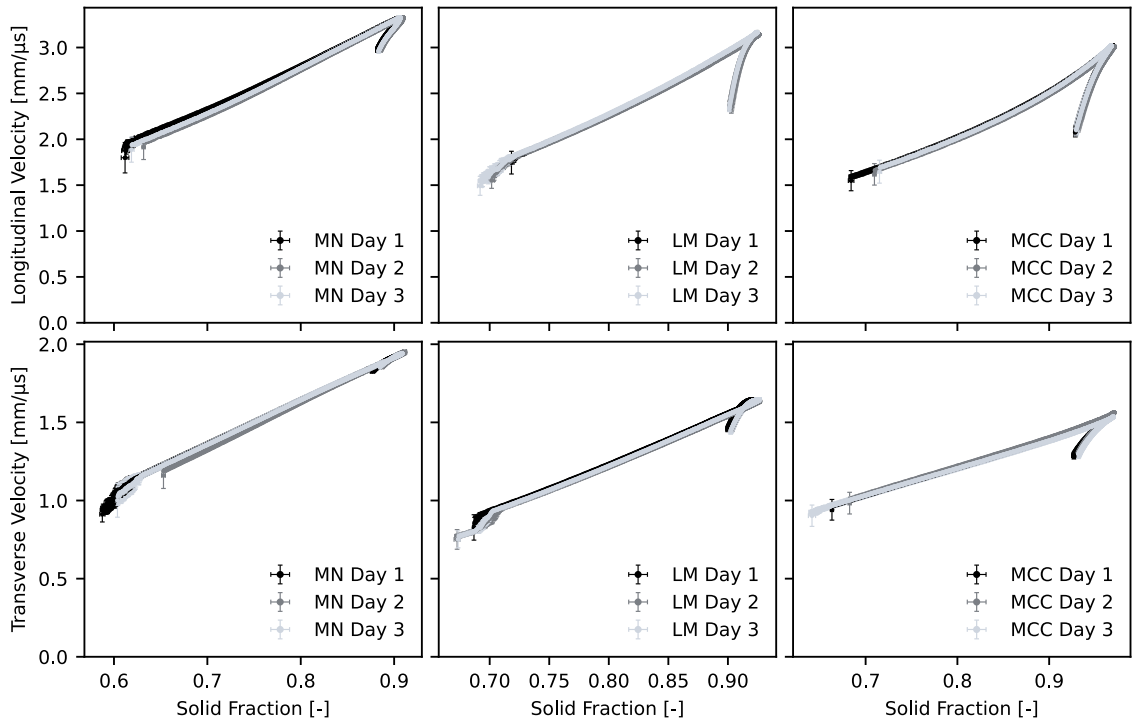

Figure 3-8: Results of repeated measurements on three different days including standard deviation (n = 8). From left to right: Parteck M 200 (MN), Tablettose 100 (LM), Vivapur 101 (MCC); Top row: Longitudinal wave velocities; Bottom row: Transverse wave velocities. Plots in one row share y-axis; plots in one column share x-axis. Published in Kern et al. (2022).

The standard deviation of the steady compression signal was below 1% in all cases for consecutive measurements. However, there was a relatively high variability at the beginning of the measurements. This was caused by the comparatively low signal amplitudes at low solid fractions as discussed before. At low amplitudes the KIM++ software did not always identify the maximum (resp. minimum for transverse measurements) of the ultrasonic signal correctly since the signal-to-noise ratio was too low. To illustrate the variability in the signal start, the eight consecutive unfiltered longitudinal measurements of Parteck M 200 performed on the first day of experiments are depicted in Figure 3-9. Not only did the signal start at different solid fractions, the earliest at 0.55 and the latest at 0.61, but the velocity fluctuations at the beginning of the compression process also differed between measurements conducted in succession. This further illustrates the necessity of a filtering step in order to not overinterpret results at low amplitudes where the precision of the signal detection is low.

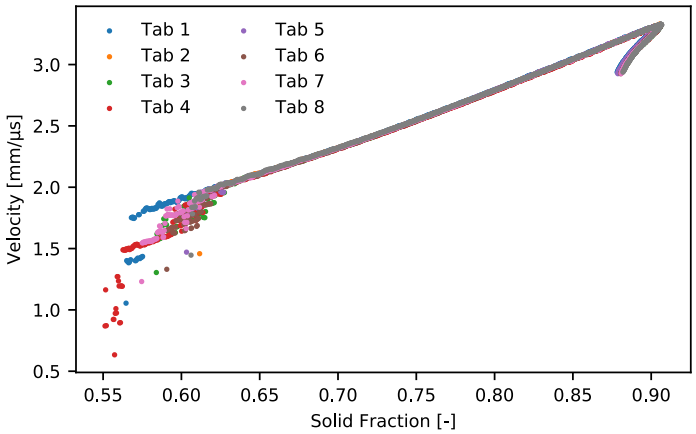

Figure 3-9: Eight consecutive measurements of the compaction process of Parteck M 200 performed in succession on the first day of experiments.

The highest variability between measurements performed on different days was observed for the MN velocity results as seen in Figure 3-10. The relative standard deviation was highest at low solid fractions, surpassing 1%, a threshold which was not surpassed by successive measurements. LM and MCC, however, did not show an increase in relative deviations compared to intraday measurements. Overall, the repeatability of the measurements was high, which shows that even with the disassembling and reassembling of the set-up the KIM system generates reliable results. At the same time, it has to be kept in mind that small variabilities in the overall velocity and the velocity profiles may occur when the measurements are not performed consecutively.

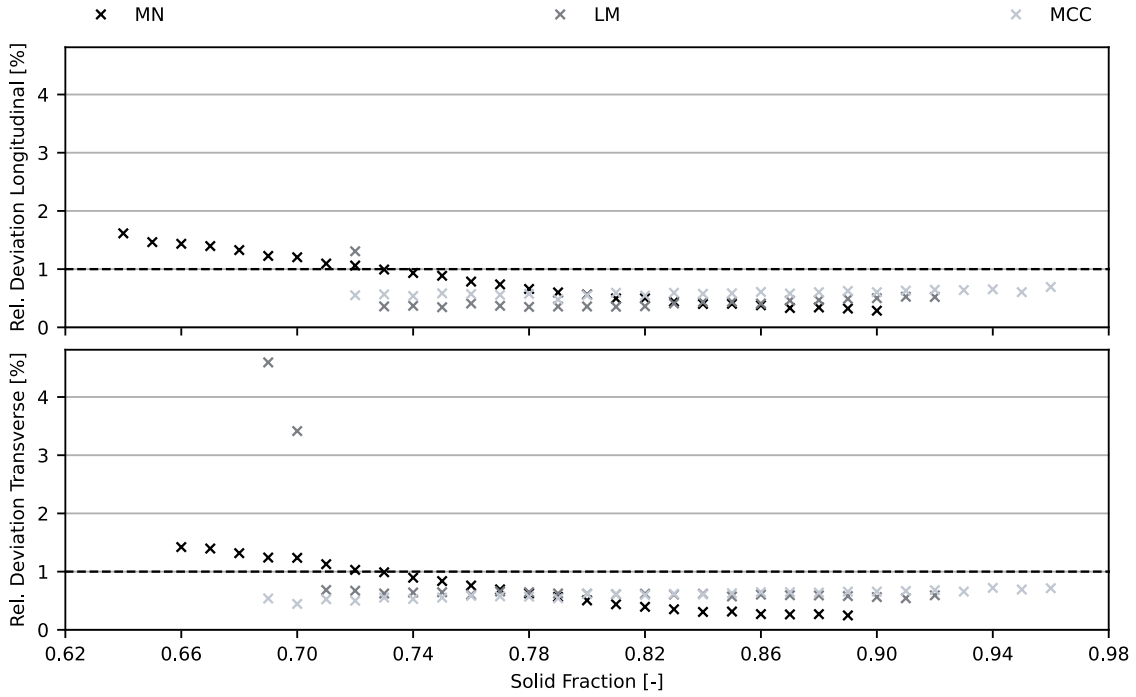

Figure 3-10: Relative standard deviations of longitudinal (top) and transverse (bottom) ultrasonic velocities between measurements conducted on three separate days (n = 24). MN = Parteck M 200, LM = Tablettose 100, MCC = Vivapur 101. Plots share x-axis.

3.1.4 Compaction Speed

Another essential point to be aware of is the influence of the compaction speed on the KIM results. For two materials the longitudinal and transverse velocities over the compaction process are depicted in Figure 3-11 (further examples can be found in Appendix Figure A-1). The fastest profile (100 ms compaction time) resulted in the highest fluctuations of the displacement measurements at high solid fractions, which in turn also resulted in fluctuations of the velocity values. This was most pronounced for the transverse MN measurements. However, in the tested range, the compaction speed did not systematically influence the velocity during compression or the shape of the decompression signal even for the viscoelastic MCC, where a time dependence of the deformation was expected (Desbois et al., 2020; Rippie and Danielson, 1981), especially during decompression as theorised by Hagelstein et al. (2019). Either the KIM system is not sensitive enough to detect those differences, or the punch movement profiles were too similar to result in changes in the compact (Ruegger and Çelick, 2000).

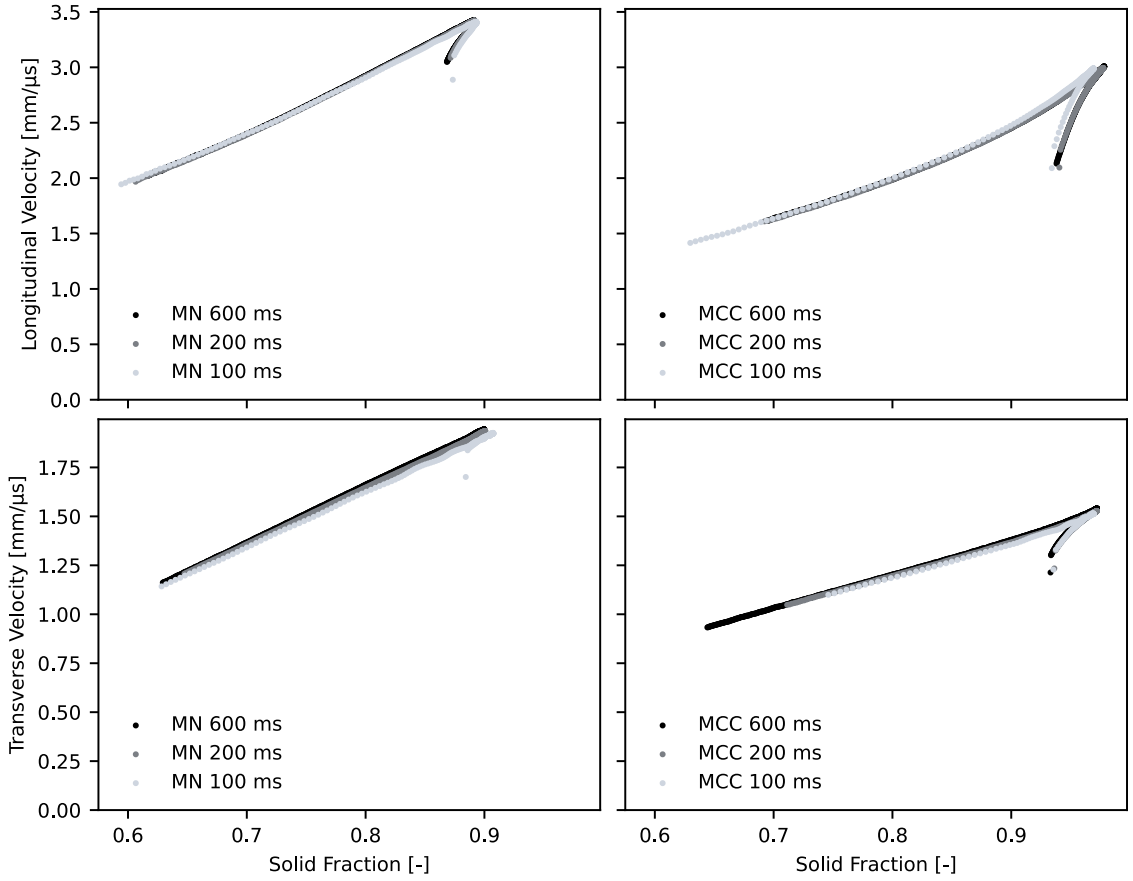

Figure 3-11: Longitudinal and transverse US velocity through Parteck M 200 (MN) and Vivapur 101 (MCC), recorded using three different compaction profiles. The compaction times were 600, 200 and 100 ms, respectively (n = 3). Plots in one row share y-axis; plots in one column share x-axis.

Since the sample rate of the KIM system is capped at 5 kHz, a higher punch speed resulted in fewer data points. Therefore, the slowest compaction profile was set as the standard setting for all other experiments to improve the quality of the data for further processing and calculations.

3.1.5 Standard KIM Measurements

In Figure 3-12 the results of the KIM measurements of different substances are shown. All materials show an overall similar behaviour: the velocity increases with increasing SF until a maximum is reached and subsequently, during the decompression phase, both decrease until the contact is lost between compact and punches. At the same time there are several differences visible between the materials, mainly regarding maximum velocity and SF, rate of velocity increase, and shape of the decompression signal. Further characterisation of the different parts of the compression process could, therefore, offer new insights into the differences in the compact formation process of different materials which had also been briefly suggested by Hagelstein et al. (2019). The repeatability was high for all materials (relative sd < 1%) except for ACP where the standard deviations were consistently above the 1% threshold and increased up to 2.5% as seen in Appendix Figure A-2.

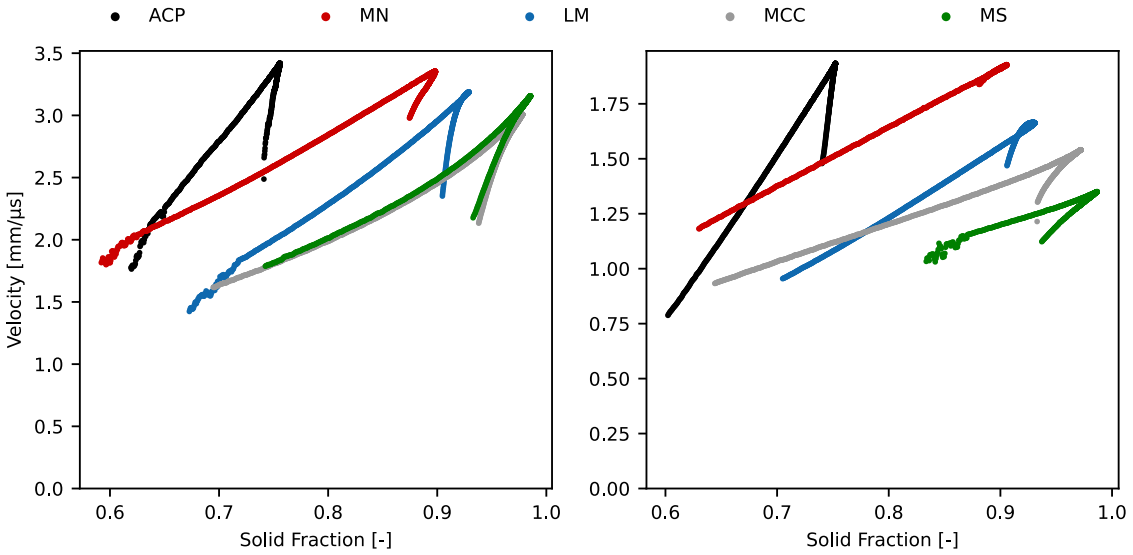

Figure 3-12: Longitudinal (left) and transverse (right) measurements of one grade each of the five different excipients (n = 3).

At the same SF the longitudinal velocity was always higher compared to the transverse velocity, which was to be expected as longitudinal sound waves through a solid material are always faster than transverse sound waves (Schmerr, 2016). However, the trends were the same for both modes. The velocity increase of ACP for example was the steepest and at the same time the maximum velocity was the highest, while the maximum SF reached was the lowest in both modes compared to the other materials. The only major difference was exhibited by MS: while its

longitudinal velocity and length of the signal were almost identical to MCC, the velocity was lower, and the signal started later during the transverse measurements. In general, the compression signal was more linear in transverse mode. The drop of the signals during decompression was more pronounced for the longitudinal velocity which could be explained by longitudinal measurements being more sensitive to small changes in porosity (Asmani et al., 2001; Xu et al., 2020).

While the transverse sound waves can only propagate through the solid medium as explained in Chapter 1.4.1, the longitudinal sound waves could theoretically move in a straight line through the compact. However, the velocity profiles generally showed a similar length of the compression signal for the two wave forms as well as an abrupt stop of the decompression signal at the same SF and exhibited higher velocities at all solid fractions in longitudinal mode compared to transverse. This all points towards the sound waves only passing through the solid phase of the compact, even in longitudinal mode, as already proposed by Takatsubo and Yamamoto (1991; 1996).

3.1.6 Comparing Different Grades of the Same Excipient

Since the SOS through a medium is generally considered specific for a certain material (see Chapter 1.4.1), it is of interest to determine whether the same relates to the velocity increase with increasing relative density. In Figure 3-13 the KIM results of four different mannitol grades are shown. As is evident, the velocity profiles were not identical for all grades. However, they could be grouped according to their velocity increases during compression: the velocity through Parteck M 200 and Pearlitol 200SD increased in parallel, as it did through Parteck Delta M and D(-)-Mannit. These groups did not separate the mannitol grades depending on their crystal modifications since Parteck M 200 and D(-)-Mannit are both comprised of the β-modification. Instead, they coincide with the intended purpose of the grades: direct compression (Parteck M 200 and Pearlitol 200SD) and granulation (Parteck Delta M and D(-)-Mannit), respectively. It needs to be mentioned that Parteck M 200 and Pearlitol 200SD which show similar curve progressions are both pre-processed through spray drying. It is, therefore, possible that there is a change in deformation behaviour of mannitol when processed, something that has already been proposed for lactose (Lamešić et al., 2018), which becomes visible through the US profiles.

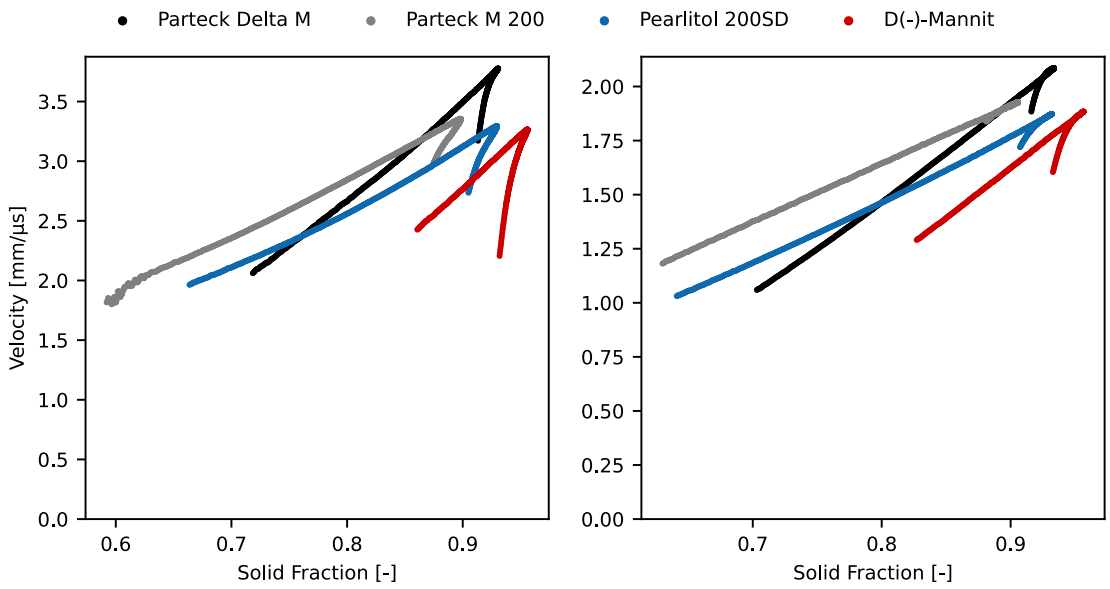

Figure 3-13: Longitudinal (left) and transverse (right) measurements of four different mannitol grades (n = 3).

3.1.7 The Influence of Particle Size

Since the velocity curves shown in Figure 3-13 also separate the mannitol grades with the large particles from those with smaller particles, the influence of particle size distribution (PSD) on the velocity profiles was investigated. The results are shown in Figure 3-14. The signals seem to start at lower solid fractions with decreasing particle size in the case of MN. In Chapter 3.1.3, it has been shown, however, that the signal start varied even when the same material was measured in repetition, i.e., the first signal was detected within a certain SF range, not at a specific SF value. Therefore, the start of the compression signal should not be used to differentiate between materials.

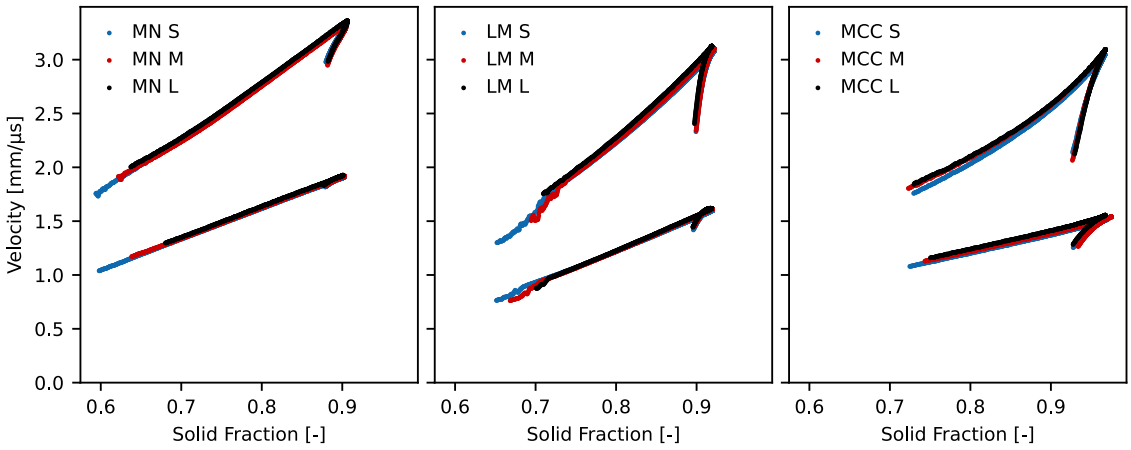

Figure 3-14: KIM measurements of three particle size classes (S: Small; M: Medium; L: Large) of three exemplary excipients with a wide PSD (n = 3): Parteck M 200 (MN), Tablettose 100 (LM), and Vivapur 102 (MCC). All plots contain longitudinal and transverse measurements, with longitudinal waves always exhibiting higher velocities. Plots share y-axis. Published in Kern et al. (2022).

For MCC larger particles resulted in slightly higher velocities at the same SF during compression as seen in Figure 3-15. A similar trend has been observed by Hakulinen et al. (2008) who found a decrease in velocity at the same SF through starch acetate tablets with decreasing particle size. They explained their finding with the pore size: bigger particles form tablets with bigger, but fewer pores in the matrix which leads to fewer encounters of the sound wave with pores, and consequently a more direct path.

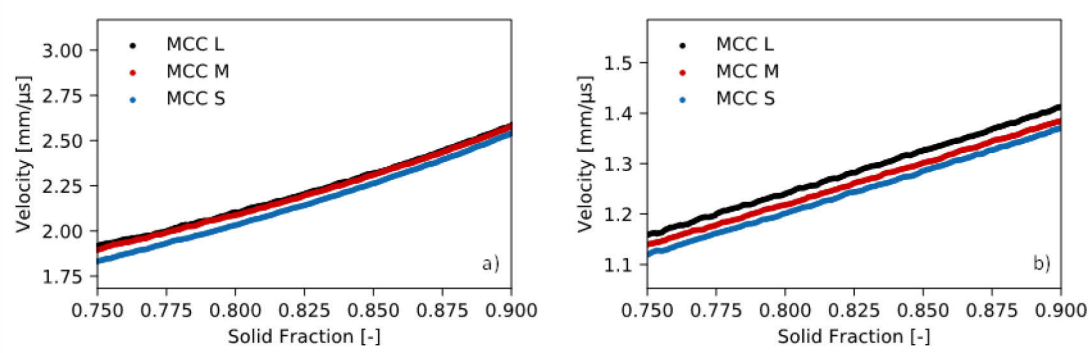

Figure 3-15: Velocities through different sieve classes of Vivapur 102 (MCC): a) longitudinal, b) transverse (n = 3). Published in Kern et al. (2022).

The relative standard deviations of the velocity through the sieve classes at the same SF are depicted in Figure 3-16. As expected from Figure 3-14, in the case of MCC the deviation was higher than the previously observed 1% threshold. For the longitudinal measurements of LM, the relative deviations were around 1%, only slightly above consecutive measurements of the same size class.

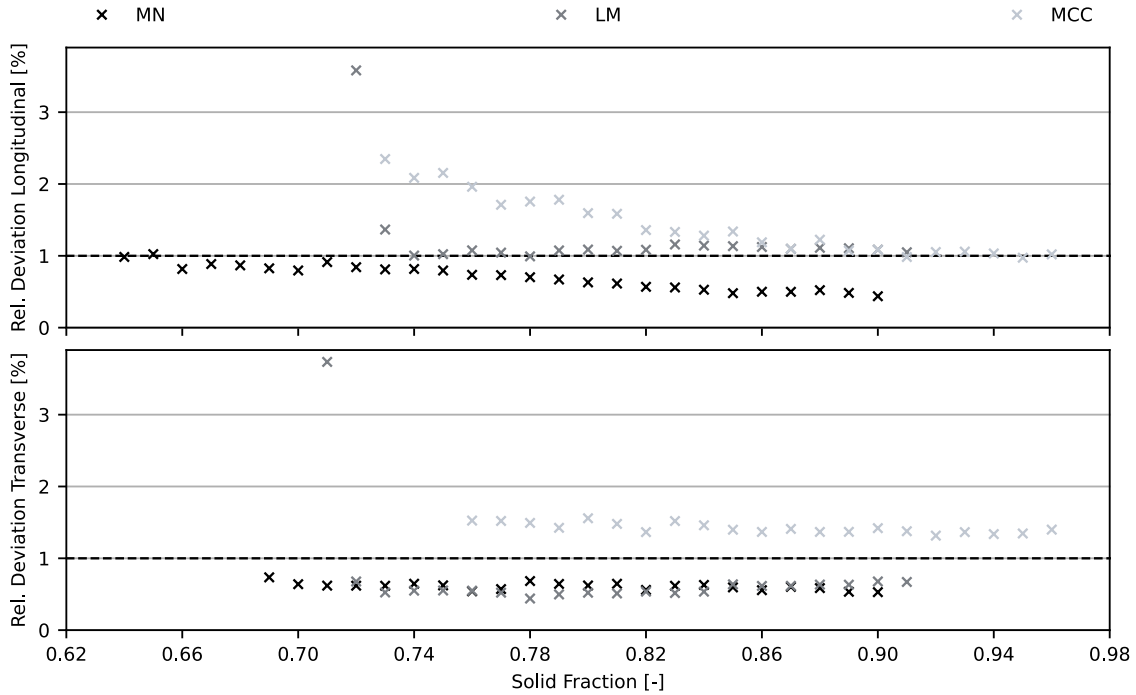

Figure 3-16: Relative standard deviations of the velocities measured through different sieve classes of the materials (n = 9). MN = Parteck M 200, LM = Tablettose 100, MCC = Vivapur 101. Plots share x-axis. Published in Kern et al. (2022).

MN also showed an increase in deviations in longitudinal measurement mode. This can be seen in more detail in Figure 3-17. While the measurements of the same size class were almost identical (Figure 3-17b, each measurement constitutes one produced tablet, hence Tab), there was a visible discrepancy between the classes (Figure 3-17a). However, in contrast to the MCC results, the velocity did not decrease with smaller particle sizes. The discrepancies could, therefore, not be explained by the PSD. This was interesting to note as a higher number of smaller pores should increase the distance the sound wave needs to cover in order to arrive at the lower punch more than a smaller number of bigger pores. This suggests that either, the pore size distribution is not pronouncedly different during compression at the same SF, independent of the size class, or the variance is too low and within the resolution of the method. An insufficient separation of the size classes is also a possibility. However, as seen in Appendix Figure A-3, while there is an overlap between the medium size class and the two others, the small and large classes are neatly separated.

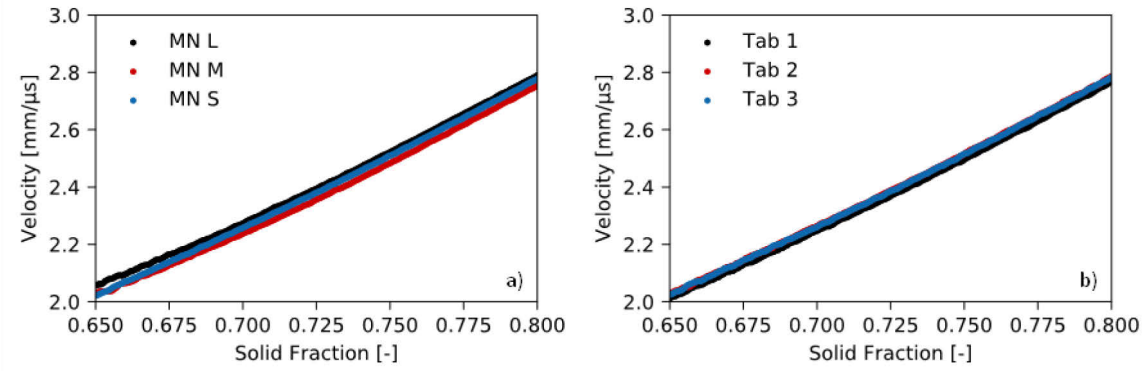

Figure 3-17: Longitudinal velocity through Parteck M 200 (MN): a) Different sieve classes (each plot is the mean of three measurements); b) Three consecutive measurements through samples of the smallest sieve class (Tab = tablet). Published in Kern et al. (2022).

While there was a slight decrease in velocity detected for the ductile MCC, the overall shape of the in-die velocity profiles were the same for all materials, no matter the initial particle size or measurement mode. This implies, that while the particle size may have had a minor influence on the velocity measurements, it was not the root cause for the differences shown by the different mannitol grades in Figure 3-13. The differences seen there, therefore most probably result from the deformation behaviour of the materials as it has been proposed that pre-processing of mannitol might increase its plasticity (Ohrem et al., 2014). Although the fragmentation rate has been shown to increase with higher particle sizes (De Boer et al., 1986; Skelbæk-Pedersen et al., 2020), the innate differences in the material properties do not change (Lamešić et al., 2018; Nordström et al., 2012; Salbu et al., 2010; Yohannes et al., 2016). The velocity profiles could therefore be an indication of the predominant deformation mechanism of a material.

3.1.8 Moisture Content

As explained in Chapter 1.4.1 sound propagation is dependent on the material properties and might change with the inclusion of a second substance such as for example water. Since some of the excipients chosen in this study are hygroscopic, especially MCC and MS (Rowe et al., 2009), it should be tested whether water content has an influence on the velocity measurements. Samples of the same materials stored under different relative humidity conditions were therefore measured using the KIM system. The loss on drying (LoD) of the materials after storage is shown in Table 3-1. The ambient storage condition refers to the non-treated materials as supplied by the respective manufacturers stored at non-monitored ambient conditions. The grades used for this experiment were chosen since they have comparatively low water contents resulting in even more pronounced changes by storing under high humidity.

Table 3-1: LoD of the samples in % after storage at different relative humidities. Arithmetic mean ± sd (n = 3).

Storage Condition	Vivapur 112	Starch 1500
30°C / Vacuum	0.51 (± 0.12)	0.76 (± 0.12)
Ambient	2.38 (± 0.18)	8.80 (± 0.11)
60% relative humidity	6.24 (± 0.16)	11.17 (± 0.15)
75% relative humidity	8.12 (± 0.10)	14.08 (± 0.19)

The results of the KIM measurements for MCC and MS are displayed in Figure 3-18. Several trends could be observed between the different samples. The velocity at a certain SF during compression decreased with increasing water content. This agrees with Wang et al. (2002) who found a decrease in longitudinal velocity with increasing moisture in lumber. The shape of the signal changed as well. The curvature of the longitudinal compression velocity increased with increasing moisture, while the increase of the transverse velocity became less steep. At the same time the decompression signal shortened. The dried samples showed a very pronounced velocity drop as well as a vast difference between velocity at compression and decompression at the same SF. The drop decreased with increasing water content. In addition, the intensity of the sound wave reaching the lower punch decreased in transverse mode. For both materials the amplification had to be increased from a gain, i.e., amplification, of 5 dB (dried sample) to 15 and 17 dB (highest water content) for MCC and MS, respectively. This resulted in a shortening of the compression signal due to the difficulties with the peak detection as described in Chapter 3.1. For the starch sample with the highest water content, a minimum detection was not possible.

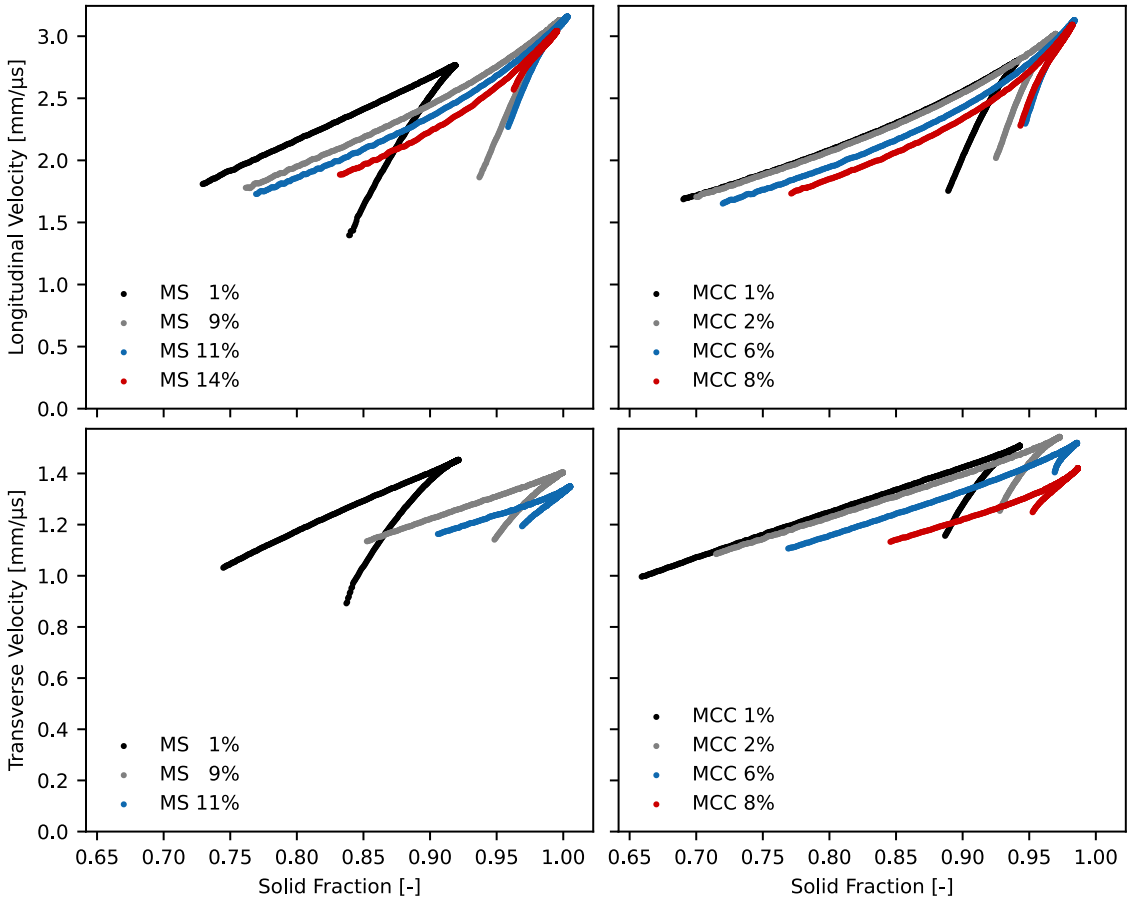

Figure 3-18: Longitudinal and transverse velocities of the Vivapur 112 (MCC) and Starch 1500 (MS) samples containing varying amounts of water. Plots in one row share y-axis; plots in one column share x-axis.

The raw signal of the transverse MS measurements with an LoD of about 14% are exemplarily shown in Figure 3-19. While a peak was detected in the upper picture, the KIM software did not find a minimum in the second measurement even though both signals look identical. However, the second signal exhibited a slightly lower amplitude, which could explain why it was not recognized as a peak. Additionally, the typical signal was not visible. This indicates that high water contents make transverse velocity measurements difficult or even impossible as seen here for the 14% sample. This sensitivity to water content also explains the observed difference in the length of the compression signal of maize starch in Chapter 3.1.5. The LoD was over 10% which is within the range observed here, where the transverse signal was not detected at lower solid fractions.

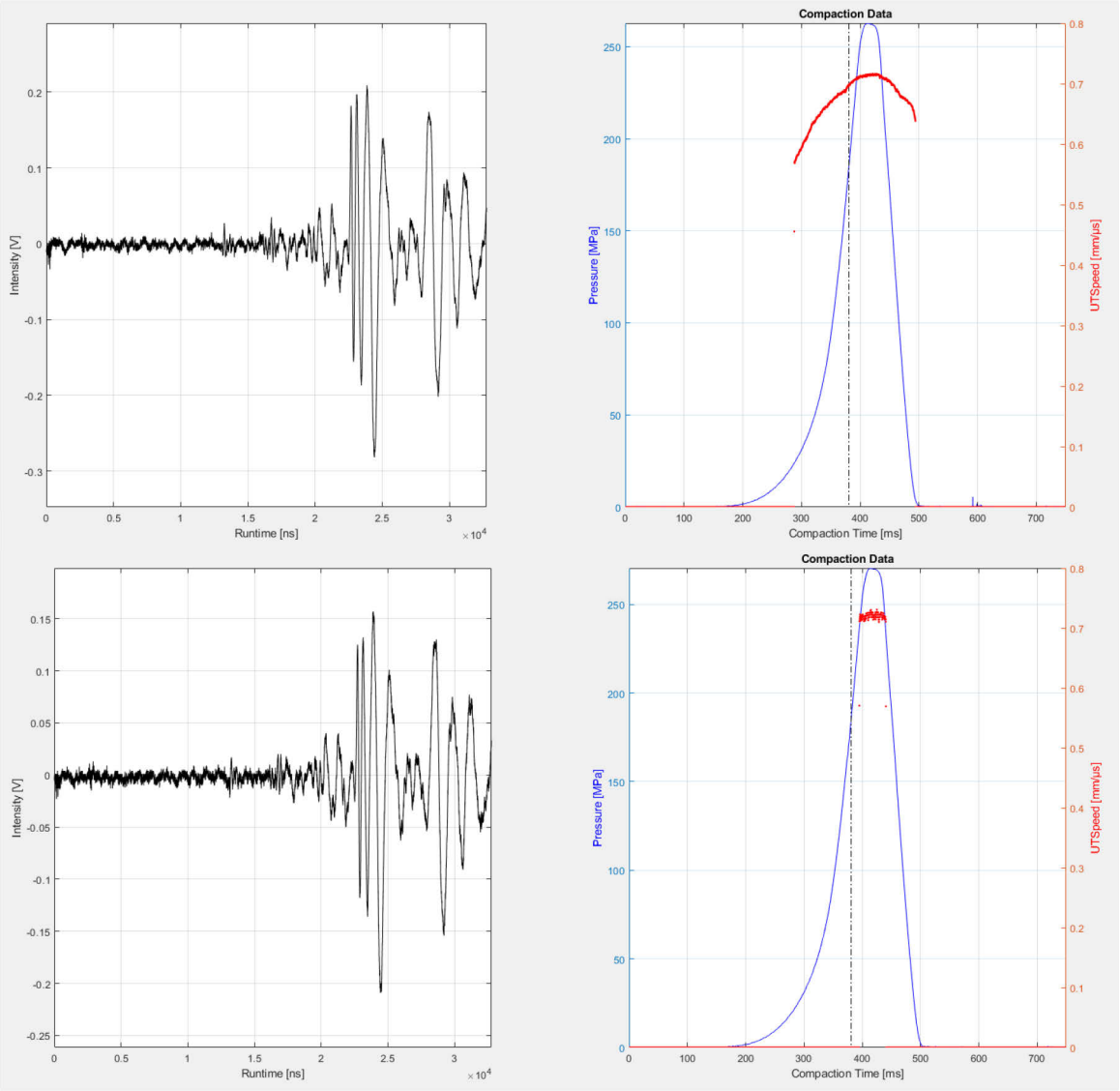

Figure 3-19: Two transverse measurements of Starch 1500 containing 14% of water as depicted by the TabAnalyzer software. On the left, the raw ultrasonic signal generated at the 390 ms timepoint is shown. On the right, the pressure (blue) and calculated velocity (red) over time are depicted.

Overall, the water content was shown to have an influence on the detected signals which must be kept in mind when comparing the results of hygroscopic materials, and considering batch-to-batch variability.

The response to water content could be caused by one or more of the following reasons: a) The SOS in water is lower than in either MCC or MS which results in a decrease of velocity with increasing water content when both materials have to be traversed, b) Integration of a foreign substance decreases the velocity through the medium, probably caused by the sound wave circumventing the included material (Krautkrämer and Krautkrämer, 1990), or c) Water changes the mechanical properties and subsequently the deformation behaviour of the materials (Amidon and Houghton, 1995) which could then be observed through the velocity measurements. As a

pronounced impedance mismatch and the associated dampening of the sound intensity is expected between water and the respective materials, the arrival probability of the signal at the transducer in the lower punch would be very low for a sound wave traversing the water. In addition, transverse waves do not propagate in liquids at all. This leaves possibility a) unlikely. Water can be present either in pores and capillaries as a separate phase or be absorbed into the structure of the material (Bauer-Brandl and Ritschel, 2012). If it was solely occupying pore space, the velocity progression should be similar if not identical to the dried samples as the pores are circumvented as well. The most likely possibility is therefore c). This hypothesis is further strengthened by the increased compressibility of the materials shown by the pressure/SF plots in Figure 3-20 when the moisture content is increased. The increased curvature of the compression signal could, therefore, be an indication of the changing compaction properties caused by the inclusion of moisture into the materials.

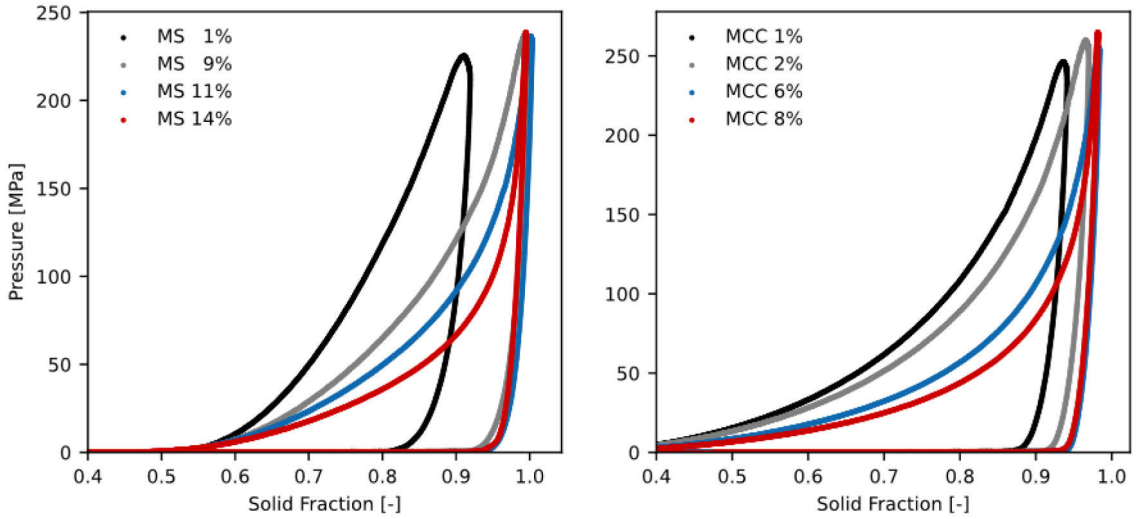

Figure 3-20: Pressure/SF plots of the two materials with varying moisture content (n=3). MS = Starch 1500, MCC = Vivapur 112.

3.1.9 Summary

The intensity of the ultrasonic signal is related to the acoustic properties of the materials and might need to be amplified or dampened to be in the target range usable by the KIM software. Nonetheless, low signal intensities at the beginning of the measurement did lead to difficulties with the TOF detection, which in turn influenced the velocity calculations. Once the steady part of the signal started, the results of the ultrasonic in-die measurements were highly repeatable. Consecutive measurements of the same material showed relative standard deviations below 1%. Dismantling and reassembling did increase the variability slightly, but still remained below 2%. This needs to be kept in mind when comparing results obtained on different days in order not to overinterpret small variabilities.

While it was possible to perform the measurements at elevated punch speeds, the accuracy of the obtained results decreased. In addition, more data points were generated at a lower punch speed which makes subsequent quantification of the results more precise. The compression profiles of different materials showed vastly different progressions in both measurement modes. Since the velocity increase varied for different grades of the same material, as demonstrated for mannitol even if comprised of the same polymorph, the chemical composition was not the only cause for the different velocity profiles. Neither was it the PSD, even though the particle size seems to have a minor impact on the velocity through the ductile MCC. The more brittle materials LM and MN showed no obvious correlation between particle size and measured velocity.

One factor influencing the KIM-measurements is the moisture content of the samples. The velocity through the same material decreased with increasing moisture content. Simultaneously, the curvature of the longitudinal velocity profiles increased, and the rate of velocity increase of the transverse profiles decreased. This needs to be kept in mind when working with hygroscopic materials, since the water content is prone to changing with storage as well as between batches. As moisture content can be related to the compaction behaviour of materials, the observed changes could indicate the sensitivity of the ultrasonic in-die measurements to changes in the compaction behaviour of the materials.

3.2 Signals During Compression

The tableting process can be separated into different phases. In this work loading (= compression) and unloading (= decompression) will be further explored, as during those two phases of the compaction process ultrasonic transmission measurements can be performed in transmission mode.

3.2.1 Fitting the Compression Signals

The hypothesis of the deformation behaviour of a material being the reason for the different progressions of the velocity during compression mentioned in Chapter 3.1.6 was established based on the findings of Takatsubo and Yamamoto (1991; 1996) who showed that not only pore volume but also pore shapes influence the velocity of a sound wave through a porous solid. The measured ultrasonic velocity through a porous medium is in conclusion influenced by the SOS through the solid medium, the relative pore volume and the pore structure (i.e., size and shape). The velocity changes through the compact with changing porosity during compression and decompression are thus indicative of the changes in the microstructure within the sample. Since the pore structure evolution with applied pressure depends on the deformation behaviour of a material (Cooper and Eaton, 1962), it is feasible to assume that differences thereof could be seen by characterising the velocity changes during compression. Brittle materials consolidate through fragmentation of particles. Those fragments can then occupy smaller pores, which were previously inaccessible (Kalman, 2020). Ductile materials deform plastically on the contact areas between particles which are on the pore edges (Cooper and Eaton, 1962). It could, therefore, be of interest to be able to investigate different materials depending on their velocity profiles and being able to compare and classify them.

While the relationship between transverse velocity and SF was almost linear for all materials, the longitudinal velocity showed a pronounced deviation from a linear trend for several substances, as exemplarily shown on the example of Vivapur 101 in Figure 3-21. While a coefficient of determination (R^2) of 0.980 in some cases might be acceptable for assuming a linear correlation, this does not apply if the calculated results using said equation systematically over- and underestimate the actual data as seen here through the residuals. Using linear regression of the complete compression process to compare the changes of the longitudinal velocity was, therefore, not feasible as the slope overestimated the increase at low solid fractions and underestimated it at high solid fractions. It did, therefore, not yield any usable information for the comparison of different materials. As shown through the residuals, there was also a systematic error present in the linear regression of the transverse velocity increase during compression,

however, in contrast to the longitudinal regression the determined slope does give a more realistic impression of the velocity increase.

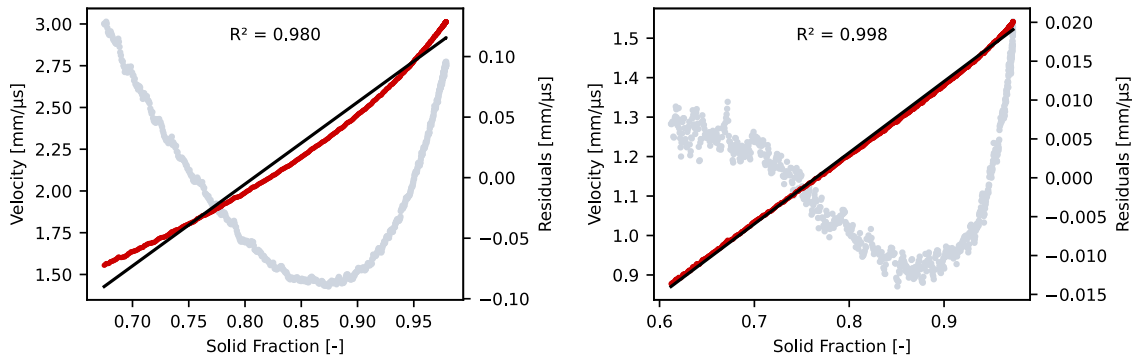

Figure 3-21: Linear regression of the compression process of one exemplary longitudinal (left) and transverse (right) Vivapur 101 measurement each. Red: Experimental data; Dashed line: Fit; Grey: Residuals.

While a linear relationship between input and response parameter is always preferable, several authors have resorted to the usage of exponential equations to describe the relationship between tablet parameters and porosity. Their main focus points were tensile strength (Duckworth, 1953) and Young's Modulus (Phani and Niyogi, 1987; Spriggs, 1961). Their aim in fitting experimental data to these equations was twofold: firstly, characterising and comparing materials using the fit parameters, and secondly: to extrapolate to zero porosity and thus obtaining the material characteristics theoretically which are often impossible to measure experimentally in porous solids. Those parameters were then used to compare the material properties independent of the porosity (Busignies et al., 2004; Van Der Voort Maarschalk et al., 1997).

Therefore, three exponential equations ((3-2) - (3-4)) with different variables (*y0*, *a*, *b* and *c*) were tested. The fit was performed in Python using the scipy.optimize package. The only set condition was 'positive values for *a, b* and *c*'. The maximum number of iterations was set to 10,000.

$$v = b * e^{c*SF} \tag{3-2}$$

$$v = y0 + b * e^{c*SF} \tag{3-3}$$

$$v = y0 + ax + b * e^{c*SF} \tag{3-4}$$

When looking at the fit using Equation (3-2) in Figure 3-22 in the top row, exemplarily shown for GranuLac 200 (left) and Vivapur 101 (right), the residuals show that the fit did not match the velocity profiles measured for either of the substances. Different parts of the compression signal

were either over- or underestimated. However, the equation fit the GranuLac 200 data better. Adding a third variable (second row) improved the fit but was still systematically off for the velocity profiles of both materials. It is interesting to note that the progression of the residuals changed. While certain parts of the compression data were still systematically over- or underestimated, the values of the residuals were decreased from 0.02 and 0.04 to 0.01 and 0.02 mm/µs, respectively. In addition, they changed from a maximum or minimum (for GranuLac 200 and Vivapur 101, respectively) in the middle part of the compression to a sine shape. The third equation is a combination of a linear and an exponential term and resulted in the best fit as seen in the bottom row, which made Equation (3-4) the equation of choice.

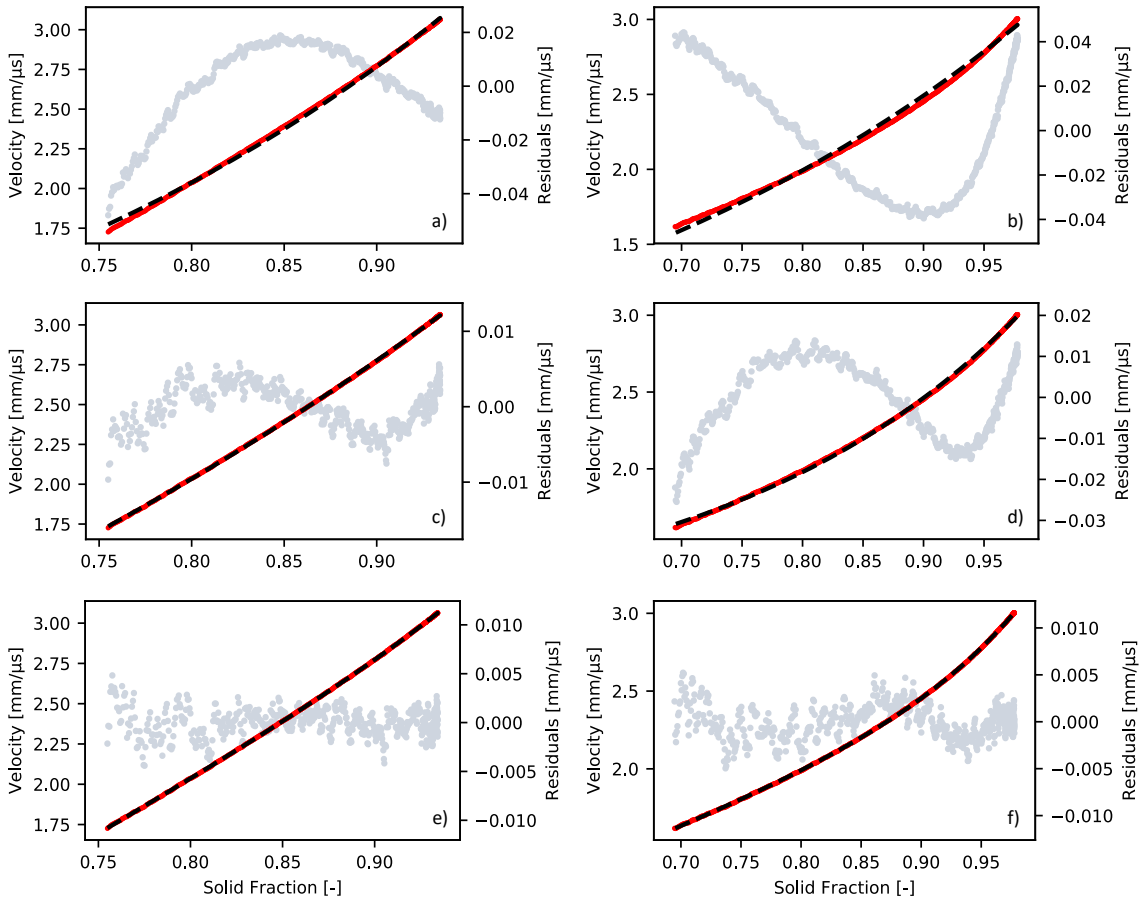

Figure 3-22: Equations (3-2), (3-3) and (3-4) (from top to bottom) fitted to the experimental data of one exemplary measurement of GranuLac 200 (a, c, e) and Vivapur 101 (b, d, f). Red: experimental data; Black: fit; Grey: residuals.

In Figure 3-23 the fit to Equation (3-4) of the other samples previously shown are depicted. As can be seen, the goodness of fit varied between materials. In the case of ACP (a) there seemed to be a systematic error below a SF of 0.7, while the fit at higher solid fractions was good. The worst fit was reached for the Parteck M 200 (b) velocity increase. For the Tablettose 100 (c) and maize starch (d) profiles the residuals were randomly distributed around zero.

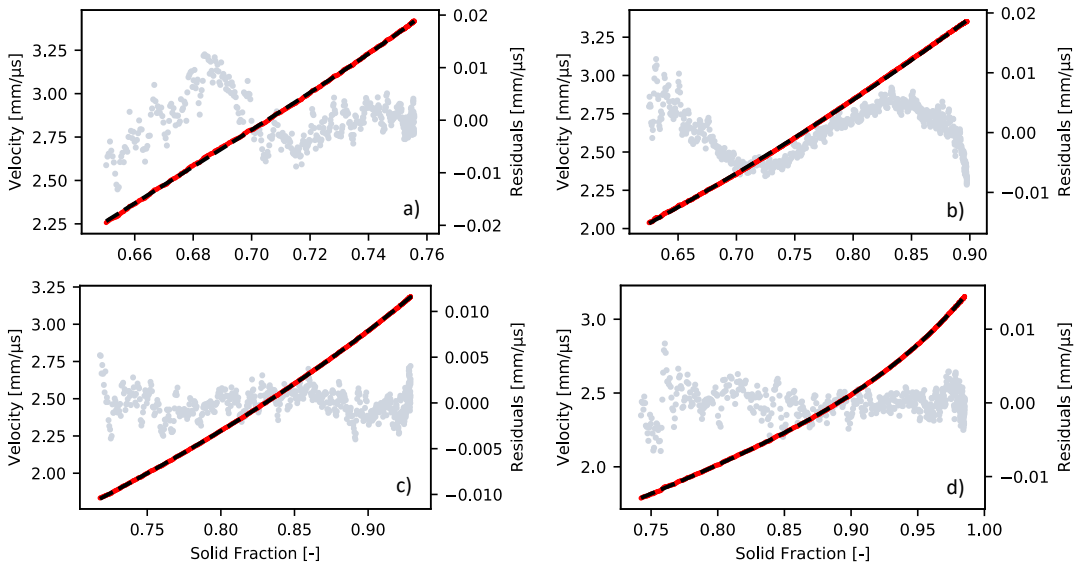

Figure 3-23: Fit of Equation (3-4) to longitudinal experimental data of a) ACP, b) Parteck M 200, c) Tablettose 100, d) maize starch. Red: Experimental data; Dashed line: Fit; Grey: Residuals.

When fitting each tablet individually and then calculating the mean values of each parameter, the resulting equations did not fit the experimental data. Instead, they overestimated the velocity at high solid fractions as depicted in Figure 3-24 on two exemplary materials. This was especially apparent for GranuLac 200 shown in Figure 3-24b) where the mean value fit did not meet the measured velocity at all. To avoid this, one fit was performed for all consecutive measurements together. The results are also shown in Figure 3-24.

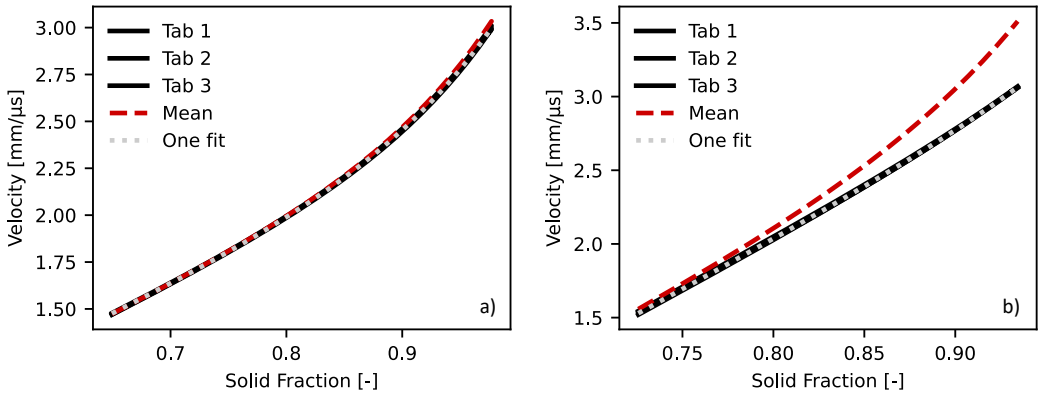

Figure 3-24: Three consecutive longitudinal measurements of a) Vivapur 101 and b) GranuLac 200 including the fit according to Equation (3-4). Black: Experimental data (n = 3); Red: fit using the mean values of the individually fitted parameters; Grey: fit using the parameters of the fit performed for all three measurements together.

The results of the non-linear regression compared to the experimental data of the three measurements can be found in Figure 3-25 for the longitudinal and Appendix Figure A-4 for the transverse measurements. Overall, the complete fit seemed to match the experimental data. The only observable difference was shown by ACP due to the comparatively low repeatability as mentioned in Chapter 3.1.5.

When separating the equation into a linear ($y0 + ax$) and an exponential (be^{c*SF}) part as depicted in Figure 3-25 and calculated using the parameters shown in Appendix Table A-6, it can be seen that for most materials, the exponential expression did not have an influence at SFs below 0.8. As at least one material (ACP) did not even reach this SF, and the *b* parameter showed values close to zero for most velocity profiles, comparison of the exponential expression parameters was not feasible. Neither was an extrapolation to zero porosity to determine the velocity through the fully solid material as the equation seemed to overfit the data. This is also evident when observing the low SF range, as the calculated velocity became negative. The fit parameters can therefore only be used to describe the measured values and not to predict the velocity at higher or lower solid fractions.

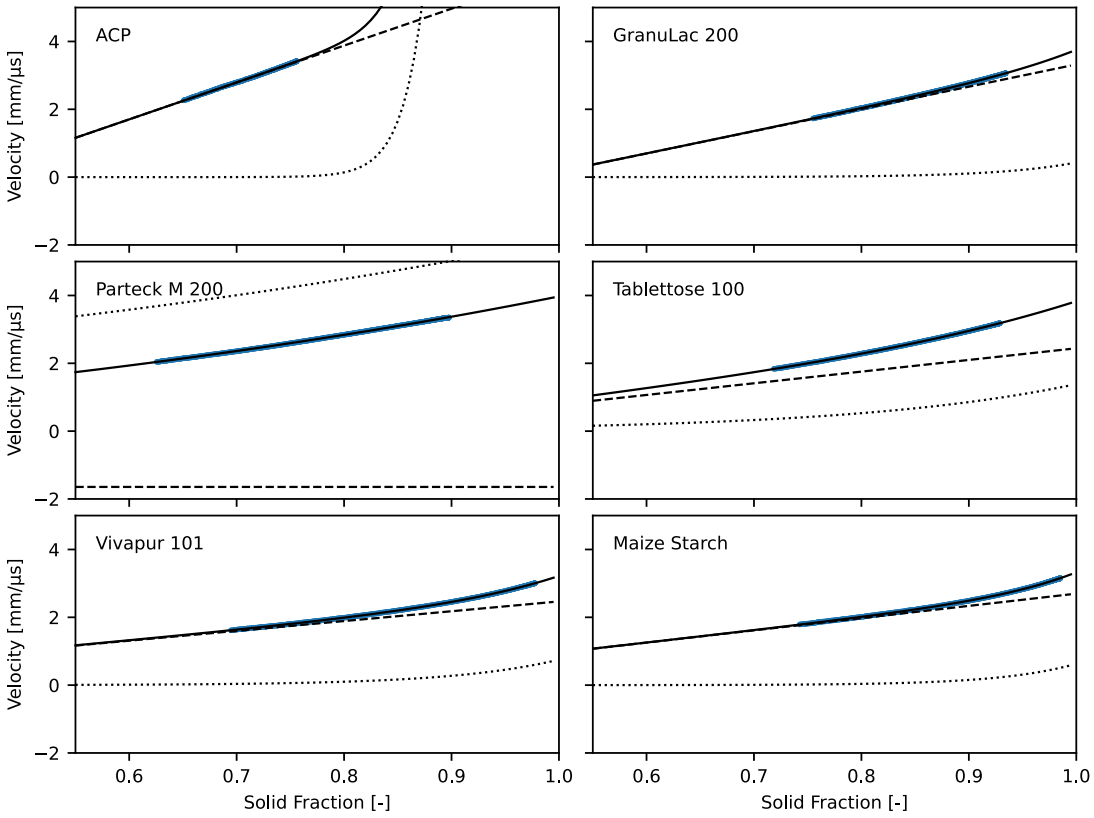

Figure 3-25: Fit of Equation (3-4) to the experimental data measured in longitudinal mode including the mean of the three individual measurements (blue) and the complete fit (solid line), linear expression, i.e. $y0 + ax$ (dashed line) and exponential expression of the equation, i.e. be^{c*SF} (dotted line). Plots in one row share y-axis; plots in one column share x-axis.

However, since it has been observed that most of the substances exhibited an almost linear increase towards the start of the compression, instead of performing non-linear regression of the complete compression process, slope of the linear portion of the compression signal was determined. The approach was adapted from the Heckel equation where the slope of the linear increase is determined to calculate the yield pressure.

The linear fit performed at the beginning of the compression signal is depicted in Figure 3-26 exemplarily for one measurement per material. The linear part was defined as all data points between the start of the steady compression signal until the last data point where an $R^2 > 0.998$ was reached. It was determined by repeatedly performing linear regression and calculating the R^2 value, starting with a fit over the whole compression, and then each iteration excluding one more data point at high solid fractions.

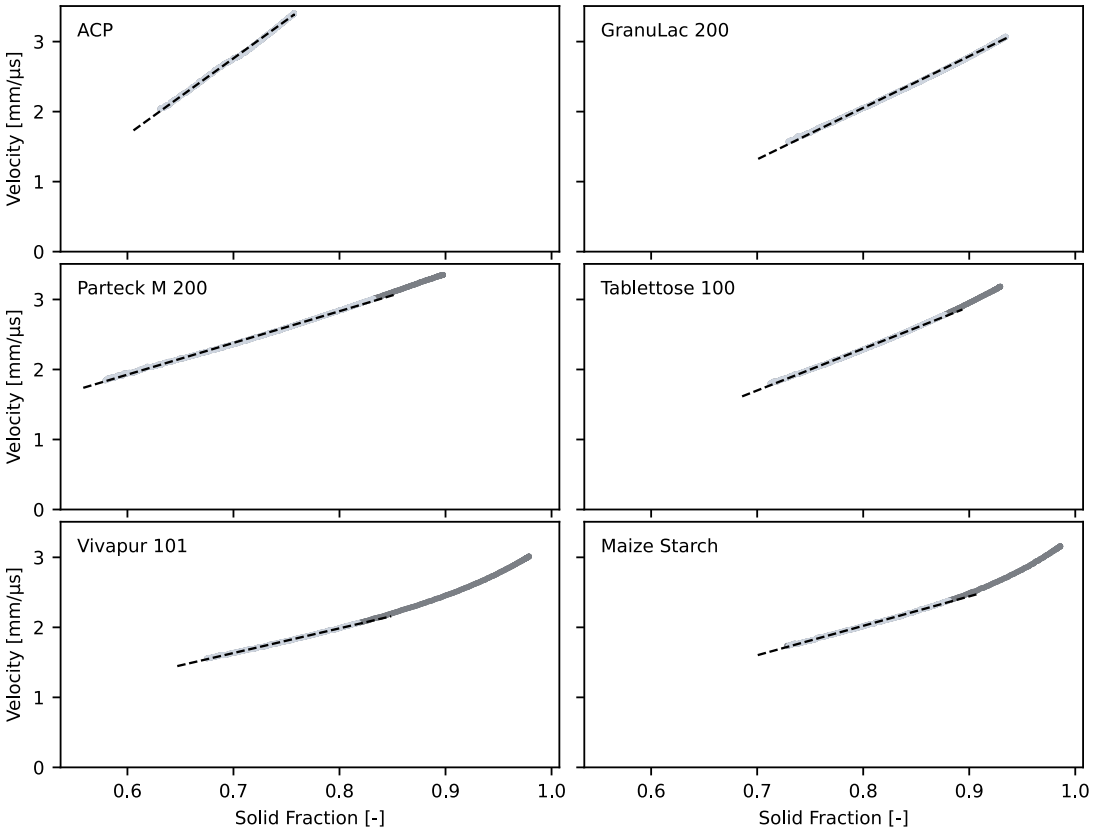

Figure 3-26: Compression signal exemplarily shown for one measurement each of six substances. Dark grey: Whole compression between start of the steady signal and maximum US velocity; Light grey: Data points used for linear fit; Dashed line: Linear fit. Published in Kern et al. (2022). Plots in one row share y-axis; plots in one column share x-axis.

The first observation that could be made was the overall linearity of the signal. While for ACP and GranuLac 200 the whole compression signal showed a relatively high linearity, some data points towards the end of the compression had to be excluded for Parteck M 200 and Tablettose 100. The high linearity here was surprising as both had shown a pronounced influence of the exponential expression of Equation (3-4) before, seen in Figure 3-25. Nonetheless, the substances which showed the highest deviation from a linear increase at high solid fractions were Vivapur 101 and maize starch where only about half of the compression process was in the linear range. One possible explanation for the observed deviations from a linear increase could be a shift from interconnected to isolated pores, or complete closure of smaller voids at higher solid

fractions which would then exponentially decrease the length of the solid pathways through the compact. This could explain why the softer, more elastic substances showed more of a deviation from a linear trend towards the end of the compression as they are the materials which could be compressed to the highest solid fractions.

The second major difference between the materials was the rate of increase during compression, expressed through the slope of the linear fit shown for one exemplary grade per material in Figure 3-27. The other materials are shown in Appendix Table A-5. Since the SF is a dimensionless number, the slope has the same unit as the velocity: mm/µs. The steepest increase was exhibited by ACP, followed by Parteck Delta M, D(-)-Mannit and GranuLac 200. While there was a rather large discrepancy of over 2 mm/µs between ACP and the other materials, Vivapur 101 and maize starch, the substances with the shallowest increase rate, were rather similar. As seen in Chapter 3.1.6, the increase rate of Pearlitol 200SD and Parteck M 200 is quite similar, same as D(-)-Mannit and Parteck Delta M. A steeper increase over the same SF range for one sample could potentially be caused by the difference in SOS through the completely solid material. However, since Parteck M 200 showed a higher velocity throughout the whole compression process than e.g., GranuLac 200 while exhibiting a decidedly shallower compression slope this does not seem to be the cause. It has to be noted that the relationship between velocity and SF was not perfectly linear for any of the substances, even though the R^2 was rather high. Nevertheless, the linear fit did give an idea as to how much the materials differed in their initial curve progression.

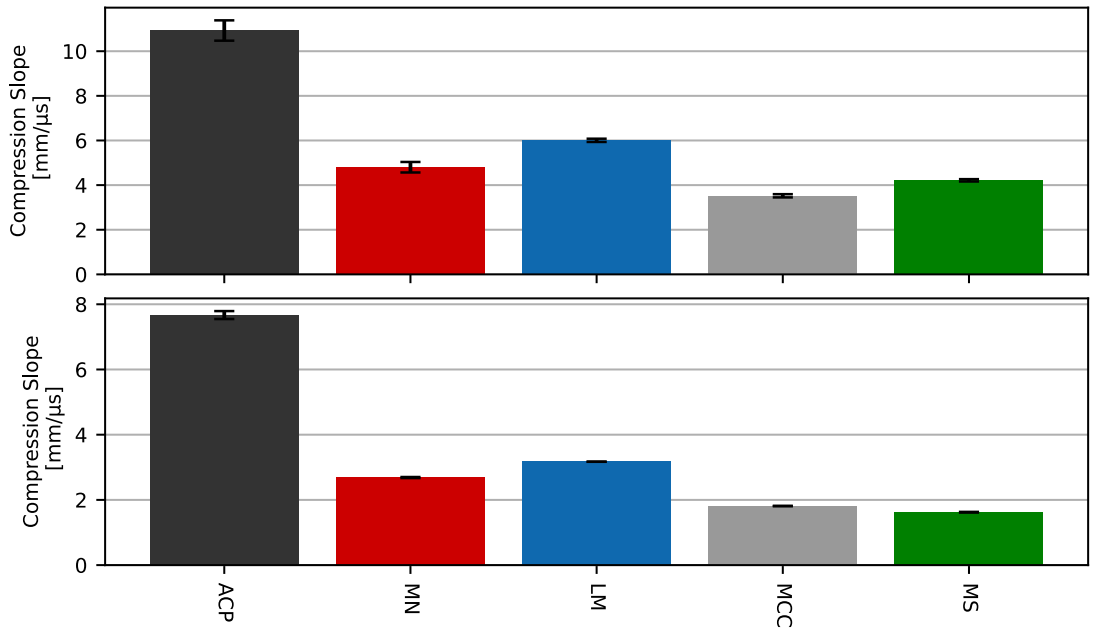

Figure 3-27: Slope of the linear fit calculated using the longitudinal (top) and transverse (bottom) measurements. Arithmetic mean ± sd (n = 3). ACP = anhydrous calcium phosphate, MN = Parteck M 200, LM = Tablettose 100, MCC = Vivapur 101, MS = maize starch.

When comparing the increase rate to the in-die Heckel yield pressure depicted in Figure 3-28 (an overview over the yield pressures of all the grades can be found in Appendix Figure A-5), calculated as described in Chapter 5.2.4.5, commonly used to characterise the deformation behaviour of powder materials, a correlation could be seen. The materials with the higher yield pressure were those with the steepest velocity increase. This would point towards a relationship between compaction behaviour and velocity change with increasing SF. One possible explanation are the changes in the pore structure caused by the different deformation mechanisms as already mentioned above. The only exceptions were Parteck M 200 and Pearlitol 200SD where the velocity increase was lower than for the lactose grades, while the yield pressure was higher. This could be caused by the two different approaches to describe the same process. The Heckel equation describes the changes in pore volume with increasing pressure, whereas the ultrasound velocity changes with decreasing pore fraction help identify the differences in the pore structure evolution. While the yield pressure then gives an idea about the pressure needed to induce plastic deformation in the particles, a steeper velocity increase could show a more pronounced fragmentation propensity. All in all, the yield pressures of all four mannitol grades were quite similar. The ultrasonic data, however, suggests that there actually are differences between pre-processed and other mannitol grades with the structured varieties showing higher plasticity not seen through the yield pressure. Another advantage of the compression slope over the Heckel approach is its independence of the density measurements. While the *y0* parameter will be influenced by inaccurate density values through a shift on the x-axis, the slope value will not change. In the Heckel analysis, however, small discrepancies of the density values of as little as 0.03 g/mL will result in a significant difference in the determined yield pressure (Krumme et al., 2000).

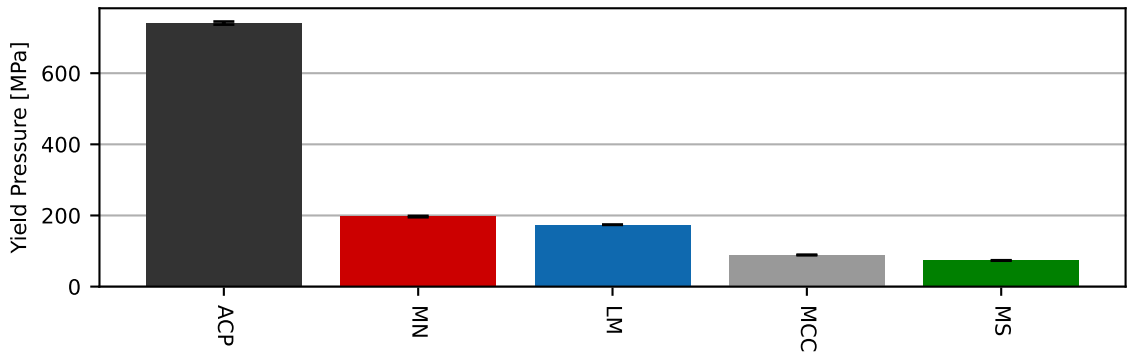

Figure 3-28: Heckel yield pressure of exemplary excipients. Arithmetic mean ± sd (n = 3). ACP = anhydrous calcium phosphate, MN = Parteck M 200, LM = Tablettose 100, MCC = Vivapur 101, MS = maize starch.

3.2.2 Elasticity Parameters

As during compression both longitudinal and transverse velocity were measured, apparent Young's Modulus (YM) and Poisson's Ratio (PR) were calculated according to the equations presented in Chapter 1.4.3. In addition, the apparent Shear Modulus (SM) was calculated using the transverse velocity. Apparent, because during compression the compact is under stress and elastically deformed, and the values will probably not correspond to those obtained out-die at the same SF. Henceforth, every mention of YM, PR and SM will refer to the apparent in-die values. As in both modes three measurements were conducted each, nine different combinations for the κ ratio c_L/c_T (see Chapter 1.4.3) were possible. The calculations were performed for solid fractions between 0.5 and 1 in steps of 0.01. The results of the PR, YM and SM calculations are presented in Figure 3-29 and Appendix Figure A-6 to Figure A-8. The YM increased for all materials with increasing SF. However, while the increase was rather steep for ACP up to values of 20 GPa at a SF of 0.75, the maximum reached for starch was at around 7.5 GPa at a SF of 0.98. The YM of the two lactose grades increased in parallel, Tablettose 100 always exhibiting slightly higher values than GranuLac 200 at the same SF. Overall, these findings agreed well with those of other authors who found an increase in YM with decreasing porosity and deduced the elasticity parameters to be porosity dependent (Hagelstein et al., 2019; Mazel et al., 2012).

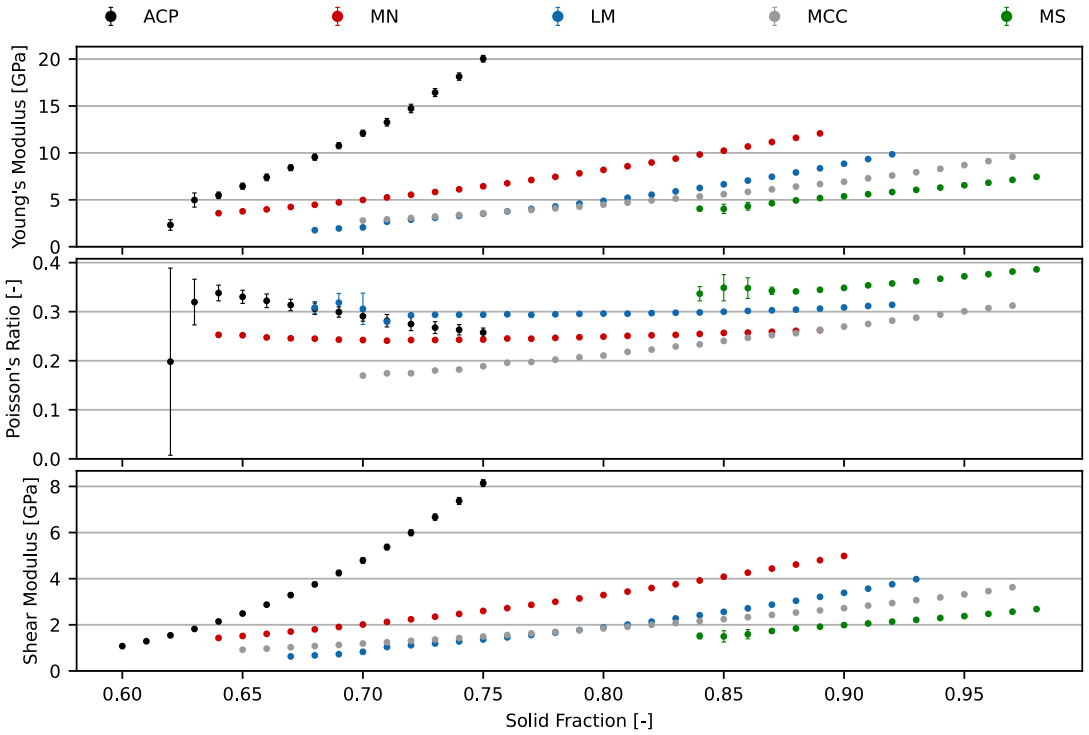

Figure 3-29: Apparent Young's Modulus and Poisson's Ratio calculated using longitudinal and transverse ultrasonic velocity and apparent Shear Modulus calculated using transverse velocity through the materials during compression. Arithmetic mean ± sd (YM and PR: n = 9; SM: n = 3). ACP = anhydrous calcium phosphate, MN = Parteck M 200, LM = Tablettose 100, MCC = Vivapur 101, MS = maize starch. Plots share x-axis.

For the PR there were different trends observed. The values for MS and MCC increased with increasing relative density. The LM and MN PR did not increase but remained almost steady around 0.3 and 0.25, respectively. The ACP PR decreased with increasing SF. At the same time, this substance showed the highest standard deviation. The tendency that the PR changes differed between ductile substances like MCC and brittle ones such as ACP was also observed by Hagelstein et al. (2019). However, so far, no explanation was proposed as to why the materials showed those trends. Mathematically this increasing ratio of the plastically deforming materials is a result of the increasing difference in longitudinal and transverse velocity with decreasing porosity, i.e., the deviation from a linear velocity increase at low porosities.

The SM also increased with increasing relative density. Overall, the trends were the same as observed for the YM. However, the SM values were generally lower by half compared to the YM. This agrees with the results presented by Roberts et al. (1994). The increase in YM and SM implies an increased resistance against deformation with increased relative density. The lowest moduli were shown by starch which is known to show particularly elastic behaviour.

When comparing the elasticity parameters described in this work with those obtained by other authors, discrepancies will be noted (Cunningham et al., 2004; Mazel et al., 2012). Possible reasons could be the method used for the determination, the equation used for calculations, the difference between in- and out-die values, or a combination of the factors. The values determined using the same set-up, however, could still be used to compare different materials to each other, especially YM and SM which are directly linked to the resistance of a material towards deformation.

3.2.3 Summary

While the velocity increase in transverse mode was mostly linear in relation to the SF increase, the relationship was more complex in longitudinal mode: The best fit was found using an equation consisting of a linear and an exponential term. It was shown that the velocity increase differed between materials. While ACP and GranuLac 200 showed an almost linear relationship between velocity and SF over the whole compression process, only about half of the compression showed a linear increase for Vivapur 101 and maize starch. In addition, the slope of the linear fit determined for the beginning of the compression process differed. The velocity increase was steepest for ACP, followed by the lactose and non-processed mannitol grades, Parteck M 200 and Pearlitol 200SD, maize starch, and finally Vivapur 101. This was almost the same order as the yield pressure decrease which is commonly used to classify materials according to their deformation behaviour. Only Parteck M 200 and Pearlitol 200SD did not follow this trend. In contrast to the

yield pressure derived from the Heckel plot, the velocity profiles seemed to be able to differentiate between processed and non-processed mannitol grades, implying increased plasticity in processed grades

Since ultrasound can be used to not only determine the relative pore volume of a material but is also sensitive to changes in the shape and structure of pores, it is possible that the differences observed here are rooted in variances in the evolution of the pore structure with increasing pressure. The proposed relation between velocity increase rate and deformation behaviour could then be explained by differences in pore size reduction. Through fragmentation of particles, openings could be crossed fast by particle fragments being pushed into the openings and thus allowing a more direct pathway across the pore area, while ductile and elastic deformation would result in a convergence of the pore edges and a gradual decrease in pore size until smaller pores and interconnections are closed completely. The steeper increase at higher solid fractions could be explained by complete closure of interconnections between bigger pores which results in a more direct pathway for the sound wave and can only be reached by softer materials such as starch and MCC.

With the SF, the Young's Modulus and Shear Modulus also increased. This implies that the resistance against deformation increased with decreasing porosity. The PR showed no general tendency. However, it needs to be kept in mind that the elasticity parameters are directly linked to the measured velocity and consequently to the pore structure. This leads to the conclusion that the elastic parameters as determined here are linked to the microstructure of the compacts, and that there will be a difference between the parameters in-die and out-die at the same SF. Nonetheless, the elasticity parameters are interesting to take note of when comparing different materials.

3.3 Signals during Decompression

While the loading or compression part of the compaction process has been the focus of Chapter 3.2, this chapter will more closely examine the decompression signal.

3.3.1 Double Compaction Experiments

One characteristic shared by all velocity profiles is the discrepancy between the velocity during compression and decompression. In most cases the velocity measured during compression was higher compared to the velocity at the same SF during decompression, best seen in Figure 3-4. The only exception were the lactose grades in transverse mode where the velocity stays at its maximum during the initial stage of unloading. This velocity discrepancy has been proposed to be caused by actual differences between the compact during compression and decompression by Stephens et al. (2013a), as sound waves are not only influenced by pore volume, but also by pore shape. However, the punches move in opposite directions during the two phases of the compaction process. Since the displacement measurements are essential to the velocity calculations, it is necessary to assess whether the TOF and tablet height are paired correctly, i.e., there is no time delay between the recording of the sound wave arrival and the displacement determination. If not, the difference in direction could artificially create a discrepancy in the velocity. Therefore, double compaction experiments were performed. While during the first compression irreversible and reversible deformation occur simultaneously, the second cycle is primarily elastic (Mazel et al., 2012). The second cycle should then be a reversal of the first decompression which is driven by elastic recovery (Aburub et al., 2007). The results of the ultrasonic measurements are exemplarily shown for MS and MCC in Figure 3-30 and Appendix Figure A-11 for additional materials.

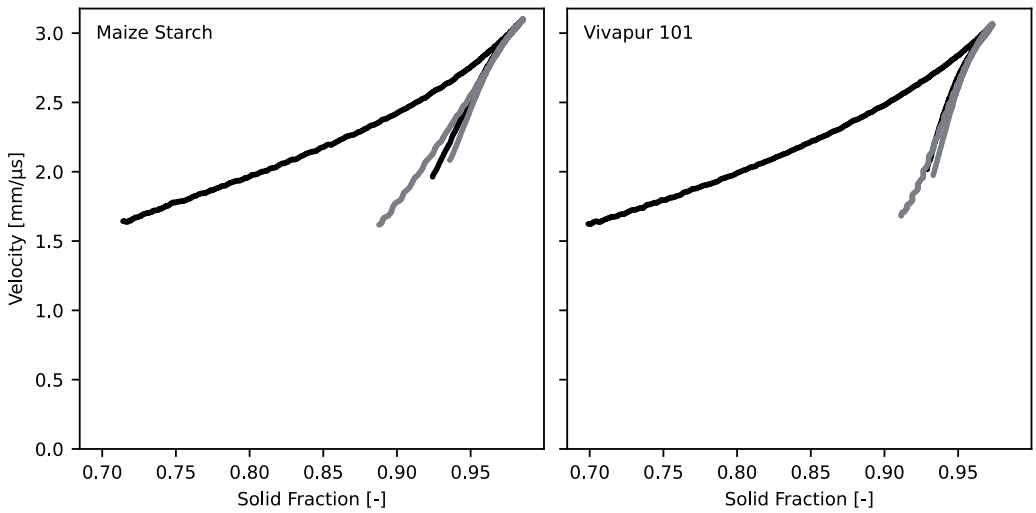

Figure 3-30: Longitudinal velocity of one exemplary measurement each, through maize starch and Vivapur 101. First compression: Black; Second compression: Grey. Plots share y-axis.

Even though there was a small discrepancy visible at the beginning of the second compaction cycle compared to the decompression signal for maize starch, it was noticeably lower compared to the first compression. Since the punch movement was the same during both cycles, trouble with the pairing of TOF and displacement values would have also appeared during the second compression. The observed discrepancy between compression and decompression in the velocity profiles was, therefore, not caused by the measurement set-up, but was instead an indication of irreversible deformation taking place inside the compact. Compared to the compression at the same SF during decompression the compact had undergone more irreversible deformation – either plastic or brittle – and was at the same time already partly relaxed. The different velocity could then be attributed to the difference in the structure of the tablet.

What has to be noted, however, is the start of the second compression. During the second cycle the contact was established at a lower SF than the one where contact was lost between punches and sample at the end of the first cycle, and the velocity was lower than previously measured. This could be observed for all materials, most pronounced for MS. The elastic recovery was, therefore, not over once the signal stopped. Instead, the volume increase of the material became slower and could not keep up with the punch movement during decompression. The same could be observed when looking at the classical compression plots in Figure 3-31 and Appendix Figure A-12. However, instead of an almost identical signal progression during the second compression as for the velocity measurements, here a hysteresis was seen due to the pressure increase upon contact.

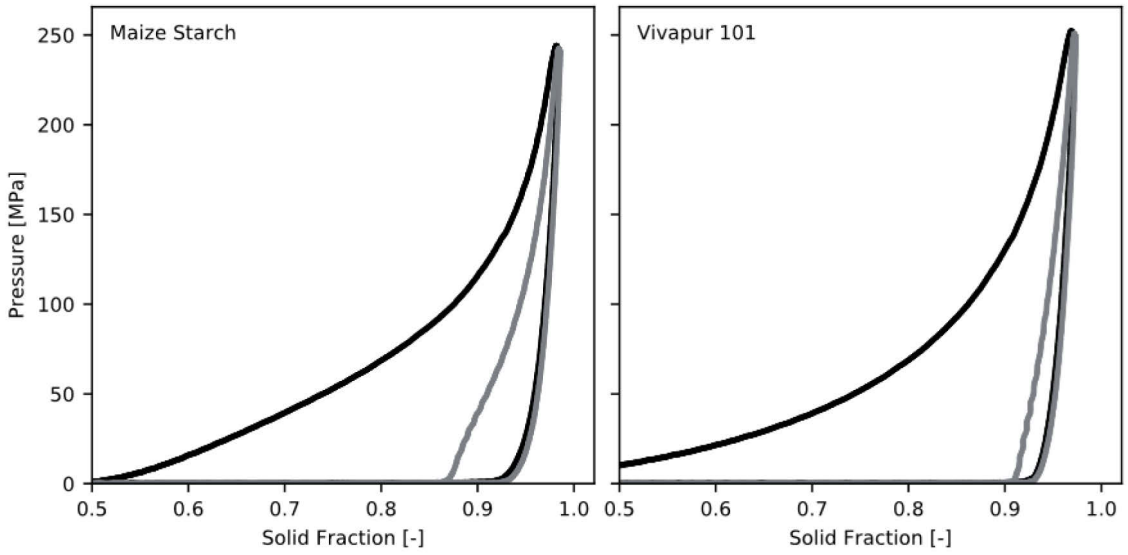

Figure 3-31: Pressure-SF plots of the double compaction experiments. First compression: Black; Second compression: Grey. Plots share y-axis.

This hysteresis has been proposed as a proof of more energy being put into the compact during the second compression, resulting in an altered and stronger tablet (Gamlen et al., 2015). But, when looking at the tensile strength of the tablets prepared with a single or double compaction cycle shown in Figure 3-32, the only material showing a significant increase in strength was MS (t-test, $P = 0.000$, $\alpha = 0.05$) even though the hysteresis was visible for all materials. Instead, the deviation from a linear relationship between pressure and SF towards the start of the second compression, only exhibited by MS, could be indicative of the second compression not being purely elastic in this case (Mazel et al., 2012). This additional irreversible deformation could be the reason why starch showed the highest discrepancy in velocity during the second cycle.

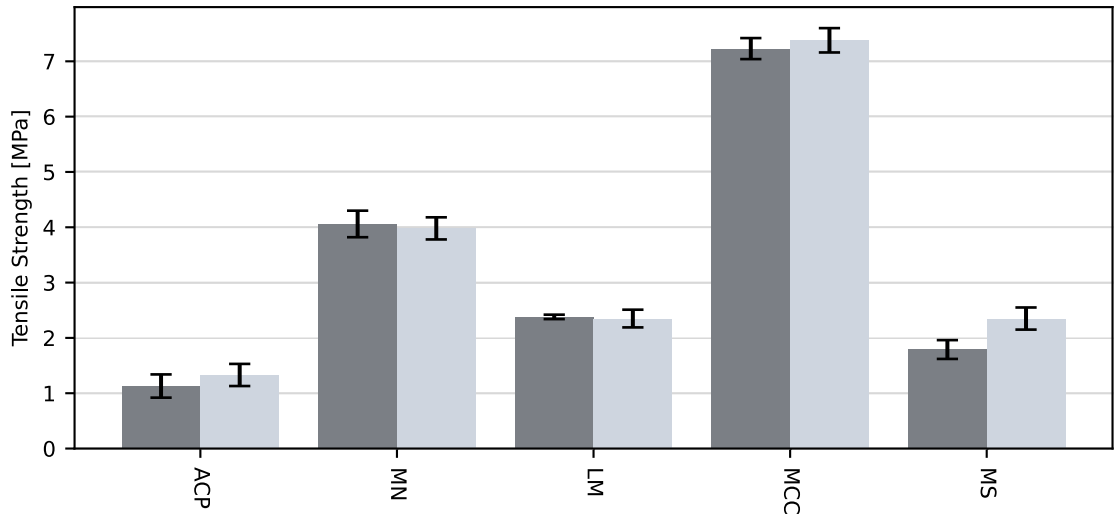

Figure 3-32: Tensile strength after single (dark grey) and double (light grey) compaction to 250 MPa. Arithmetic mean ± sd (n = 10). ACP = anhydrous calcium phosphate, MN = Parteck M 200, LM = Tablettose 100, MCC = Vivapur 101, MS = maize starch.

Overall, it needs to be kept in mind that the elastic recovery is not completed once the force signal drops to zero or the US signal stops, but instead continues afterwards. Nonetheless, it should be possible to use the decompression profiles of the ultrasonic measurements to evaluate the elasticity of a material and the changes undergone by the compact during elastic recovery. This will be further explored in the following chapter.

3.3.2 Parameters Derived from Decompression Signals

When comparing the decompression signals of velocity vs. SF to pressure vs. SF as shown in Figure 3-33, it is obvious that there is more of a variation between the velocity profiles of different materials. While the pressure plots all show a drop from 250 MPa to zero, there are certain differences between the velocity profiles of the materials: the maximum velocity differed and so did the speed of the sound waves before the contact was lost. The shape of the signal also varied more greatly for the velocity profile. Whereas there was only a slight variability of the curvature

of the pressure plots towards the end of the decompression, depending on the elasticity of the materials, the velocity signals went from almost linear (ACP and MN), over slightly concave (MCC and MS), to a pronounced curvature (LM). It is, therefore, possible that the decompression signal could offer additional information about the decompression process of different materials, especially concerning the evolution of the pore structure. This is especially interesting as the pore structure, which is essential for the performance of tablets (Sun, 2017), has been shown to be heavily influenced by the compact relaxation during decompression (Van Veen et al., 2002).

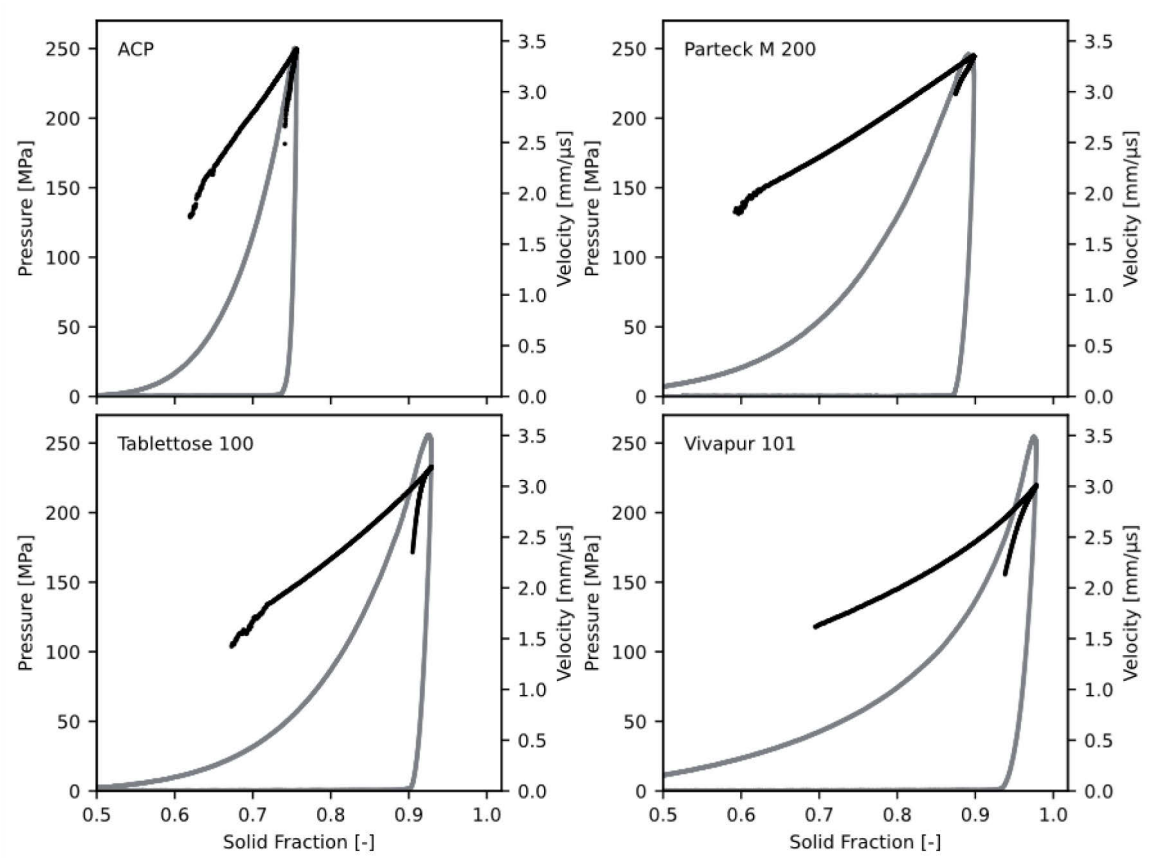

Figure 3-33: Comparison of longitudinal velocity (black) and pressure (grey) plots of four exemplary materials (n = 3). Plots in one column share x-axis.

In this chapter several attempts to characterise the decompression part of the velocity profiles are presented.

3.3.2.1 Immediate Elastic Recovery

The most forward approach to quantify the elasticity of a substance is the immediate elastic recovery (*%iER*). Generally, the volume increase between minimum distance between punches and volume at loss of contact is quantified as has been discussed in Chapter 1.2.4. In this work the *%iER* is determined through the SF decrease and calculated according to Equation (3-5).

$$\%\boldsymbol{iER} = \frac{\boldsymbol{SF_{max} - SF_{end}}}{\boldsymbol{SF_{max}}} * \mathbf{100}\% \quad (3\text{-}5)$$

%iER: *Immediate elastic recovery [%]*

SF_{max}: *Maximum SF [-]*

SF_{end}: *SF at which the last ultrasonic signal is detected during decompression [-]*

The calculated *%iER*s of the different excipients are shown in Figure 3-34 and Appendix Figure A-13. The highest values relating to the highest elasticity were exhibited by the starch grades, where the loss in SF was over 5.5% compared to the maximum reached during compression. Starch 1500 even surpassed 6%. It was followed by the MCC grades at around 4%. The smallest recovery was shown by ACP and Parteck Delta M at 2%, followed by the other mannitol and lactose grades, all below 3%. Those results are in good agreement with the elastic work during decompression reported by Aburub et al. (2007). There was also a correlation to the YM calculated using the ultrasonic data as shown in Chapter 3.2.2. The materials with the highest YM showed the lowest *%iER* values. However, there was a pronounced discrepancy between ACP and the lactose grades in the maximum YM (compare Figure 3-29): ACP showed values of around 20 GPa which was about twice as high as either lactose grade, whereas the *%iER* values were similar. The difference between MN and LM was also more pronounced, with MN exhibiting higher YM values.

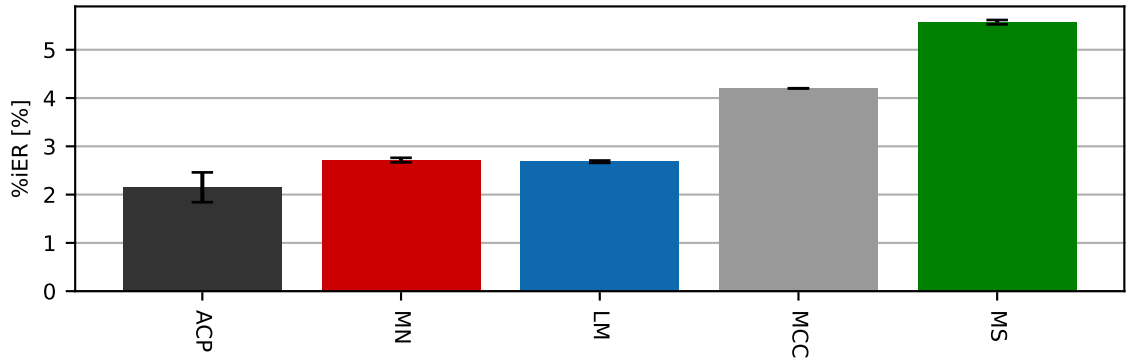

Figure 3-34: Immediate elastic recovery in % of the materials used in this work calculated using the longitudinal measurements. Arithmetic mean ± sd (n = 3). ACP = anhydrous calcium phosphate, MN = Parteck M 200, LM = Tablettose 100, MCC = Vivapur 101, MS = maize starch.

It has to be kept in mind, however, that the *%iER* does not incorporate the whole elastic relaxation as shown by the double compaction experiments in Chapter 3.3.1. When looking at the SF 24 h after compaction (SF_{24h}) compared to SF_{max} as shown in Figure 3-35, the relative SF decrease had more than doubled for most materials from SF_{end}. Only ACP did not show a pronounced volume increase in the 24 h after compression. Nevertheless, the *%iER*, albeit not returning the full picture, can be used to get a first idea about the elasticity of a material in relation to others and will be used as an indicator of elasticity from here on out.

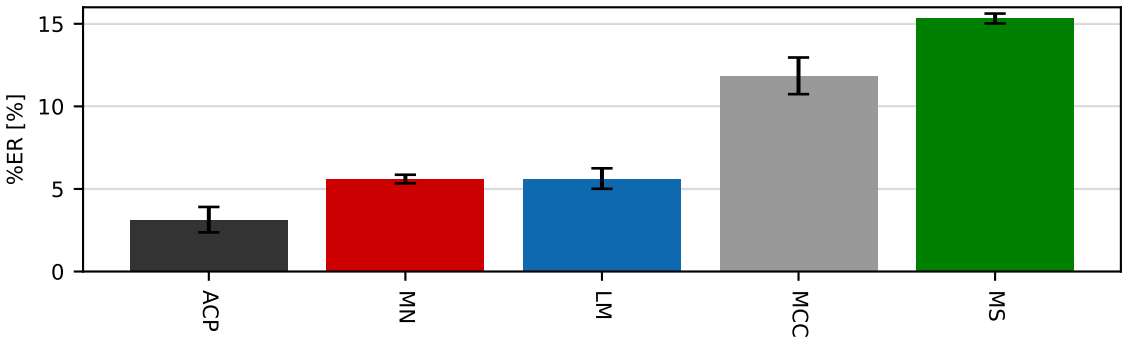

Figure 3-35: Elastic recovery between SF_{max} and SF_{24h}. Arithmetic mean ± sd (n = 10). ACP = anhydrous calcium phosphate, MN = Parteck M 200, LM = Tablettose 100, MCC = Vivapur 101, MS = maize starch.

3.3.2.2 Decompression Slope and Ratio

While the detection of the *%iER* was limited by the speed of the tablet relaxation and subsequent volume increase, the relationship of velocity and SF decrease was almost independent as shown during the second compression of the double compaction experiments. It has been proposed that the more pronounced the velocity drop, the less elastic the material (Hagelstein et al., 2019): the more elastic the material, the longer the contact between punch tips and compact which results in a shallower decompression signal. To test this hypothesis, linear regression was performed on the decompression signals of the excipients. The results of the decompression slope determinations can be found in Figure 3-36.

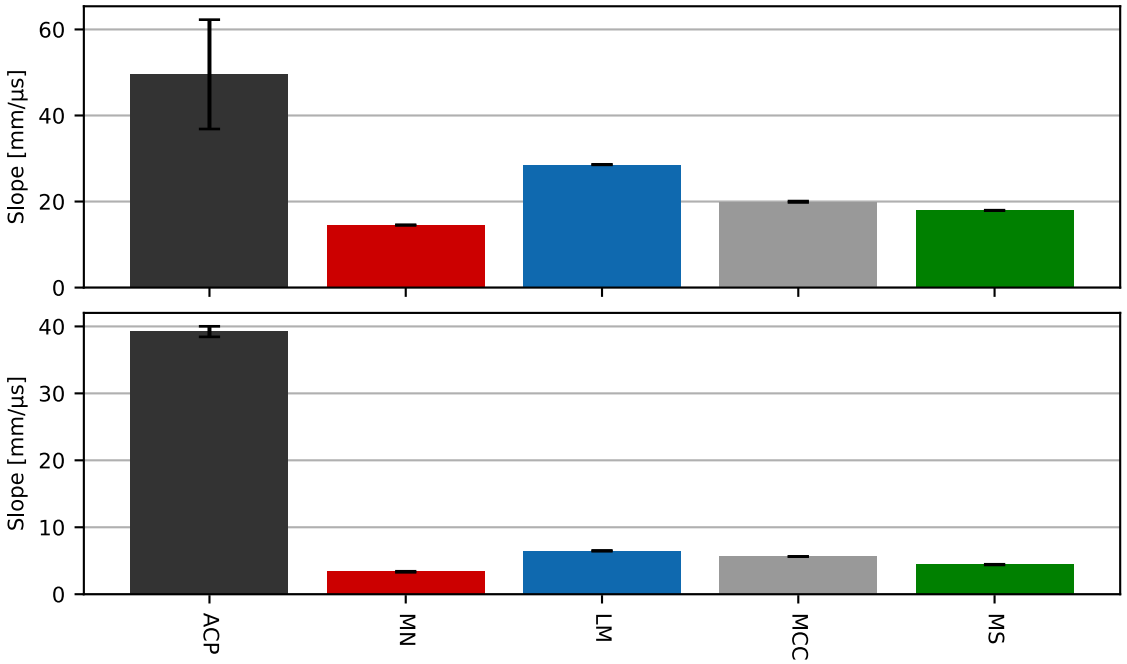

Figure 3-36: Decompression slope of five exemplary excipients calculated using the longitudinal (top) and transverse (bottom) measurements. Arithmetic mean ± sd (n = 3). ACP = anhydrous calcium phosphate, MN = Parteck M 200, LM = Tablettose 100, MCC = Vivapur 101, MS = maize starch.

The steepest slope was observed for ACP, followed by LM although only about half as steep. The shallowest *Slop*e was shown by MN which did not fit to the low *%ER* exhibited by the mannitol grades. This indicates that elasticity wasn't the sole parameter factoring into the *Slope*. In addition, while the MCC *Slope* was steeper than the MS *Slope*, the difference in the steepness did not do the actual difference in elasticity justice.

The main issue in the determination of the *Slope* was the overall shape of the signal. While Parteck M 200 showed an almost linear relationship between SF and velocity during decompression ($R^2 = 0.998$), the same did not apply to Tablettose 100 ($R^2 = 0.881$) as seen in Figure 3-37. A linear decrease would be an indication towards a steady increase in pore size, whereas a strong deviation from linearity can be assumed to be caused by a variation in the pore size increase at different points during unloading. As pores and cracks inside the compact present obstacles the sound wave needs to circumvent, the decompression velocity becoming steeper as the SF decreases, points towards there being a shift from the enlarging of existing pores to the formation of interconnections between pores impeding the sound transmission. In addition, the direction of the pore enlargement might have an impact on the apparent velocity: Elongation of pores in axial direction will not decelerate the sound wave as much as a crack formation perpendicular to the direction of propagation.

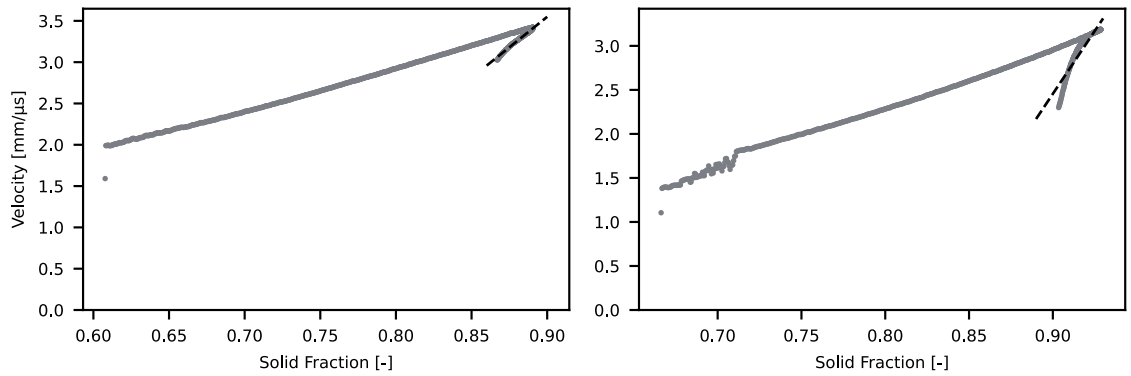

Figure 3-37: Linear regression (visualised through dashed line) of the decompression signal, exemplarily shown for one longitudinal measurement each of Parteck M 200 (left) and Tablettose 100 (right).

Another possibility to quantify the velocity decrease with decreasing SF is the ratio of velocity drop to the SF decrease calculated according to Equation (3-6):

$$\boldsymbol{Ratio} = \frac{\boldsymbol{US_{max} - US_{end}}}{\boldsymbol{SF_{max} - SF_{end}}} \tag{3-6}$$

Ratio: *Ratio of velocity drop to SF decrease during decompression [mm/µs]*

SF_{max}: *Maximum SF [-]*

SF_{end}: *Last SF at which signal is detected in the lower punch [-]*

US_{max}: *Maximum velocity [mm/µs]*

US_{end}: *Velocity at SF_{end} [mm/µs]*

The decompression *Ratio*s calculated for the excipients are depicted in Figure 3-38. The results showed the same tendency as the *Slope* calculations. While the trend of low elasticity equals pronounced velocity drop was true for most materials, MN showed a different behaviour. As might be expected, the closer the decompression signal was to a linear progression, the more similar were *Slope* and *Ratio*. The LM grades showed the highest difference, about 7 mm/µs, which showed their decompression signal deviated most from a linear relationship. This deviation indicated there might be different phases in the decompression process.

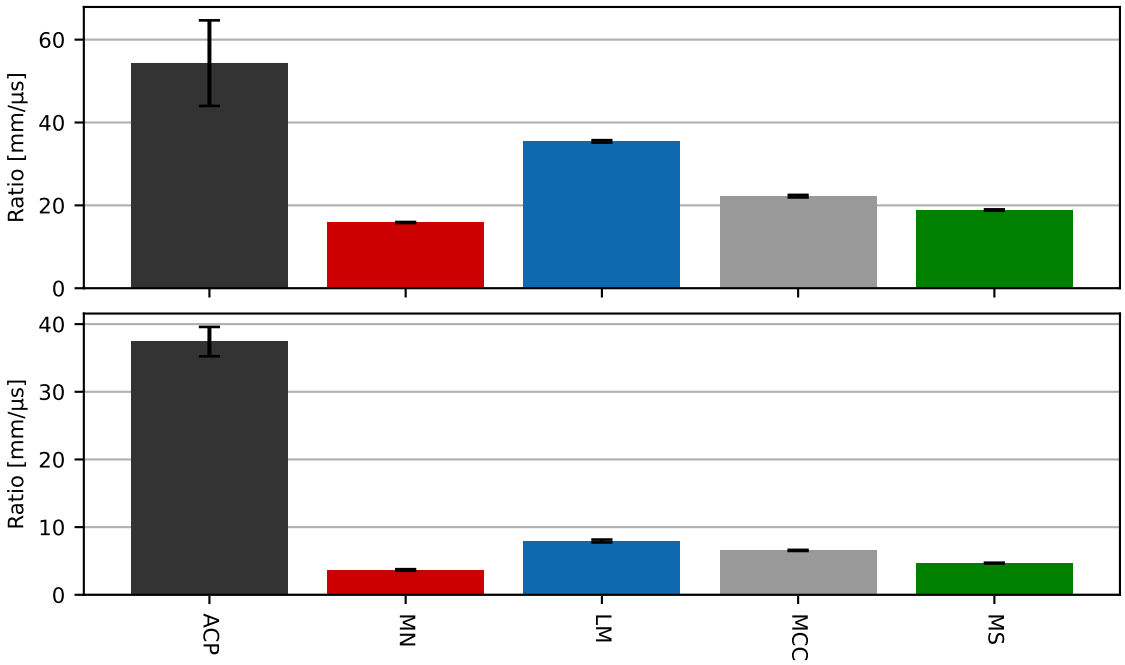

Figure 3-38: Ratio of US velocity drop to SF decrease calculated using longitudinal (top) and transverse (bottom) measurements. Arithmetic mean ± sd (n = 3). ACP = anhydrous calcium phosphate, MN = Parteck M 200, LM = Tablettose 100, MCC = Vivapur 101, MS = maize starch.

3.3.2.3 AUC calculations

To incorporate the different shapes of the decompression signals, the area under the decompression curve, dubbed *AUC*, was calculated according to Equation (3-7). To also incorporate the velocity drop and exclude the differences in the maximum velocity, the area at velocities lower than US_{end} was excluded as illustrated in Figure 3-39.

$$\boldsymbol{AUC} = \left| \int_{\boldsymbol{SF_{max}}}^{\boldsymbol{SF_{end}}} \boldsymbol{v_{US}} * \boldsymbol{dSF} \right| - \boldsymbol{US_{end}} * (\boldsymbol{SF_{max}} - \boldsymbol{SF_{end}}) \tag{3-7}$$

AUC: *Area under the decompression signal until US_{end} [mm/µs]*

SF_{max}: *Maximum SF [-]*

SF_{end}: *Last SF at which signal is detected in the lower punch [-]*

US_{end}: *Velocity at SF_{end} [mm/µs]*

v_{US}: *Ultrasonic velocity [mm/µs]*

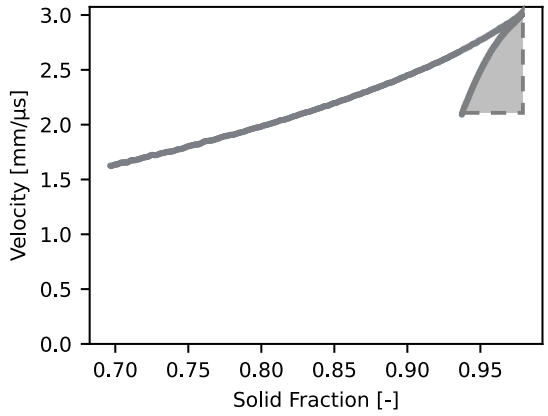

Figure 3-39: Depiction of the AUC (grey area between decompression signal and dashed lines) on the example of one longitudinal Vivapur 101 measurement.

The results of the *AUC* measurements are shown in Figure 3-40. The longitudinal and transverse measurements showed the same overall trend, however, the difference between MS and MCC was less pronounced when using the transverse measurements for the calculations. The values showed the same tendency as the *%iER*: the more elastic a substance, the higher the value. In direct comparison, however, the differences were more pronounced. While the *%iER* was 5.5 and 4.1% for MS and MCC, respectively, the *AUC*s were 0.033 and 0.023 mm/µs, both calculated using longitudinal results. This translated to the *%iER* of MCC being 4/5th of MS and the *AUC* 2/3rd. Similarly, the differences between the ACP and LM *AUC*s were higher which better reflected the SF decrease after 24 h. MN was the only material where the *%iER* and out-die data did not correlate with the *AUC* as it showed the smallest area under the decompression curve in both

measurement modes, indicating a lower elasticity than ACP. A similar trend was observed for the *Slope* and *Ratio*. What those three parameters have in common, however, is that they all incorporate the velocity decrease during decompression which was not very pronounced for MN.

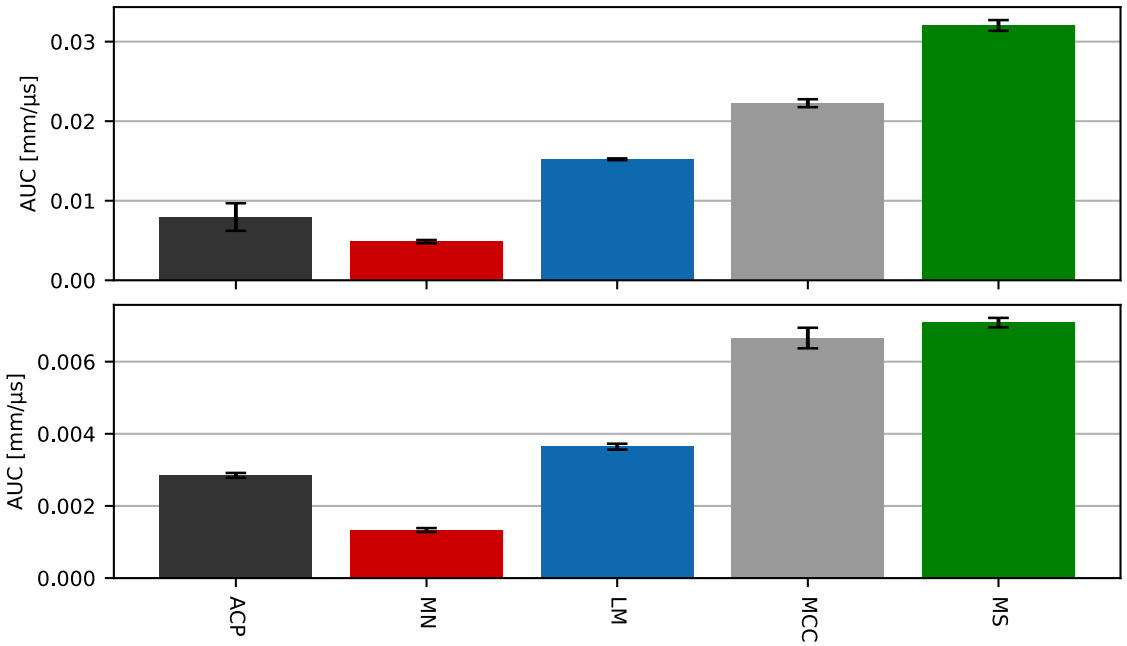

Figure 3-40: AUC calculated using the longitudinal (top) and transverse (bottom) velocity measurements. Arithmetic mean ± sd (n = 3). ACP = anhydrous calcium phosphate, MN = Parteck M 200, LM = Tablettose 100, MCC = Vivapur 101, MS = maize starch.

As both, the length of the signal in x- (*ΔSF*) and y-direction (*ΔUS*) influenced the *AUC* as calculated above, ACP with its only slightly lower *%iER,* but at the same time vastly more pronounced velocity drop during decompression compared to MN will inevitably show a larger *AUC*. To cancel out this effect and use the *AUC* to get a better grasp of the elastic recovery, the complete *AUC* (= AUC_{Full}) was calculated according to Equation (3-8). The AUC_{Full} is schematically depicted in Figure 3-41.

$$\boldsymbol{AUC_{Full}} = \left| \int_{\boldsymbol{SF_{max}}}^{\boldsymbol{SF_{end}}} \boldsymbol{v_{US}} * \boldsymbol{dSF} \right| \tag{3-8}$$

AUC_{Full}: *Area under the complete decompression signal [mm/µs]*

SF_{max}: *Maximum SF [-]*

SF_{end}: *Last SF at which signal is detected in the lower punch [-]*

v_{US}: *Ultrasonic velocity [mm/µs]*

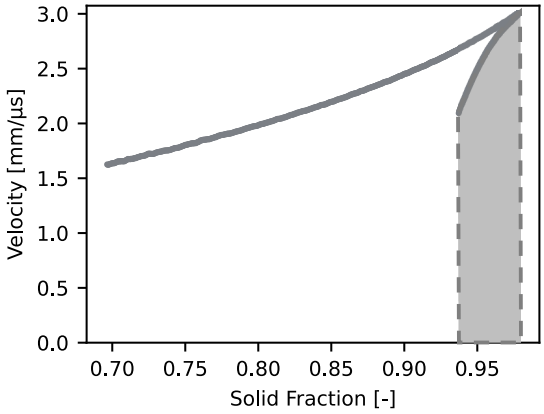

Figure 3-41: AUC_{Full} (area in light grey) exemplarily shown for one longitudinal Vivapur 101 measurement.

The AUC_{Full} of the excipients can be found in Figure 3-42. While this parameter described the difference in elasticity between MS and MCC quite well, it underestimated the difference in elasticity between LM and MS. It needs to be noted that while the *AUC* is influenced by the velocity drop, the AUC_{Full} is contingent upon $US_{max.}$ The draw-back of using the AUC_{Full} parameter could be, that the speed of sound through a material is reversely correlated to its elasticity as explained in Chapter 1.4.1. As shown by LM and MCC, LM was less elastic according to the *%iER,* discussed in Chapter 3.3.2.1. At the same time the maximum velocity reached during compression was higher. The lower SF reached by the inelastic materials did, to a degree, minimise this effect but did not nullify it.

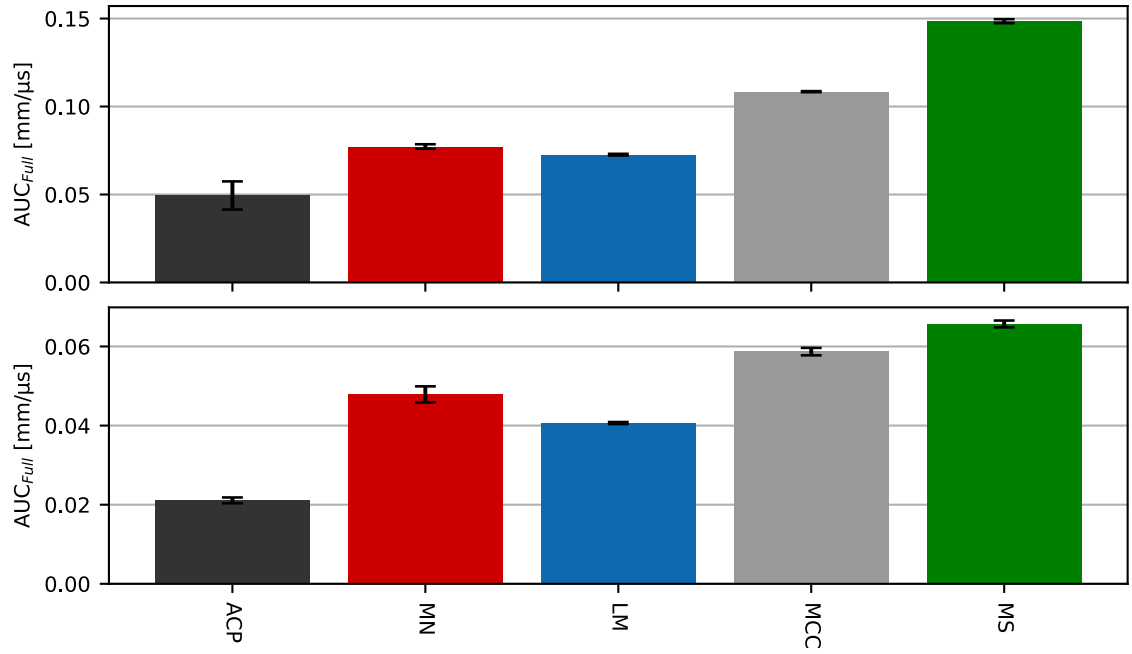

Figure 3-42: Complete AUC calculated according to Equation (3-8) using the data generated in longitudinal (top) and transverse (bottom) mode. Arithmetic mean ± sd (n = 3). ACP = anhydrous calcium phosphate, MN = Parteck M 200, LM = Tablettose 100, MCC = Vivapur 101, MS = maize starch.

Nonetheless, when comparing the AUC_{Full} to the *ERW* calculated according to Equation (1-5) and depicted in Figure 3-43, it becomes obvious that the *ERW* underestimated the elasticity of MS in comparison to the other materials. The AUC_{Full} seemed to have a higher predictability of the total elastic recovery for the materials tested here despite the difference in US_{max}.

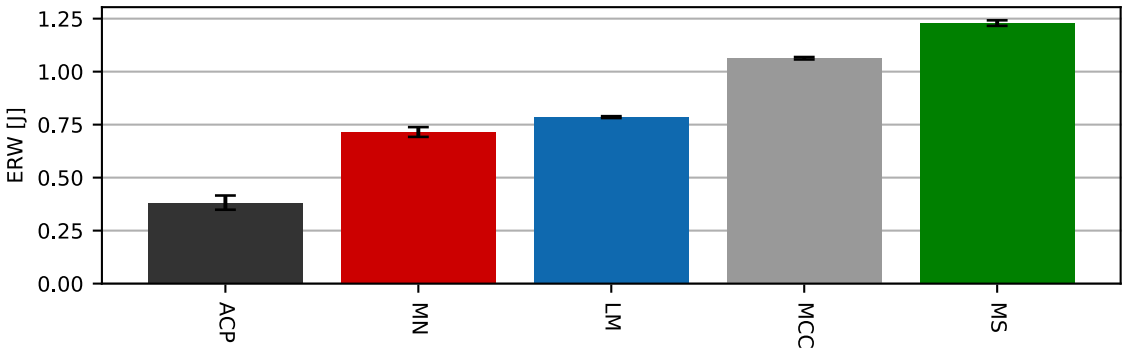

Figure 3-43: *ERW* calculated for the excipients. Arithmetic mean ± sd (n = 3). ACP = anhydrous calcium phosphate, MN = Parteck M 200, LM = Tablettose 100, MCC = Vivapur 101, MS = maize starch.

3.3.2.4 Analysing the Signal Shape

It has become clear that one major distinguishing factor between the materials was the progression or shape of the decompression signal. One descriptor incorporating the signal shape, the *AUC*, has already been discussed. However, this parameter is also influenced by the velocity drop and the decrease in SF during decompression. Since most materials showed a shallow velocity decrease towards the beginning of the decompression process – best seen on the example of the transverse LM measurements where the velocity initially did not decrease at all as shown in Figure 3-12 – and a more pronounced drop towards the end, the decompression signal could generally be described as concave. As seen when calculating the *Slope*, the curvature of the decompression velocity profiles varied between materials. To get an idea about the margin of the bend in the decompression, the area between the measured signal and a perfectly linear line between the maximum and end signal was calculated as:

$$\boldsymbol{A_c = AUC - \frac{\Delta SF * \Delta US}{2}} \tag{3-9}$$

A_C: *Area between measured signal and linear line [mm/µs]*

AUC: *Area under the decompression signal until US_{end} [mm/µs]*

ΔSF: *SF decrease during decompression [-]*

ΔUS: *Decrease in ultrasonic velocity during decompression [mm/µs]*

A_c is illustrated in Figure 3-44.

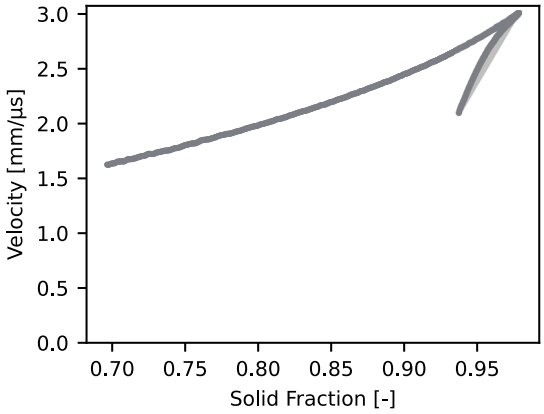

Figure 3-44: A_c (area in light grey) exemplarily shown for one longitudinal Vivapur 101 measurement.

The A_C of the materials is depicted in Figure 3-45. As with all parameters incorporating the velocity, the results calculated using the transverse measurements were overall lower. The relation between the values of the different materials was in most cases, however, quite similar. As a result of their pronounced deviation from a linear relationship in both measurement modes, the largest A_C was shown by LM and MCC. The other side of the spectrum was MN. While the A_C of MS calculated using the longitudinal data was about the same as MCC, the value was noticeably lower in transverse mode. This was caused by a higher linearity of the decompression signal in transverse mode ($R^2 > 0.99$). Since it was shown before that the longitudinal velocity changes are more sensitive to small differences in the high SF range, it is possible the transverse results are not capable of discerning small differences as well, which would mean the longitudinal velocity could be the better descriptor for the decompression process.

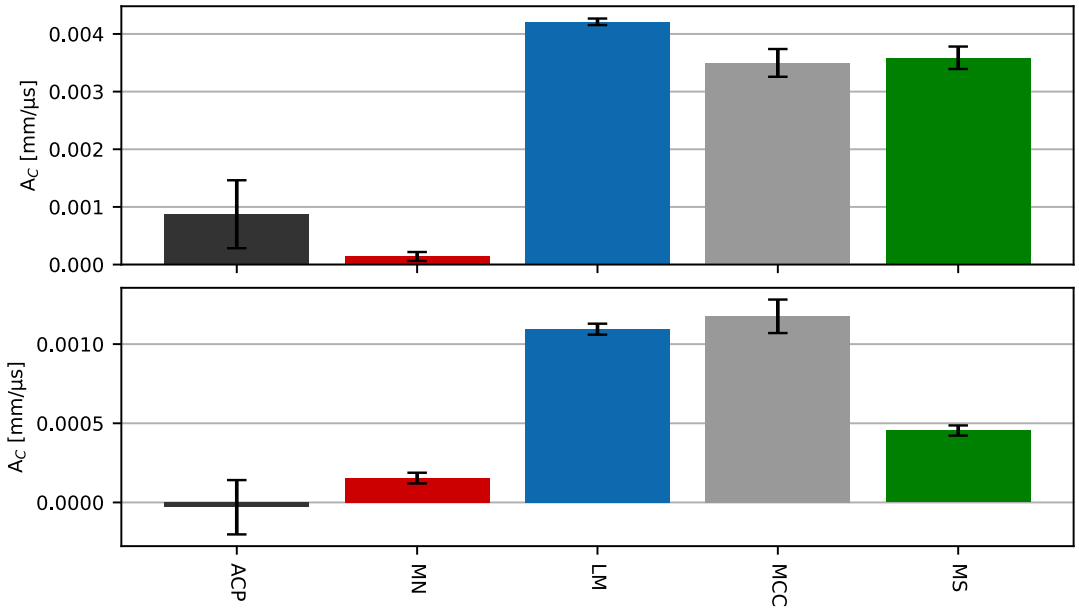

Figure 3-45: A_c calculated for five exemplary excipients using the data generated in longitudinal (top) and transverse (bottom) mode. Arithmetic mean ± sd (n = 3). ACP = anhydrous calcium phosphate, MN = Parteck M 200, LM = Tablettose 100, MCC = Vivapur 101, MS = maize starch.

It is interesting to note that LM and MCC showed similar values concerning the A_C values even though they are vastly different in their elasticity according to the *%iER*. This was caused by the "tilting" of the decompression signal described best through the *Ratio*. While length and curvature seemed to be quite similar, the SF decrease was higher for MCC. This illustrates that the parameters must always be assessed together. One factor alone will never be enough to get a complete picture of the decompression signal. This is mainly due to several processes occurring simultaneously: the compact expands due to elastic relaxation (Hiestand et al., 1977), bonds previously formed during compression might break, enlarging of existing and opening of new pores, as well as in some cases the formation of new bonds (DeCrosta et al., 2001). As many of these factors influence one another, separating them is not an easy task. Ultrasonic in-die measurements may, however, be a tool capable of helping in the identification of the different processes happening during unloading.

3.3.2.5 Velocity Decrease

The decrease in ultrasonic velocity during decompression (*ΔUS*) has been shown to influence several of the parameters calculated before, mainly *Slope*, *Ratio* and *AUC*. The results of the velocity decrease measurements are depicted in Figure 3-46. As already suspected due to the steeper velocity increase during compression, the velocity decrease was more pronounced for the longitudinal velocity measurements. For most substances the difference between maximum velocity and last detected signal was about four times as high in longitudinal mode compared to transverse. The only exception was ACP where it was only about twice as high.

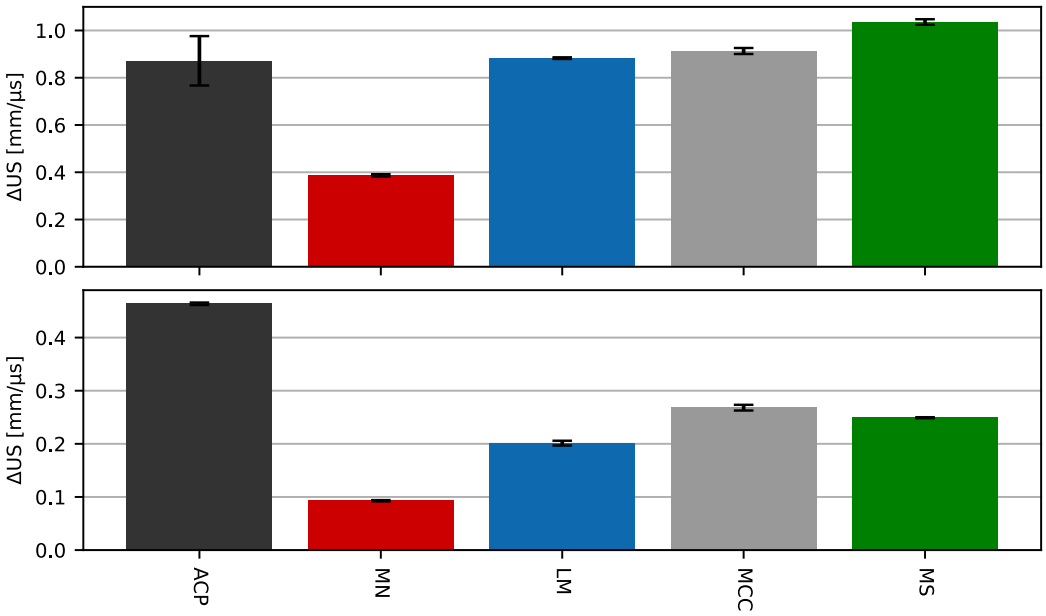

Figure 3-46: *ΔUS* calculated for the longitudinal (top) and transverse (bottom) velocity profiles. Arithmetic mean ± sd (n = 3). ACP = anhydrous calcium phosphate, MN = Parteck M 200, LM = Tablettose 100, MCC = Vivapur 101, MS = maize starch.

As the changes in velocity have been proposed to be indicative of changes in the pore structure, the velocity decrease during decompression could help in the characterisation of the changes undergone by the compact during elastic recovery. A pronounced decrease would then signify abrupt changes within the compact, especially in radial direction. Therefore, it should be possible to detect micro cracks or defects occurring during decompression which could subsequently lead to lamination of the tablets (Xu et al., 2018b). However, as the ultrasonic measurements were limited by the KIM set-up, the tool shape, which has a pronounced influence on the processes within the compact during unloading (Mazel et al., 2015), could not be changed and in the current set-up no lamination was observed for any of the materials. Nonetheless, as the changes in pore structure are likely related to the breaking of bonds during decompression, the in-die parameters could be of help in the characterisation of the finished tablets which will be investigated in Chapter 3.3.4.

3.3.3 Varying the Maximum Compaction Pressure

Since the maximum SF reached in-die by the materials when using the same maximum pressures varied as seen in Figure 3-12, the question whether the shapes of the decompression curves would assimilate, if the SF was the same, needs to be addressed. In Figure 3-47 the velocity profiles of four materials are depicted, all compacted to an in-die SF of 0.9. The first observable difference between the materials was the maximum velocity. In transverse mode it decreased in the following order: MN > LM > MCC > MS. The maximum longitudinal velocity reached for MS and MCC on the other hand was almost identical. Apart from this, the order was the same. The different velocities can be attributed to two factors previously discussed in Chapter 3.2.1: the material properties, primarily concerning elasticity, as well as the pore structure. For the materials tested in this study, the velocity at a SF of 0.9 was reversely correlated to the elasticity according to the YM and SM (refer to Figure 3-29). It could, therefore, be possible that the porosity was low enough for the material properties being the factor primarily influencing the measured velocity at this SF.

The decompression signals of the materials were still different, especially observable for the longitudinal velocity. The decompression signal of MN was the shortest and also exhibited the least pronounced velocity drop. The LM signal, however, showed an almost vertical decrease after an initially steady velocity with decreasing SF. The difference was especially apparent for MS and MCC which were basically identical during compression (longitudinal only) and reached the same velocity at a SF of 0.9 while the decompression profiles were not superimposable. The decompression signal was detected over a longer SF range and less steep for MS, which is an indication of its higher elasticity.

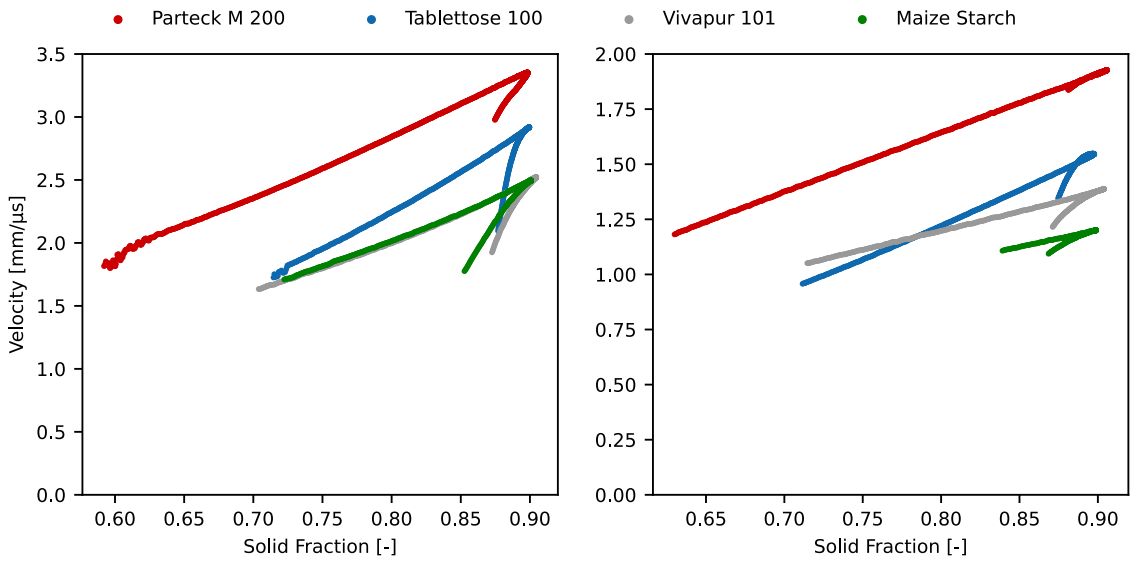

Figure 3-47: Longitudinal (left) and transverse (right) velocity through four exemplary materials compacted to the same in-die SF (n = 3).

When looking at the pressure plots in Figure 3-48, there seemed to be a correlation between maximum velocity and pressure needed to reach the target SF. One possible explanation is the elasticity and plasticity of the materials as low plasticity is associated with more resistance against compression (Çelik and Marshall, 1989). Another possibility is the overall hardness of the material. This agrees with the yield pressure shown in Figure 3-28 which is also an indicator of the hardness of a material.

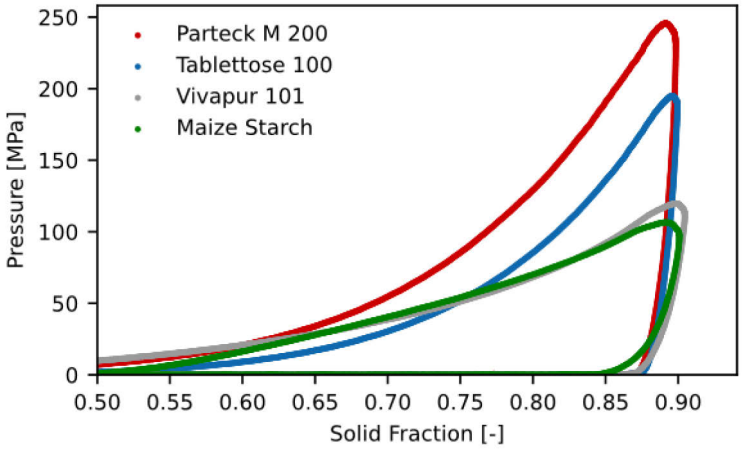

Figure 3-48: Pressure-SF plots of the four materials, compacted to an in-die SF of 0.9 (n = 3).

The differences in the curve progression mentioned before could also be seen when comparing the decompression parameters calculated for the longitudinal compression profiles as shown in Figure 3-49. First of all, the *%iER* of MS was the highest of the four materials, followed by MCC, even though the stress applied was lower as evident in Figure 3-48. The values of MCC and MS were closer in transverse mode, probably caused by difficulties of the signal detection due to the

higher water content of MS which could also explain the higher standard deviations in transverse mode. All in all, all parameters showed the same tendencies that were exhibited before when the materials had been subjected to the same stress, albeit they assimilated. The one parameter clearly most influenced by the reduced maximum SF was the AUC_{Full}. Since it incorporates the maximum velocity reached during the compaction process, which decreased with higher porosities, this trend was to be expected.

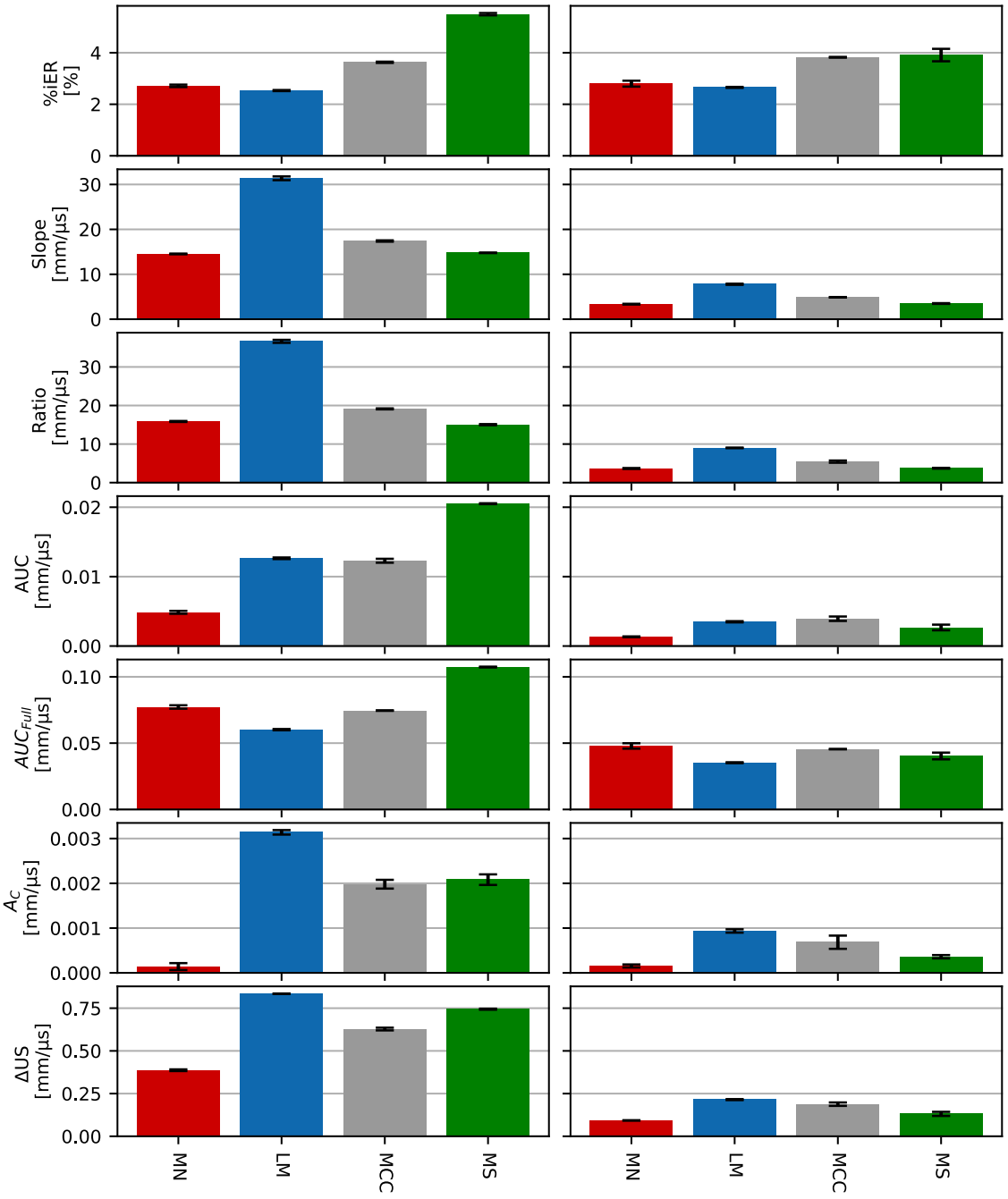

Figure 3-49: Decompression parameters, discussed in Chapter 3.3.2 calculated using the longitudinal (left) and transverse (right) measurements of four excipients compacted to the same in-die SF. Arithmetic mean ± sd (n = 3). MN = Parteck M 200, LM = Tablettose 100, MCC = Vivapur 101, MS = maize starch. Plots in one row share y-axis.

The pressure used in the standard KIM measurements was 250 MPa, which is rather high and has been chosen to cover a long SF range during the compression process. However, since the pressure used for the manufacture of tablets varies depending on the performance of the powder material, the influence of the applied pressure on the decompression signal needs to be considered. Therefore, Figure 3-50 depicts the KIM results through three exemplary materials when different maximum pressures were used. As expected, the velocity during compression at the same SF was independent of the maximum pressure applied. However, the maximum SF reached increased with increasing pressure applied. The higher SF caused an increase in maximum velocity. Due to their different starting point, i.e., the maximum SF reached, the decompression signals proceeded in parallel to one another as the shape stayed overall the same. Slight differences could be seen when comparing the loop shown by the transverse measurements of LM. With decreasing pressure, the area between the compression and decompression decreased. The decompression signals of the longitudinal and transverse measurements of LM and MCC showed the same tendencies: as the loop shown by the transverse LM measurements decreased, so did the SF range over which compression and decompression velocity were the same. A possible explanation for a more pronounced velocity drop towards the beginning could be that the radial expansion of the pores started earlier in the decompression process if lower pressures were applied.

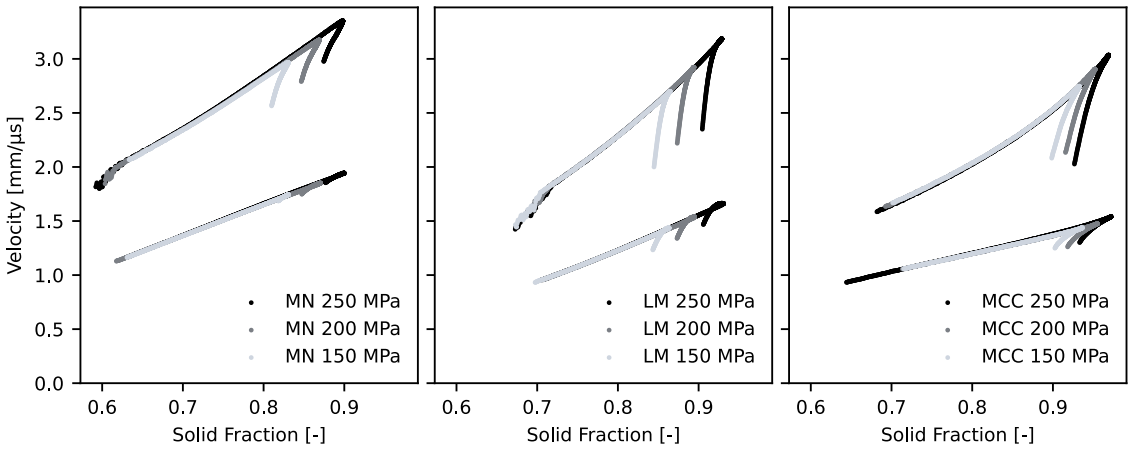

Figure 3-50: Velocity profiles of Parteck M 200 (MN), Tablettose 100 (LM) and Vivapur 101 (MCC) compacted using different maximum pressures. Each plot contains longitudinal and transverse measurements (n = 3). Plots share y-axis. Published in Kern et al. (2022).

The velocity before the signal stopped decreased with decreasing compaction pressure in the case of LM. In contrast, MCC showed almost the same minimum velocity during decompression independent of the applied pressure. As the SF at which the last signal was detected was markedly different for both, MN and LM, depending on the pressure applied and the SOS is known to be porosity dependent, the reduced velocity was expected. For MCC, the SF difference was less

pronounced which could explain why the measured velocity before loss of contact was comparatively similar. As before with the compression the tendencies were the same independent of the measurement mode. This shows that either wave type can be used in the assessment of the velocity changes.

Of the parameters calculated for the decompression, shown in Figure 3-51 only two showed the same trend with decreasing maximum pressure for all three materials: *%iER* and AUC_{Full} which both increased with increasing pressure. Since the maximum velocity, which decreased with lower compression pressures, plays a huge part in the AUC_{Full} calculations this trend was expected. The decrease in *%iER* indicates that elastic deformation will occur until the end of the compression process which then results in more relaxation, the more stress the materials had been subjected to. This agrees with other authors who found the volume reduction at high solid fractions to be mainly caused by elastic deformation of the compact (Sun and Grant, 2001). The most pronounced difference could be observed for MCC, probably caused by its comparatively high elasticity. An interesting trend could be observed when comparing *Slope* and *Ratio* of LM. While the *Slope* increased with decreasing compression pressure, the *Ratio* was basically identical at all three stress levels. The values of the two parameters were most similar for the 150 MPa measurements. This indicates that the lower the applied pressure, the more linear the decompression signal for this material which fits with the observations made in Figure 3-50 concerning the short overlap between compression and decompression velocity towards the beginning of the decompression signal. The values shown in Figure 3-51 further show that the *AUC* is not an appropriate measure for the elasticity. While the *%iER* was at all pressure levels highest for MCC, its *AUC* at 150 MPa was about the same as for LM at 250 MPa. This was caused by the more pronounced velocity drop exhibited by LM.

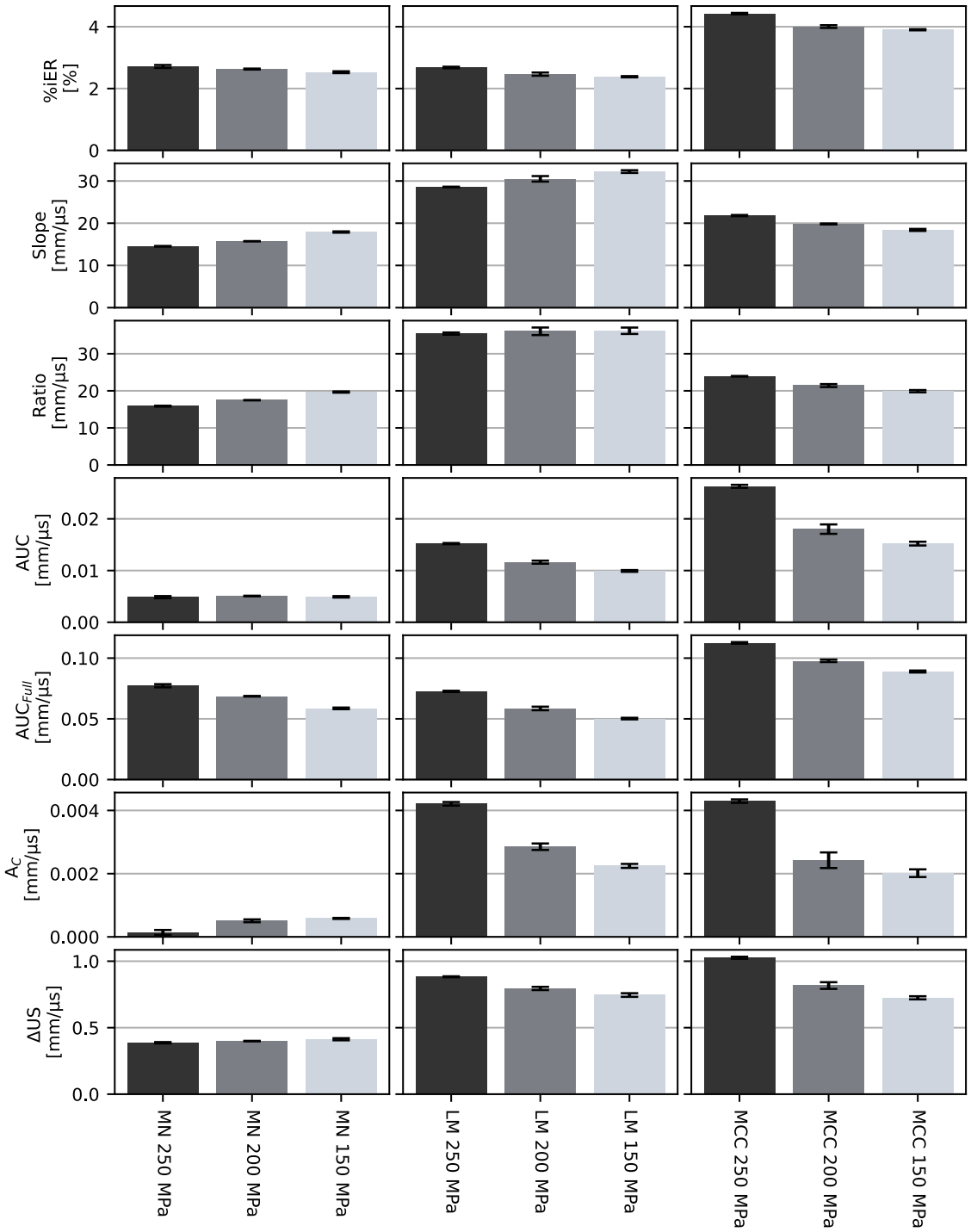

Figure 3-51: Parameters calculated for the decompression signals of the longitudinal velocity profiles after compression with three different maximum compression pressures. Arithmetic mean ± sd (n = 3). MN = Parteck M 200, LM = Tablettose 100, MCC = Vivapur 101. Plots in one row share y-axis.

As the pressure was decreased, the decompression profile of MN became slightly more concave in shape. For the decompression parameters this resulted in an increase in A_C, and an increase of *Slope* and *Ratio.* However, the *AUC* was about the same no matter the maximum pressure. For LM and MCC the *AUC* decreased as the pressure was decreased. which was caused by the pronounced decrease in convexity at lower pressure levels. This showed again that the *AUC*

is a product of several other parameters, each with its own implications: the *%iER* which is indicative of elasticity, *ΔUS* relating to the changes in pore structure between the compact at maximum compression and end of the immediate elastic recovery, and A_C which could possibly indicate differences in the pore size increase in radial direction during the decompression process.

3.3.4 Correlating Ultrasound Parameters and Tablet Properties

As the velocity through tablets of MCC and LM and their binary mixtures has been shown to correlate with their tensile strength (Xu et al., 2018a), it is a possibility that the decompression signal could offer insights into the tablet strength as well. A comparison of the out-die parameters of tablets compacted from the mannitol grades previously used in Chapter 3.1.6 at 250 MPa is shown in Figure 3-52. The tensile strength decreased from Parteck M 200 at 4 MPa, over Pearlitol 200SD at 3.6 MPa and Parteck Delta M at 3.2 MPa, to D(-)-Mannit at 1.6 MPa. The SF was reversely correlated to the tensile strength. This showed that low porosity does not necessarily equal high tensile strength.

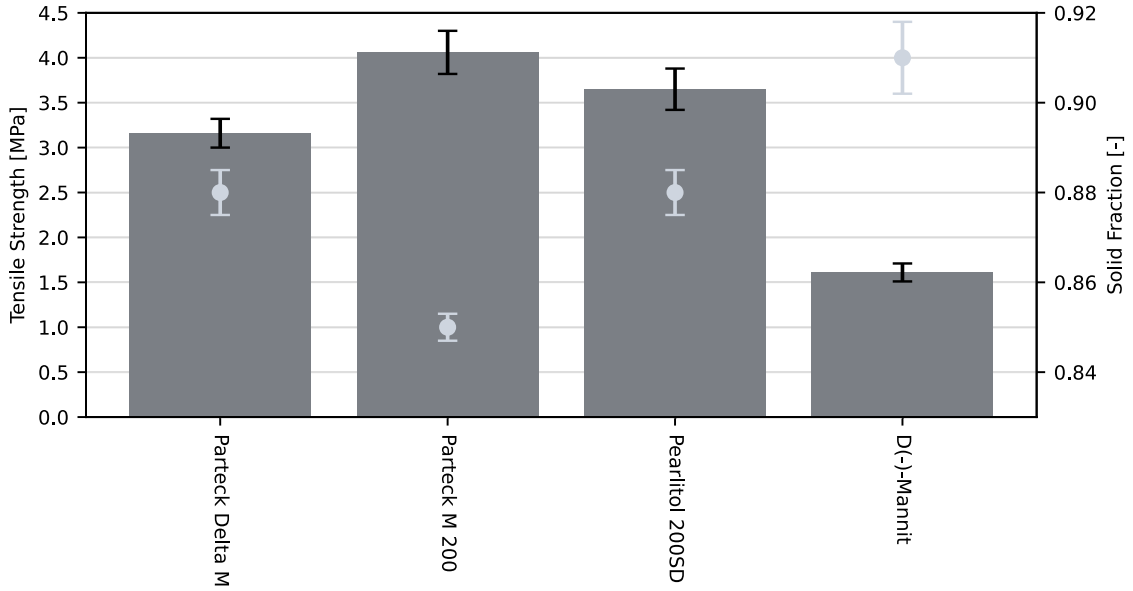

Figure 3-52: Tensile strength (bars) and out-die SF (markers) of the four mannitol grades 24 h after compaction. Arithmetic mean ± sd (n = 10).

When looking at the decompression parameters, a reverse correlation between the parameters incorporating the velocity decrease and the tensile strength could be seen. A direct comparison between the TS and one exemplary parameter – the *AUC* – is shown in Figure 3-53. As a pronounced drop in velocity could be indicative of pronounced changes in the pore structure of the tablets during decompression as discussed before in Chapter 3.3.2.5, the *AUC* relates to the pore size increase during decompression, as well as the elasticity, both of which could negatively affect TS.

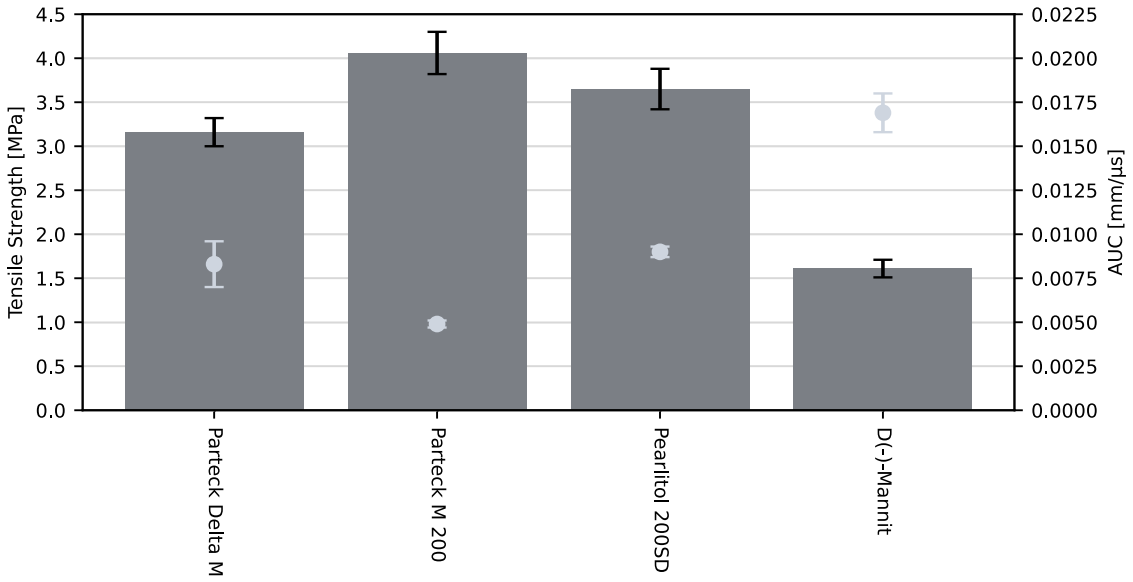

Figure 3-53: Tensile strength (bars; n = 10) and AUC calculated using the longitudinal signals (markers; n = 3) of the four mannitol grades. Arithmetic mean ± sd.

However, this tendency could not be seen when comparing different materials to one another. The tensile strength and *AUC* of five different excipients are shown in Figure 3-54. The second highest *AUC* was exhibited by MCC which at the same time produced the strongest tablets by far. At the same time ACP showed the second lowest value while yielding the weakest tablets. As the *AUC* also incorporates the elastic recovery of a material and MCC was shown before to be one of the more elastic substances used in this work and ACP the least, these results were not surprising. The elasticity of a substance, or the lack thereof, is then not necessarily indicative of the tablet strength.

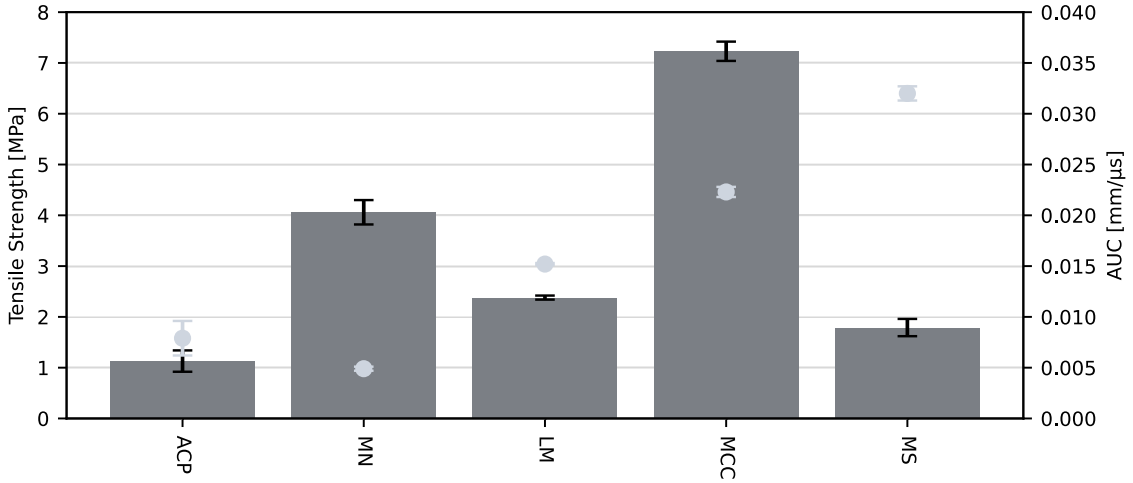

Figure 3-54: Tensile strength (bars; n = 10), and AUC calculated using the longitudinal velocity profiles (markers; n = 3) of six different excipients. Arithmetic mean ± sd. ACP = anhydrous calcium phosphate, MN = Parteck M 200, LM = Tablettose 100, MCC = Vivapur 101, MS = maize starch.

Only using the velocity drop as displayed in Figure 3-55 did not explain the differences in strength either. The value of MCC was close to those of ACP and LM. This implies that the changes undergone by the compact are not the only factor that needs to be kept in mind when assessing the tablet strength. While the microstructure change might have an influence on the strength as shown by the mannitol grades it was not capable to explain differences between materials which possibly exhibit different bonding strength. This agrees with Firestone (1946) who made a similar observation when comparing the strength of welds. In addition, the transmission measurements performed with the KIM set-up are not capable of measuring the velocity during ejection, where additional changes are undergone by the compact (DeCrosta et al., 2001), as the upper punch is not in contact with the sample anymore. Similar to other parameters determined in-die such as immediate elastic recovery, or the yield pressure, no direct assumption about the tablet strength can be made based on the ultrasonic parameters alone, as the pore size increase is just one factor of many playing into the formation of the final compact.

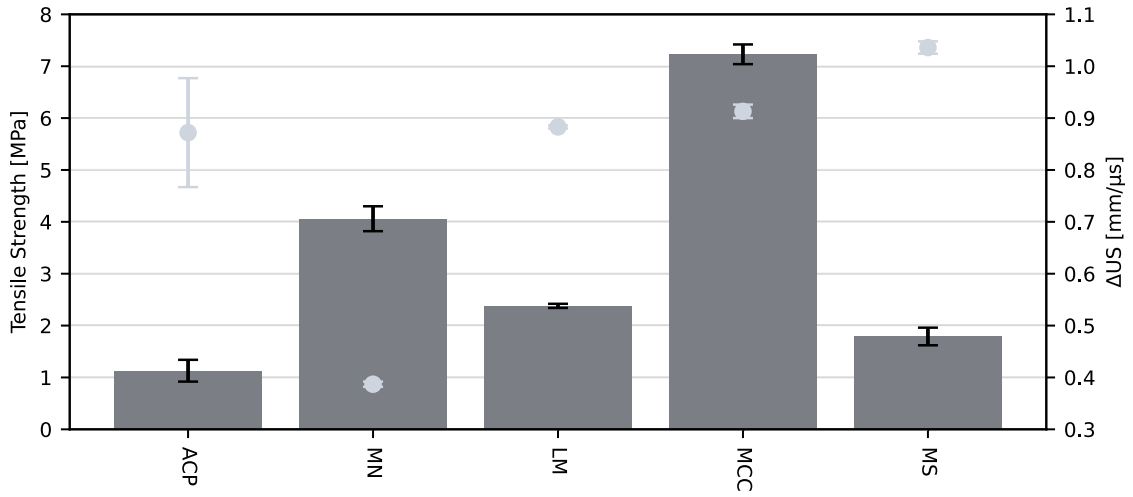

Figure 3-55: Tensile strength (bars; n = 10) and longitudinal velocity drop (markers; n = 3). Arithmetic mean ± sd. ACP = anhydrous calcium phosphate, MN = Parteck M 200, LM = Tablettose 100, MCC = Vivapur 101, MS = maize starch.

3.3.5 Summary

The decompression signal of the velocity profiles is caused by the elastic relaxation of the material when the stress is decreased. It was found to be characteristic for the materials under investigation. Since it is indicative of the volume increase of the compact during unloading, it can be consulted to quantify the immediate elastic recovery. The main benefit here compared to the determination using force and displacement data was the complete stop of the signal once the contact between punches and compact was lost, which made the determination of the loss of contact fairly easy. Furthermore, the velocity does not drop to zero after compression like the pressure. The velocity decrease as well as the velocity before the signal stops could then give

additional information about the structure of the compact. In addition to the absolute increase in pore volume, the different relationships between SF and velocity of different materials could be indicative of the changes in the pore structure which in turn could be one of the factors determining the performance of the finished tablets.

Of all the parameters proposed to describe the decompression signals, the AUC_{Full} showed the highest correlation to the complete elastic recovery, while the *AUC* was possibly the most exhaustive descriptor of the decompression signal as it incorporates shape, velocity decrease and SF decrease. This, however, also shows one of the drawbacks of the decompression parameters: They are often related to multiple factors. The *AUC*, e.g., increases if the *%iER* increases, but also if *ΔUS* is more pronounced. The *AUC* is, thus, indicative of both, elasticity of the material, and changes in pore structure, which are not necessarily correlated. One factor alone does, therefore, not offer the full picture of the decompression process.

The *AUC* parameter was in good agreement with the tensile strength of the different mannitol grades. The higher the *AUC* the lower the strength of the tablets. This indicated that the more pronounced changes in microstructure resulted in weaker tablets. However, these findings could not be confirmed when different substances were compared. Especially MCC did not behave in the same manner. Even though it showed pronounced elastic recovery and the resulting pore expansion, the tensile strength was about three times as high as LM. This could either mean MCC showed a higher number of bonds between particles, or the bonds that were retained during decompression were stronger. The *AUC* alone is, therefore, not capable of estimating the tensile strength exhibited by the tablets comprised of the material.

3.4 Excipient Blends

It has been shown that the ultrasonic velocity during compaction, or to be more specific the velocity profile, is dependent on the material in use. Since the finished drug product will always contain a combination of API and different excipients to improve the tablet and flow properties, investigating the interactions between the materials and the impact of the different substances on the process is of high interest during the development phase. However, all experiments so far were performed using single components. In this chapter the profiles of samples containing more than one material in the solid phase are shown.

3.4.1 Internal Lubrication

Figure 3-56 shows the KIM results of internally lubricated samples as well as the previously shown externally lubricated materials. In the tested range between 0 and 2% of magnesium stearate (MgSt) the velocity profiles of the samples were almost identical.

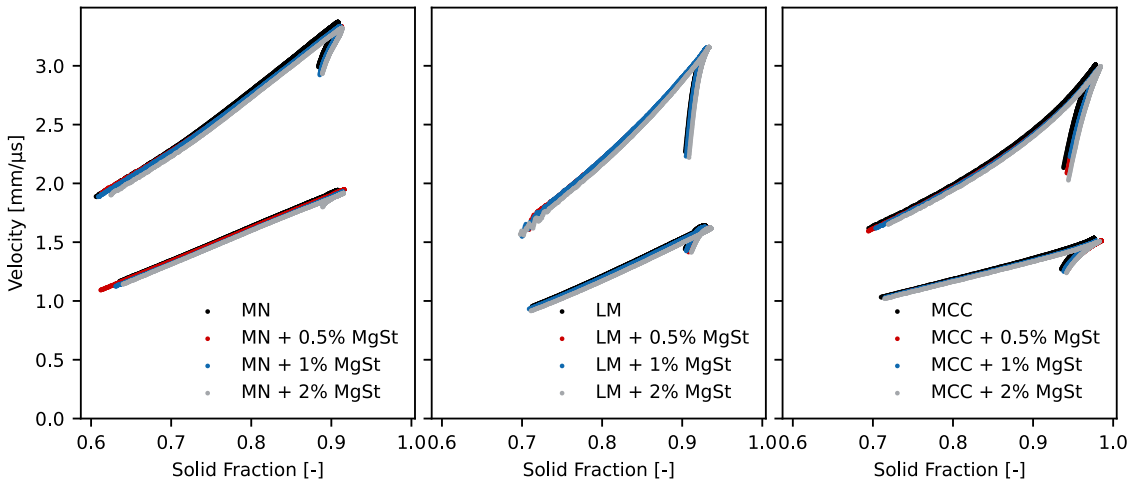

Figure 3-56: Longitudinal and transverse velocity through the lubricated samples (n = 3). MN = Parteck M 200, LM = Tablettose 100, MCC = Vivapur 101. Plots share y-axis. Published in Kern et al. (2022).

There was, however, a slight increase in relative deviations when comparing the samples containing different amounts of MgSt. The highest deviations could be seen for the longitudinal MN and the transverse LM results as seen in Figure 3-57.

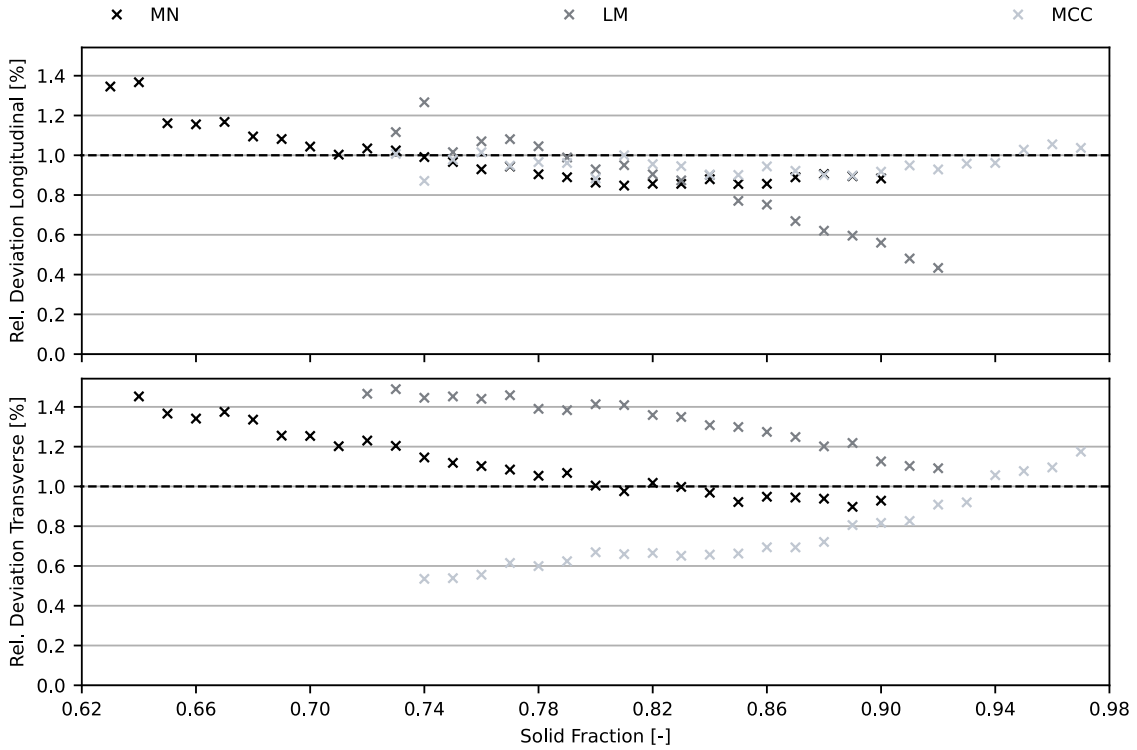

Figure 3-57: Relative standard deviations of longitudinal and transverse velocity through the materials. Non-lubricated materials and blends containing 0.5, 1 and 2% of MgSt (n = 12). MN = Parteck M 200, LM = Tablettose 100, MCC = Vivapur 101. Plots share x-axis. Published in Kern et al. (2022).

Figure 3-58 shows an excerpt of the compression phase of the longitudinal MN (a) and the transverse LM (b) velocity measurements of the different samples. If only the non-lubricated and 2% samples are compared, there seems to be a decrease in velocity with the addition of lubricant at the same SF. However, the 0.5 and 1% samples do not fit into this finding. For MN those two blends showed about the same velocity throughout the whole compression, albeit in between the other two samples. In case of LM, the velocity through the 1% mixture was higher than through the 0.5% blend. As with the different particle sizes there was no systematic change visible. This seems to indicate that there was no general effect of decreased velocity with increasing MgSt content in the observed range up to 2%. A similar observation was made by Hakulinen et al. (2008) who did not find a systematic influence of caffeine content up to 25% on the measured sound velocity through tablets of binary mixtures with starch acetate out-die.

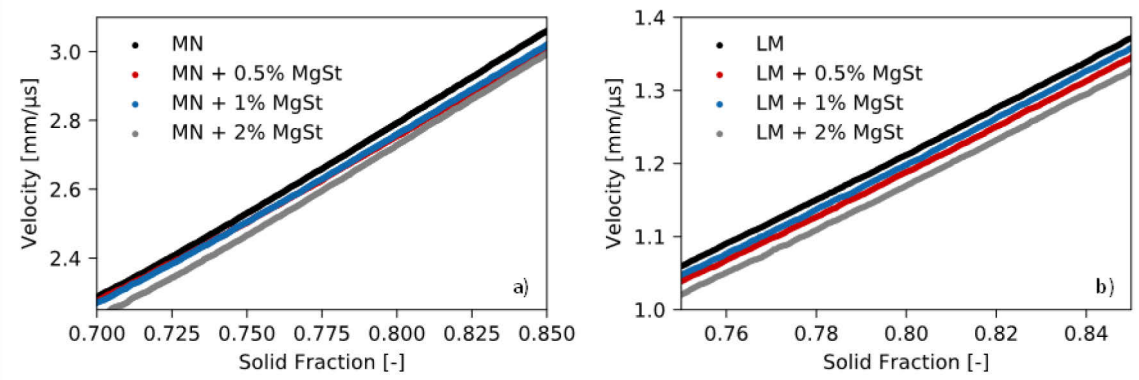

Figure 3-58: Ultrasonic velocity through blends containing varying amounts of lubricant: a) MN (Parteck M 200) in longitudinal mode, and b) LM (Tablettose 100) in transverse mode (n = 3). Published in Kern et al. (2022).

Leskinen et al. (2013) had previously found that ultrasonic measurements were sensitive to changes in the blending time of MgSt. They compared samples blended for 2 min and 10 min at 22 rpm and found an increase in measured velocity during compaction with increased blending time. They explained their finding by better acoustic coupling between particles through the MgSt which, over time, would more and more be pushed into smaller pores. As in the current work the blending times had been kept short to mimic those routinely used for pharmaceutical formulations (Rowe et al., 2009), this effect had probably not taken place, yet. An increase in velocity caused by a closing of pores does, however, align with the pore hypothesis proposed before.

3.4.2 Binary Mixtures Containing Two Fillers in Equal Amounts

In contrast to the results shown above where only small amounts of the second component were used, there was a pronounced change in the velocity profile when blends of two components in equal amounts were analysed using ultrasound as seen in Figure 3-59. As ultrasonic velocity is postulated to decrease when a second component is added (Krautkrämer and Krautkrämer, 1990) a velocity lower than either of the components could be expected. However, the velocity of the binary mixture seemed to be a mix of the velocity through its components which agrees with the measurements conducted out-die by Xu et al. (2018a) who reported similar results in the low porosity range. In both measurement modes the velocity at a given solid fraction was in between its respective raw materials. For MN and LM (a+d) the increase was almost parallel. In the case of MN and MCC (b+e) the velocity discrepancy increased with increasing SF. The LM and MCC samples showed a similar behaviour in longitudinal mode (c), although the velocity towards the beginning was almost identical. In transverse mode (f) the velocity profiles crossed during compression. Below 0.78 the velocity was higher through MCC, above the velocity was higher through LM. This could be explained by the SOS through a porous solid being influenced by the

velocity through the material itself as well as the pore structure. Below the mentioned SF threshold, the pore structure was then mainly responsible for the overall velocity. One possible cause is a comparatively high number of interconnections or a more horizontal orientation of the pores, both of which would obstruct the most direct pathway the sound wave could take through the compact in axial direction. At higher solid fractions when there are less pores obstructing the sound wave's path, the velocity through the material, which is in all likelihood higher through LM, probably becomes the more influential factor. Due to the limitations of the KIM system concerning the maximum pressure which could be applied during compression, it was not possible to measure the velocity through the materials at higher solid fractions to get a better idea of the speed of sound through a non-porous sample, i.e., SF = 1. Therefore, the higher velocity through LM is an assumption based on its lower elasticity compared to MCC. While the velocity is influenced by both components, at first glance there seemed to be a tendency towards the profile of the LM/MCC blend being closer to the one of plain LM.

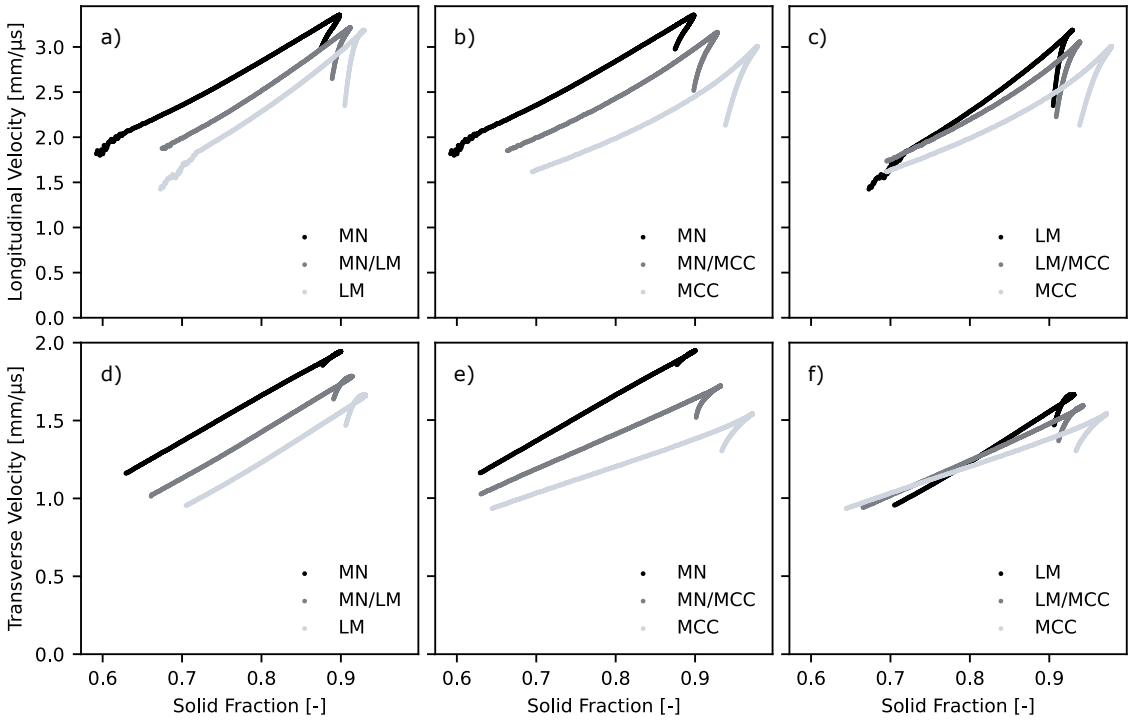

Figure 3-59: Longitudinal (top) and transverse (bottom) velocity through binary mixtures (50:50 %w) and their components (n = 3). MN = Parteck M 200, LM = Tablettose 100, MCC = Vivapur 101. Published in Kern et al. (2022). Plots in one row share y-axis; plots in one column share x-axis.

The velocity increase during compression is depicted in Figure 3-60. In all cases and both modes the determined slope values of the binary mixtures were between the ones of their components. It is interesting to note that while the longitudinal signal shape of the LM/MCC blend seemed more similar to LM in Figure 3-59 due to the proximity of the two curves, the determined slope was actually closer to the slope of the MCC profile. Since MCC is the softer of the two materials, this

could be caused by a more pronounced deformation of MCC at the same pressure level, meaning the overall structure is more defined by the softer, more plastically deforming material (Ilkka and Paronen, 1993). The steepest increase was, as expected, exhibited by the MN/LM blend as the inclusion of MCC decreased the slope. If the compression slope is as hypothesised indicative of the deformation behaviour of the material, this approach could be used to track those changes in the overall behaviour of the blends with varying concentrations of the components.

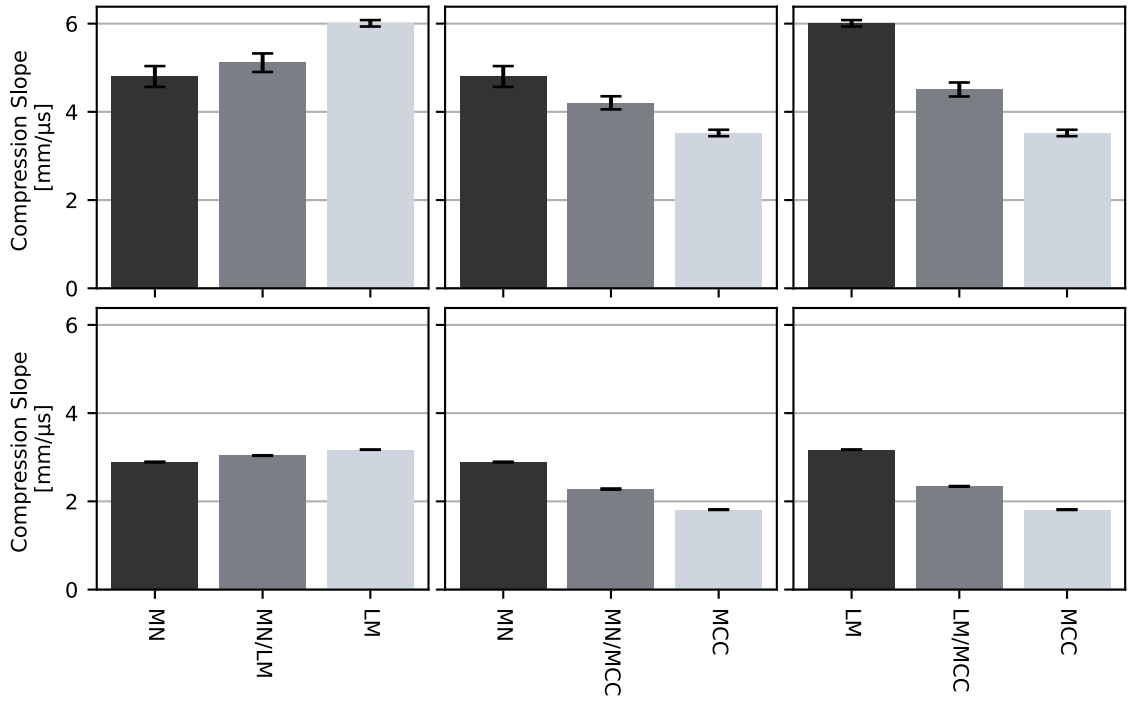

Figure 3-60: Slope of the compression signal using the longitudinal (top) and transverse (bottom) ultrasonic velocity. Arithmetic mean ± sd (n = 3). MN = Parteck M 200, LM = Tablettose 100, MCC = Vivapur 101. Plots in one row share y-axis.

A similar observation can be made when comparing the classic Heckel plots and the yield pressure derived thereof as shown in Figure 3-61. The yield pressure of the blend was in all cases in between the single components of which the mixture was comprised. A dependency of the yield pressure of a binary mixture on the respective components has been observed before, although not necessarily linear in nature (Ilkka and Paronen, 1993; Roopwani and Buckner, 2011). However, as it cannot be expected to see an actual change in the material properties of the single particles it can be surmised that the yield pressure of the mixture is an average of all the particles being compacted.

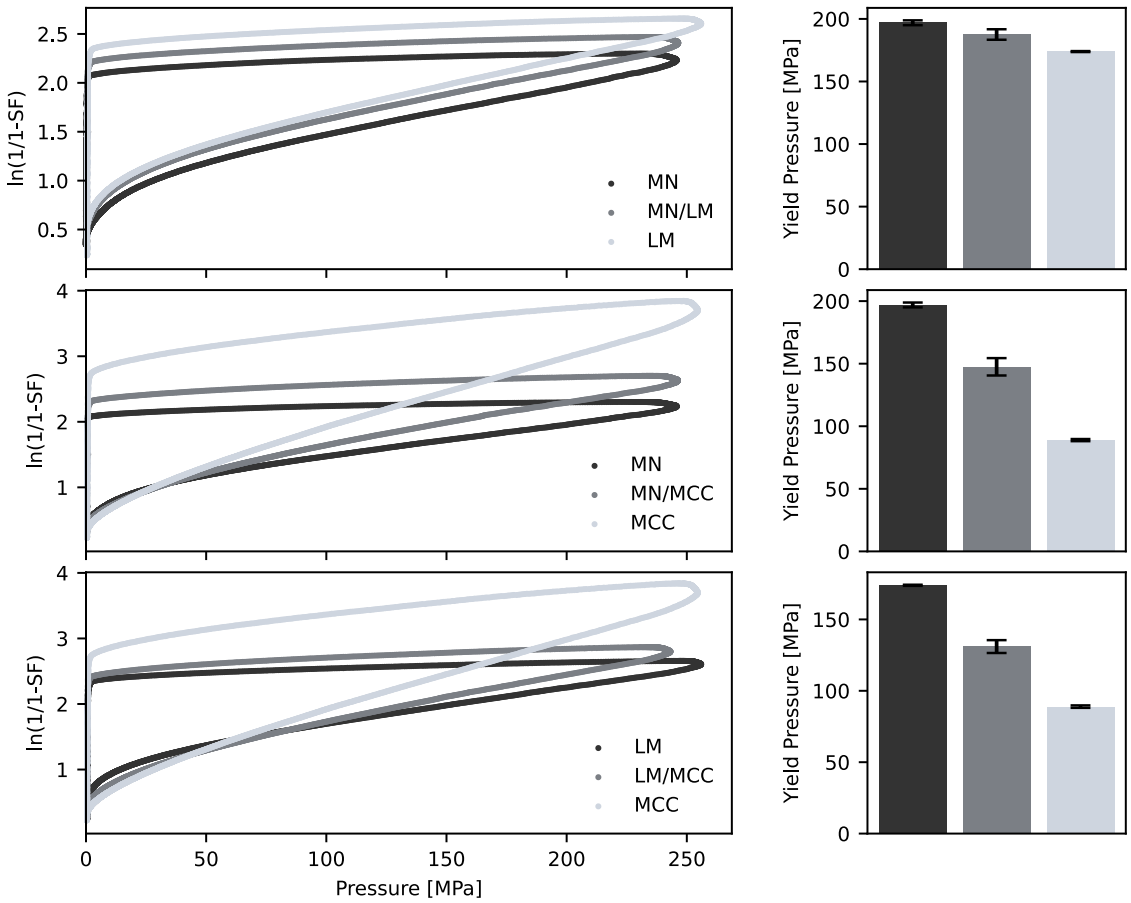

Figure 3-61: Heckel plots determined using the displacement values measured during the ultrasonic measurements (left) and the yield pressure thereof (right). Yield pressure: Arithmetic mean ± sd (n = 3). MN = Parteck M 200, LM = Tablettose 100, MCC = Vivapur 101. Plots in one column share x-axis.

The decompression parameters are depicted in Figure 3-62 and Appendix Figure A-14. As with the compression slope, the decompression parameters of the blends were between the ones of their components. Concerning elasticity, the less elastic substances (MN and LM) seemed to influence the *%iER* slightly more than the more elastic MCC. The same could be observed for the *AUC* and AUC_{Full}, where the values were closer to LM and MN than MCC. Even though the curves were clearly different for the substances, some parameters were rather similar. Those were *%iER* and AUC_{Full}, the parameters previously associated with elasticity, for the MN/LM samples and *ΔUS* which is thought to be indicative of the changes in pore structure within the sample for LM/MCC, however only in longitudinal mode. This further illustrates that it is not possible to use just one parameter to fully understand the changes caused by the addition of a second component. The ultrasonic parameters could, however, help in the identification of factors influencing the performance of the finished tablets made of more than one component.

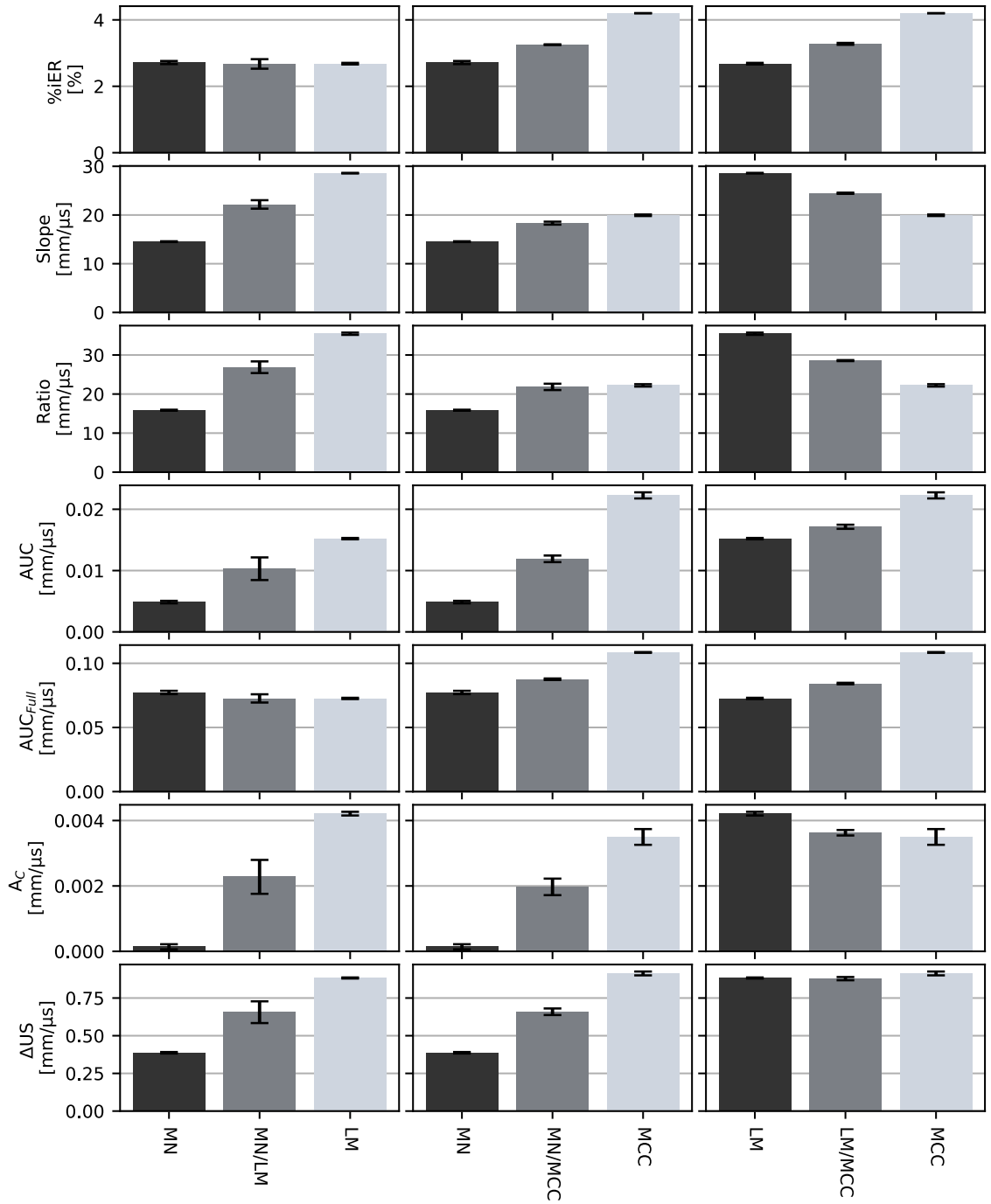

Figure 3-62: Decompression parameters calculated using the longitudinal velocity profiles. Arithmetic mean ± sd (n = 3). MN = Parteck M 200, LM = Tablettose 100, MCC = Vivapur 101. Plots in one row share y-axis.

Several authors have so far correlated the TS and SF of single components to binary mixtures thereof (Busignies et al., 2006; Michrafy et al., 2007; Patel and Bansal, 2011; Schmidtke et al., 2017; Van Veen et al., 2000). Wu et al. (2005a) for example could predict the TS of binary mixtures using the volume fraction and the parameters of the Ryshkewich-Duckworth equation (Duckworth, 1953). As the correlation between tablet performance, expressed through the tensile strength, and proportion of the components is not necessarily linear (Sun, 2016), the question was

whether the US profiles might give an indication towards which component the tensile strength of a binary mixture might lean.

The parameter that could be correlated with tensile strength in the case of the different mannitol grades was the *AUC* (refer to Chapter 3.3.4). As seen in Figure 3-63 the tensile strength of the binary mixtures was right between the respective components. Especially the addition of MCC improved the strength of the resulting tablets which agrees with the finding of other authors (Jetzer, 1986; Kim et al., 1998). The *AUC* on the other hand was not, which was especially apparent for the LM/MCC blend. While the tensile strength doubled with the addition of MCC to LM, the *AUC* did only slightly change. In addition, the *AUC* of MCC was higher than that of either LM or their blend, which is at odds with the results shown by the mannitol grades where an increase in *AUC* corresponded to a lower tablet strength. Using this parameter to determine which of its components a binary mixture resembles most, and especially which material exhibits the higher tensile strength, was, therefore, not successful. This is in line with the findings before in Chapter 3.3.4 where Parteck M 200 and Vivapur 101, the two materials reaching the highest tablet strengths, showed the highest discrepancy in the *AUC* value.

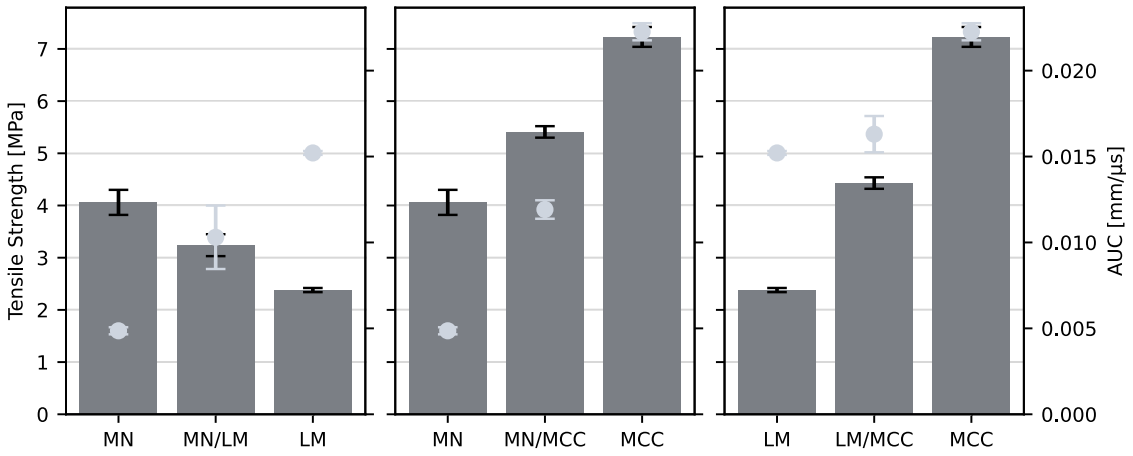

Figure 3-63: Comparison of tensile strength (bars) and *AUC* calculated using the longitudinal velocity profiles (markers) of the binary mixtures and their components. Arithmetic mean ± sd (n = 3). MN = Parteck M 200, LM = Tablettose 100, MCC = Vivapur 101. Plots share both y-axes.

3.4.3 Binary Mixtures of Changing Composition

Three additional sets of binary mixtures with gradually changing composition were compared. The components were ACP, MCC (Vivapur 101) and MS. They were chosen as they represent materials with vastly different compaction properties: brittle, ductile and elastic, respectively. The results of the measurements are depicted in Figure 3-64. The blends containing ACP and MCC showed a gradual change with increasing MCC content in both measurement modes (a+d). The maximum SF increased while the maximum velocity decreased. The shape of both compression

and decompression also changed with increasing MCC content. The behaviour of the ACP/MS blends (b+e) showed similar trends. However, while the blends containing MCC were evenly fanned out between the raw materials, those containing MS were shifted towards MS on the x-axis. In addition, the transverse signal during compression became shorter with an increasing proportion of MS probably owing to the increased water content introduced into the blend through MS.

As the longitudinal MCC and MS velocity profiles were very similar to begin with (refer to Figure 3-12), their binary mixtures (c+f) did not show as much variability as the blends containing ACP. In transverse mode there was a decrease in velocity and a later signal start with increasing MS content visible in all likelihood caused by the increased water content with the addition of more MS. The only exception concerning the velocity decrease was the 75% MCC blend which was almost identical to 100% MCC profile. In longitudinal mode, this blend showed a slightly higher velocity and a lower SF compared to its raw materials. However, it needs to be kept in mind that the pycnometric density determined for this particular blend was also higher as seen in Appendix Table A-4. As mentioned before, the determination of the true density used for a material containing high amounts of water can be problematic. It is, therefore, possible that the observed higher velocity was caused by a shift of the curve on the x-axis due to a density value too high. Nevertheless, the shape of the signal could still be assessed.

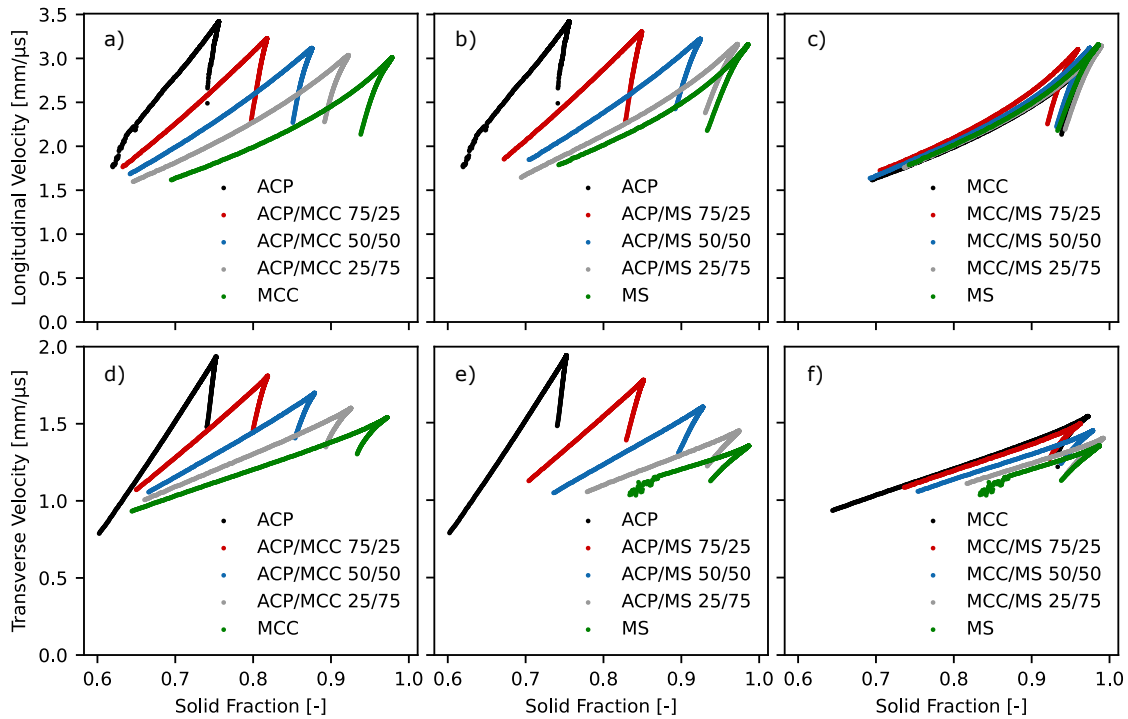

Figure 3-64: Longitudinal and transverse velocity through binary mixtures and their respective components with varying composition (n = 3). The numbers denote the composition of the blends in %w. ACP = anhydrous calcium phosphate, MCC = Vivapur 101, MS = maize starch. Plots in one row share y-axis; plots in one column share x-axis.

To better assess the MCC/MS blends, the velocity profiles were shifted on the x-axis (Figure 3-65). There was an increase in maximum velocity with increasing MS content visible. At the same time the decompression signal became slightly longer and less steep.

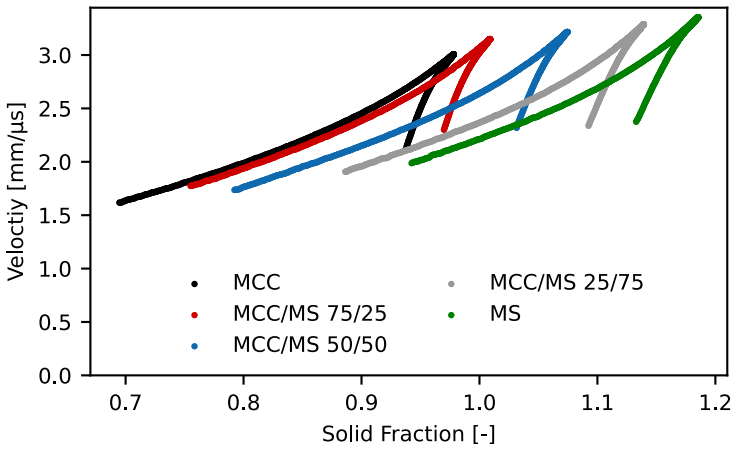

Figure 3-65: Longitudinal velocity through MCC, MS and their respective blends (n = 3). The results are shifted on the SF axis by 0.05 (25/75), 0.1 (50/50), 0.15 (75/25) and 0.2 (MS). MCC = Vivapur 101, MS = maize starch.

As with the binary mixtures in Chapter 3.4.2, the intermixture of a second component did not generally decrease the measured velocity through a material. In the case of MCC/MS the measured velocity did not change at all, while the addition of as little as 25% ACP even increased the velocity compared to both, MCC and MS. This contrasts the findings of Leskinen et al. (2013) who reported a decrease in velocity through binary mixtures of MCC and paracetamol with increasing API content which is in line with the general assumption that the inclusion of a second component decreases the sound velocity through a matrix (Krautkrämer and Krautkrämer, 1990). However, they did note, that this could partially be caused by the difference in porosity. Additionally, they did not measure the velocity through 100% paracetamol. It is, therefore, possible that the decrease was caused by an overall lower velocity through the API. Hakulinen et al. (2008) on the other hand found no change in longitudinal velocity through tablets of binary mixtures of starch acetate and caffeine with a caffeine content as high as 25% at the same SF. However, they also did not measure the velocity through tablets of pure caffeine. One possibility for their observation is then that the overall velocity is similar through the two materials similar to what was observed for MCC and MS.

With the velocity, the elasticity parameters also gradually changed, shown here on the example of the ACP/MCC blends in Figure 3-66. The other two combinations can be found in Appendix Figure A-9 and Figure A-10. YM and SM were fanned out between the components, all increasing with decreasing porosity implying an increased resistance against deformation. The calculated

values resembled more closely the raw component with the higher elasticity, MCC and MS, respectively. This agrees with Bassam et al. (1991) who found a deviation from a linear relationship of the YM and amount of the respective components, favouring the more elastic material. The PR, however, changed in shape. While it decreased for ACP as the compression progressed, it increased for all blends containing MCC, gradually increasing the slope with MCC content. The two combinations containing MS showed similar behaviour. In the case of the MCC/MS mixture though, both blends containing 75% of one component showed pronounced similarities in the progression of the YM and SM to the plain excipient of the same material. Since they both use the transverse velocity for the calculations, this was expected, as the measured velocity during compression of especially the 75% MCC blend was almost identical to the 100% MCC measurement.

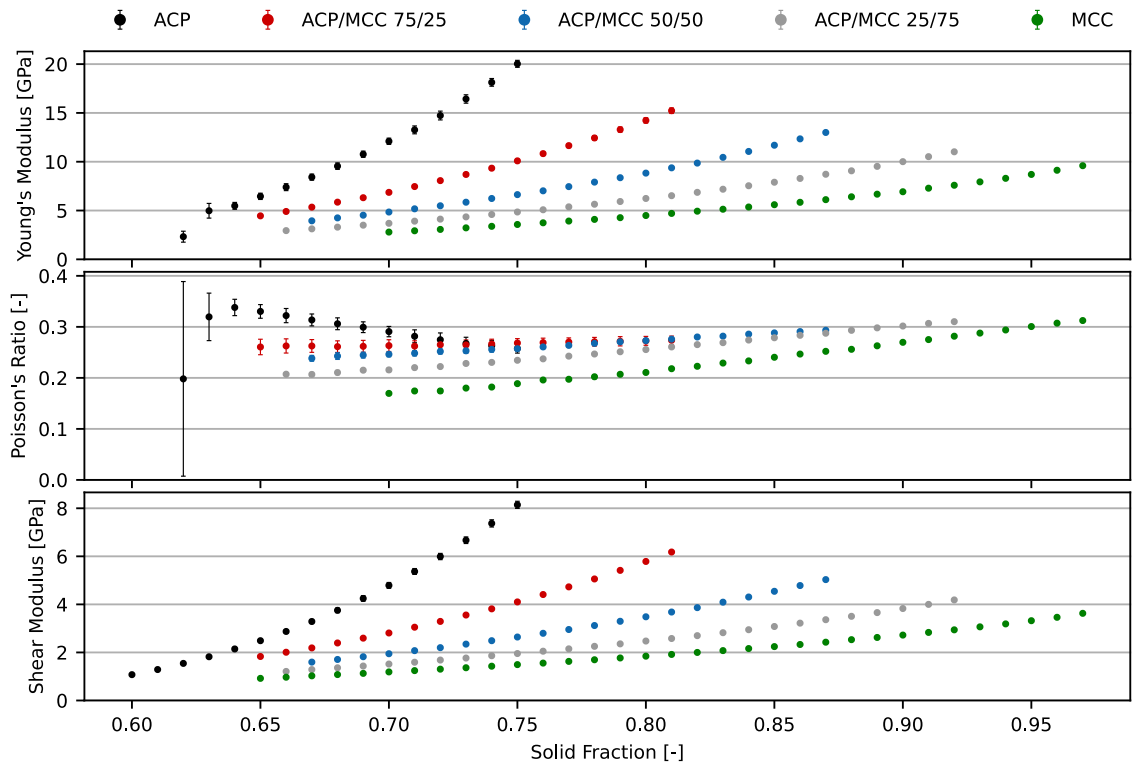

Figure 3-66: YM, PR and SM calculated for ACP (anhydrous calcium Phosphate), MCC (Vivapur 101) and their blends. Arithmetic mean ± sd (YM and PR: n = 9; SM: n = 3). Plots share x-axis.

The slope of the initial velocity increase is depicted for all materials in Figure 3-67. For the mixtures containing ACP the slope became less steep with increasing amount of the second component. In both cases there was an almost exponential decrease of the slope with decreasing amount of ACP. The MCC/MS blends showed opposite behaviour in longitudinal and transverse mode. While there was an increase of the slope of the longitudinal velocity with increasing MS content, there was a decrease in transverse mode. One possible explanation is the difference in length and consequently the number of datapoints used for the determination of the compression

slope. As there was a divergence from a linear trend observed in the high SF range as shown in Chapter 3.2.1, primarily for the longitudinal velocity profiles, the lower number of datapoints in the low SF rage measured when starch was included in the blend, could explain the slightly higher slope values.

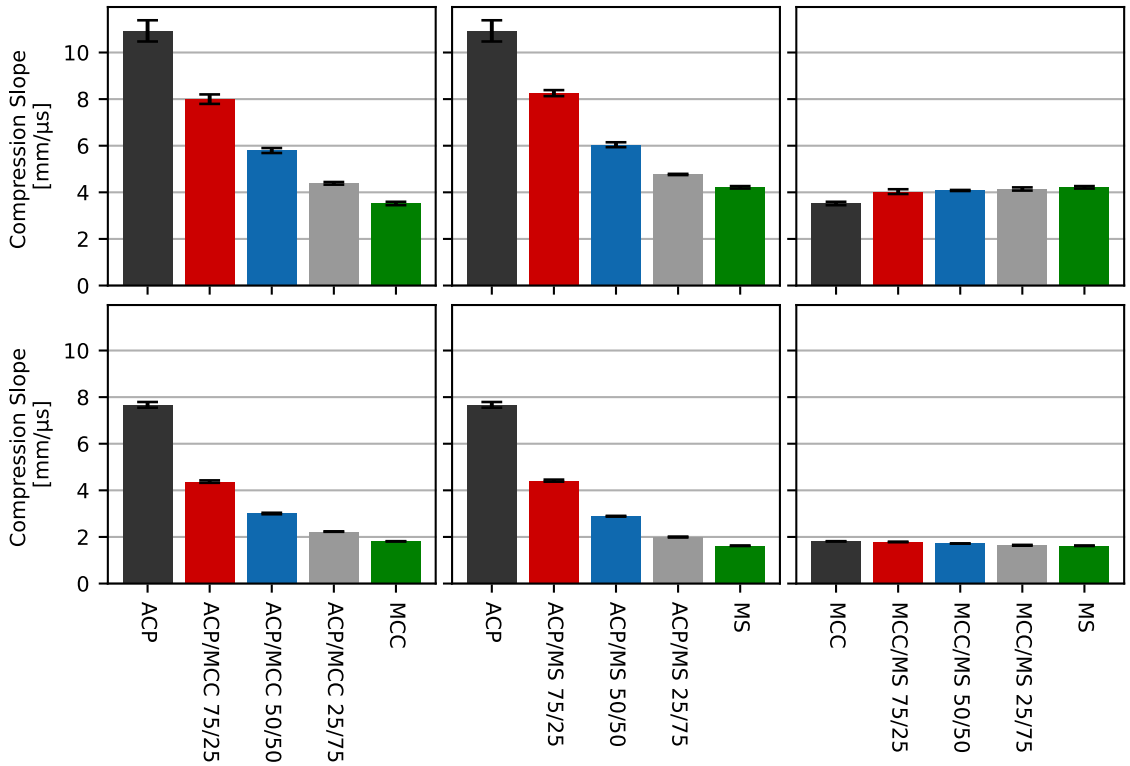

Figure 3-67: Slopes of the compression signal calculated as described in Chapter 3.2.1. Top: Longitudinal; Bottom: Transverse. Arithmetic mean ± sd (n = 3). ACP = anhydrous calcium phosphate, MCC = Vivapur 101, MS = maize starch. Plots in one row share y-axis.

The true density of ACP is much higher than the density of the other materials. This results in a discrepancy between weight and volume percent which could explain the non-linear decrease of the slope with decreasing ACP content. Figure 3-68 depicts the relationship between calculated slope and amount of secondary component in weight and volume percent. The correlation between compression slope and %V was better compared to %w. As the volume more closely corresponds to the distance the sound wave needs to travel through this might be expected.

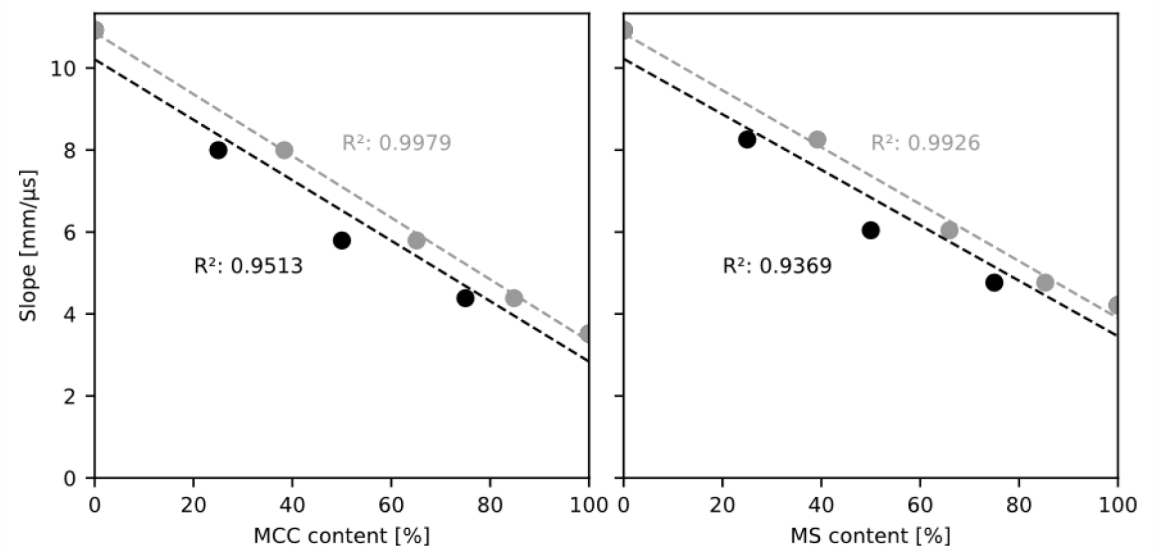

Figure 3-68: Slope of the compression curve as a function of a) MCC (Vivapur 101), b) MS (maize starch) content in combination with ACP (anhydrous calcium phosphate). Black: %w; Grey: %V. Arithmetic mean ± sd (n = 3). Plots share y-axis.

In addition to the compression parameters, the decompression parameters of the blends were determined as well. An overview is shown in Figure 3-69 for longitudinal measurements and in Appendix Figure A-15 for transverse. For most parameters there was a gradual change with an increasing amount of the second component. The one exception was the drop in velocity during decompression of the binary ACP mixtures: the blends containing 75% of ACP had in both combinations the most pronounced drop, while the 25% ACP blends exhibited less velocity decrease than either of the components. The velocity drop of a mixture is then not necessarily a combination of its components. However, this was only the case for the longitudinal measurements. In transverse mode the blends were evenly fanned out between the raw materials with the exception of the blend containing 25% MS which showed a similar decrease as 100% ACP. The overall most noticeable discrepancy between longitudinal and transverse results concerned, again, ACP. While in longitudinal mode all parameters were rather close to the 75% blends, in transverse mode *Slope* and *Ratio* of 100% ACP showed values about twice as high as the 75% blend. It must be noted that of all materials ACP showed the highest standard deviation in longitudinal mode. The absolute values of the decompression parameters should, therefore, only be used cautiously in this case. Nonetheless, there was a tendency visible that *AUC*, AUC_{Full} and A_C, the parameters describing the shape of the signal, were more influenced by ACP than the respective second component, most noticeably for the blends containing starch. This was interesting to note as the decompression is, as mentioned before, indicative of the elastic recovery and ACP was in both combinations the less elastic component. Hence, the implication was that ACP hindered the elastic expansion of the second component which was at odds with the previous observation that the YM favoured the more elastic material. The MCC/MS parameters were

overall closer together as there was not as much a discrepancy between the two materials to begin with. It could be seen, however, that the blend containing 75% of MCC was in all parameters almost identical to MCC.

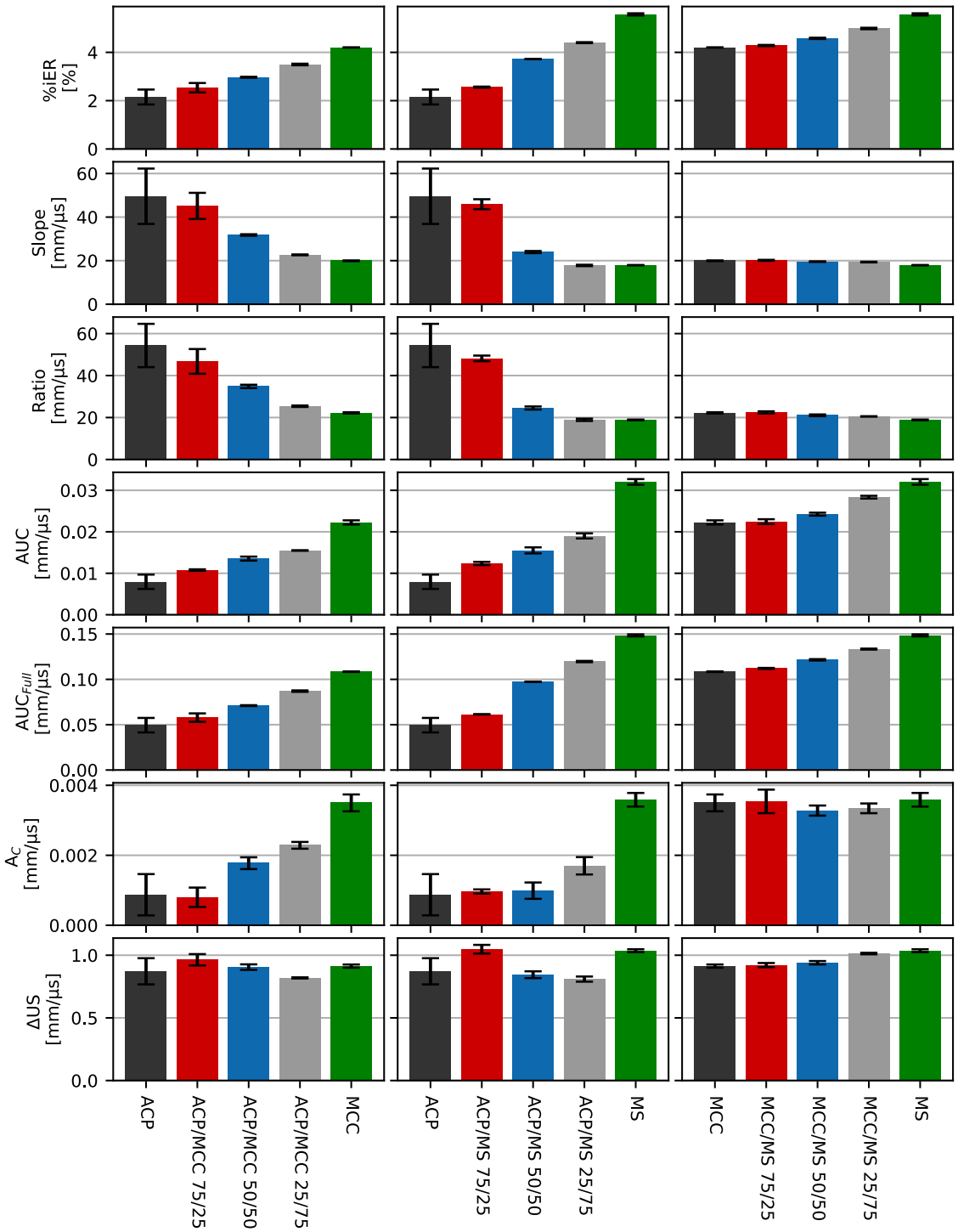

Figure 3-69: Decompression parameters calculated using the longitudinal velocity as described in Chapter 3.3.2. Arithmetic mean ± sd (n = 3). ACP = anhydrous calcium phosphate, MCC = Vivapur 101, MS = maize starch. Plots in one row share y-axis.

3.4.4 Velocity Profiles Through Two Components in Blends and Layers

When talking about the ultrasonic velocity through a mixture of materials one question that needs answering concerns the pathway of the ultrasonic pulse. Two scenarios are possible: a) There is a high impedance mismatch between particles of different materials which will result in high reflections and the arrival probability of the sound wave will be higher if the sound wave circumvents the material with the less favourable properties, or b) The sound wave will indiscriminately traverse both materials only slowed down by the pores. Scenario a) is favoured by the basic assumption mentioned before, that the inclusion of a second component generally lowers the SOS through a material (Krautkrämer and Krautkrämer, 1990). Although not clearly stated this implies the sound wave bypasses the foreign material, similar to what has been shown for pores in a solid matrix (Takatsubo and Yamamoto, 1991). However, as shown in Chapters 3.4.2 and 3.4.3, this was not the case for the binary blend of equal amounts of the two materials or a 75/25 %w ratio.

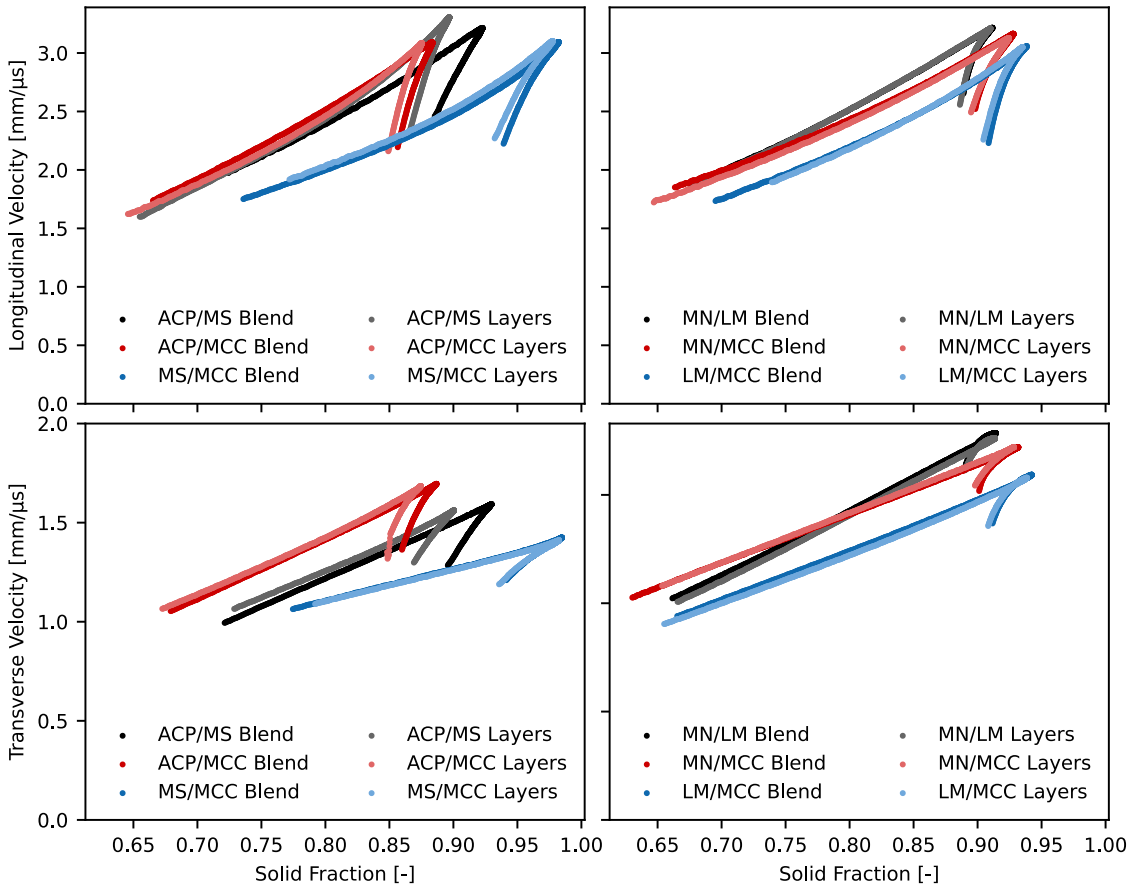

Figure 3-70: Longitudinal ultrasonic velocity through binary mixtures (50/50 %w) and two-layer tablets of MCC, MN and LM on the left, as well as MCC, MS and ACP on the right (n = 3). ACP = anhydrous calcium phosphate, MN = Parteck M 200, LM = Tablettose 100, MCC = Vivapur 101, MS = maize starch. Plots in one row share y-axis; plots in one column share x-axis.

In order to elucidate the propagation mechanism through the blend, experiments were performed in which the sound wave was forced to pass through both materials, by separating them into two distinct layers. When the ultrasonic velocity through a binary blend and through a two-layer tablet of the same composition as shown in Figure 3-70 were compared, the velocity profiles were basically identical in most cases. The only deviation could be observed if ACP was one of the components, especially when combined with MS.

When comparing the classic Heckel plots in Figure 3-71, it is visible that the blends and layers showed a similar behaviour. However, the MS/MCC combination showed more variation in the Heckel plot compared to the velocity profiles, owing to the slightly higher SF reached by the blend at the same applied pressure. One possible explanation could be that the amount of material was not entirely equal for the two layers. While the blends were prepared beforehand and thus had a consistent composition, the layers were added individually which could lead to inconsistencies. In addition, some material was pushed out of the die during compression which especially for the upper layer resulted in a decrease of material and a subsequent change in weight percent.

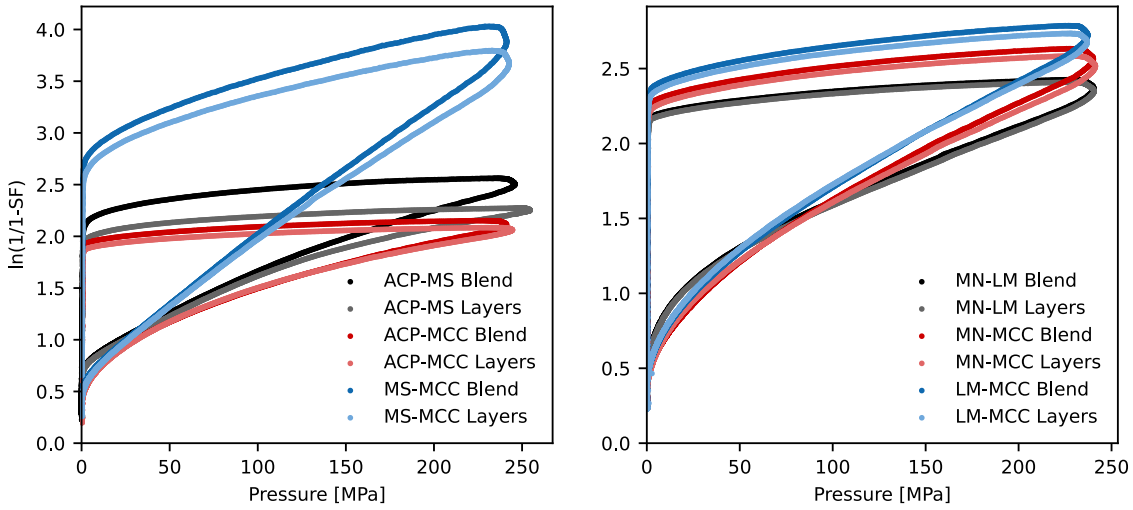

Figure 3-71: Heckel plots of the binary mixtures and layers (n = 3). ACP = anhydrous calcium phosphate, MN = Parteck M 200, LM = Tablettose 100, MCC = Vivapur 101, MS = maize starch.

Nonetheless, the overall close resemblance between the blends and layers in the velocity plots indicates the sound waves traverse both materials in a binary mixture. Additionally, this indicates the deformation of the single particles is, to a point, independent of the presence of a second material with different properties, e.g., hardness, in close proximity. The only obvious deviation was observed for the blends containing ACP. This could either signify the material exhibits substantially different acoustic properties, deformation behaviour, or both. As it was compacted with MS and MCC, both of which are markedly more elastic and also less dense, ACP is almost certainly the acoustically harder material which could lead to pronounced attenuation of the

signal if the sound wave passed between the two materials. It is, therefore, possible the arrival probability of the sound wave increased in this case if the acoustically softer material was circumvented. However, the Heckel plots also showed markedly different profiles. The second scenario where the different profiles are caused by the difference in compression behaviour between blends and layers can, therefore, not be excluded.

3.4.5 Ternary Mixtures

A tabletting mixture is usually composed of more than two components. Therefore, in addition to the binary mixtures shown above, three ternary mixtures were prepared to see whether there were tendencies visible concerning the calculated parameters in relation to the component concentrations. The results of the ultrasonic measurements are depicted in Figure 3-72. The ternary mixture of ACP, MCC and MS was closer to MS and MCC concerning the maximum SF and velocity. This was expected since the corresponding binary mixtures showed a similar behaviour. In addition, the volume fraction of ACP in this blend was only about 20%. However, the shape of the signal was clearly different compared to MS and MCC: the velocity was higher, the compression slope steeper, and there was no overlap towards the beginning of the decompression process with the compression velocity. This was the case for longitudinal and transverse velocity profiles, although there was a short range over which the transverse velocity through the mixture was almost the same as through MCC, albeit slightly steeper. In addition, in transverse mode, the compression signal was rather short compared to MCC, even though not as short as the starch signal.

For the second set of excipients, maximum velocity and SF were close to LM. The velocity increase during compression, however, was different. The increase was less steep, the velocity drop during decompression less pronounced and in transverse mode the velocity through the mixture was higher. One observable difference between longitudinal and transverse measurements was the maximum velocity: while it was lower than LM in longitudinal mode, it was slightly higher in transverse mode. It must be noted that in longitudinal mode the maximum velocity reached through the three components was overall closer than in transverse mode.

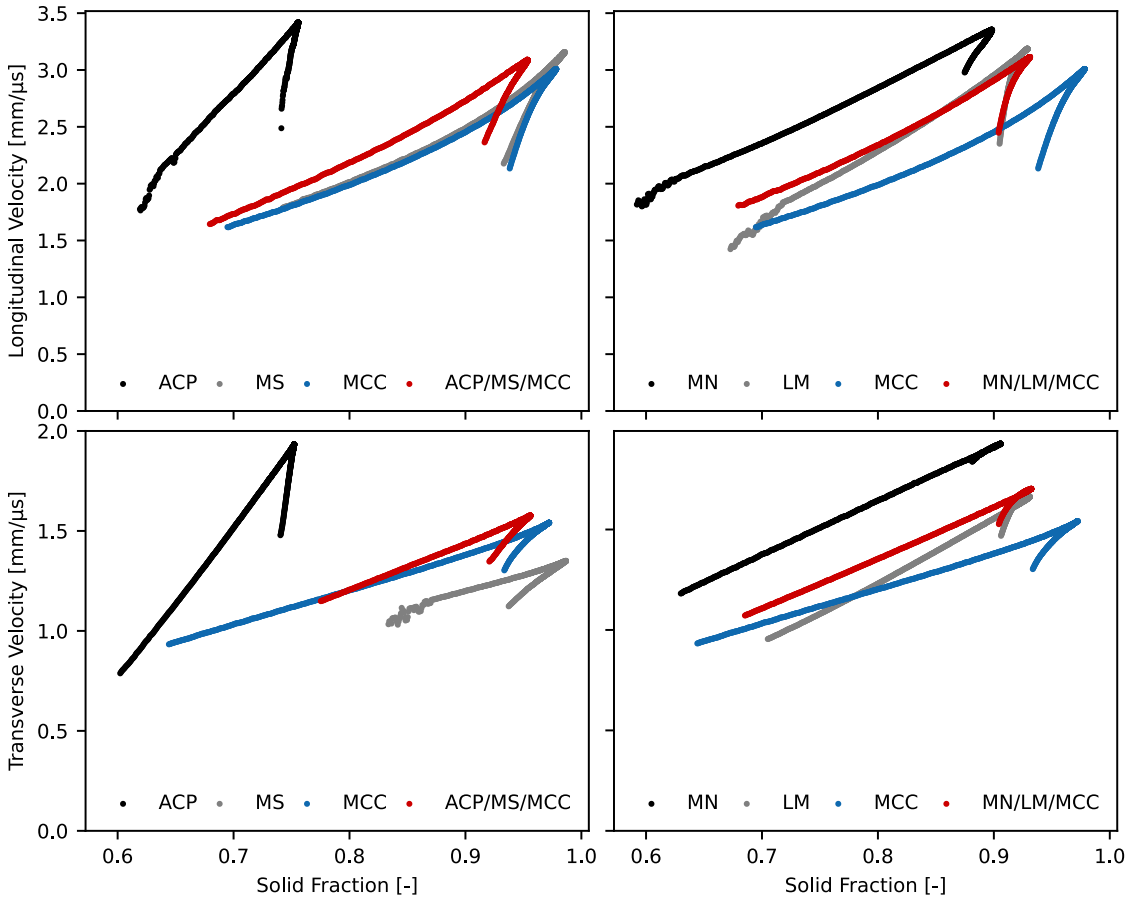

Figure 3-72: Ultrasonic measurements through ternary mixtures (red) and their respective components (n = 3). ACP = anhydrous calcium phosphate, MN = Parteck M 200, LM = Tablettose 100, MCC = Vivapur 101, MS = maize starch. Plots in one row share y-axis; plots in one column share x-axis.

To better compare the mixtures to their components, the compression slope was calculated and is shown in Figure 3-73. The steepest slope by far was shown by ACP, followed by LM. The two mixtures showed about the same rate of increase, slightly less steep than MN. This is interesting to see as it shows that the influence of ACP was not as pronounced as that of MS and MCC on the overall velocity increase. This can be related to the discrepancy between %V and %w fraction. The increase rate through the second mixture was right in between its components.

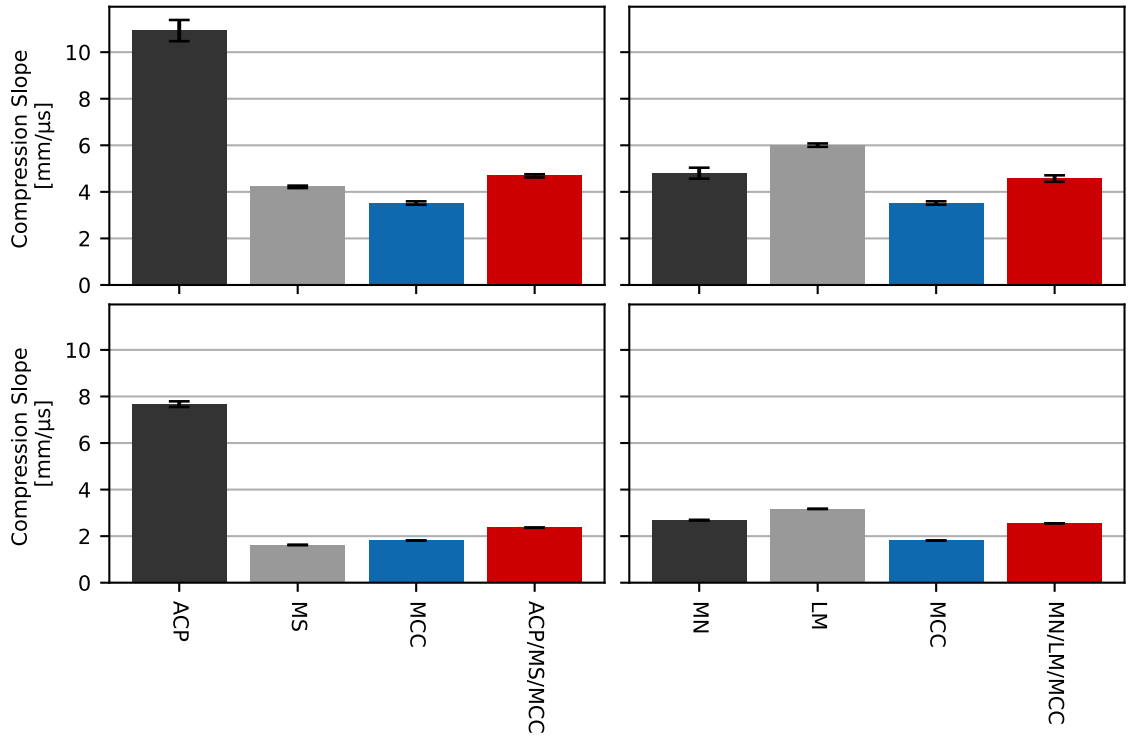

Figure 3-73: Compression slope calculated using the longitudinal (top) and transverse (bottom) velocity measurements. Arithmetic mean ± sd (n = 3). ACP = anhydrous calcium phosphate, MN = Parteck M 200, LM = Tablettose 100, MCC = Vivapur 101, MS = maize starch. Plots in one row share y-axis.

The decompression parameters calculated using the longitudinal velocity are depicted in Figure 3-74. For the ACP/MCC/MS set, the tendencies were similar to those previously observed for the binary mixtures. The decompression *Slope* and *Ratio* were similar to the elastic substances MCC and MS, while *AUC* and A_C were closer to the inelastic ACP. Only the AUC_{Full} was right in between the three materials. There was no similar tendency visible for the second combination. All parameters were a blend of the individual parameters of the components. The only notable exception was the A_C value which was almost as high for the blend as MCC, much higher than MN. This showed the curvature was more pronounced for the mixture than for MN.

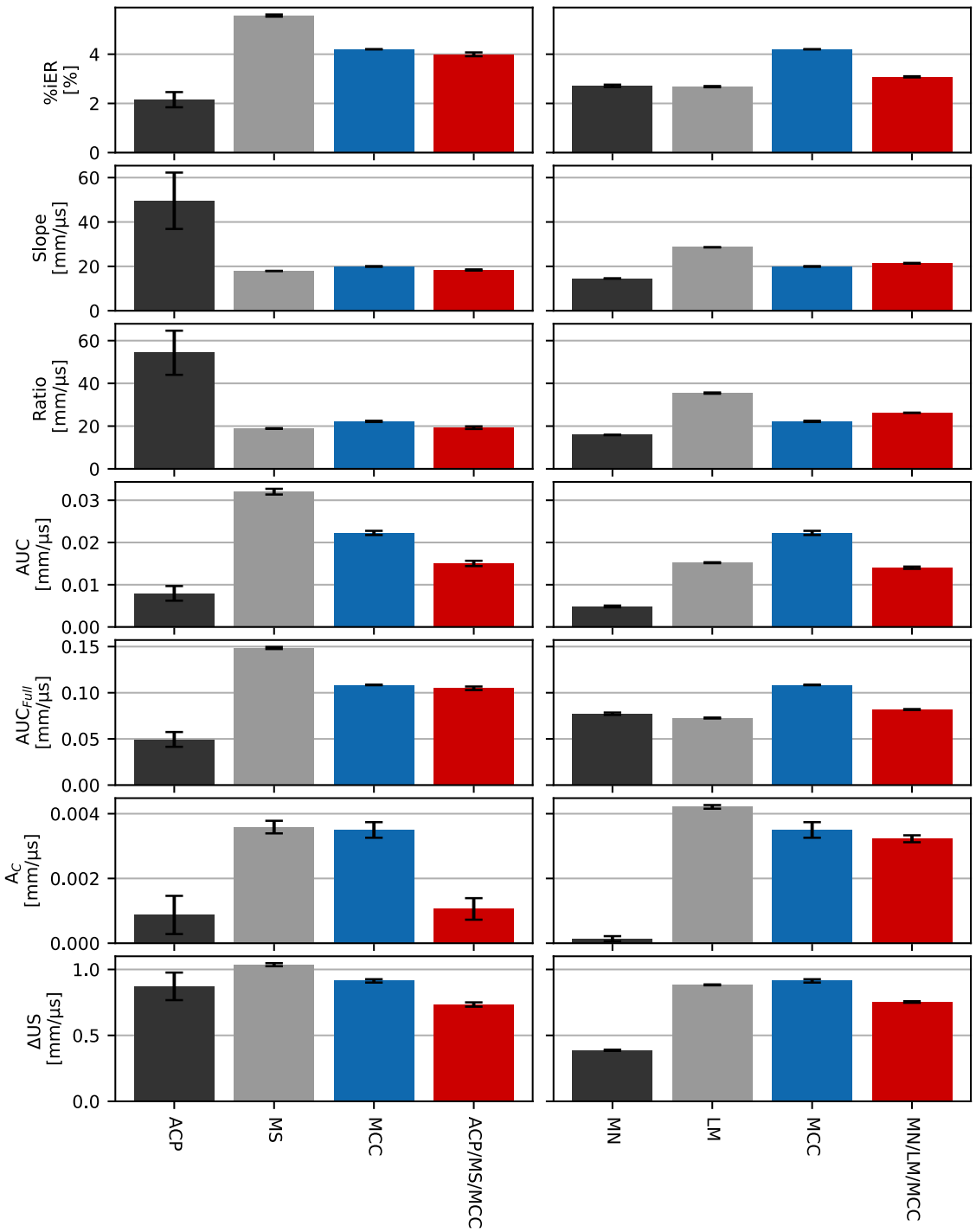

Figure 3-74: Decompression parameters calculated using the longitudinal velocity results. Arithmetic mean ± sd (n = 3). ACP = anhydrous calcium phosphate, MN = Parteck M 200, LM = Tablettose 100, MCC = Vivapur 101, MS = maize starch. Plots in one row share y-axis.

3.4.6 Summary

It has been shown that the velocity through a binary mixture was influenced by both of its components. However, as seen with the lubricated samples at concentrations of the second component up to 2% there was no systematic velocity decrease or change of the velocity profiles in either measurement mode visible. At higher concentrations of the second component the

profiles gradually changed, both, during compression and decompression. The slope of the compression signal was shown to be proportionally related to the volume fractions of the respective components in blends containing ACP. In the case of the MCC blends with MN and LM, the slope was slightly closer to MCC even though there was not much difference between volume and weight fraction which probably relates to its comparative softness. This was especially interesting as the depiction of the compression process seemed to imply the progression was closer to LM. This seeming similarity could be explained by the similar maximum solid fraction reached and resulting close proximity of the compression curves. It also showed that exhibiting similar velocities at the same SF did not necessarily mean the curve progression was the same.

The decompression parameters were related to the respective components as well. Aside from the velocity drop during decompression, all the other parameters were gradually changing with varying composition. Here, there did not seem to be a correlation between volume fraction and parameter. *AUC, AUC_{Full}* and A_C resembled ACP more closely than either MCC or MS. This seemed to imply that ACP had a higher influence on those parameters and consequently the pore size increase during decompression.

Similar to the behaviour of binary mixtures, the velocity profiles were also related to all components in a ternary mixture. Again, the influence on the compression was roughly proportional to the volume fraction of the components. For the decompression parameters it was difficult to tell which component primarily influenced the shape of the signal as there are many factors to consider.

4 Summary

The aim of this work was the evaluation of the KIM system and its applicability to the characterisation of pharmaceutical materials. It has been shown that the set-up is capable of performing highly repeatable velocity measurements, for longitudinal and transverse ultrasonic waves, both in succession and on consecutive days, which in turn allows the comparison of data gathered at different time-points. The amplitudes of the sound waves on the other hand are prone to fluctuations, which makes their assessment difficult. The visualisation chosen for the measurements was velocity as a function of SF which offered additional information about the relative density of the materials reached during compression and facilitated spotting differences between the materials. The two different measurement modes gave similar results. However, the longitudinal velocity was always higher compared to transverse and was more sensitive to small changes in the porosity at high solid fractions.

All velocity profiles showed the same basic progression: the velocity increased during compression, reached a maximum at roughly the maximum SF, and then decreased during decompression until the signal stopped. However, the exemplary excipients used for the measurements showed noticeable differences in their velocity profiles concerning maximum velocity reached, maximum SF, rate of velocity increase and velocity drop. Those differences were not exclusive to different chemical structures, but also observed for different grades of the same material. In addition, it was shown that the different velocity profiles were not caused by different initial particle sizes, although especially for MCC which is known to densify through plastic deformation, a slight decrease in velocity with decreased particle size was observed.

As ultrasound is known to be influenced by the pore volume of a material and the shape of the pores, the explanation for the different profiles currently deemed most likely is the changing pore structure during compaction exhibited by the materials depending on their deformation behaviour. The initial linear increase of velocity during compression correlated with the fragmentation of a material: the more prone to fragmentation, the steeper the slope during compression of the material. The decompression signal was indicative of the elasticity or more precisely, the immediate elastic recovery of a material. In addition, the changes in ultrasonic velocity, i.e., the velocity drop, could be an indication towards the changes undergone inside the compact during decompression caused by the elastic recovery. As the KIM system is limited to one set of flat punch tips and a rather slow compaction profile, there was no lamination observed.

As the speed of sound is linked to the elasticity parameters of a material, apparent Young's Modulus, Poisson's Ratio and Shear Modulus could be calculated. YM and SM were shown to

increase with increasing SF which is a sign of increased resistance against elastic and shear deformation with decreasing porosity. This has also been observed by other authors using different means for the calculation of the moduli. The change in PR on the other hand was different for different materials.

Lastly, the changes in the profiles with intermixture of a second component was investigated. Internal lubrication with up to 2% of MgSt did not systematically alter the results. Adding a second component in higher amounts (25 and 50% were tested here), however, changed the velocity profiles. The calculated parameters, elasticity parameters, as well as the maximum velocity and SF were in between the respective components which could allow observing changes in the behaviour of a material in regard to its components with varying composition.

Overall, ultrasonic in-die measurements could help in the better understanding of the compaction process, by offering insights into the changes in pore structure during compression and decompression. However, it must be noted that none of the parameters calculated using the velocity profiles so far could explain the differences in tensile strength observed for the different materials. They are then not a measure of the bonding strength of a material. As there was only one set of punch tips available, whether these results could be transferred to different punch diameter and shape, both of which have a huge impact on the tablet properties, could not be affirmed. To find a practical application for the system, several steps must be taken: a) Different punches must be tested to check whether the results presented here are independent of punch size and shape, b) The data set needs to be expanded by adding materials with a wider variety of compression characteristics to better being able to separate the different processes happening simultaneously, and c) Establish a number of parameters to perform statistical analysis, e.g., through multi variate data analysis, to investigate whether one or a combination of in-die parameters can be used to predict the out-die performance of a single material or a tabletting mixture.

5 Experimental Part

Parts of this section have already been published in the International Journal of Pharmaceutics (Kern et al., 2022). The content was linguistically adapted, and data sets were partly extended.

5.1 Materials

Five commonly used excipients were chosen as exemplary materials in this work to cover a wide variety of compaction behaviours. In some cases, several different grades were used to account for different requirements depending on the experiment.

Table 5-1: Pharmaceutical excipients used for the ultrasonic in-line analysis.

Substance	Abbreviations	Grade	Supplier
Calcium hydrogen phosphate, anhydrous	ACP	Milled	Merck Millipore, Darmstadt, Germany
Microcrystalline Cellulose	MCC	Vivapur® 101	JRS Pharma, Rosenberg, Germany
		Vivapur® 102	JRS Pharma, Rosenberg, Germany
		Vivapur® 112	JRS Pharma, Rosenberg, Germany
Mannitol	MN	Parteck® M 200	Merck Millipore, Darmstadt, Germany
		Parteck® Delta M	Merck Millipore, Darmstadt, Germany
		D(-)-Mannit	Roquette, Lestrem, France
		Pearlitol® 200SD	Roquette, Lestrem, France
Maize Starch	MS	Native	Roquette, Lestrem, France
		Starch 1500®	Colorcon, Harleysville, USA
α-Lactose Monohydrate	LM	Tablettose® 100	Meggle, Wasserburg, Germany
		GranuLac® 200	Meggle, Wasserburg, Germany

Additionally, magnesium stearate (MgSt; Peter Greeven, Bad Münstereifel, Germany) was used as lubricant.

5.2 Methods

5.2.1 Powder Characterisation

5.2.1.1 Particle Density

For the determination of the particle density of the powders the UltraPyc 1200e gas expansion pycnometer (Quantachrome, Boynton Beach, Florida) was used. The apparatus contains a sample and a reference cell, where the sample cell is filled with a powder sample of a defined mass. The volume of both empty cells is known.

At the beginning of the measurement the air was removed from both cells through vacuum. Then they were separated, and the sample cell was filled with a gas – in this case nitrogen – up to the target pressure of 19 psig. Once the pressure was stable, the connection between the cells was opened and due to the expansion of the gas, the pressure fell. The sample volume could now be calculated using the Boyle-Mariotte law:

$$\mathbf{V_s} = \mathbf{V_c} + \frac{\mathbf{V_r}}{\mathbf{1} - \frac{\mathbf{P_1}}{\mathbf{P_2}}} \tag{5-1}$$

V_s: *Sample volume [g/mL]*

V_c: *Volume of empty sample cell [g/mL]*

V_r: *Volume reference cell [g/mL]*

P_1: *Pressure after filling of the sample cell [bar]*

P_2: *Pressure after opening connection [bar]*

Since this method is based on the determination of the gas volume displaced by the solid material, intraparticular cavities or pores too small for the gas to enter will be interpreted as solid. The particle density is, therefore, lower than the true density of the material, but is commonly used as an estimate or a substitute.

There are four measurement cells available: micro, small, medium and large. The medium cell with a sample volume of 40 mL was used in this study. The cell was filled with the powder up to 80% of its volume and the sample mass was determined. Each sample was measured until the relative standard deviation of three consecutive runs dropped below 0.05%. The mean value of those three runs was calculated. Per material, three samples were measured.

The pycnometric density of every substance and blend measured using the KIM system was determined. The results of each material can be found in Appendix Table A-1 and Table A-4.

5.2.1.2 Particle Size Distribution

The particle size distribution (PSD) of the different powders was determined using the Camsizer X2 (Retsch Technology GmbH, Haan, Germany). The underlying measuring principle is the dynamic image analysis (DIA) according to ISO 13322-2.

Two cameras – the Basic camera with a range of 50 – 3000 µm and the Zoom camera which detects particles between 1 and 100 µm – are positioned opposite of two light sources. Each camera takes about 300 pictures per second. Whenever a particle passes between camera and light source, a shadow appears on the picture. The diameter of the particles is then measured through the number of pixels appearing black. Five different size definitions are available with the Camsizer (Figure 5-1). In this work xc_min has been chosen, as it is closest to the diameter measured via sieve analysis, which is still the standard method of PSD analysis in many places.

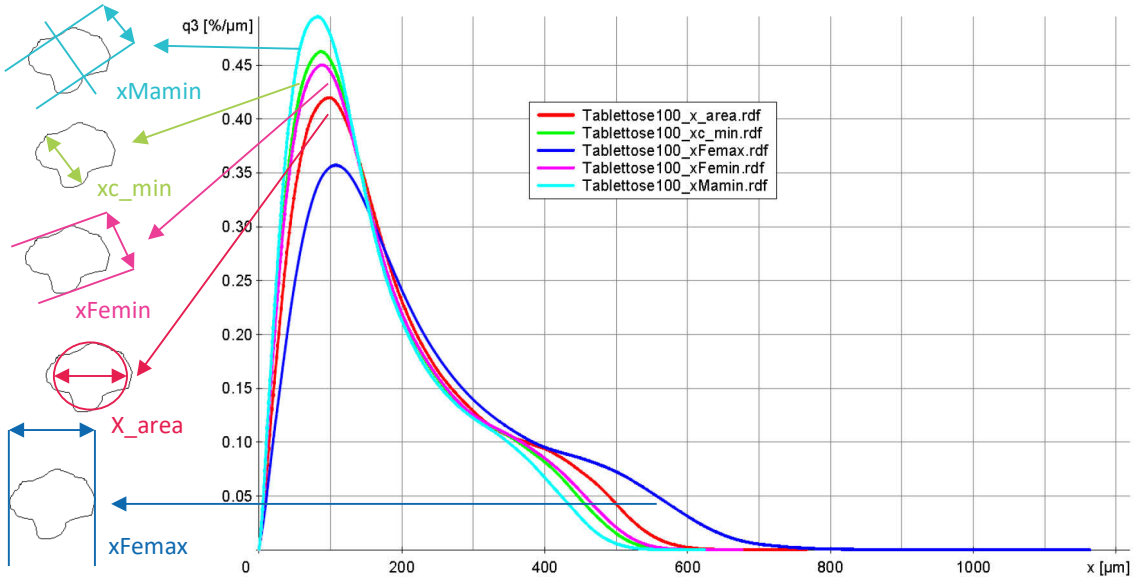

Figure 5-1: Size definitions available with the Camsizer X2. xMamin = length of smallest area bisector (Martin diameter), xc_min = inner particle width, xFemin = smallest Feret diameter, x_area = diameter of circle of same area as particle projection, xFemin = largest Feret diameter.

For dry powders the measurement can be carried out using two different cartridges: X-Fall and X-Jet. With X-Fall the sample falls vertically through the measuring gap and is dispersed via gravity. With X-Jet the dispersion is done by compressed air.

In this study the X-Jet module was used with an applied pressure of 20 kPa. Per run, 10 mL sample were used, and each material was measured in triplicate.

5.2.1.3 Loss on Drying

The LoD was determined for all pure substances used in this study with the Moisture Analyzer HE53 (Mettler Toledo, Columbus, Ohio). The sample was spread out on an aluminium pan and heated to 105 °C until the mass reduction was below 1 mg in 50 s. The LoD measurements were performed in triplicate.

5.2.2 Powder Compaction

5.2.2.1 Tablet Preparation

All compression experiments were performed on the compaction simulator Styl'One Evolution (Medelpharm, Lyon, France), an instrumented single station tablet press capable of mimicking the punch movements of production scale rotary tablet presses. The force exerted during compression is measured by two piezo-electric load cells per punch capable of covering forces up to 50 kN. The displacement is determined by two incremental sensors for UP and LP, each. The punches move individually which allows for adjustment of the movement profile as needed for the experiments.

To correlate tablet properties with the ultrasonic data, tablets were prepared for the single substances as well as the excipient blends explained in Chapter 5.2.3.5.11. 11.28 mm round, flat Euro norm B punches were used for the experiments. The 300-300 compression profile, shown in Chapter 5.2.3.5.1, was chosen. The target force was 25 kN, corresponding to 250 MPa. For Vivapur 101, Parteck M 200 and Tablettose 100 additional tablets with 15 and 20 kN were prepared. The lower forces were reached by increasing the compression thickness, i.e., the minimum distance between punches, while keeping the sample mass constant. Per force level 10 tablets were prepared. The die was filled manually and externally lubricated using MgSt powder applied with a brush to minimise the influence of the lubricant on the resulting tablets. The sample weight was 300 mg (± 2 mg) for all substances except ACP where the weight was increased to 450 mg (± 2 mg). The samples were prepared on an XS204 balance (Mettler Toledo, Langen, Germany).

5.2.2.2 Double Compression

The same materials as before were used for the double compaction experiments. The compression part of the 300-300 profile was doubled as depicted in Chapter 5.2.3.5.8. The compression thickness was set to the same value as the 25 kN tablets of the force study to allow comparison between the two tablet groups.

5.2.2.3 Tablet Characterisation

After 24 h the tablets produced according to Chapters 5.2.2.1 and 5.2.2.2 were individually fed into the Multicheck VI (Erweka, Langen, Germany) where in succession tablet mass, height, diameter, and breaking force were measured. The breaking force of the tablets was determined via diametral compression test: the tablets were placed between a static metal wall and a moving platen. The platen moved towards the wall with a velocity of 2.30 mm/s, thus applying a force to the tablet. The force at which tablet failure occurs is registered and referred to as breaking force.

5.2.3 The KIM System

5.2.3.1 Set-Up

The ultrasonic measurement were performed with the KIM system introduced by Hagelstein et al. (2019), an add-on to the Styl'One Evolution. The KIM system consists of several hardware components which have to be installed prior to the measurements: two sets of transducers (longitudinal: Olympus V112-SM 10 MHz; transverse: Olympus V156-RM 5 MHz; Olympus Europe, Hamburg, Germany), two sets of punches, four external incremental displacement sensors (upper punch: Magnescale DK812SAR5; lower punch: Magnescale DK25PR5; Magnescale Europe, Wernau, Germany), a pulser and a receiver unit (both OLYMPUS 5077PR, Olympus Europe, Hamburg, Germany), and a work station. The measurement set-up inside the tablet press can be seen in Figure 5-2.

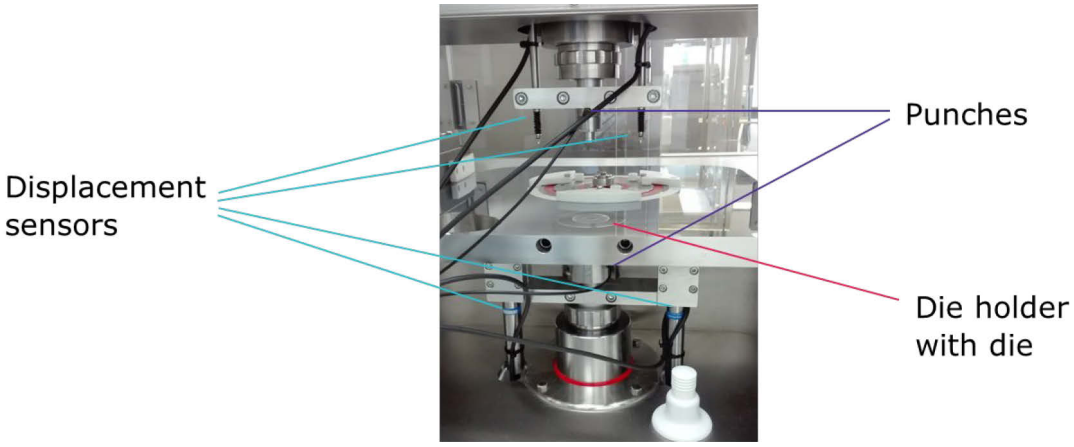

Figure 5-2: Set up of the KIM-System. Published in Kern et al. (2022).

The punches are custom made, hollow, Euro norm D punches with removable 13 mm, round, flat punch tips as shown in Figure 5-3. While there is one set of punches for each measurement mode (transverse and longitudinal), the same punch tips are used in all cases.

Figure 5-3: Punch set used for transverse KIM measurements including removable punch tips.

The sound waves are generated by vibrations of the piezoelectric transducers generated through transformation of an electrical signal. The sound pressure is proportional to the voltage used in the generation of the signal. Reversely, the voltage of the received signal is proportional to the pressure of the detected sound wave. The piezoelectric US-transducers are integrated into the punches and connected to the punch tips through a couplant which allows the transmission of the signal into the punch tips. The recommended coupling agents are glycerol for longitudinal and honey for the transverse transducers. In the KIM set-up, the transducer in the upper punch (UP) generates the sound wave and also receives signals, whereas the transducer in the lower punch (LP) only receives. The measurements are done during the whole compaction process in the pitch-catch, i.e., transmission, mode: The signal is sent by the transducer in the UP and received in the LP as depicted in Figure 5-4.

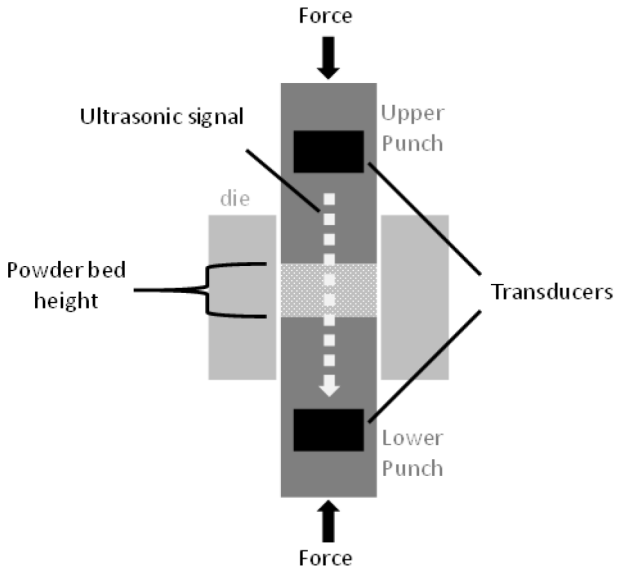

Figure 5-4: Measuring principle of the KIM-System. Published in Kern et al. (2022).

5.2.3.2 Data Acquisition and Pre-Processing

The ultrasonic data, the displacement measurements and the recorded forces are sent to the workstation where the pre-processing is taking place. Figure 5-5 shows an US signal recorded by the LabView based KIM++ software (Romaco Kilian, Cologne, Germany). The blue signals are the reflections detected by the transducer in the UP and the red signals are the transmissions. The TOF is measured from the start of the excitation pulse (first blue signal) to the maximum of the first transmission pulse for longitudinal measurements. In transverse mode the minimum is detected instead. The amplitude of the ultrasonic signal can be adjusted by changing the gain setting and thus the amplification of the signal in the receiver unit connected to the transducer in the lower punch. The clearest signal peaks are detected at amplitudes between 0.1 and 1 V. Depending on the acoustic properties of the powder, the signal has to be amplified or dampened. Since longitudinal sound waves are faster than transverse waves, the time window for the peak detection is set to 16 and 32 µs, respectively.

Figure 5-5: Screenshot of US signal as detected by the KIM++ software (blue: reflection; red: transmission).

The trigger signal sent by the Styl'One after the start of the compression process is detected by the KIM++ software and provides the starting point of the data recording. However, to decrease the size of the resulting files it is possible to manually adjust the time window, by adding a waiting time before the recording starts, and setting the length of the acquisition. Additionally, the sample rate can be changed. The maximum setting is 5000 Hz. Time, TOF, measured signal amplitude, force and displacement are then displayed as shown in Figure 5-6, and summarised in a text file for each measurement.

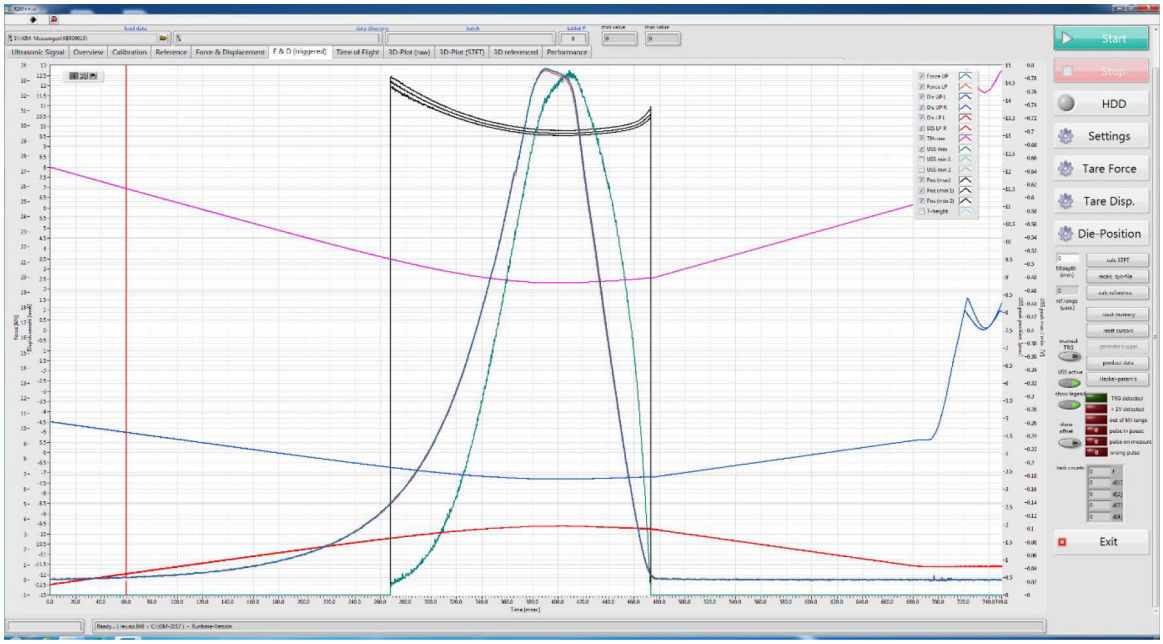

Figure 5-6: Data as recorded using the KIM++ software; UP displacement (blue), LP displacement (red), distance between punches (pink), US intensity (green), TOF (black), compression force (dark red and blue).

The further processing of the data is performed with the MATLAB-based TabAnalyzer V 2.4 (Romaco Kilian, Cologne, Germany). The punch diameter, powder density, mass of the compact after ejection, gain and corrections to be applied (refer to 5.2.3.4) are entered and the text files are loaded into the software. The additional parameters solid fraction, pressure, ultrasonic velocity and actual amplitude are then calculated, and the results displayed to check the plausibility of the results. The processed data can then be exported as .csv or Excel file.

5.2.3.3 Calibration

Before each measurement, force and displacement need to be tared. To tare the displacement sensors a 5 mm metal tablet is used. A force between 2.7 and 3 kN is applied via a specially prepared slow compression profile with extended dwell time. The first input parameter is the punch position at the minimum distance between the punches, i.e., the metal tablet height, the second input parameter is the position of the lower punch after ejection, i.e., the zero position.

Afterwards the metal tablet is measured to check the success of the taring and if the height is within a 5 µm margin of the true value (4.9976 mm) before the measurements can be performed. The tablet height is determined again after the measurements are performed to check the displacement sensors and to rule out dislocation of the holders during the compaction process.

5.2.3.4 Correction Values

Three correction values had to be determined beforehand and then applied to the raw data: TOF through the punches, punch deformation, and changes of TOF with increasing pressure during compaction. The factors were determined in triplicate each on three consecutive days resulting in nine values per factor.

5.2.3.4.1 Time of Flight Through the Punch Tips

For the velocity calculations only the TOF through the powder bed is of interest. Therefore, the residence time of the signal in the punch tips had to be measured and subtracted from the total TOF. For the determination the punches were placed tip-on-tip, connected by the respective coupling agent, and an ultrasonic pulse was sent. Then the TOF ultrasonic data was transferred from the KIM++ software to an Excel sheet prepared by Solids Development Consult (SDC). The determination was performed for both modes.

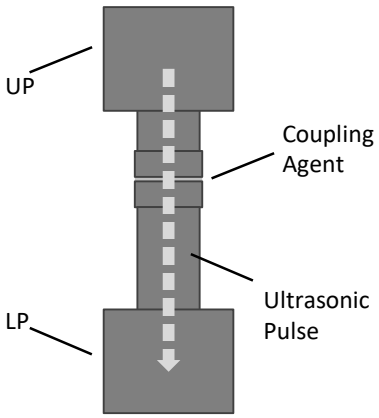

Figure 5-7: Set-up of the punch-on-punch measurements for the determination of the US velocity through the punch tips.

5.2.3.4.2 Punch Deformation

During a compression cycle on a tablet press, the forces applied do not only induce changes in the powder bed but also in the punches, if to a lesser extent. This can be seen when looking at the compaction of the 5 mm metal tablet used for taring of the system as depicted in Figure 5-8. The measured tablet height decreases linearly even though the distance between the punches is constant at 5 mm, due to the metal tablet placed between them. This was caused by the deformation of the punches.

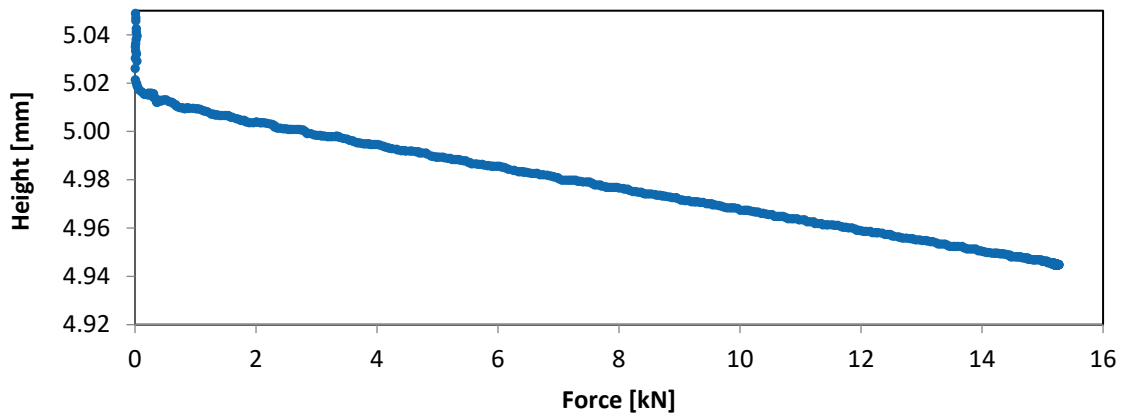

Figure 5-8: Compaction of the metal tablet using the longitudinal punch set, recorded using the external displacement sensors of the KIM system.

The correction factor was obtained by performing punch-on-punch measurements and determining the slope of the height decrease with increasing compression force using an Excel template provided by SDC.

5.2.3.4.3 TOF Correction

With increasing compression pressure and resulting punch deformation, the TOF of the ultrasonic signal through the punches decreases as well. Therefore, the change in velocity was determined analogue to the punch deformation. The tablet height was swapped with the TOF as shown in Figure 5-9 and the slope of the linear decrease was calculated.

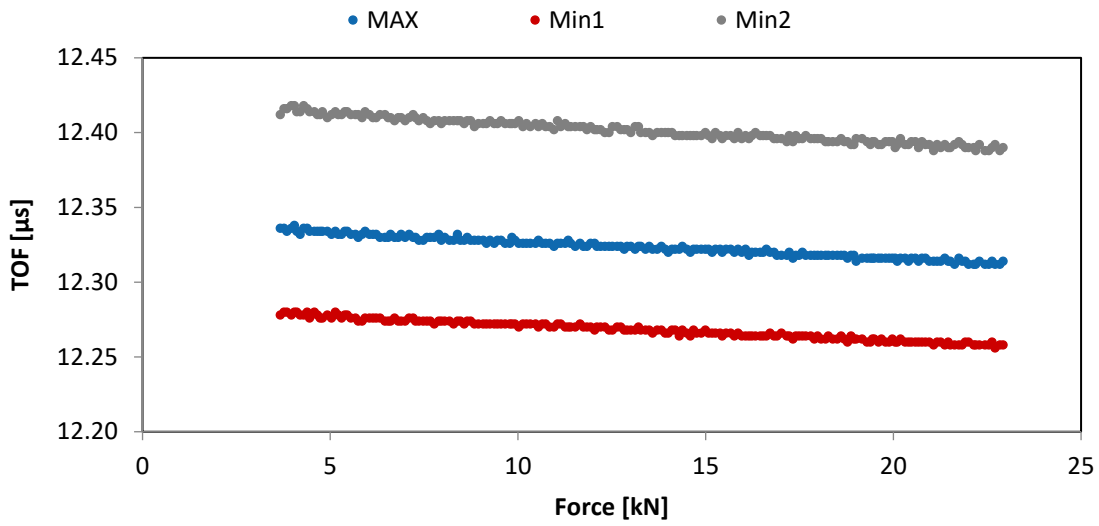

Figure 5-9: TOF of the longitudinal signal with applied pressure. Maximum (MAX) used for velocity determination. Minima before and after maximum peak.

5.2.3.4.4 Calculations

The correction factors determined for the KIM system are summarised in Table 5-2.

Table 5-2: Correction values used for the calculation of the velocity throughout the compaction process; standard deviation in brackets.

Mode	$TOF_{Punches}$ [µs]	Punch Deformation [mm/kN]	TOF_{corr} [µs/kN]
Longitudinal	12.3102 (± 0.0046)	3.9608 (± 0.0101)	1.2345 (± 0.1118)
Transverse	20.5998 (± 0.0120)	3.4294 (± 0.0092)	0.9388 (± 0.0705)

The actual distance between punches, i.e., corrected powder bed height was calculated via an extended linear correction:

$$\boldsymbol{h = TH + (Def_{corr} * F_{avg} - Def_{corr} * F_{Ref})} \quad (5\text{-}2)$$

h: *Corrected powder bed height [mm]*

TH: *Measured tablet height [mm]*

Def_{corr}: *Punch deformation [mm/kN]*

F_{avg}: *Applied force during compression [kN]*

F_{Ref}: *Reference force measured during taring [kN]*

The reference force is used to compensate the non-linear deformation at lower forces. It is the force used during the taring.

The TOF through the powder bed is calculated using the following equation:

$$\boldsymbol{ToF_{Powder} = ToF_0 - (ToF_{UP+LP} - TOF_{corr} * F_{avg})} \quad (5\text{-}3)$$

TOF_{Powder}: *TOF through the powder bed [µs]*

TOF_0: *Measured TOF [µs]*

TOF_{UP+LP}: *TOF through upper and lower punch [µs]*

TOF_{corr}: *Change of TOF with applied pressure [µs/kN]*

F_{avg}: *Average compaction force of UP and LP [kN]*

Using *TOF_{powder}*, and *h*, the velocity of the sound wave can be calculated:

$$\boldsymbol{c = \frac{h}{ToF_{Powder}}} \quad (5\text{-}4)$$

c: *Velocity of the ultrasonic wave (longitudinal or transverse) [mm/µs]*

h: *Corrected powder bed height [mm]*

TOF_{Powder}: *TOF through the powder bed [µs]*

5.2.3.5 Ultrasonic Measurements

5.2.3.5.1 Standard Set-Up

The ultrasonic measurements were done in hand-fill mode on the Styl'One. The samples were individually weighed on a XS204 balance (Mettler Toledo, Langen, Germany) before being transferred into the die. The fill-depth was in most cases 10 mm, except for the Vivapur grades where it was adjusted to 13 mm to account for the low bulk density of the materials. Lubrication was in most cases done externally with magnesium stearate powder applied with a brush. The only exception were the lubrication experiments where the lubricant was added to the powder material.

The default compaction profile used in this work was the V-shaped 300-300 profile depicted in Figure 5-10. The compression time was set to 600 ms with compression and decompression each taking 300 ms, and no extended dwell time. The compaction was performed symmetrically which means the force was applied by both punches.

Figure 5-10: 300-300 compaction profile. All numbers are time in ms.

The sample weight was in most cases 500 mg (± 2 mg). The exception was ACP with its high density and the corresponding powder mixtures. The target maximum pressure applied during compaction was 250 MPa which corresponds to approximately 32 kN using 13 mm punches. The receiver gain was adjusted, so an amplitude between 0.3 and 1 V was reached (refer to Appendix Table A-2). The produced tablets were weighed again after compression. The measurements were performed in triplicate per mode and substance.

Measurements were excluded and repeated if one of the following criteria was not met: maximum compression force above 30 kN, intact tablet obtained, maximum ultrasonic amplitude between 0.3 and 1 V, an intensity maximum detected for longitudinal or a minimum for transverse and the tablet thickness of the metal disc used for calibration was within 5 µm of the true height when checked with the KIM system after the measurements.

The standard KIM measurements were performed for every substance mentioned in Table 5-1.

5.2.3.5.2 Repeatability

When establishing and evaluating a new characterisation method it is important to ensure its repeatability, both consecutively and on different days. Therefore, eight back-to-back measurements were performed per substance and mode. The materials chosen for this study were Parteck M 200, GranuLac 200, Tablettose 100 and Vivapur 101. Afterwards, the KIM set-up was dismantled. The next day, punches and displacement sensors were reassembled, and the same materials were measured again. This was repeated on three separate days.

5.2.3.5.3 Compaction Speed

In addition to the aforementioned 300-300 profile, two faster compression profiles were tested on six substances: Vivapur 101, GranuLac 200, Tablettose 100, native maize starch, ACP and Parteck M 200. The profiles were identical apart from the actual compaction time. It was reduced from 600 to 200 and 100 ms, respectively. The target mass and the compression thickness were identical to the standard measurements.

5.2.3.5.4 Different Particle Sizes

Three substances previously measured using the KIM system with comparatively large PSD were separated into three sieve classes each. The sieves were chosen to ensure a) clear distinction between the smallest and the largest class, and b) about the same amount of material in every class. An overview of the materials and the respective size classes can be found in Table 5-3.

Table 5-3: Analysed materials and their size classes

Material	Size class S [µm]	Size class M [µm]	Size class L [µm]
Parteck M 200	< 100	100 – 180	> 180
Vivapur 102	< 90	90 – 180	> 180
Tablettose 100	< 90	90 – 200	> 200

The two sieves were stacked on top of each other, and 120 g of material were placed on the top sieve with the bigger mesh size. The separation was done on a vibratory sieve shaker (Retsch Technology, Haan, Germany) for 10 min. Afterwards the PSD was determined with the Camsizer X2 according to Chapter 5.2.1.2.

The KIM measurements were done as described in Chapter 5.2.3.5.1. The settings were adopted from the previous compressions done using the full particle size range.

5.2.3.5.5 Maximum Pressure

The standard KIM measurements were conducted at a maximum pressure of 250 MPa. To check differences in the behaviour when lower pressures are applied, additional measurements with 200 and 150 MPa were performed by increasing the compression thickness. The used target thicknesses are listed in Appendix Table A-2.

5.2.3.5.6 Target Maximum Solid Fraction

The substances chosen were Parteck M 200, GranuLac 200, Tablettose 100, Vivapur 101 and native maize starch. The target SF was 0.9, which was the SF_{max} reached by Parteck M 200 when 250 MPa were applied. As this far surpassed the maximum SF reached by ACP (SF_{max} = 0.75), this substance was not included in the experiment. The target SF was reached for the other substances by increasing the compression thickness and thereby decreasing the maximum pressure compared to the standard measurements as summarised in Appendix Table A-3.

5.2.3.5.7 Influence of Moisture Content

Starch 1500 and Vivapur 112 two excipients known for their hygroscopicity, were stored under two different storage conditions for 8 weeks. The conditions were reached by adding saturated saline solutions into three different desiccators: The largest desiccator was prepared with sodium chloride to reach a relative humidity of 75% and two smaller ones with sodium bromide which resulted in 60% relative humidity. To keep the exposure time of the samples to the ambient after storage as short as possible, 15 samples of 500 mg powder per humidity were filled into glass vials which were closed immediately after the desiccators were opened. The individual samples were weighed before and after storage.

Figure 5-11: Desiccators containing the powder samples and the saturated salt solutions.

Additionally, fifteen samples were prepared per substance and dried for 24 h at 30°C in a vacuum drying cabinet (PINK, Wertheim, Germany). The materials were then measured with the KIM system using the same settings as for the non-treated samples previously characterised. The remaining samples were used to determine the LoD in triplicate.

5.2.3.5.8 Double Compaction

The compaction profile used for the double compaction experiments is shown in Figure 5-12. A short relaxation time and a second identical compression cycle were added to the 300-300 profile.

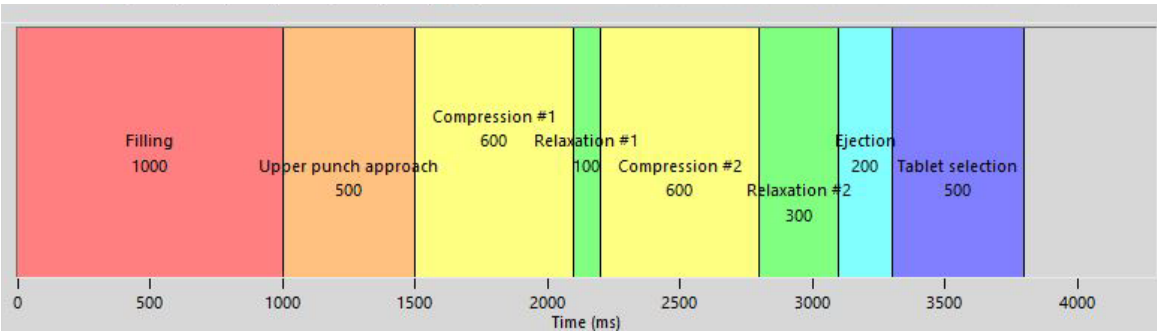

Figure 5-12: Multi-compression profile. All numbers denote time in ms.

The target pressure was 250 MPa in both compressions. The settings were adopted from the single compression experiments.

5.2.3.5.9 Lubrication

The standard KIM measurements were all done with external lubrication. In addition, measurements were performed on Vivapur 101, Parteck M 200 and Tablettose 100 with varying MgSt concentrations in the commonly used range: 0.5, 1 and 2%.

The components were weighed, and the MgSt was sieved through a 500 µm sieve to loosen possible agglomerates and added to the other component, before being blended for 5 min at 32 rpm in the Turbula T2C tumble blender (Willy A. Bachofen, Muttenz, Switzerland). The Pycnometric density of the blends was then determined in triplicate. The compression experiments were conducted following the procedure described for the externally lubricated materials in Chapter 5.2.3.5.1 without the addition of MgSt powder before compaction.

5.2.3.5.10 Blends and Layers

The ultrasonic velocity through binary mixtures of previously studied excipients was measured and compared to the velocity through two layers of the same materials. Overall, five materials in six combinations were tested which can be summarised into two groups as shown in Table 5-4.

Table 5-4: The five excipients divided into two groups. Each excipient was combined with the other two materials in its group

Group 1	Group 2
Native maize starch	Parteck M 200
ACP	Tablettose 100
Vivapur 101	Vivapur 101

Of every combination in a group a binary mixture consisting of equal weight parts was prepared by sieving the materials through a hand sieve with a 500 µm mesh size to loosen agglomerates and improve the miscibility, and then blending them in the Turbula blender for 15 min at 32 rpm. The blends were compacted on the Styl'One and analysed using the KIM system according to the standard KIM procedure.

In parallel, two-layer tablets were produced by weighing the components individually (250 mg per substance except for the combinations containing ACP where 280 mg per component were used) and pouring them consecutively into the die. To prevent intermixing of the layers, the first substance was flattened using a specially designed 3D-printed cylindrical devise (dubbed Mylinder and shown in action in Figure 5-13) before the second component was added.

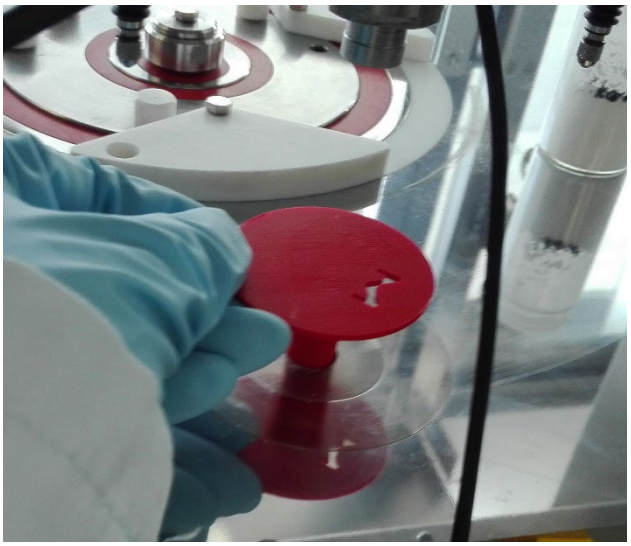

Figure 5-13: Flattening of the lower substance with the Mylinder before addition of the second component.

5.2.3.5.11 Binary Mixtures

Additional blends of Group 1 were prepared to track the changes in velocity with varying composition. 25/75 and 75/25% (%w) blends were prepared as described in Chapter 5.2.3.5.10. The blends were then measured via the standard KIM measurement approach using the 300-300 profile.

5.2.3.5.12 Ternary Mixtures

Two ternary mixtures were made using equal amounts (%w) of the substances of groups 1 and 2 respectively (Chapter 5.2.3.5.10). The KIM measurements were then performed as described above.

5.2.4 Data Processing

The ultrasonic data exported using the TabAnalyzer software was processed using a script written in Python 3. The main packages used in the calculations and later plotting of the data were scipy, pandas, numpy and matplotlib

5.2.4.1 Data Filtering and Separation

The first point that was removed was the first velocity value which was in all cases calculated using an artificially created velocity value of zero by the TabAnalyzer software. The initial jump of the velocity caused by the erroneously assigned later peak as the main peak was filtered by excluding all data points during compression where a velocity increase of 0.03 (longitudinal) or 0.015 (transverse) was detected, which corresponds roughly to one fifth of the arrival difference between the peaks in the two measurements modes.

For the subsequent calculation, compression and decompression were separated through the maximum SF and velocity. The compression was defined as starting at the beginning of the steady signal and ending at the velocity maximum, while the decompression was defined as starting at the SF maximum ending at the signal stop.

5.2.4.2 Relative Standard Deviations

To assess the repeatability of the measurements and the effect of e.g., PSD or lubrication on the measured velocity, the standard deviations during compression were calculated in SF steps of 0.1. First the standard deviation was calculated at the same SF for successive measurements of the same material, then the deviation at the same SF was calculated for the different conditions, e.g., the same material at different days, or with different amounts of added lubricant. For the repeatability measurement, e.g., this resulted in the standard deviation between 24 single measurements (eight measurements on three days) while it was 12 for the lubrication samples (3 measurements for each of the 4 lubrication levels). Since the absolute velocity values differed throughout the compression process and between different materials, the relative deviation in percent is given.

5.2.4.3 Elasticity Parameters

For the calculations of Young's Modulus, Poisson's Ratio and Shear Modulus, equations (1-18), (1-19), and (1-15) – the latter solved for the Shear Modulus – were used. They were calculated during the whole compression phase in the same SF increments as the standard deviations. As for YM and PR both, longitudinal and transverse velocities are needed, for each substance, nine values were obtained, owing to the nine different combinations of longitudinal and transverse measurement. On the other hand, only three Shear Modulus values were obtained, since for the calculations only the transverse velocity is needed.

5.2.4.4 Compression and Decompression Parameters

The compression and decompression parameters were calculated as described in Chapters 3.2 and 3.3.2. Each parameter was determined for every measurement performed with the respective material.

5.2.4.5 Heckel Yield Pressure

The linear part of the Heckel plot was defined through the inflection point, i.e., the point of the compression where the first derivative was at its minimum. From this point on, the end of the linear portion was defined as the pressure at which the first derivative deviated more than 15% from the minimum. The start was determined through repeated linear regression until the R^2 between start and determined endpoint first surpassed 0.998.

Bibliography

Aburub, A., Mishra, D., Buckner, I., 2007. *Use of compaction energetics for understanding particle deformation mechanism*. Pharmaceutical Development and Technology 12, 405-414.

Adams, M.J., McKeown, R., 1996. *Micromechanical analyses of the pressure-volume relationships for powders under confined uniaxial compression*. Powder Technology 88, 155-163.

Akseli, I., Becker, D.C., Cetinkaya, C., 2009a. *Ultrasonic determination of Young's moduli of the coat and core materials of a drug tablet*. International Journal of Pharmaceutics 370, 17-25.

Akseli, I., Cetinkaya, C., 2008a. *Acoustic testing and characterization techniques for pharmaceutical solid dosage forms*. Journal of Pharmaceutical Innovation 3, 216-226.

Akseli, I., Cetinkaya, C., 2008b. *Air-coupled non-contact mechanical property determination of drug tablets*. International Journal of Pharmaceutics 359, 25-34.

Akseli, I., Dey, D., Cetinkaya, C., 2010. *Mechanical property characterization of bilayered tablets using nondestructive air-coupled acoustics*. AAPS PharmSciTech 11, 90-102.

Akseli, I., Hancock, B.C., Cetinkaya, C., 2009b. *Non-destructive determination of anisotropic mechanical properties of pharmaceutical solid dosage forms*. International Journal of Pharmaceutics 377, 35-44.

Akseli, I., Iyer, S., Lee, H.P., Cuitiño, A.M., 2011. *A quantitative correlation of the effect of density distributions in roller-compacted ribbons on the mechanical properties of tablets using ultrasonics and X-ray tomography*. AAPS PharmSciTech 12, 834-853.

Akseli, I., Ladyzhynsky, N., Katz, J., He, X., 2013. *Development of predictive tools to assess capping tendency of tablet formulations*. Powder Technology 236, 139-148.

Akseli, I., Libordi, C., Cetinkaya, C., 2008a. *Real-time acoustic elastic property monitoring of compacts during compaction*. Journal of Pharmaceutical Innovation 3, 134-140.

Akseli, I., Mani, G.N., Cetinkaya, C., 2008b. *Non-destructive acoustic defect detection in drug tablets*. International Journal of Pharmaceutics 360, 65-76.

Aliabouzar, M., Zhang, G.L., Sarkar, K., 2018. *Acoustic and mechanical characterization of 3D-printed scaffolds for tissue engineering applications*. Biomedical Materials (Bristol) 13.

Amidon, G.E., Houghton, M.E., 1995. *The Effect of Moisture on the Mechanical and Powder Flow Properties of Microcrystalline Cellulose*. Pharmaceutical Research: An Official Journal of the American Association of Pharmaceutical Scientists 12, 923-929.

Armstrong, N.A., 1989. *Time-dependent factors involved in powder compression and tablet manufacture*. International Journal of Pharmaceutics 49, 1-13.

Asmani, M., Kermel, C., Leriche, A., Ourak, M., 2001. *Influence of porosity on Youngs modulus and poisson's ratio in alumina ceramics*. Journal of the European Ceramic Society 21, 1081-1086.

Bassam, F., York, P., Rowe, R.C., Roberts, R.J., 1991. *The Young's modulus of binary powder mixtures*. Powder Technology 65, 103-111.

Bauer-Brandl, A., Ritschel, W.A., 2012. *Die Tablette - Handbuch der Entwicklung, Herstellung und Qualitätssicherung*, 3rd fully revised Edition. Editio Cantor-Verlag, Aulendorf.

Boccaccini, D.N., Boccaccini, A.R., 1997. *Dependence of ultrasonic velocity on porosity and pore shape in sintered materials*. Journal of Nondestructive Evaluation 16, 187-192.

Busignies, V., Leclerc, B., Porion, P., Evesque, P., Couarraze, G., Tchoreloff, P., 2006. *Investigation and modelling approach of the mechanical properties of compacts made with binary mixtures of pharmaceutical excipients*. European Journal of Pharmaceutics and Biopharmaceutics 64, 51-65.

Busignies, V., Tchoreloff, P., Leclerc, B., Hersen, C., Keller, G., Couarraze, G., 2004. *Compaction of crystallographic forms of pharmaceutical granular lactoses. II. Compacts mechanical properties*. European Journal of Pharmaceutics and Biopharmaceutics 58, 577-586.

Çelik, M., Marshall, K., 1989. *Use of a compaction simulator system in tabletting Research*. Drug Development and Industrial Pharmacy 15, 759-800.

Chang, L.S., Chuang, T.H., Wei, W.J., 2000. *Characterization of alumina ceramics by ultrasonic testing*. Materials Characterization 45, 221-226.

Chen, Z., Wang, X., Giuliani, F., Atkinson, A., 2015. *Microstructural characteristics and elastic modulus of porous solids*. Acta Materialia 89, 268-277.

Chowhan, Z.T., Chow, Y.P., 1980. *Compression behavior of pharmaceutical powders*. International Journal of Pharmaceutics 5, 139-148.

Cooper, A.R.J., Eaton, L.E., 1962. *Compaction behavior of several ceramic powders*. Journal of the American Ceramic Society 45, 97-101.

Cunningham, J.C., Sinka, I.C., Zavaliangos, A., 2004. *Analysis of tablet compaction. I. Characterization of mechanical behavior of powder and powder/tooling friction*. Journal of Pharmaceutical Sciences 93, 2022-2039.

Dai, S., Xu, B., Zhang, Z., Yu, J., Wang, F., Shi, X., Qiao, Y., 2019. *A compression behavior classification system of pharmaceutical powders for accelerating direct compression tablet formulation design*. International Journal of Pharmaceutics 572.

De Boer, A.H., Vromans, H., Leur, C.F., Bolhuis, G.K., Kussendrager, K.D., Bosch, H., 1986. *Studies on tableting properties of lactose - Part III. The consolidation behaviour of sieve fractions of crystalline α-lactose monohydrate*. Pharmaceutisch Weekblad Scientific Edition 8, 145-150.

DeCrosta, M.T., Schwartz, J.B., Wigent, R.J., Marshall, K., 2001. *Thermodynamic analysis of compact formation; compaction, unloading, and ejection: II. Mechanical energy (work) and thermal energy (heat) determinations of compact unloading and ejection*. International Journal of Pharmaceutics 213, 45-62.

Denny, P.J., 2002. *Compaction equations: A comparison of the Heckel and Kawakita equations*. Powder Technology 127, 162-172.

Desbois, L., Tchoreloff, P., Mazel, V., 2020. *Characterization and modeling of the viscoelasticity of pharmaceutical tablets*. International Journal of Pharmaceutics 587.

Diarra, H., Mazel, V., Busignies, V., Tchoreloff, P., 2013. *FEM simulation of the die compaction of pharmaceutical products: Influence of visco-elastic phenomena and comparison with experiments*. International Journal of Pharmaceutics 453, 389-394.

Diarra, H., Mazel, V., Busignies, V., Tchoreloff, P., 2018. *Sensitivity of elastic parameters during the numerical simulation of pharmaceutical die compaction process with Drucker-Prager/Cap model*. Powder Technology 332, 150-157.

Duckworth, W., 1953. *Discussion of Ryshkewitch Paper by Winston Duckworth*. Journal of the American Ceramic Society 36, 68-68.

Eren, E., Kurama, S., Solodov, I., 2012. *Characterization of porosity and defect imaging in ceramic tile using ultrasonic inspections*. Ceramics International 38, 2145-2151.

Fariñas, L., Sanchez-Torres, E.A., Sanchez-Jimenez, V., Diaz, R., Benedito, J., Garcia-Perez, J.V., 2021. *Assessment of avocado textural changes during ripening by using contactless air-coupled ultrasound*. Journal of Food Engineering 289.

Fell, J.T., Newton, J.M., 1970. *Determination of tablet strength by the diametral-compression test*. Journal of Pharmaceutical Sciences 59, 688-691.

Fell, J.T., Newton, J.M., 1971. *Effect of particle size and speed of compaction on density changes in tablets of crystalline and spray-dried lactose*. Journal of Pharmaceutical Sciences 60, 1866-1869.

Firestone, F.A., 1942. *Flaw detecting device and measurement instrument* (US2280226A). United States Patent Office. https://patents.google.com/patent/US2280226A/en (accessed: 16.02.2021)

Firestone, F.A., 1946. *The supersonic reflectoscope, an instrument for inspecting the interior of solid parts by means of sound waves*. Journal of the Acoustical Society of America 17, 287-299.

Gamlen, M.J.D., Martini, L.G., Al Obaidy, K.G., 2015. *Effect of repeated compaction of tablets on tablet properties and work of compaction using an instrumented laboratory tablet press*. Drug Development and Industrial Pharmacy 41, 163-169.

Gustafsson, C., Bonferoni, M.C., Caramella, C., Lennholm, H., Nyström, C., 1999. *Characterisation of particle properties and compaction behaviour of hydroxypropyl methylcellulose with different degrees of methoxy/hydroxypropyl substitution*. European Journal of Pharmaceutical Sciences 9, 171-184.

Hagelstein, V., Frindt, B., Hucke, M., Carstens, J., Pieper, J., Lammens, R.F., 2018. *Ultrasonic in-die measurement of deformation properties*, 11th World Meeting on Pharmaceutics, Biopharmaceutics and Pharmaceutical Technology; Granada, Spain.

Hagelstein, V., Frindt, B., Hucke, M., Pieper, J., Carstens, J., Lammens, R.F., Wagner, K.G., 2019. *Novel ultrasonic in-die measurements during powder compression at production relevant speed*. International Journal of Pharmaceutics 571, 118761.

Hakulinen, M.A., Pajander, J., Leskinen, J., Ketolainen, J., Veen, B., Niinimäki, K., Pirskanen, K., Poso, A., Lappalainen, R., 2008. *Ultrasound transmission technique as a potential tool for physical evaluation of monolithic matrix tablets*. AAPS PharmSciTech 9, 267-273.

Hardman, J.S., Lilley, B.A., 1970. *Deformation of particles during briquetting*. Nature 228, 353-355.

Heckel, R.W., 1961. *Density-pressure relationship in powder compaction*. Transactions of the Metallurgical Society of AIME 221, 671-675.

Hersey, J.A., Rees, J.E., 1971. *Deformation of particles during briquetting*. Nature Physical Science 230, 96-96.

Hiestand, E.N., 1997. *Principles, tenets and notions of tablet bonding and measurements of strength*. European Journal of Pharmaceutics and Biopharmaceutics 44, 229-242.

Hiestand, E.N., Wells, J.E., Peot, C.B., Ochs, J.F., 1977. *Physical processes of tableting*. Journal of Pharmaceutical Sciences 66, 510-519.

Ilkka, J., Paronen, P., 1993. *Prediction of the compression behaviour of powder mixtures by the Heckel equation*. International Journal of Pharmaceutics 94, 181-187.

Jetzer, W.E., 1986. *Compaction characteristics of binary mixtures*. International Journal of Pharmaceutics 31, 201-207.

Kachrimanis, K., Malamataris, S., 2004. *"Apparent" Young's elastic modulus and radial recovery for some tableted pharmaceutical excipients*. European Journal of Pharmaceutical Sciences 21, 197-207.

Kalman, H., 2020. *Phenomenological study of particulate materials compression – From individual through bed compression to tableting*. Powder Technology 372, 161-177.

Katz, J.M., Roopwani, R., Buckner, I.S., 2013. *A material-sparing method for assessment of powder deformation characteristics using data collected during a single compression-decompression cycle*. Journal of Pharmaceutical Sciences 102, 3687-3693.

Kawakita, K., Lüdde, K.-H., 1971. *Some considerations on powder compression equations*. Powder Technology 4, 61-68.

Kawakita, K., Tsutsumi, Y., 1966. *A Comparison of Equations for Powder Compression*. Bulletin of the Chemical Society of Japan 39, 1364-1368.

Kern, M., Riedel, T., Breitkreutz, J., 2022. *Investigating key properties of model excipients and binary powder blends using ultrasonic in-die measurements on a compaction simulator*. International Journal of Pharmaceutics 613.

Kim, H., Venkatesh, G., Fassihi, R., 1998. *Compactibility characterization of granular pectin for tableting operation using a compaction simulator*. International Journal of Pharmaceutics 161, 149-159.

Kinsler, L.E., Frey, A.R., Coppens, A.B., Sanders, J.V., 2000. *Fundamentals of Acoustics*, 4th Edition. John Wiley and Sons, New York, NY.

Klevan, I., Nordström, J., Bauer-Brandl, A., Alderborn, G., 2009. *On the physical interpretation of the initial bending of a Shapiro-Konopicky-Heckel compression profile*. European Journal of Pharmaceutics and Biopharmaceutics 71, 395-401.

Klevan, I., Nordström, J., Tho, I., Alderborn, G., 2010. *A statistical approach to evaluate the potential use of compression parameters for classification of pharmaceutical powder materials*. European Journal of Pharmaceutics and Biopharmaceutics 75, 425-435.

Kohout, T., Karlqvist, R., Lassila, I., Eskelinen, J., Hortling, A., Pesonen, L.J., Hæggström, E., 2013. *Ultrasonic determination of porosity in homogeneous ceramic samples*. Geophysica 49, 25-32.

Krautkrämer, J., Krautkrämer, H., 1990. *Ultrasonic Testing of Materials*, 4th Edition. Springer-Verlag, Berlin.

Krumme, M., Schwabe, L., Frömming, K.H., 2000. *Development of computerised procedures for the characterisation of the tableting properties with eccentric machines: Extended Heckel analysis*. European Journal of Pharmaceutics and Biopharmaceutics 49, 275-286.

Krycer, I., Pope, D.G., Hersey, J.A., 1982. *The interpretation of powder compaction data - a critical review*. Drug Development and Industrial Pharmacy 8, 307-342.

Kuentz, M., Leuenberger, H., 1999. *Pressure susceptibility of polymer tablets as a critical property: A modified Heckel equation*. Journal of Pharmaceutical Sciences 88, 174-179.

Lamešić, D., Planinšek, O., German Ilić, I., 2018. *Modified equation for particle bonding area and strength with inclusion of powder fragmentation propensity*. European Journal of Pharmaceutical Sciences 121, 218-227.

Leane, M., Pitt, K., Reynolds, G., Anwar, J., Charlton, S., Crean, A., Creekmore, R., Davies, C., DeBeer, T., De-Matas, M., Djemai, A., Douroumis, D., Gaisford, S., Gamble, J., Stone, E.H.,

Kavanagh, A., Khimyak, Y., Kleinebudde, P., Moreton, C., Paudel, A., Storey, R., Toschkoff, G., Vyas, K., 2015. *A proposal for a drug product Manufacturing Classification System (MCS) for oral solid dosage forms*. Pharmaceutical Development and Technology 20, 12-21.

Leane, M., Pitt, K., Reynolds, G.K., Dawson, N., Ziegler, I., Szepes, A., Crean, A.M., Dall Agnol, R., The Manufacturing Classification System Working, G., 2018. *Manufacturing classification system in the real world: factors influencing manufacturing process choices for filed commercial oral solid dosage formulations, case studies from industry and considerations for continuous processing*. Pharmaceutical Development and Technology 23, 964-977.

Leskinen, J.T.T., Hakulinen, M.A., Kuosmanen, M., Ketolainen, J., Abrahmsén-Alami, S., Lappalainen, R., 2011. *Monitoring of swelling of hydrophilic polymer matrix tablets by ultrasound techniques*. International Journal of Pharmaceutics 404, 142-147.

Leskinen, J.T.T., Simonaho, S.P., Hakulinen, M., Ketolainen, J., 2010. *In-line ultrasound measurement system for detecting tablet integrity*. International Journal of Pharmaceutics 400, 104-113.

Leskinen, J.T.T., Simonaho, S.P., Hakulinen, M., Ketolainen, J., 2013. *Real-time tablet formation monitoring with ultrasound measurements in eccentric single station tablet press*. International Journal of Pharmaceutics 442, 27-34.

Leuenberger, H., Lanz, M., 2005. *Pharmaceutical powder technology - From art to science: The challenge of the FDA's process analytical technology initiative*. Advanced Powder Technology 16, 3-25.

Leuenberger, H., Rohera, B.D., 1986. *Fundamentals of powder compression. I. The compactibility and compressibility of pharmaceutical powders*. Pharmaceutical Research: An Official Journal of the American Association of Pharmaceutical Scientists 3, 12-22.

Levina, M., Rubinstein, M.H., Rajabi-Siahboomi, A.R., 2000. *Principles and application of ultrasound in pharmaceutical powder compression*. Pharmaceutical Research 17, 257-265.

Liu, J., Cetinkaya, C., 2010. *Mechanical and geometric property characterization of dry-coated tablets with contact ultrasonic techniques*. International Journal of Pharmaceutics 392, 148-155.

Liu, J., Stephens, J.D., Kowalczyk, B.R., Cetinkaya, C., 2011. *Real-time in-die compaction monitoring of dry-coated tablets*. International Journal of Pharmaceutics 414, 171-178.

Lum, S.K., Duncan-Hewitt, W.C., 1996. *A comparison of elastic moduli derived from theory, microindentation, and ultrasonic testing*. Pharmaceutical Research 13, 1739-1745.

Mahmoodi, F., Klevan, I., Nordström, J., Alderborn, G., Frenning, G., 2013. *A comparison between two powder compaction parameters of plasticity: The effective medium a parameter and the Heckel 1/K parameter*. International Journal of Pharmaceutics 453, 295-299.

Markl, D., Bawuah, P., Ridgway, C., van den Ban, S., Goodwin, D.J., Ketolainen, J., Gane, P., Peiponen, K.E., Zeitler, J.A., 2018a. *Fast and non-destructive pore structure analysis using terahertz time-domain spectroscopy*. International Journal of Pharmaceutics 537, 102-110.

Markl, D., Strobel, A., Schlossnikl, R., Bøtker, J., Bawuah, P., Ridgway, C., Rantanen, J., Rades, T., Gane, P., Peiponen, K.E., Zeitler, J.A., 2018b. *Characterisation of pore structures of pharmaceutical tablets: A review*. International Journal of Pharmaceutics 538, 188-214.

Markl, D., Wang, P., Ridgway, C., Karttunen, A.P., Chakraborty, M., Bawuah, P., Pääkkönen, P., Gane, P., Ketolainen, J., Peiponen, K.E., Zeitler, J.A., 2017. *Characterization of the pore structure of functionalized calcium carbonate tablets by terahertz time-domain spectroscopy and X-ray computed microtomography*. Journal of Pharmaceutical Sciences 106, 1586-1595.

Masteau, J.C., Thomas, G., 1999. *Modelling to understand porosity and specific surface area charges during tabletting*. Powder Technology 101, 240-248.

Mazel, V., Busignies, V., Diarra, H., Tchoreloff, P., 2012. *Measurements of elastic moduli of pharmaceutical compacts: A new methodology using double compaction on a compaction simulator*. Journal of Pharmaceutical Sciences 101, 2220-2228.

Mazel, V., Busignies, V., Diarra, H., Tchoreloff, P., 2013. *On the links between elastic constants and effective elastic behavior of pharmaceutical compacts: Importance of poisson's ratio and use of bulk modulus*. Journal of Pharmaceutical Sciences 102, 4009-4014.

Mazel, V., Diarra, H., Busignies, V., Tchoreloff, P., 2015. *Evolution of the die-wall pressure during the compression of biconvex tablets: Experimental results and comparison with FEM simulation*. Journal of Pharmaceutical Sciences 104, 4339-4344.

Michrafy, A., Michrafy, M., Kadiri, M.S., Dodds, J.A., 2007. *Predictions of tensile strength of binary tablets using linear and power law mixing rules*. International Journal of Pharmaceutics 333, 118-126.

Michrafy, A., Ringenbacher, D., Tchoreloff, P., 2002. *Modelling the compaction behaviour of powders: Application to pharmaceutical powders*. Powder Technology 127, 257-266.

Millán-Jiménez, M., Galdón, E., Ferrero, C., Caraballo, I., 2017. *Application of ultrasound-assisted compression in pharmaceutical technology. Design and optimization of oral sustained-release dosage forms*. Journal of Drug Delivery Science and Technology 42, 119-125.

Nagarajan, A., 1971. *Ultrasonic study of elasticity-porosity relationship in polycrystalline alumina*. Journal of Applied Physics 42, 3693-3696.

Nicklasson, F., Alderborn, G., 2000. *Analysis of the compression mechanics of pharmaceutical agglomerates of different porosity and composition using the Adams and Kawakita equations*. Pharmaceutical Research 17, 949-954.

Nordström, J., Klevan, I., Alderborn, G., 2012. *A protocol for the classification of powder compression characteristics*. European Journal of Pharmaceutics and Biopharmaceutics 80, 209-216.

Nyström, C., Alderborn, G., Duberg, M., Karehill, P.G., 1993. *Bonding surface area and bonding mechanism-two important factors fir the understanding of powder comparability*. Drug Development and Industrial Pharmacy 19, 2143-2196.

Nyström, C., Mazur, J., Sjögren, J., 1982. *Studies on direct compression of tablets II. The influence of the particle size of a dry binder on the mechanical strength of tablets*. International Journal of Pharmaceutics 10, 209-218.

Ohrem, H.L., Schornick, E., Kalivoda, A., Ognibene, R., 2014. *Why is mannitol becoming more and more popular as a pharmaceutical excipient in solid dosage forms?* Pharmaceutical Development and Technology 19, 257-262.

Palmieri, G.F., Joiris, E., Bonacucina, G., Cespi, M., Mercuri, A., 2005. *Differences between eccentric and rotary tablet machines in the evaluation of powder densification behaviour*. International Journal of Pharmaceutics 298, 164-175.

Patel, S., Bansal, A.K., 2011. *Prediction of mechanical properties of compacted binary mixtures containing high-dose poorly compressible drug*. International Journal of Pharmaceutics 403, 109-114.

Paul, S., Sun, C.C., 2017. *Gaining insight into tablet capping tendency from compaction simulation*. International Journal of Pharmaceutics 524, 111-120.

Paulick, M., Morgeneyer, M., Kwade, A., 2015. *Review on the influence of elastic particle properties on DEM simulation results*. Powder Technology 283, 66-76.

Peiponen, K.E., Bawuah, P., Chakraborty, M., Juuti, M., Zeitler, J.A., Ketolainen, J., 2015. *Estimation of Young's modulus of pharmaceutical tablet obtained by terahertz time-delay measurement*. International Journal of Pharmaceutics 489, 100-105.

Ph. Eur. 10.5: *2.9.36. Powder Flow*, in: European Pharmacopoeia (2021), Strasbourg, Council of Europe.

Phani, K.K., Niyogi, S.K., 1987. *Young's modulus of porous brittle solids*. Journal of Materials Science 22, 257-263.

Piekarczyk, W., Kata, D., 2016. *Methodology for determining material constants of anisotropic materials belonging to the transversely isotropic system by ultrasound method*. Ultrasonics 71, 199-204.

Porion, P., Busignies, V., Mazel, V., Leclerc, B., Evesque, P., Tchoreloff, P., 2010. *Anisotropic porous structure of pharmaceutical compacts evaluated by PGSTE-NMR in relation to mechanical property anisotropy*. Pharmaceutical Research 27, 2221-2233.

Radovic, M., Lara-Curzio, E., Riester, L., 2004. *Comparison of different experimental techniques for determination of elastic properties of solids*. Materials Science and Engineering A 368, 56-70.

Ragnarsson, G., 1996. *Force-Displacement and Network Measurements*, in: Alderborn, G., Nyström, C. (Eds.), Pharmaceutical Powder Compaction Technology. Marcel Dekker, New York, NY.

Rasenack, N., Müller, B.W., 2002. *Crystal habit and tableting behavior*. International Journal of Pharmaceutics 244, 45-57.

Razavi, S.M., Callegari, G., Drazer, G., Cuitiño, A.M., 2016. *Toward predicting tensile strength of pharmaceutical tablets by ultrasound measurement in continuous manufacturing*. International Journal of Pharmaceutics 507, 83-89.

Rippie, E.G., Danielson, D.W., 1981. *Viscoelastic stress/strain behavior of pharmaceutical tablets: Analysis during unloading and postcompression periods*. Journal of Pharmaceutical Sciences 70, 476-482.

Roberts, R.J., Rowe, R.C., York, P., 1994. *The Poisson's ratio of microcrystalline cellulose*. International Journal of Pharmaceutics 105, 177-180.

Roopwani, R., Buckner, I.S., 2011. *Understanding deformation mechanisms during powder compaction using principal component analysis of compression data*. International Journal of Pharmaceutics 418, 227-234.

Rosato, D.V., Rosato, D.V., 2003. *Plastics engineered product design*, 1st Edition. Elsevier Advanced Technology, Oxford; New York.

Rowe, R.C., Roberts, R.J., 1996. *Mechanical Properties*, in: Alderborn, G., Nyström, C. (Eds.), Pharmaceutical Powder Compaction Technology. Marcel Dekker, New York, NY.

Rowe, R.C., Sheskey, P.J., Quinn, M.E., 2009. *Handbook of Pharmaceutical Excipients*, 6th Edition. Pharmaceutical Press and American Pharmacists Association, London.

Ruegger, C.E., Çelick, M., 2000. *The effect of compression and decompression speed on the mechanical strength of compacts*. Pharmaceutical Development and Technology 5, 485-494.

Rumpf, H., 1958. *Grundlagen und Methoden des Granulierens*. Chemie Ingenieur Technik 30, 144-158.

Salbu, L., Bauer-Brandl, A., Tho, I., 2010. *Direct compression behavior of low- and high-methoxylated pectins*. AAPS PharmSciTech 11, 18-26.

Sarpün, I.H., Özkan, V., Tuncel, S., 2009. *Ultrasonic determination of elastic modulus of marbles relation with porosity and CaO %*, 10th International Conference of the Slovenian Society for Non-Destructive Testing: Application of Contemporary Non-Destructive Testing in Engineering, pp. 119-125.

Sayers, C.M., 1981. *Ultrasonic velocity dispersion in porous materials*. Journal of Physics D: Applied Physics 14, 413-420.

Schlack, H., 2001. *Kompressibilität und Kompaktibilität von Hilfsstoffen bei der Tablettierung*. Albert-Ludwigs-Universität, Freiburg im Breisgau.

Schmerr, L.W., 2016. *Fundamentals of Ultrasonic Nondestructive Evaluation*, 2nd Edition. Springer, Cham.

Schmidtke, R., Schröder, D., Menth, J., Staab, A., Braun, M., Wagner, K.G., 2017. *Prediction of solid fraction from powder mixtures based on single component compression analysis*. International Journal of Pharmaceutics 523, 366-375.

Shang, C., Sinka, I.C., Pan, J., 2013. *Modelling of the break force of tablets under diametrical compression*. International Journal of Pharmaceutics 445, 99-107.

Simonaho, S.P., Takala, T.A., Kuosmanen, M., Ketolainen, J., 2011. *Ultrasound transmission measurements for tensile strength evaluation of tablets*. International Journal of Pharmaceutics 409, 104-110.

Sinka, I.C., 2007. *Modelling powder compaction*. KONA Powder and Particle Journal 25, 4-22.

Skelbæk-Pedersen, A., Vilhelmsen, T., Wallaert, V., Rantanen, J., 2019. *Quantification of fragmentation of pharmaceutical materials after tableting*. Journal of Pharmaceutical Sciences 108, 1246-1253.

Skelbæk-Pedersen, A.L., Vilhelmsen, T.K., Wallaert, V., Rantanen, J., 2020. *Investigation of the effects of particle size on fragmentation during tableting*. International Journal of Pharmaceutics 576.

Sonnergaard, J.M., 1999. *A critical evaluation of the Heckel equation*. International Journal of Pharmaceutics 193, 63-71.

Sonnergaard, J.M., 2001. *Investigation of a new mathematical model for compression of pharmaceutical powders*. European Journal of Pharmaceutical Sciences 14, 149-157.

Spriggs, R.M., 1961. *Expression for effect of porosity on elastic modulus of polycrystalline refractory materials, particularly aluminum oxide*. Journal of the American Ceramic Society 44, 628-629.

Stephens, J.D., Kowalczyk, B.R., Hancock, B.C., Kaul, G., Cetinkaya, C., 2013a. *Ultrasonic real-time in-die monitoring of the tablet compaction process - A proof of concept study*. International Journal of Pharmaceutics 442, 20-26.

Stephens, J.D., Lakshmaiah, M.V., Kowalczyk, B.R., Hancock, B.C., Cetinkaya, C., 2013b. *Wireless transmission of ultrasonic waveforms for monitoring drug tablet properties and defects*. International Journal of Pharmaceutics 442, 35-41.

Sun, C.C., 2005. *True density of microcrystalline cellulose*. Journal of Pharmaceutical Sciences 94, 2132-2134.

Sun, C.C., 2016. *A classification system for tableting behaviors of binary powder mixtures*. Asian Journal of Pharmaceutical Sciences 11, 486-491.

Sun, C.C., 2017. *Microstructure of tablet—Pharmaceutical significance, assessment, and engineering*. Pharmaceutical Research 34, 918-928.

Sun, C.C., Grant, D.J.W., 2001. *Influence of elastic deformation of particles on Heckel analysis*. Pharmaceutical Development and Technology 6, 193-200.

Takatsubo, J., Yamamoto, S., 1991. *Stochastic theory of propagation of elastic waves in porous solids for nondestructive pore characterization*. JSME International Journal, Series 1: Solid Mechanics, Strength of Materials 34, 412-420.

Takatsubo, J., Yamamoto, S., 1996. *Propagation mechanism of ultrasonic waves in porous ceramics*. JSME International Journal, Series A: Mechanics and Material Engineering 39, 266-271.

Tarlier, N., Soulairol, I., Bataille, B., Baylac, G., Ravel, P., Nofrerias, I., Lefèvre, P., Sharkawi, T., 2015. *Compaction behavior and deformation mechanism of directly compressible textured mannitol in a rotary tablet press simulator*. International Journal of Pharmaceutics 495, 410-419.

Thoorens, G., Krier, F., Leclercq, B., Carlin, B., Evrard, B., 2014. *Microcrystalline cellulose, a direct compression binder in a quality by design environment - A review*. International Journal of Pharmaceutics 473, 64-72.

Van Der Voort Maarschalk, K., Zuurman, K., Vromans, H., Bolhuis, G.K., Lerk, C.F., 1996. *Porosity expansion of tablets as a result of bonding and deformation of particulate solids*. International Journal of Pharmaceutics 140, 185-193.

Van Der Voort Maarschalk, K., Zuurman, K., Vromans, H., Bolhuis, G.K., Lerk, C.F., 1997. *Stress relaxation of compacts produced from viscoelastic materials*. International Journal of Pharmaceutics 151, 27-34.

Van Veen, B., Van der Voort Maarschalk, K., Bolhuis, G.K., Visser, M.R., Zuurman, K., Frijlink, H.W., 2002. *Pore formation in tablets compressed from binary mixtures as a result of deformation and relaxation of particles*. European Journal of Pharmaceutical Sciences 15, 171-177.

Van Veen, B., Van Der Voort Maarschalk, K., Bolhuis, G.K., Zuurman, K., Frijlink, H.W., 2000. *Tensile strength of tablets containing two materials with a different compaction behaviour*. International Journal of Pharmaceutics 203, 71-79.

Wang, J., Wen, H., Desai, D., 2010. *Lubrication in tablet formulations*. European Journal of Pharmaceutics and Biopharmaceutics 75, 1-15.

Wang, J.C., 1984a. *Young's modulus of porous materials - Part 1 Theoretical derivation of modulus-porosity correlation*. Journal of Materials Science 19, 801-808.

Wang, J.C., 1984b. *Young's modulus of porous materials - Part 2 Young's modulus of porous alumina with changing pore structure*. Journal of Materials Science 19, 809-814.

Wang, S.Y., Chiu, C.M., Lin, C.J., 2002. *Variations in ultrasonic wave velocity and dynamic Young's modulus with moisture content for Taiwania plantation lumber*. Wood and Fiber Science 34, 370-381.

Westermarck, S., Juppo, A.M., Kervinen, L., Yliruusi, J., 1998. *Pore structure and surface area of mannitol powder, granules and tablets determined with mercury porosimetry and nitrogen adsorption*. European Journal of Pharmaceutics and Biopharmaceutics 46, 61-68.

Westermarck, S., Juppo, A.M., Kervinen, L., Yliruusi, J., 1999. *Microcrystalline cellulose and its microstructure in pharmaceutical processing*. European Journal of Pharmaceutics and Biopharmaceutics 48, 199-206.

Wong, L.W., Pilpel, N., 1990. *The effect of particle shape on the mechanical properties of powders*. International Journal of Pharmaceutics 59, 145-154.

Wu, C.Y., Best, S.M., Bentham, A.C., Hancock, B.C., Bonfield, W., 2005a. *A simple predictive model for the tensile strength of binary tablets*. European Journal of Pharmaceutical Sciences 25, 331-336.

Wu, C.Y., Ruddy, O.M., Bentham, A.C., Hancock, B.C., Best, S.M., Elliott, J.A., 2005b. *Modelling the mechanical behaviour of pharmaceutical powders during compaction*. Powder Technology 152, 107-117.

Wu, S.J., Chin, P.C., Liu, H., 2019. *Measurement of elastic properties of brittle materials by ultrasonic and indentation methods*. Applied Sciences (Switzerland) 9.

Wu, Y.S., Frijlink, H.W., Van Vliet, L.J., Stokroos, I., Van Der Voort Maarschalk, K., 2005c. *Location-dependent analysis of porosity and pore direction in tablets*. Pharmaceutical Research 22, 1399-1405.

Wu, Y.S., Frijlink, H.W., van Vliet, L.J., van der Voort Maarschalk, K., 2008. *Pore shape in the sodium chloride matrix of tablets after the addition of starch as a second component*. European Journal of Pharmaceutics and Biopharmaceutics 70, 539-543.

Wu, Y.S., van Vliet, L.J., Frijlink, H.W., van der Voort Maarschalk, K., 2007. *Pore size distribution in tablets measured with a morphological sieve*. International Journal of Pharmaceutics 342, 176-183.

Wünsch, I., Friesen, I., Puckhaber, D., Schlegel, T., Finke, J.H., 2020. *Scaling tableting processes from compaction simulator to rotary presses—mind the sub-processes*. Pharmaceutics 12.

Xu, X., Coskunturk, Y., Dave, V.S., Kuriyilel, J.V., Wright, M.F., Dave, R.H., Cetinkaya, C., 2020. *Effects of compaction pressure, speed and punch head profile on the ultrasonically-extracted physical properties of pharmaceutical compacts*. International Journal of Pharmaceutics 575.

Xu, X., Mack, C., Cleland, Z.J., Vallabh, C.K.P., Dave, V.S., Cetinkaya, C., 2018a. *Correlation of solid dosage porosity and tensile strength with acoustically extracted mechanical properties*. International Journal of Pharmaceutics 542, 153-163.

Xu, X., Vallabh, C.K.P., Hoag, S.W., Dave, V.S., Cetinkaya, C., 2018b. *Early detection of capping risk in pharmaceutical compacts*. International Journal of Pharmaceutics 553, 338-348.

Yang, B.H., Wu, A.X., Miao, X.X., Liu, J.Z., 2014. *3D characterization and analysis of pore structure of packed ore particle beds based on computed tomography images*. Transactions of Nonferrous Metals Society of China (English Edition) 24, 833-838.

Yohannes, B., Gonzalez, M., Abebe, A., Sprockel, O., Nikfar, F., Kiang, S., Cuitinõ, A.M., 2016. *Evolution of the microstructure during the process of consolidation and bonding in soft granular solids*. International Journal of Pharmaceutics 503, 68-77.

Yu, S.W., Frijlink, H.W., Van Vliet, L.J., Stokroos, I., Van Der Voort Maarschalk, K., 2005. *Location-dependent analysis of porosity and pore direction in tablets*. Pharmaceutical Research 22, 1399-1405.

Zhang, Y., Law, Y., Chakrabarti, S., 2003. *Physical properties and compact analysis of commonly used direct compression binders*. AAPS PharmSciTech 4.

Zhong, H., Chan, G., Hu, Y., Hu, H., Ouyang, D., 2018. *A comprehensive map of FDA-approved pharmaceutical products*. Pharmaceutics 10.

Appendix

Table A-1: Powder characteristics of the raw materials (n = 3); Standard deviation in brackets.

Material	Density [g/mL]	D10 [µm]	D50 [µm]	D90 [µm]	LoD [%]
ACP	2.9667 (± 0.0188)	5.0 (± 0.1)	18.6 (± 0.1)	30.9 (± 0.1)	0.22 (± 0.01)
GranuLac 200	1.5548 (± 0.0038)	10.5 (± 0.3)	37.4 (± 1.1)	107.9 (± 1.0)	0.08 (± 0.02)
Tablettose 100	1.5560 (± 0.0048)	45.1 (± 0.3)	135.6 (± 1.7)	347.8 (± 4.5)	0.34 (± 0.05)
Parteck M 200	1.5210 (± 0.0117)	69.1 (± 1.6)	139.1 (± 1.5)	213.5 (± 2.3)	0.17 (± 0.05)
Pearlitol 200 SD	1.4836 (± 0.0029)	91.9 (± 0.9)	144.9 (± 0.1)	205.7 (± 0.5)	0.22 (± 0.02)
D(-)-Mannit	1.5043 (± 0.0034)	28.8 (± 0.4)	83.7 (± 0.4)	186.1 (± 1.5)	0.13 (± 0.03)
Parteck Delta M	1.5253 (± 0.0019)	15.8 (± 0.1)	47.6 (± 0.8)	151.1 (± 2.2)	0.08 (± 0.06)
Vivapur 101	1.5899 (± 0.0094)	20.5 (± 0.4)	49.7 (± 1.7)	107.7 (± 0.9)	4.56 (± 0.06)
Vivapur 102	1.5990 (± 0.0052)	31.9 (± 0.5)	109.5 (± 0.8)	199.0 (± 0.5)	4.17 (± 0.09)
Vivapur 112	1.5756 (± 0.0046)	27.2 (± 0.4)	97.7 (± 2.5)	197.2 (± 1.1)	2.38 (± 0.18)
Native Maize Starch	1.5338 (± 0.0068)	10.5 (± 0.0)	16.0 (± 0.0)	22.0 (± 0.0)	10.97 (± 0.02)
Starch 1500	1.5080 (± 0.0028)	20.5 (± 0.2)	89.7 (± 0.3)	156.5 (± 0.2)	8.80 (± 0.11)

Table A-2: Set parameters for the standard KIM measurements of the raw materials.

Material	Target thickness [mm]	Gain long [dB]	Gain trans [dB]
ACP	1.00	-3	-9
GranuLac 200	1.40	1	1
Tablettose 100	1.40	-4	-5
Parteck M 200	1.50	-1	-1
Pearlitol 200 SD	1.50	-1	3
D(-)-Mannit	1.40	-1	5
Parteck Delta M	1.45	-1	3
Vivapur 101	1.20	5	15
Vivapur 102	1.20	5	17
Vivapur 112	1.20	5	17
Native Maize Starch	1.30	7	15
Starch 1500	1.30	5	15

Table A-3: Target compression thickness set to reach different maximum pressures in mm.

Material	250 MPa	200 MPa	150 MPa
Parteck M 200	1.50	1.88	2.24
Tablettose 100	1.40	1.75	2.06
Vivapur 101	1.20	1.40	1.60

Table A-4: Pycnometric density of the mixtures prepared from the raw materials in Table A-1 (n = 3); Standard deviation in brackets.

Material	Composition [%w]	Density [g/mL]
MN/LM	50:50	1.5406 (± 0.0016)
MN/MCC	50:50	1.5658 (± 0.0022)
LM/MCC	50:50	1.5829 (± 0.0023)
ACP/MCC	75:25	2.4496 (± 0.0082)
ACP/MCC	50:50	2.0841 (± 0.0071)
ACP/MCC	25:75	1.8144 (± 0.0083)
ACP/MS	75:25	2.4050 (± 0.0057)
ACP/MS	50:50	2.0071 (± 0.0042)
ACP/MS	25:75	1.7230 (± 0.0050)
MCC/MS	75:25	1.5986 (± 0.0057)
MCC/MS	50:50	1.5638 (± 0.0022)
MCC/MS	25:75	1.5359 (± 0.0076)
ACP/MCC/MS	33:33:33	1.8247 (± 0.0052)
MN/LM/MS	33:33:33	1.5560 (± 0.0017)

Table A-5: Compression slope calculated for the materials used in this work in longitudinal and transverse mode (n=3); Standard deviation in brackets.

Material	Longitudinal Compression Slope [mm/µs]	Transverse Compression Slope [mm/µs]
ACP	10.93 (± 0.46)	7.67 (± 0.12)
GranuLac 200	7.45 (± 0.08)	3.58 (± 0.06)
Tablettose 100	6.01 (± 0.07)	3.17 (± 0.00)
D(-)-Mannit	8.79 (± 0.16)	4.53 (± 0.08)
Parteck Delta M	8.02 (± 0.43)	4.50 (± 0.02)
Parteck M 200	4.80 (± 0.24)	2.69 (± 0.02)
Pearlitol 200SD	4.40 (± 0.05)	2.92 (± 0.01)
Maize Starch	4.21 (± 0.05)	1.62 (± 0.01)
Starch 1500	4.93 (± 0.03)	1.81 (± 0.01)
Vivapur 101	3.52 (± 0.07)	1.81 (± 0.01)
Vivapur 102	3.88 (± 0.28)	1.72 (± 0.01)
Vivapur 112	3.64 (± 0.16)	1.74 (± 0.00)

Table A-6: Parameters of Equation (3-4) determined for the longitudinal velocity profiles using Python's scipy.optimize package.

Material	y0 [mm/µs]	a [mm/µs]	b [mm/µs]	c [-]
ACP	-4.82	10.88	8.95E-19	49.48
GranuLac 200	-3.24	6.56	3.57E-07	14.01
Tablettose 100	-1.00	3.44	1.13E-02	4.81
Parteck M 200	-1.65	0.00	1.82E+00	1.13
Native Maize Starch	-0.91	3.61	4.54E-07	14.14
Vivapur 101	-0.43	2.89	3.20E-05	10.07

Table A-7: Parameters of Equation (3-4) determined for the transverse velocity profiles using Python's scipy.optimize package.

Material	y0 [mm/µs]	a [mm/µs]	b [mm/µs]	c [-]
ACP	-5.85	0.00	3.51E+00	1.06
GranuLac 200	-1.75	3.60	1.26E-07	0.11
Tablettose 100	-2.36	0.00	1.80E+00	0.86
Parteck M 200	-1.30	2.68	7.91E-01	0.00
Native Maize Starch	-0.15	1.50	5.44E-18	36.42
Vivapur 101	-0.17	1.72	1.22E-14	29.69

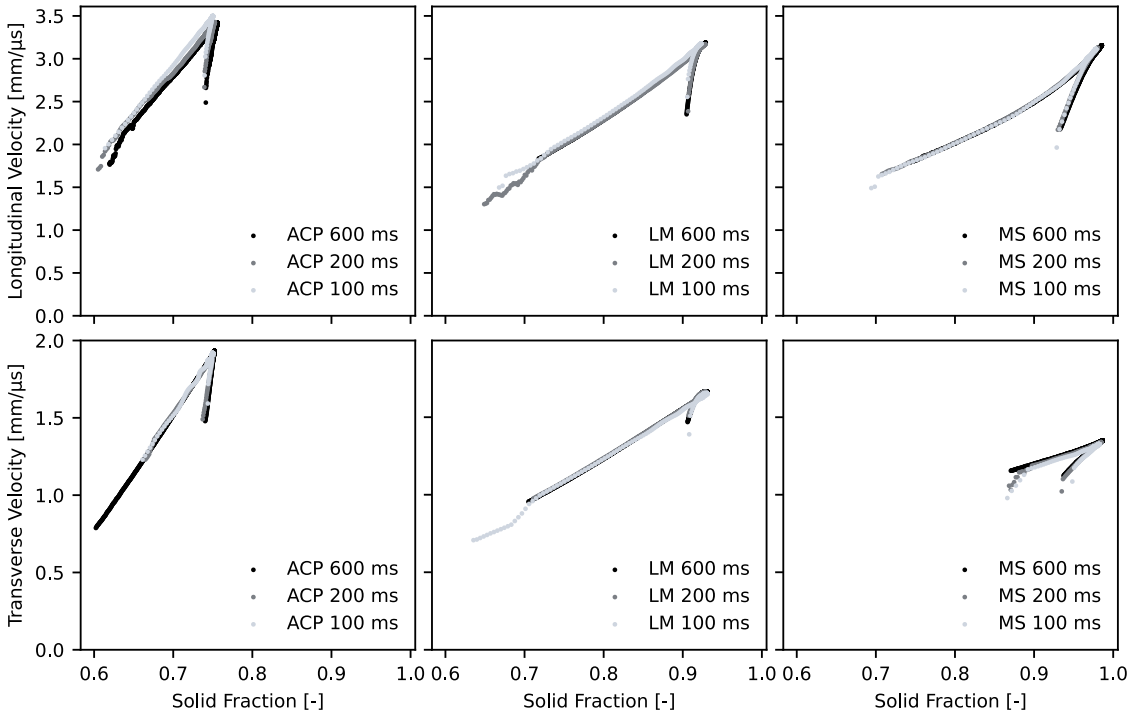

Figure A-1: Longitudinal and transverse US velocity through ACP, Tablettose 100 (LM) and maize starch (MS), recorded using three different compaction profiles. The compaction times are 600, 200 and 100 ms, respectively (n = 3). Plots in one row share y-axis; plots in one column share x-axis.

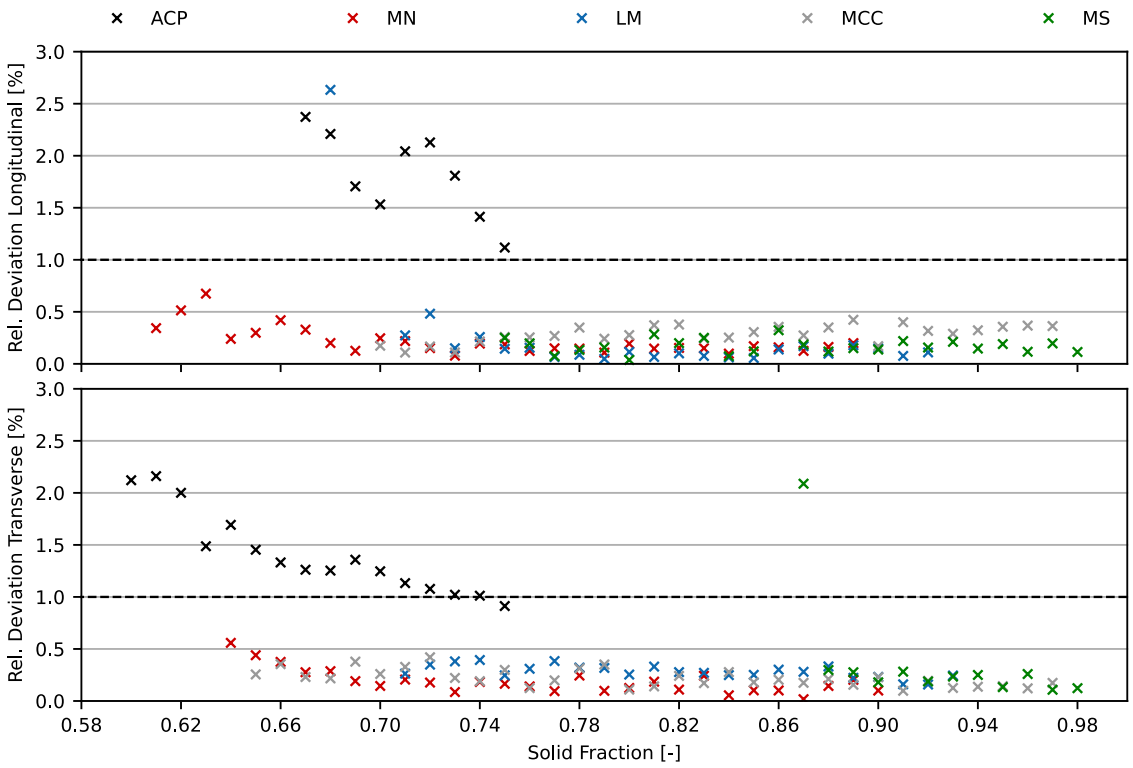

Figure A-2: Relative standard deviations between three consecutive measurements calculated for one exemplary grade per material. Plots share x-axis.

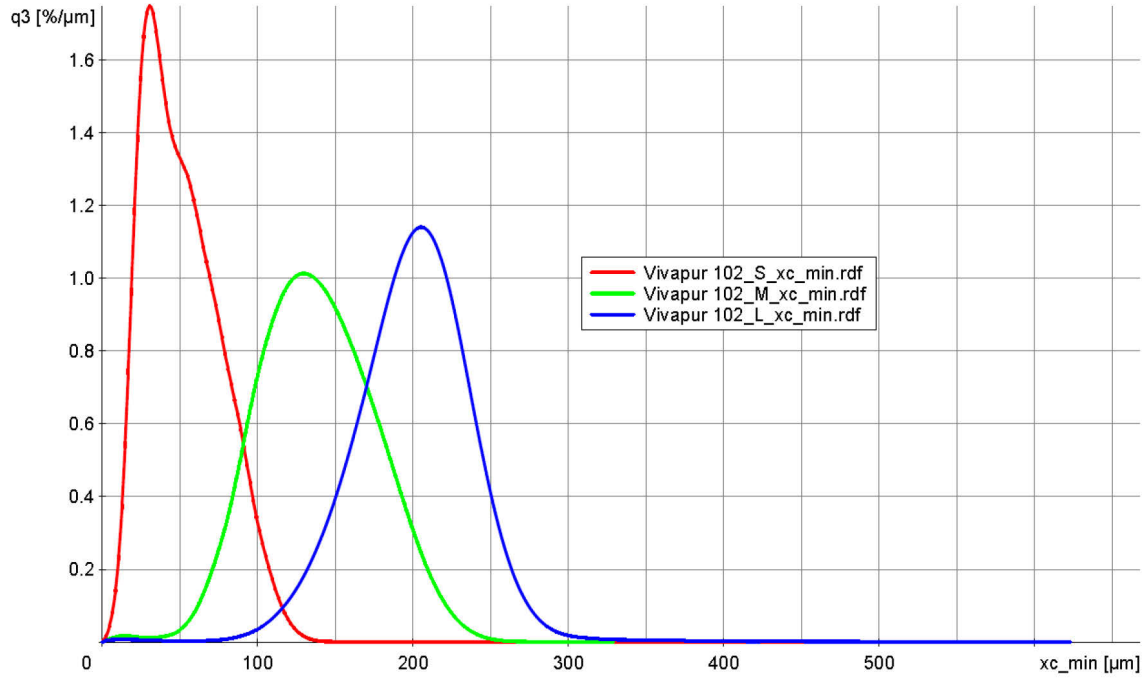

Figure A-3: PSD determined via Camsizer X2 for the three sieve classes of Vivapur 102. S = small, M = medium, L = large (n = 3).

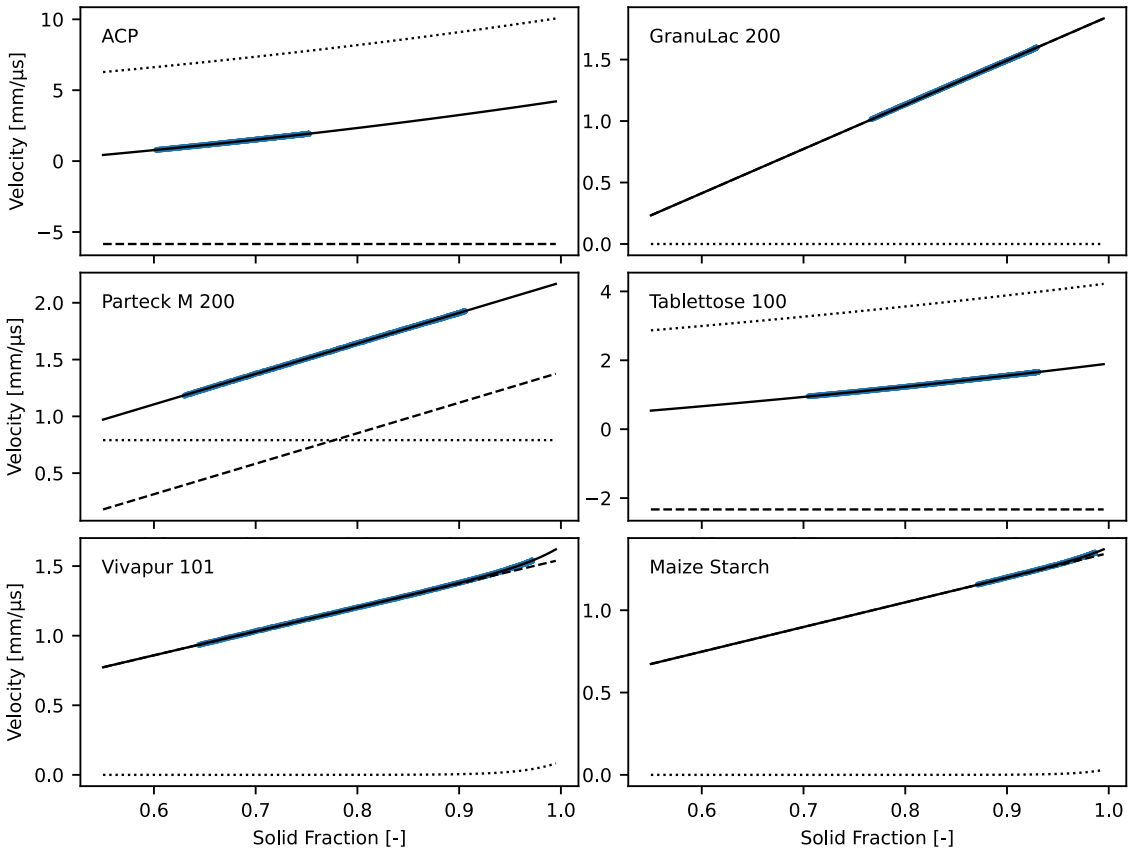

Figure A-4: Fit of Equation (3-4) to the experimental data measured in transverse mode including the mean of the three individual measurements (blue) and the complete fit (solid line), linear expression i.e. *y0 + ax* (dashed line) and exponential expression of the equation, i.e. be^{c*SF} (dotted line). Plots in one row share y-axis; plots in one column share x-axis.

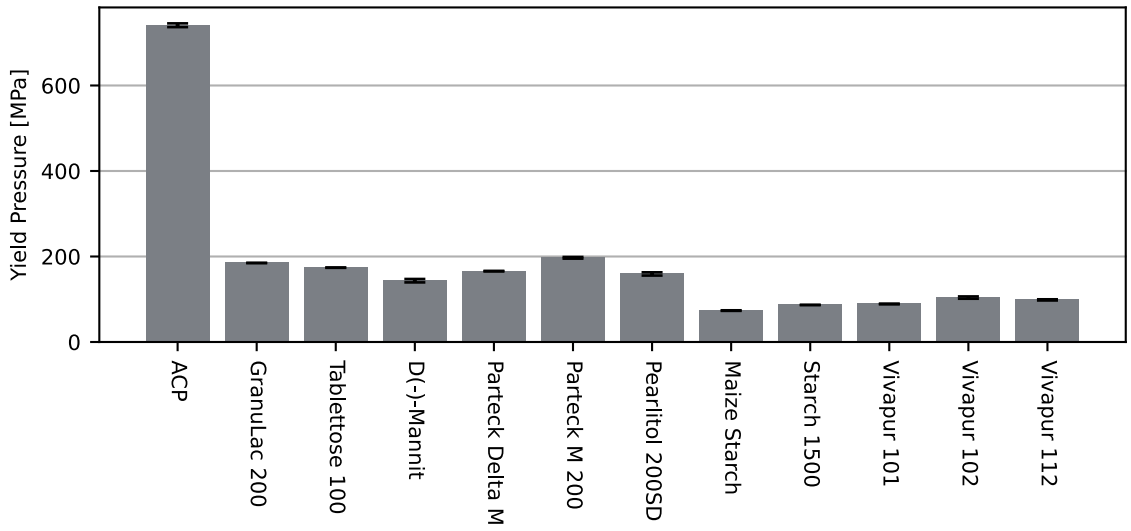

Figure A-5: Overview over the Heckel yield pressures. Arithmetic mean ± sd (n = 3).

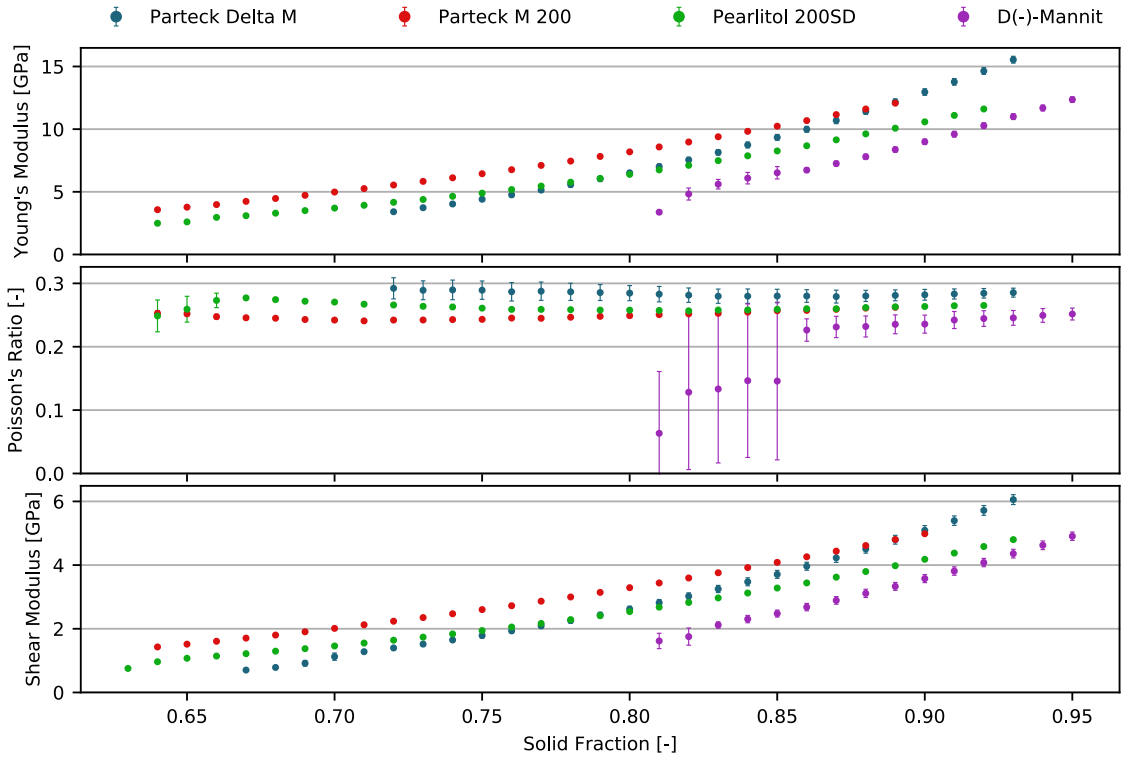

Figure A-6: Apparent Young's Modulus and Poisson's Ratio calculated for the mannitol grades using longitudinal and transverse ultrasonic velocity and apparent Shear Modulus calculated using transverse velocity through the materials during compression. Arithmetic mean ± sd (YM and PR: n = 9; SM: n = 3). Plots share x-axis.

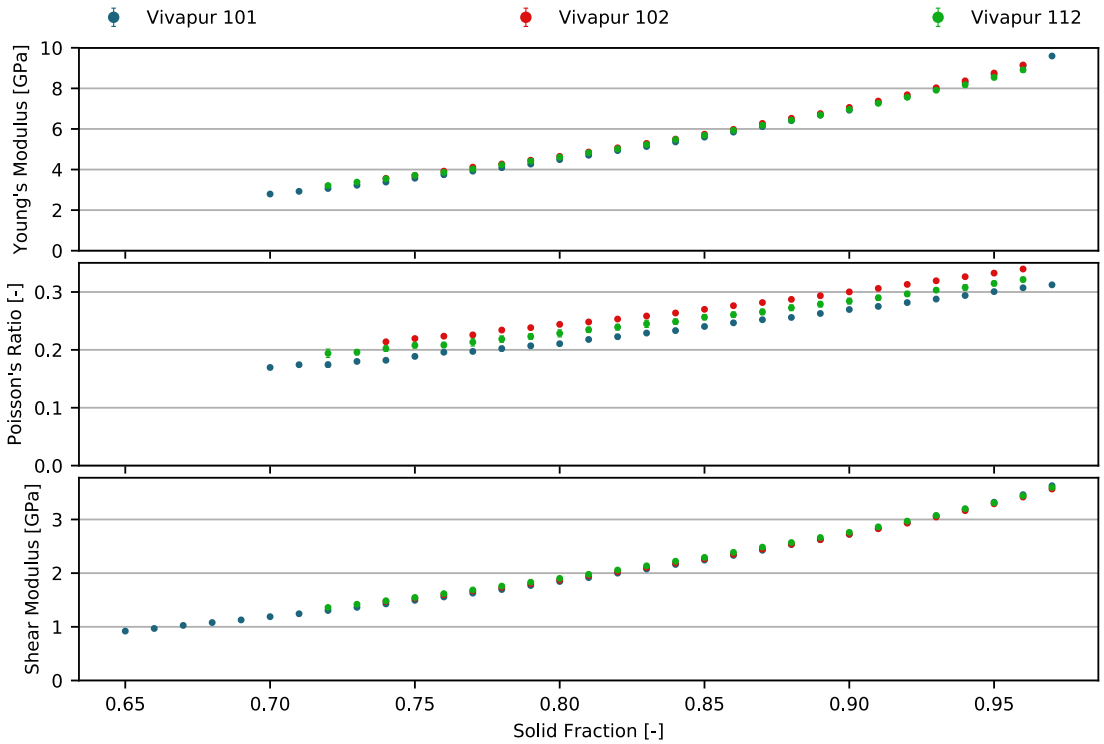

Figure A-7: Apparent Young's Modulus and Poisson's Ratio calculated for the MCC grades using longitudinal and transverse ultrasonic velocity and apparent Shear Modulus calculated using transverse velocity through the materials during compression. Arithmetic mean ± sd (YM and PR: n = 9; SM: n = 3). Plots share x-axis.

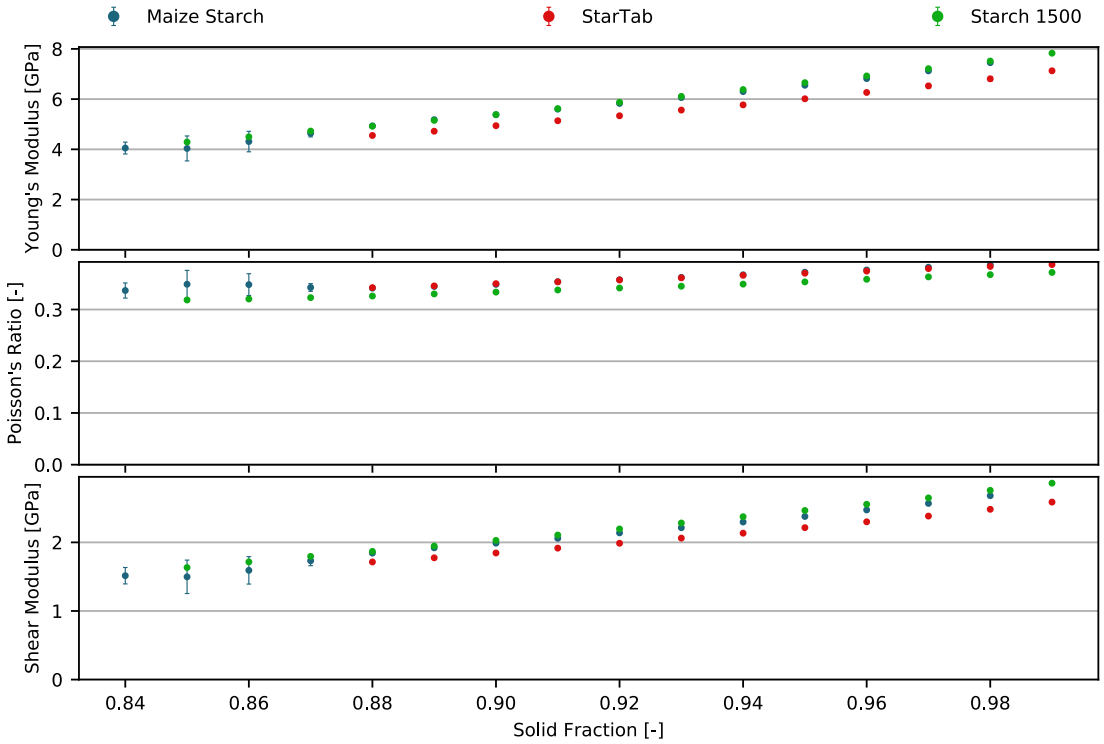

Figure A-8: Apparent Young's Modulus and Poisson's Ratio calculated for the starch grades using longitudinal and transverse ultrasonic velocity and apparent Shear Modulus calculated using transverse velocity through the materials during compression. Arithmetic mean ± sd (YM and PR: n = 9; SM: n = 3). Plots share x-axis.

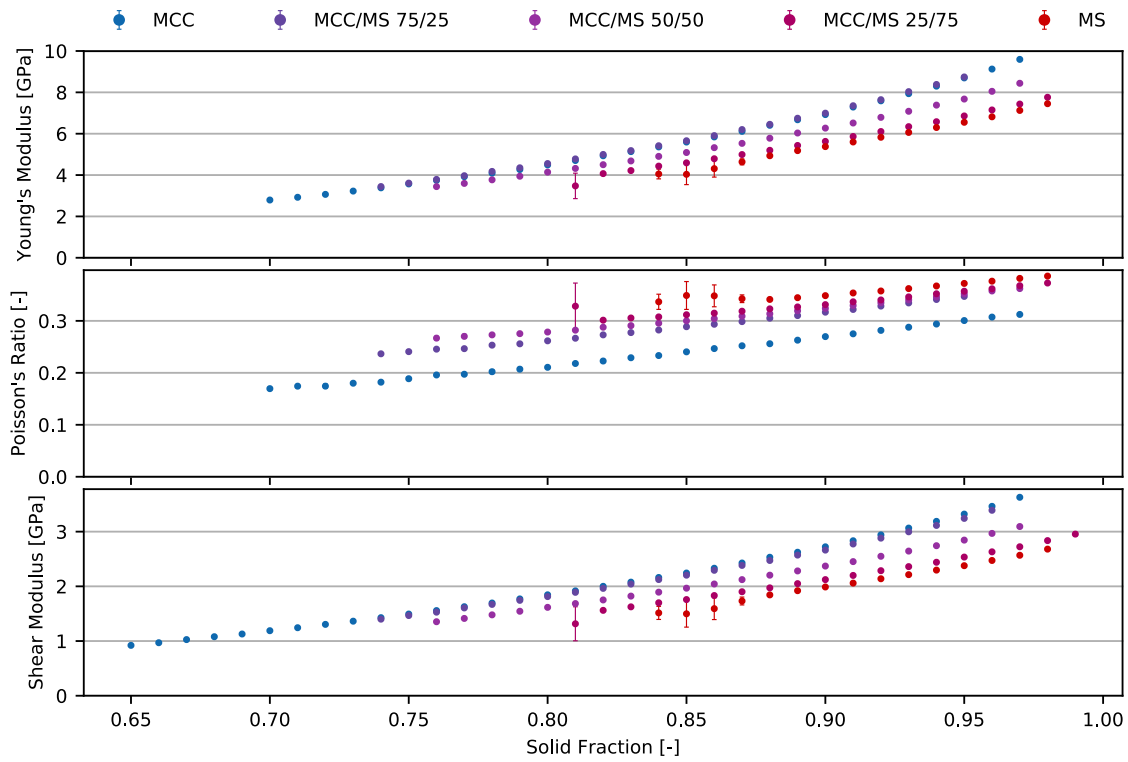

Figure A-9: YM, PR and SM calculated for MCC, MS and their blends. Arithmetic mean ± sd (YM and PR: n = 9; SM: n = 3). Plots share x-axis.

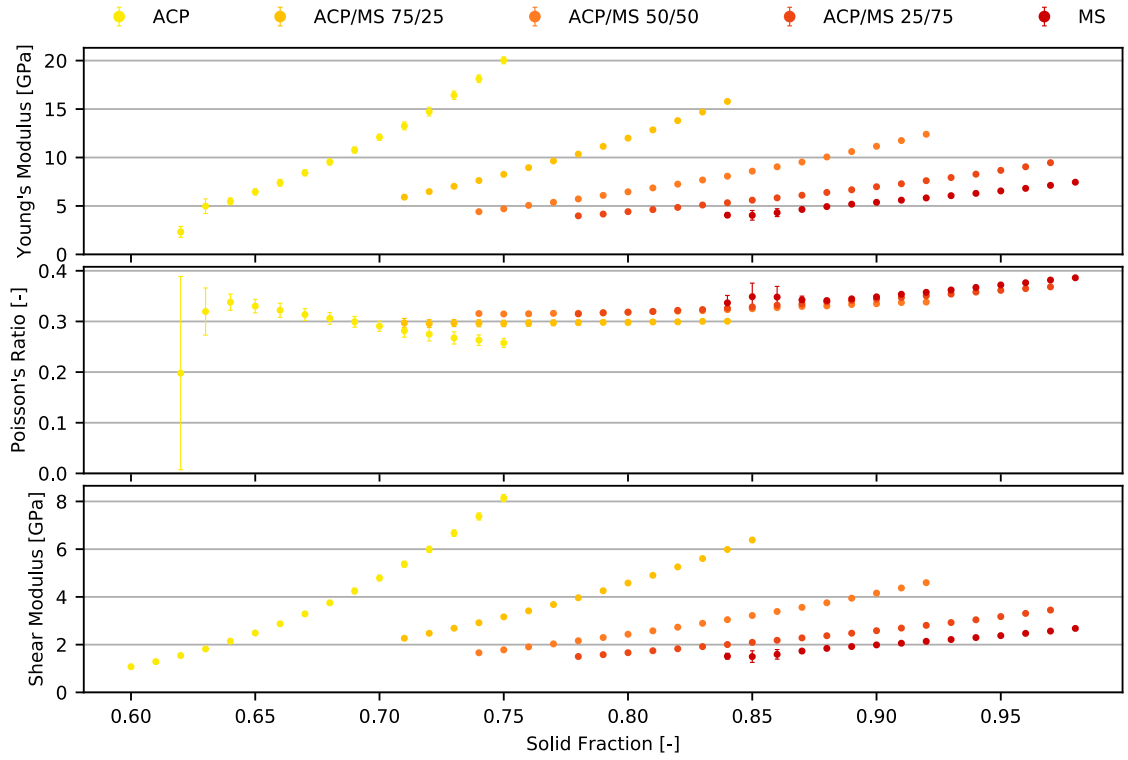

Figure A-10: YM, PR and SM calculated for ACP, MS and their blends. Arithmetic mean ± sd (YM and PR: n = 9; SM: n = 3). Plots share x-axis.

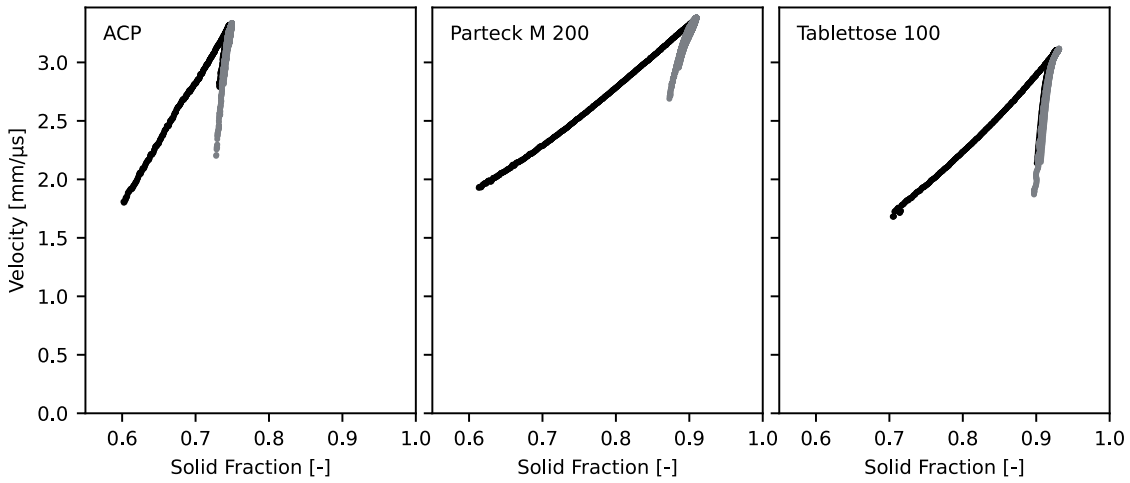

Figure A-11: Longitudinal velocity of one exemplary measurement each, through ACP, Parteck M 200 and Tablettose 100. First compression: Black; Second compression: Grey. Plots y-axis.

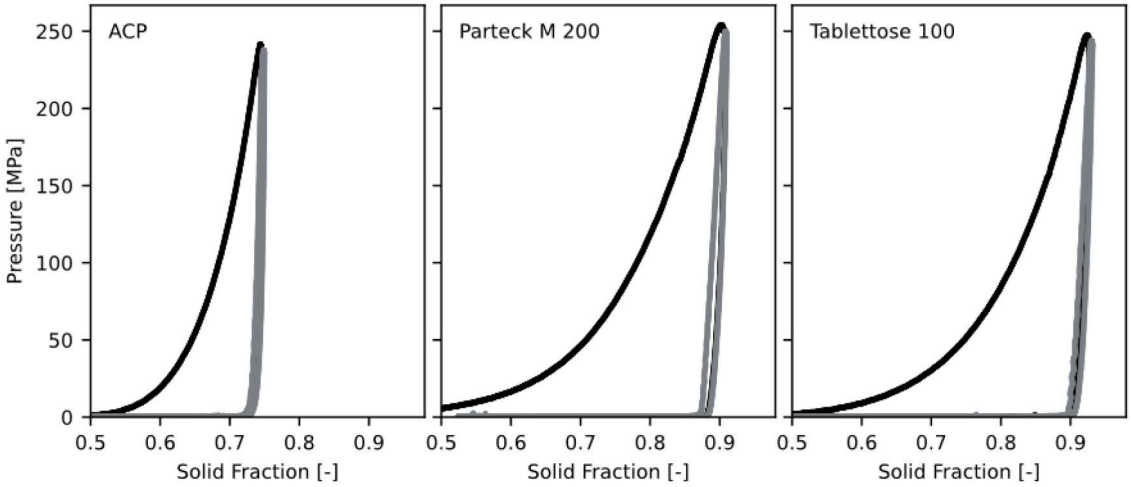

Figure A-12: Pressure-SF plots of the double compaction experiments. First compression: Black; Second compression: Grey. Plots share y-axis.

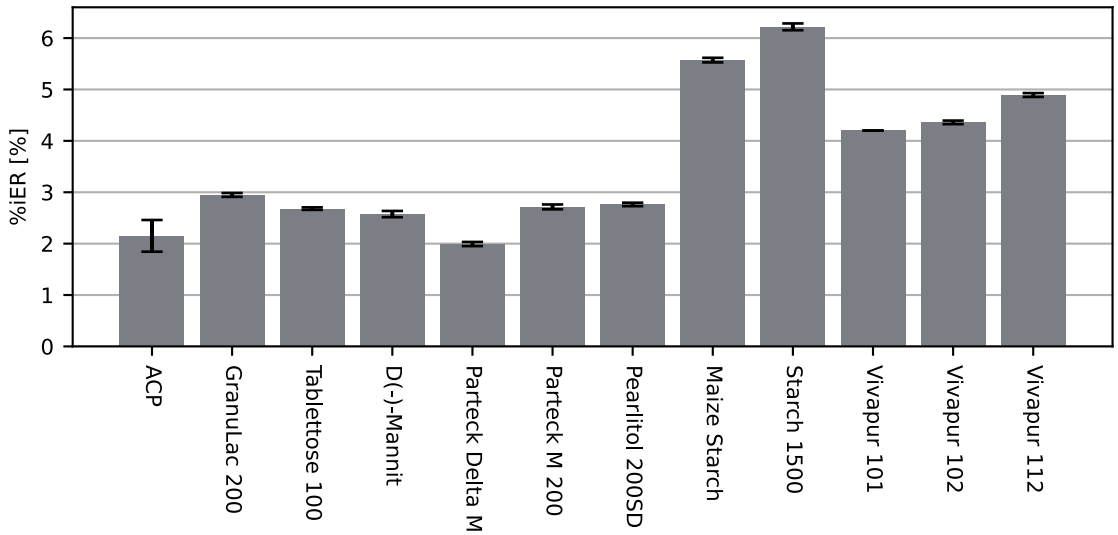

Figure A-13: %iER of the excipients calculated using Equation (3-5). Arithmetic mean ± sd (n = 3).

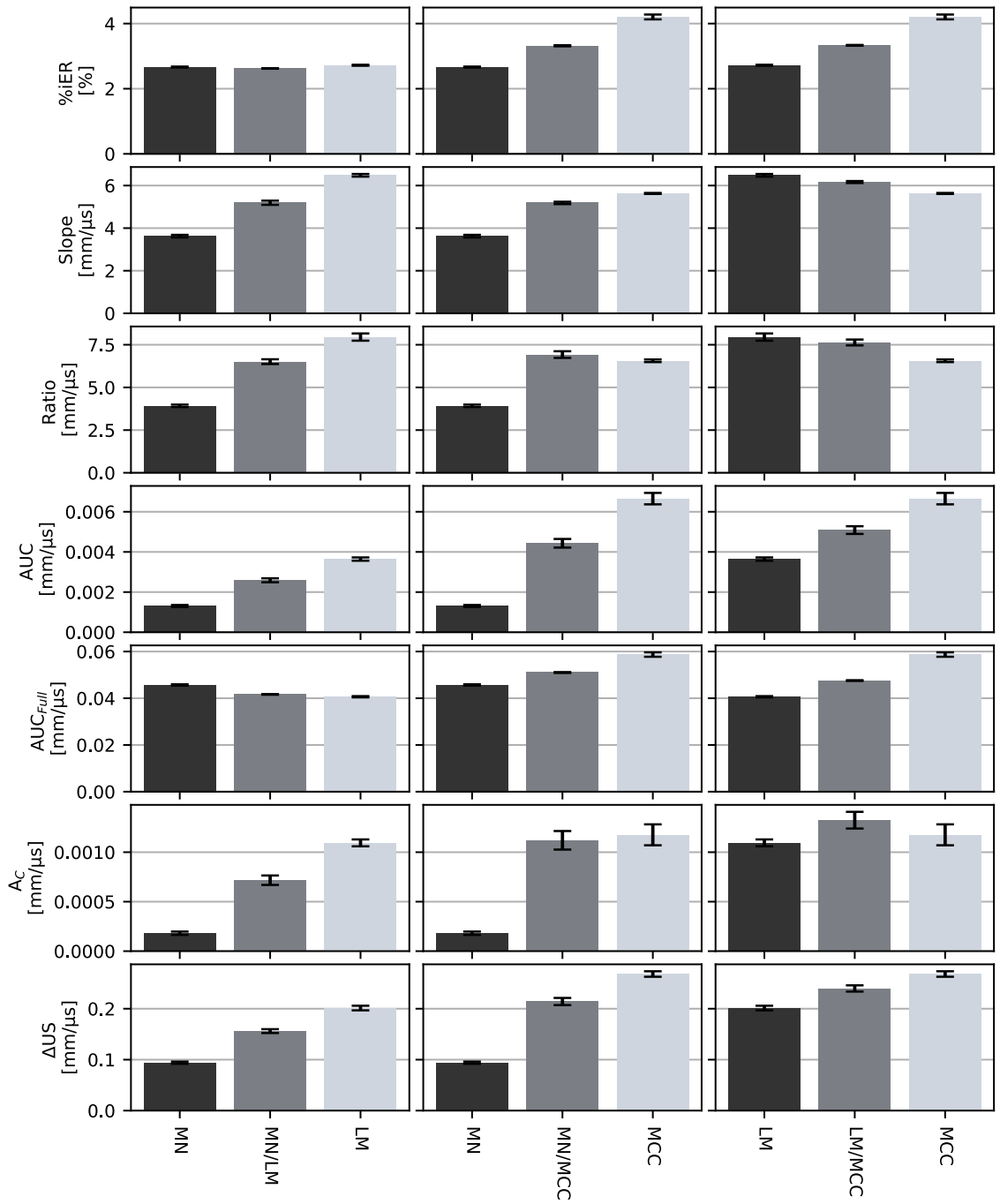

Figure A-14: Decompression parameters calculated using the transverse velocity profiles. Arithmetic mean ± sd (n = 3). MN = Parteck M 200, LM = Tablettose 100, MCC = Vivapur 101. Plots in one row share y-axis.

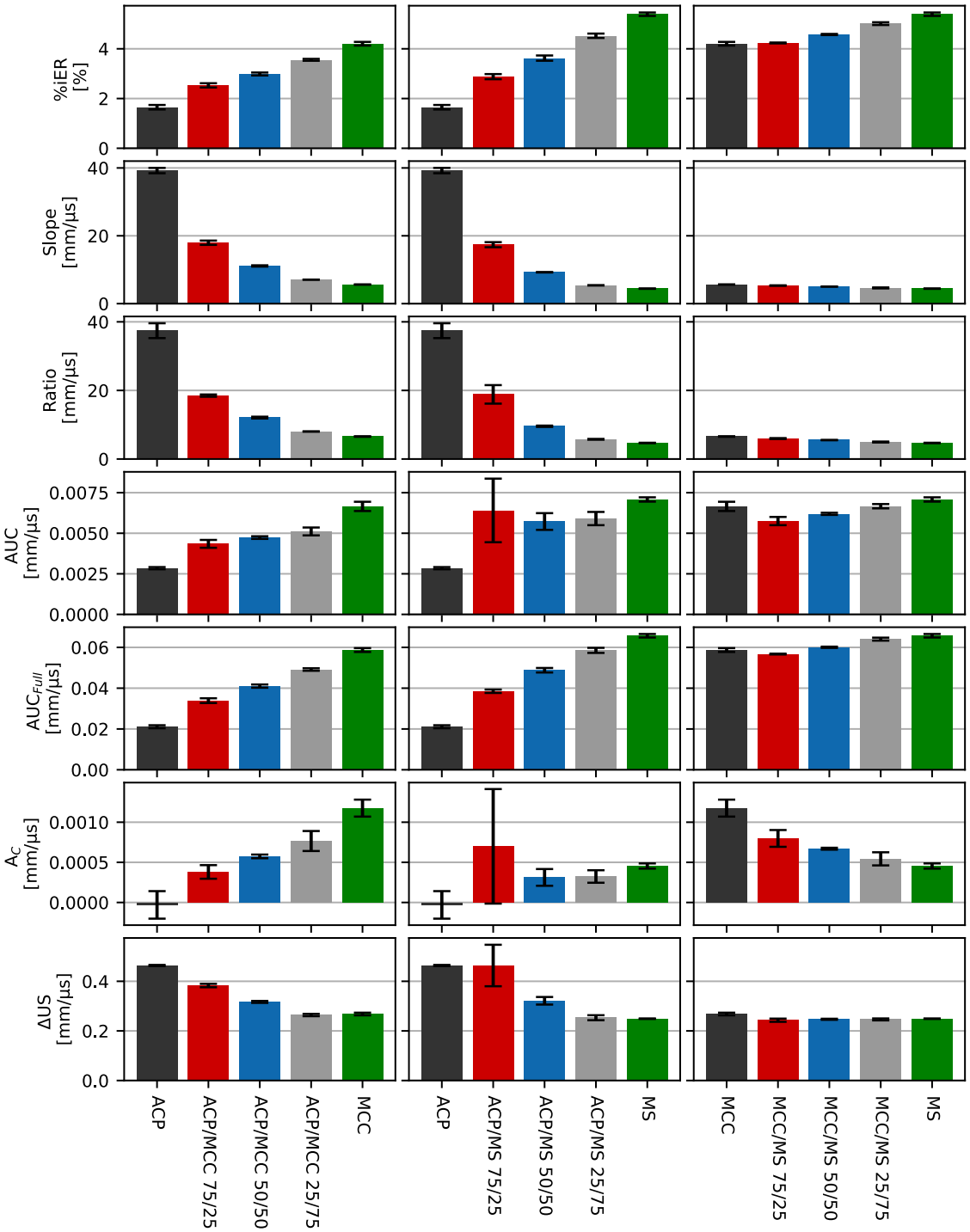

Figure A-15: Decompression parameters calculated using the transverse velocity as described in Chapter 3.3.2. Arithmetic mean ± sd (n = 3). ACP = anhydrous calcium phosphate, MCC = Vivapur 101, MS = maize starch. Plots in one row share y-axis.

Danksagung

Die vorliegende Arbeit entstand unter der Leitung von Herrn Prof. Dr. Jörg Breitkreutz (Heinrich-Heine-Universität Düsseldorf) und Betreuung von Herrn Dr. Thomas Riedel (Merck Healthcare KGaA, Darmstadt) im Rahmen meiner Tätigkeit als Doktorandin bei Merck Healthcare KGaA in der Abteilung Pharmaceutical Technologies.

Vielen Dank zunächst an Herrn Prof. Dr. Breitkreutz für die Betreuung meiner Arbeit. Trotz seines vollen Kalenders hat er sich in jedem unserer gemeinsamen Termine sehr viel Zeit für mich und die Diskussion meiner Ergebnisse genommen. Außerdem natürlich auch für die Hilfestellung was alle organisatorischen Punkte angeht, die manchmal schwer aus Darmstadt zu lösen waren.

Mein Dank geht ebenfalls an Prof. Dr. Anne Seidlitz für die Übernahme der Rolle der zweiten Gutachterin.

Ein riesiges Dankeschön geht an Dr. Thomas Riedel auch bekannt als Thomas Schmal oder (Ex-)Chef. Ich bin mir nicht sicher, ob er eine Vorstellung davon hatte, wie viel Aufwand die Betreuung einer Doktorandin (vor allem einer bestimmten Doktorandin) mit sich bringt. Zum Glück ist Doktorand Nummer 2 wesentlich pflegeleichter was den emotionalen Support und den damit einhergehenden Taschentuchverbrauch angeht.

Auch vielen Dank an Dr. Carsten Schmidt, für die Chance meine Doktorandenzeit bei DPD verbringen zu dürfen und die aktive Begleitung meiner Arbeit besonders in ihren letzten Zügen. Und natürlich die Unterstützung als es darum ging wie es in meinem beruflichen Leben weitergehen wird.

Danke auch an Romaco Kilian für das zur Verfügung stellen des KIM-systems, sowie an Rob Lammens und Benjamin Frindt von Solids Development Consult für die Installation der Hardware und den Softwaresupport.

Ein besonderes Dankeschön geht an meine Kollegen aus DPD und DDI, die mich während der letzten Jahre im Technikum unterstützt haben. Seien es die Schulungen an den Geräten, die Suche nach dem passenden Packmittel, das Ausklamüsern der Gerätebelegungen oder das Verschieben der Styl'One in einen freien Arbeitsplatz unter Einsatz des eigenen Lebens (hier seien vor allem Alexander Sander und Matthias Schäfer nochmal gesondert erwähnt). Auch Karina Schmutzler soll hier namentlich genannt werden, da sie nicht nur wann immer nötig ein zweites Händepaar zur Verfügung gestellt hat (Tabletten ausmessen geht zu zweit einfach wesentlich schneller), sondern mich auch quasi adoptiert und mich bei mehr als einer Gelegenheit durchgefüttert hat.

Einen wesentlichen Anteil am Gelingen meiner Experimente hatten auch unsere professionellen 3D-Drucker Dominique Schädel, Nadine Gottschalk und Franziska Kuhn. Zum einen natürlich durch all die kleinen Helfer, die mir das Leben erleichtert haben (die Einbauhilfe für die externen Wegmesser des KIM Systems und die Mylinder der ersten und zweiten Generation bilden hier nur die Spitze des Eisbergs), aber auch durch unsere gemeinsamen Auszeiten, nach denen das Arbeiten gleich doppelt so schnell voran ging.

Eine der grandiosesten Erfindungen früherer PharmTech Doktorandengenerationen ist wahrscheinlich das gemeinsame Frühstück. Denn seien wir mal ehrlich: wer von uns weiß auf was man als frischgebackene Doktorandin so alles achten muss? Ich bestimmt nicht. Und wo könnte man besser Informationen und Tipps austauschen als in gemütlicher Runde mit dem einen oder anderen Brötchen auf dem Teller? Vielen Dank deshalb an alle, die mit mir gemeinsam die Doktorandenzeit verbracht haben. Sowohl an die, die schon vor mir am Ziel angekommen sind, als auch an jene, die als nächstes drankommen. Vor allem möchte ich an dieser Stelle Dr. Karsten Flügel hervorheben, der (wahrscheinlich zu seinem Leidwesen) sehr schnell zu meiner go-to Person wurde, wann immer ich vor einem kleineren oder größeren organisatorischen Problem stand. Auch Katharina Krollik soll hier nicht unerwähnt bleiben. Vielen Dank für die Unterstützung und das „Mitleiden“ im letzten Jahr! Dies gilt auch meinen „neuen“ Kollegen bei RP.

Wer schonmal mit größeren Datenmengen gearbeitet hat und Tage, wenn nicht sogar Wochen, damit zugebracht hat händisch Werte von einem Excel Sheet in ein anderes zu übertragen weiß, dass es fast nichts Schöneres gibt als Abläufe zu automatisieren. Vielen Dank deshalb an Ingo Kaminski, der sich die Zeit genommen hat meine Excel Templates durch Makros up zu graden und mir dadurch nicht nur sehr viel repetitive Arbeit erspart hat, sondern es auch geschafft hat, dass ich mich für das Programmieren interessiere. Danke an dieser Stelle auch an Dr. Malte Bogdahn, der mich aus unerfindlichen Gründen in seine Digital Guild aufgenommen hat weshalb ich ab Jahr drei nicht mehr mit fünf verschiedenen Templates und drei verschieden Programmen umherhantieren und meinen Doktorandenvertrag wahrscheinlich um mehrere Jahre verlängern hätte müssen, weil Excel sich immer wieder aufgehängt hätte. Danke auch an Marcel Franke, der sich das eine oder andere Mal mit mir Gedanken über meine Skripte gemacht hat und Dr. Meike Harms, für die gemeinsamen „Heckeln für Anfänger“ Sessions und das zur-Verfügung-stellen ihres Auswerteskripts für die Styl’One Kraft-Weg Daten, das ich für meine Zwecke adaptieren und übersetzen durfte. Zuletzt sei hier auch Dr. Markus Riehl genannt, der sich mehr als einmal bereiterklärt hat mich durch Korrekturlesen zu unterstützen. Danke dafür! Und natürlich auch dafür, dass ich meinen PJ Platz damals bei DPD bekommen habe, was der Ausgangspunkt meiner PharmTech-Laufbahn war, obwohl mein Vorstellungsgespräch definitiv Luft nach oben hatte.

Wer mich kennt weiß, dass es für mich essenziell ist, dass ich mich mit meinen Kollegen gut verstehe und mich in meinem Umfeld wohlfühle. Was das angeht habe ich wahrscheinlich den Jackpot gezogen. Auch was meine Bürokollegen angeht. Was gibt es Besseres als, als frische Doktorandin zwischen zwei Kollegen gesetzt zu werden, die gerade in den letzten Zügen ihrer eigenen Doktorarbeit sind? Danke deshalb an Dr. Simone Hansmann und Dr. Aaron Ruff, die immer einen Tipp für mich parat hatten. Auch mit meinem zweiten Sitzplatz hätte ich es nicht besser treffen können. Vielen Dank an Jessica Grieser und Martina Jeschke, die mich so herzlich bei sich aufgenommen haben und mich immer auf dem aktuellen Stand gehalten haben was gewisse TV-Formate angeht, die hier nicht weiter erläutert werden sollen…

Außerdem möchte ich mich bei meinen Freunden aus der Heimat bedanken, die mir immer wieder gezeigt haben, dass es auch ein Leben außerhalb der Pharmazie und Merck gibt und mich nicht aufgegeben haben, selbst wenn ich das Antworten auf Nachrichten zwischendurch immer mal wieder vergessen hatte. Aber was sind schon sechs Monate Funkstille, wenn man sich seit 20 Jahren kennt? Oder weit über 20 Jahre in manchen Fällen (gell, Rahel Ritter und Lena Ziroli?).

Mein abschließender Dank geht an meine Familie, ganz besonders meine Eltern und Großeltern, die mich mein ganzes Leben lang unterstützt haben, auch wenn sie es nicht immer leicht mit mir hatten. Ich hab euch lieb!! Gerne hätte ich mit euch allen gefeiert, aber dafür war ich leider zu langsam.

Eidesstattliche Erklärung

Ich versichere an Eides Statt, dass die Dissertation von mir selbständig und ohne unzulässige fremde Hilfe unter Beachtung der „Grundsätze zur Sicherung guter wissenschaftlicher Praxis an der Heinrich-Heine-Universität Düsseldorf“ erstellt worden ist.

Melinda Kern